UV-VISIBLE MICROSCOPE SPECTROPHOTOMETRIC POLARIZATION AND DICHROISM WITH INCREASED DISCRIMINATION POWER IN FORENSIC ANALYSIS

by

DALE KEVIN PURCELL

A dissertation submitted to the Graduate Faculty in Criminal Justice, Forensic Science Specialization, in partial fulfillment of the requirements for the degree of Doctor of Philosophy, The City University of New York

2013

This manuscript has been read and accepted by the

Graduate Faculty in Criminal Justice in satisfaction of the
Dissertation requirement for the degree of Doctor of Philosophy

Thomas A. Kubic, M.S., J.D., Ph.D.

_____	_____
Date	Chair of Examining Committee

Joshua D. Freilich, J.D., Ph.D.

_____	_____
Date	Executive Officer

John A. Reffner, Ph.D.

Robert P. Nolan, Ph.D

Fran Adar, Ph.D.

Supervisory Committee

THE CITY UNIVERSITY OF NEW YORK

ABSTRACT

UV-VISIBLE MICROSCOPE SPECTROPHOTOMETRIC POLARIZATION AND DICHROISM WITH INCREASED DISCRIMINATION POWER IN FORENSIC ANALYSIS

by

DALE KEVIN. PURCELL

Advisor: Thomas A. Kubic, M.S., J.D., Ph.D.

Microanalysis of transfer (Trace) evidence is the application of a microscope and microscopical techniques for the collection, observation, documentation, examination, identification, and discrimination of micrometer sized particles or domains. Microscope spectrophotometry is the union of microscopy and spectroscopy for microanalysis. Analytical microspectroscopy is the science of studying the emission, reflection, transmission, and absorption of electromagnetic radiation to determine the structure or chemical composition of microscopic-size materials. Microscope spectrophotometry instrument designs have evolved from monochromatic illumination which transmitted through the microscope and sample and then is detected by a photometer detector (photomultiplier tube) to systems in which broad-band (white light) illumination falls incident upon a sample followed by a non-scanning grating spectrometer equipped with a solid-state multi-element detector. Most of these small modern spectrometers are configured with either silicon based charged-couple device detectors (200-950 nm) or InGaAs based diode array detectors (850-2300 nm) with computerized data acquisition and signal processing being common.

A focus of this research was to evaluate the performance characteristics of various modern forensic (UV-Vis) microscope photometer systems as well as review early model instrumental designs. An important focus of this research was to efficiently measure ultraviolet-visible spectra of microscopically small specimens for classification, differentiation, and possibly individualization. The first stage of the project consisted of the preparation of microscope slides containing neutral density filter reference materials, molecular fluorescence reference materials, and dichroic reference materials. Upon

completion of these standard slide preparations analysis began with measurements in order to evaluate figures of merit for comparison of the instruments investigated. The figures of merit investigated included: 1) wavelength accuracy, 2) wavelength precision, 3) wavelength resolution stability, 4) photometric accuracy, 5) photometric precision, 6) photometric linearity, 7) photometric noise, and 8) short-term baseline stability. In addition, instrument intrinsic polarization effects were investigated to determine the impact of these properties on spectral interpretation and data quality.

Finally, a set of recommendations were developed which describe instrument performance characteristics for microscope and spectrometer features and functions, and specific instrument parameters that must be controlled in order to acquire high quality data from an ultraviolet-visible forensic microscope spectrophotometer system for increased discrimination power.

ACKNOWLEDGEMENTS

I wish to express my sincere appreciation to Dr. Thomas A. Kubic, Associate Professor of Forensic Sciences for serving as the Chairperson and advisor for this dissertation. I benefitted from numerous, practical, and patient discussions about instrumentation and microscopy with Dr. Kubic. I am indebted to Dr. John A. Reffner, Assistant Professor of Forensic Sciences whose knowledge, acute observations, invaluable insight and ability to simplify complicated surmise significantly assisted in the direction and completion of this dissertation. I am also extremely grateful for many insightful discussions and guidance to understand many physics related questions and answers from Dr. Fran Adar, Raman Principal Scientist with HORIBA Jobin Yvon, Inc. Lastly, but not least, I wish to express my appreciation to Dr. Robert P. Nolan, Professor and Director of Earth and Environmental Sciences at The Graduate Center, City University of New York for his constructive suggestions, helpful criticisms, and infectious enthusiasm. Without the guidance of these four members of my dissertation committee, the accomplishment of this dissertation would not have been possible.

I wish to express my deep respect and appreciation to Dr. Selman Berger, Professor Emeritus at John Jay College for your friendship and support through many discussions and encouragements. A special thank you is expressed to Dr. JoAnn Buscaglia, Research Chemist with the Federal Bureau of Investigation in the Counterterrorism and Forensic Science Research Unit. I appreciate your many contributions to my education, my personal growth as a forensic scientist and your mentor during my tenure as a Visiting Scientist. I am forever grateful for the opportunity to participate in the Visiting Scientist Program sponsored by the Oakridge Institute for Science and Education (ORISE) and the Federal Bureau of Investigation.

There are many other people whom have contributed to the success of this dissertation and manuscript and whom I want to express my appreciation: Dr. Nicholas D.K. Petraco, Assistant Professor of Forensic Sciences, Professor Nicholas Petraco, Sr., Dr. Brooke W. Kammrath, Assistant Professor of Forensic Sciences at the University of New Haven. I extend my sincere appreciation to my fellow doctoral students and colleagues, Ms. Pauline Leary, Mr. Thiti Mahacharoen, Police Major of Royal Thai Police, Thailand, and Mr. Peter Diaczuk.

I also wish to express my gratitude to Dr. Lawrence Kobilinsky, Department of Sciences Chairperson, John Jay College of Criminal Justice, Mr. Nikolay Azar, Mr. Argeliz Pomales, Ms. Natalia T. Timmer, and Ms. Kiezia Lawrence, to name only a few, but whom stand out in my mind as making significant contributions to the success of this dissertation.

I would like to thank many of my undergraduate and graduate school professors, all of whom have contributed in their own way to my education, personal growth, and personal friendships: Dr. David Wild, Dr. Pete E. Poston, Dr. Arlene Courtney, Dr. Rahim Kazerouni, Dr. Peter R. De Forest, and the late Dr. Richard Culp.

I wish to express special appreciation to friends who I was so fortunate to meet during my eighteen months as a Marine Security Guard at the American Embassy in Ouagadougou, Burkina Faso, West Africa: Ambassador Dr. Edward P. Brynn, currently of Washington, DC, and Historian at the United State Department of State; Dr. Joseph "Joe" Hilts and his wife Margaret, currently of Green Bay, Wisconsin, and fellow Packer-Backers; I hold a very special space in my life for my "Mom & Pops", Tom and Carol Holbrook, currently of Hudson, Florida. My life has been greatly enriched by all of you. I am forever grateful to have shared a short time working with each of you only to gain a lifetime of friendship and fellowship with you still today. I value every visit and conversation we share reminiscing about West Africa and our joint contributions to serving our country as foreign diplomats.

All of this would not be remotely possible without the love and support from William R. "Bill" and Connie Ford III, and their children, Will and Addie. I am forever grateful to you all for welcoming me into your home and inviting me to be an integral part of your family. I can think of no earthly way to express my sincere gratitude to each of you. I remain humbled by your earnest devotion to my every endeavor with endless support and encouragement to move forward with my dreams and my career. I remain forever grateful for your selfless commitment and support for my many years of continued education and personal development. I also want to express my sincere gratitude to "Grandma and Grandpa Ford" for opening your home to me from the very beginning of my relationship with Bill and Connie, and I will always remember our first family Christmas together in 1983. Thank you all from the innermost being of my soul.

In the forefront of my life is my wife Patti. I am sincerely grateful for your personal sacrifices to help make this dissertation research and the pursuit of this Ph.D. a reality. Your constant words of encouragement, your endless devotion, and everlasting commitment to help this dissertation and manuscript come to fruition cannot be matched by any words of thanks. Patti is my rock! I am forever indebted to you for your fastidious push to finish under strong stride. This accomplishment is as much yours as it is mine.

TABLE OF CONTENTS

LIST OF TABLES

LIST OF FIGURES

GLOSSARY OF TERMS

Absorbance, A – the logarithm to the base 10 of the reciprocal of the transmittance, (T).

$$A = \log_{10} (1/T) = - \log_{10} T$$

Absorption coefficient, α – a measure of absorption of radiant energy from an incident beam as it traverses an absorbing medium according to Bouguer's law, $P / P_0 = e^{-\alpha b}$.

Absorptivity, a – the absorbance divided by the product of the concentration of the substance and the sample pathlength. a = A/bc, The units of b and c shall be specified. IUPAC recommends the unit of measure for b is the centimeter, and the unit for c is kilogram per cubic meter or equivalent, g/dm^3, g/L, mg/cm^3.

Angle of incidence, θ – the angle between an incident radiant beam and a perpendicular to the interface between two media.

Background – apparent absorption caused by anything other than the substance for which the analysis is being made.

Baseline – any line drawn on an absorption spectrum to establish a reference point representing a function of the radiant power incident on a sample at a given wavelength.

Bathochromic shift – change of a spectral band to a longer wavelength (lower frequency) because of structural modifications or environmental influences, also known as "red shift".

Beer's law – the absorbance of a homogeneous sample containing an absorbing substance that is directly proportional to the concentration of the absorbing substance.

Bouguer's law – the absorbance of a homogeneous sample is directly proportional to the thickness of the sample in the optical path.

Certified Reference Material, (CRM) – a reference material, the composition or properties of which are certified by a recognized standardizing agency or group. A certified reference material produced by the National Institute of Standards and Technology (NIST) is designated a Standard Reference Material (SRM).

Charged-couple device, CCD – a silicon-based semiconductor chip consisting of a two-dimensional matrix of photosensors or pixels.

Concentration, c – the quantity of the substance contained in a unit quantity of sample. For solutions, the recommended unit of concentration is grams of solute per liter of solution.

Dark current – a current that occurs naturally through the thermally generated electrons in the electronic circuitry of a photo detector. It is intrinsic to semiconductors and is independent of incident photons.

Dark noise – the shot noise associated with the dark current for the given exposure time, and is approximately equal to the square root of the dark current times the exposure time used. It is usually expressed in terms of number of electrons.

Dynamic range – the ratio of the full well saturation charge to the system noise level. It represents the ratio of the brightest signals a detector can measure in a single measurement (A true 16-bit detector will have a dynamic range of 65,535:1).

Filter, Neutral Density – a filter that attenuates the radiant power reaching the detector by the same factor at all wavelengths within a prescribed wavelength region.

Fluorescence – the emission of radiant energy from an atom, molecule, or ion resulting from absorption of a photon and a subsequent transition to the ground state without a change in the spin quantum number. The initial and final states of the transition are usually both singlet states. The average time interval between absorption and fluorescence is usually less than 10^{-6} second.

Internal conversion – a transition between electronic states of the same total spin quantum number (multiplicity).

Intersystem crossing – a transition between electronic states that differ in total spin quantum number (multiplicity).

Level one (1) tests – a simple series of measurements designed to provide quantitative data on various aspects of instrument performance and information on which to base the diagnosis of problems.

Level zero (0) tests – a routine check of instrument performance that can be done in a few minutes, and designed to detect significant changes in instrument performance and provide a database to determine instrument function over time.

Linear dispersion – the derivative, $dx/d\lambda$, where x is the distance along the exit focal plane of a grating or prism-based spectrograph or monochromator, and λ is the wavelength.

Luminescence – the emission of radiant energy during a transition from an excited electronic state of an atom, molecule, or ion to a lower electronic state. The recommended unit of measure for "specimen pathlength" is centimeters.

Monochromator – a device or instrument that, with an appropriate light source, may be used to provide a continuous calibrated output of electromagnetic energy at known wavelengths or frequency range.

Noise – unwanted random variations of output signal that are added to the real signal and are not subtractable. Noise arises from the statistical variations of both thermal and photon generated signal as well as from electron conduction through resistive material, and variations in the readout electronics.

Numerical aperture – the sine of one half of the vertex angle of the largest cone of meridional rays that can enter or leave an optical system or element, multiplied by the refractive index (n) of the medium in which the cone is located. AA is the acceptance angle of the microscope objective.

$$NA = n \sin \frac{AA}{2}$$

Peltier cooler – solid-state device that uses the thermal electric effect to cool a CCD. A thermal electric cooler has a hot and cold side. The cold side is connected to the back of the CCD. This enables the temperature of the CCD to be reduced. The hot side is connected to a heat sink which enables excess heat to be dissipated.

Phosphorescence – the emission of radiant energy from an atom, molecule, or ion resulting from absorption of a photon from the ground state, and then transition to a lower excited state with different spin value, followed by a subsequent transition to the ground state with a change in the total spin quantum number. The initial state of the transition is usually a triplet state. The average time interval between absorption and phosphorescence is usually greater than 10^{-6} second.

Photodetector – an electronic device that yields an output electrical signal in response to or as a replica of the input radiant energy.

Photometer – a device so designed that it furnishes the ratio, or a function of the ratio, of the radiant power of two electromagnetic beams. These two beams may be separated in time, space, or both.

Photometric linearity – the ability of a photometric system to yield a linear relationship between the radiant power incident on its detector and some measurable quantity provided by the system.

Pixel – abbreviation for picture element. The smallest unit in an optical device in which charge is collected as a signal. CCD detectors typically have 26 μm square pixels, however, pixel sizes of 8, 13, 16, and 20 μm square are also available.

Quantum efficiency (QE) – a measure of the sensitivity of the CCD chip or PMT to convert photons to photoelectrons at a given wavelength. It is defined as the ratio of the detected to the incident photons at the given wavelength and is normally expressed as a percentage.

Radiant energy – energy transmitted as electromagnetic waves.

Radiant power, P – the rate at which energy is transported in a beam of radiant energy.

Ratioed spectrum – the calculated ratio of two single-beam spectra, one of which is a background (source) spectrum.

Reference material – a material or substance one or more properties of which are sufficiently well established to be used for calibration of an apparatus, the assessment of a measurement method, or for assigning values to materials.

Reflectance, R – the ratio of the radiant power reflected by the specimen to the radiant power incident on the specimen.

Refractive index – the phase velocity of radiant power in a vacuum divided by the phase velocity of the same radiant power in a specified medium. When light enters a medium from a vacuum, n is the ratio of the sine of the angle of incidence to the sine of the angle of refraction.

Resolving power, R – the ratio $\lambda/\Delta\lambda$ where λ is the wavelength of radiant energy and $\Delta\lambda$ is the resolution expressed in wavelength units.

Resolution, $\Delta\lambda$ – the wavelength interval, $\Delta\lambda$, of radiant energy leaving the exit slit of a monochromator measured at half the peak detected radiant power.

Practical resolution, $(\Delta\lambda)^{\pi}_{S/N}$ – is the resolution applicable to an instrument operated at a given integration period, π, and a given signal-to-noise, S/N, measured at or near 100% on a transmission scale.

Limiting resolution, $(\Delta\lambda)_L$ – is the maximum resolution achievable under optimum experimental conditions.

Theoretical resolution, $(\Delta\lambda)_0$ – is the computed resolution. This term should be used sparingly and only when all the factors in the computation of resolution are given.

NOTE: **Resolving power** is an instrument property, specifying the smallest detail that a Microscope and Photometer can resolve in both the image and spectrum of an ideal (possibly hypothetical) specimen. This quantity is determined both by instrument design and by properties of the imaging radiation (λ). The related quantity, **Resolution**, refers to the detail actually revealed in the image (spectrum) of a given specimen. The achievement of resolution not only requires adequate instrumental resolving power but also depends on the contrast properties of both microscope and specimen; these are somewhat competing properties.

Sample spectrum – a spectrum, either single-beam or ratioed, that contains spectral features due to an analyte of interest.

Shot noise limited – the detection level where the minimum measurable signal is limited by the shot noise and not by the CCD detector's electronics-related noise sources.

Signal-to-noise ratio, S/N – the ratio of the signal, S, to the noise, N, as indicated by the instrument read-out indicator. Noise as used here is the random variation of signal with time.

Silicon- a tetravalent, semiconducting element whose crystal is used in the fabrication of integrated circuits including CCDs.

Single-beam spectrum – a spectrum determined through one physical optical path. This spectrum may be simply the instrument response function as measured by the detector, or it may include spectral features resulting from the presence of a sample or sampling device.

Single-beam reference spectrum (I_0) – a spectrum determined through one physical optical path consisting of the instrument response function measured by the detector through the sample preparation without the sample in the optical path being measured.

Single-beam sample spectrum (I) – a spectrum determined through one physical optical path consisting of the sample preparation to include the sample.

Single-beam ratioed spectrum (I/I_0) – the calculated ratio of two single-beam spectra, one of which is a reference spectrum.

Specimen pathlength, b – the distance, measured in the direction of propagation of the beam of radiant energy, between the surface of the specimen on which the radiant energy is incident and the surface of the specimen from which it is emergent.

Spectral position – the wavelength of an essentially monochromatic beam of radiant energy.

Spectral rate – a value describing the number of fully vertically binned spectra per second that can be produced by the CCD. Usually expressed in spectra per second or Hz.

Spectral slit width – the mechanical width of the exit slit, divided by the linear dispersion in the exit slit plane.

Spectrograph – an instrument with one slit that uses s photographic detector such as a CCD to obtain a record of a spectral range simultaneously. The radiant power passing through the optical system is integrated over time, and the quantity recorded is a function of radiant energy.

Spectrometer – an instrument for measuring some function of power, or other physical quantity, with respect to spectral position within a spectral range.

Spectrometry – the branch of physical science treating the theory and practice of the measurement of spectra.

Spectrophotometer – a spectrometer with associated equipment, so designed that it furnishes a ratio, or a function of the ratio, of the radiant power of two beams as a function of spectral position. The two beams may be separated in time, space, or both.

Spectroscopy – the branch of physical science treating the theory and interpretation of spectra.

Spectrum – any actual or notational arrangement of the component parts of any phenomenon, as electromagnetic waves or particles, ordered in accordance with the magnitude of a common physical property, as wavelength, frequency, or mass.

Specular reflection – reflection without diffusion, in accordance with the laws of optical reflection, as in a mirror. Angle of reflection equals angle of incidence.

Standard Reference Material, (SRM) – a certified reference material produced by the National Institute of Standards and Technology (NIST).

Surface reflection – reflection in which radiant energy is returned exclusively at the surface of the specimen.

Thermoelectric cooling – method to reduce the temperature of a CCD by direct or near direct contact with a Peltier cooling device.

Throughput – the vector product of the area and solid angle of a beam at its focus and the square of the refractive index of the medium in which the beam is focused.

Transmittance, T – the ratio of radiant power transmitted by the specimen to the radiant power incident on the specimen.

CHAPTER 1. INTRODUCTION

A. Statement of the problem

The purview of forensic science to determine the identity of materials, to establish the exchange of materials between objects or people, to determine the source of the materials, to establish a link between a person and a crime scene, the inference of common origin or identity of source, and to interpret the significance of physical evidence to assist the legal system is unique to forensic science. The growing expectation by the legal system to answer these questions has placed extreme demands on laboratory methods for analysis and chemical instrumentation to become more technologically advanced, more sensitive with a higher degree of discrimination, all the while remaining within the fiscal limits of laboratory budgets. These are formidable challenges for the development of instruments and methods that are capable of analyzing many different types of physical evidence materials or transfer (Trace) evidence. Transfer evidence is useful in the evaluation of contact between two or more objects, people or locations in order to establish associations, and in the reconstruction of events. The fundamental principle that transfer evidence produces a record of past events is best stated by Dr. Paul Leland Kirk in the preface of his book, *Crime Investigation (1953)*:

> Wherever he steps, whatever he touches, whatever he leaves, even unconsciously, will serve as silent evidence against him. Not only his fingerprints or his footprints, but his hair, the fibres from his clothes, the glass he breaks, the tool mark he leaves, the paint he scratches, the blood or semen he deposits or collects – all these and more bear mute witness against him. This is evidence that does not forget. It is not confused by the excitement of the moment. It is not absent because human witnesses are. *It is factual evidence.* Physical evidence cannot be wrong; it cannot perjure itself; it cannot be wholly absent. Only its interpretation can err. Only human failure to find it, study and understand it, can diminish its value (Kirk, 1935, italic emphasis in the original).

Instrumental analysis and the evaluation of transfer evidence present formidable challenges for microscope spectrophotometry instrumentation that address forensic science needs. The critical instrumental attributes include the necessity to observe and analyze small, microscopic sized particles, and the discrimination of source attribution (association) when dealing with different samples. Any discussion of inference of contact and association generally defaults to a demand for better methodologies of individualization. In a forensic science context, the meaning of individualization is to draw a conclusion of common source between two items. Logically, any single item is unique, this is not the question, but rather whether two or more individual items once shared a common source (came from the same individual item). The demands placed on the forensic applications of instrumentation to establish inference of source or inference of contact is more stringent than those demands required by most other scientific disciplines, which deal mostly with the identification of materials and not the inference of source or contact. Association is an inference of contact between two objects, and is the only way in which legally relevant evidence can be generated by a scientist. A distinction between source determination and inference of contact becomes increasingly easier with more ambiguous evidence, in which the leap from source determination to an inference of contact requires more assumptions. Therefore, the definition for association is an inference of contact between two objects, the source of the evidence, and the target on which it was located.

Microscope spectrophotometry, in its most rudimentary sense, is the measurement of the wavelength dependence of the transmittance or reflectance of electromagnetic radiation by a microscopic sized specimen, which is much too small to be measured on a typical bench top spectrophotometer. In addition to dealing with limitations in specimen size, capabilities exist to determine optical properties of the specimen such as, morphology, refractive indices, birefringence, homogeneity, phase differences (polymorphisms), cross-section, and dichroism, to name only a few for which a microscope is ideal. Microscope spectrophotometry is a specialized method within the realm of molecular electronic, vibrational, and rotational spectral analysis. Configuration of the essential equipment necessary to perform reliable microspectrophotometric measurements is challenging for an instrument design that allows the analyst to control many of the critical parameters. Some of the most critical parameters include photometric stability over long data acquisition times, sufficiently high spectral resolution, and rapid data

collection and processing time. Historically, many of the early instruments required long data acquisition times, were large and cumbersome, but they did have very adequate control of critical microscope settings such as field diaphragm sizes, magnification, and spectrometer features such as spectral bandwidth selection and the selection of different diffraction gratings. Notwithstanding instrumental differences, the underlying theory and principle of operation is relatively similar to most bench top spectrophotometers, with the most important exception being the microscope as the optical bench. Many of the important microscope parameters such as illumination with polarized light, image formation, and the physical configuration of critical optical elements need to be reviewed to determine whether they are accessible to the operator for proper adjustment and control. What is still lacking in the forensic sciences is a document that outlines parameters that are critical for instrument operation and training. The primary focus of this dissertation is to bridge the gap between the theoretical understanding and the practical operation of an ultraviolet (UV) -visible microscope spectrophotometer. This dissertation will guide a forensics scientist to make logical, informed decisions about which instrument parameters must be controlled in order to obtain the highest quality spectral data. Properly controlled instrument parameters optimize instrument resolving power, which in turn optimizes spectral resolution and improves the power of discrimination. Approximately eighty percent of colored fibers exhibit dichroism. Alas this dissertation provides guidance to forensic scientists to understand and implement procedures for the collection and interpretation of dichroic spectra using polarized light microscope spectrophotometry.

B. Principles of Electromagnetic Radiation (Light):

Wavelengths of electromagnetic radiation in the UV and visible ranges are generally expressed in nanometers (nm), with the ultraviolet region being between 200–400 nm and the visible region between 400-800 nm (Skoog et al., 2007). The energy of electromagnetic radiation is defined by the relationship, $E = h\nu$, where E is energy (in Joules, J), h is Planck's constant (6.62×10^{-34} J*second), and ν (the Greek letter nu) is frequency (in Hertz, Hz, where Hz = cycles/second). Electromagnetic radiation is the combination of alternating, orthogonal electric and magnetic fields that propagate through space as a transverse wave. As a result, the wave may be classified by its frequency (ν) or wavelength (λ) which are related by, $\nu = c / \lambda$, where c is the speed of light (2.998×10^{8} m/s) in a vacuum. Light can be described

by its amplitude, wavelength and direction of the electric vector. The direction of travel is called the propagation direction, which is always transverse (that is, perpendicular) to the wavefront. The amplitude varies as a sine function according to Equation 1.1:

$$y = r \sin \omega t, \qquad \text{Equation 1.1}$$

where r is the maximum amplitude, t is the time, and ω is the angular velocity.

When electromagnetic radiation interacts with matter, many possible resulting processes may occur such as scattering, reflection, refraction, absorption, emission, fluorescence, phosphorescence, and/or decomposition. Since light in the form of energy may be absorbed, this energy may promote electronic excitation within molecules. The total energy of a molecule is fundamentally represented by the sum of its electronic (E_e), vibrational (E_v), and rotational (E_r) energies by the relationship $E_T = E_e + E_v + E_r$. In ultraviolet-visible spectroscopy, the photons have enough energy to promote electronic transitions, whereas in the infrared spectral region the photons only have only enough energy to promote vibrational and rotational transitions. In most molecules, vibrational and rotational energy levels will interact, which results in band spectra. In liquids and solids there is additional band broadening as a result of molecular interactions and collisions. Consequently spectral peaks are characterized by their shape, intensity, width, and wavelength. Usually the peak width is expressed as the width in energy (wavelength) at half the peak height, which is commonly referred to as full-width-at-half-maximum (FWHM).

In a molecule, the total internal energy is composed of the additive contributions from the energy of the electronic states, the vibrational motions of the constituent atoms in the molecule, and the rotational motion of the molecule as a unit. These various contributions are quantized, meaning that they exist in discrete energy levels. The quantized motions of molecules add spectral complexities not present in atoms, which produce line spectra. In any electronic state a molecule may exist in a number of vibrational states, separated by relatively small energy level differences. In any vibrational state many rotational energy levels are possible that are separated by even smaller energy level differences. Therefore, when the energy absorbed by the molecule is able to promote electronic transitions there are a large number of vibrational and rotational transitions possible as well. The spectrum of a molecular gas associated with a single electronic transition, contains a number of bands, each one associated with a

definite vibrational change. Upon further resolution, the bands may be found to contain a larger number of lines each associated with a particular rotational state. In liquids and solutions, heterogeneous interactions between absorbing solute and solvent molecules, broaden the energy levels such that the rotational and most vibrational energy level structure is lost in the spectrum. A discussion of the instrument attributes and features that contribute to the ability to measure spectra is discussed in more detail below.

C. Principles of Microscope Spectrophotometry:

The perceived color of a specimen depends on the relative spectral power distribution of the light source, the spectral reflectance and absorbance of the colored specimen, and the spectral sensitivity of the human eye or detector. Cones in the human eye are able to detect color as electromagnetic radiation in the narrow visible region approximately between 400-700 nm, while the rods provide black and white vision. Cones exist in three types: 1) erythrolabe, which are sensitive to red light; 2) chlorolabe, which are most sensitive to green light; and 3) cyanolabe, which are sensitive to blue light. All visible colors can be described by a set of parameters called the tristimulus values, determined from the response of the average human eye for the primary colors red (X), blue (Z), and green (Y) (ASTM D2244, 1993). The human eye is most sensitive to green light at approximately 550 nm (Blackwell, 1946). The eye-brain detector system reacts to physiological stimulus that is registered as light, brightness (intensity) and color (frequency). It is well-known that when the three primary colors are blended by the human eye, they are perceived as white. The subjectivity of human color interpretation is in the way we communicate the differences in observed color. The normal human eye responds to light between approximately 400 – 800 nm, in the visible region of the spectrum. Microscope spectrophotometry provides a systematic way to analyze spectral data within and outside the spectral range of the human eye.

Microscope spectrophotometry has found forensic value using fluorescence, cathodoluminescence, bright-field and dark-field reflected light, and bright-field transmission measurements. The application of microscope spectrophotometry to contrast methods such as phase contrast, differential interference contrast, Hoffman modulation contrast, and crossed-polar interference color birefringence measurements may prove to be of forensic value and the subjects of future research.

To this point, the majority of the forensic science applications of visible microscope spectrophotometry are in the analysis and comparison of transfer evidence with a few reported applications using ultraviolet light for the analysis of automobile clear coat paints. The vast majority of the visible light applications include analysis of dyes and pigments common to fibers and textiles, to ink and paper, to coating materials used in architectural, automotive, and artistic paints, and to dyes used to color human and animal hair. A review of these applications is presented in the literature review of Chapter 2.

The key advantage of microscope spectrophotometry over bulk analysis using a bench top spectrometer is the ability to characterize the inherent optical structure and characteristics, and the chemical properties of a small, micrometer size specimen. This is achieved by making observations of magnified images of the specimen that may be documented using digital photomicrography, and by using metrology to determine physical measurements. Optical measurements are made to determine characteristic properties such as refractive index, birefringence, and sign of elongation, to name only a few. In addition, the microscope spectrophotometer will provide chemical information about a specimen's absorption spectrum. In brightfield microscope spectrophotometry, for example, to understand the spectral characteristics of a specimen, a photodetector is used to measure the intensity of light transmitted through a specimen as a function of wavelength. The transmittance for one wavelength (λ) may be defined by Equation 1.2:

$$\text{Transmittance, } T(\lambda) = \frac{I_t(\lambda)}{I_i(\lambda)} = e^{-abc} \qquad \text{Equation 1.2}$$

where $I_t(\lambda)$ is the intensity of the transmitted light and $I_i(\lambda)$ is the intensity of the incident light, measured at a specific wavelength (λ). From this, the absorbance $A(\lambda)$ at any wavelength can be calculated by using the Bouguer-Beer-Lambert law, Equation 1.3:

$$\text{Absorbance, } A(\lambda) = -log_{10}\frac{I_t(\lambda)}{I_i(\lambda)} = -log_{10}T(\lambda) = 2 - log_{10}(\%T) = abc \qquad \text{Equation 1.3}$$

where the absorption coefficient (*a*) is a measure of absorption of radiant energy from an incident beam as it traverses an absorbing homogeneous medium of a specific concentration, (*c*) is directly proportional to the thickness of the sample, and (*b*) in the optical path. This needs to be explained in more detail, in terms of oblique transmitted light.

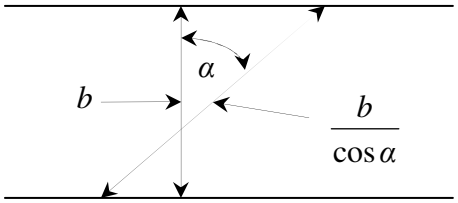

Figure 1.1: Change of optical path in a uniform thickness (parallel) specimen for light paths diverging from normal incident angles.

As illustrated in Figure 1.1, in a parallel-sided specimen (i.e., a cuvette) the light path increases as the light moves away from the surface normal by angle (α), making the optical light path proportional to 1/cos α. The angle of refraction is dependent upon the refractive index of the homogeneous specimen. If absorbance in the direction normal to the specimen surface is $A_0 = ab$, then absorbance in the direction (α) in a specimen is measured using Equation 1.4:

$$A(\alpha) = \frac{A_0}{\cos \alpha} \qquad \text{Equation 1.4}$$

where the absorption in a specimen at the direction normal (α = 0) is expressed by $A_0 = ab$. This relationship holds true for illumination that is cylindrical or collimated and very thin. In properly aligned Köehler illumination (Goldberg, 1980) which is necessary for high resolution magnified microscope images, the illumination is conical with the optical axis of the cone being the normal to the specimen's surface, and the maximum angle (α) being determined by the aperture angle (u) according to the law of refraction: $n = \frac{\sin(u)}{\sin(\alpha)}$, where n is the refractive index of the specimen. Therefore, the relationship between absorbance and illumination angle is dependent on the optical characteristics of the specimen (dispersion, refraction, and reflection) and the optical characteristics of the microscope (Piller, 1977).

In measuring the spectroscopic information of materials, the interpretation of spectra is often a complicated endeavor that requires a theoretical understanding of the underlying physical phenomenon and quantum mechanics. Instrumental effects are introduced because of inherent limiting spectra resolution, power fluctuations in illumination, the increase in spectral radiance or color temperature in which the wavelength shifts to the blue (shorter wavelengths) as the temperature of the radiant source increases, and variations in the signal-to-noise (S/N) ratio due to differences in quantum efficiency of the photodetector at the different wavelengths. There are many additional instrumental attributes that contribute to the quality of spectral data and these will be discussed in more contextual details below.

D. Microscope Spectrophotometer Configurations:

There are three configurations or types of microscope spectrophotometer systems identified in the literature, see Figure 1.2. All three configurations consist of a microscope optical system, a photometer head containing a diaphragm or slit, and a photodetector electrical assembly. The primary difference between each system is the optical geometry of the photometric reference beam path.

The first configuration is known as a single beam system with stage-object switching (Figure 1.2a). In a single beam configuration the geometry of both the microscope (illumination) and the photometric electrical assembly remain fixed when the reference and specimen are interchanged. In addition, the operation of the illumination and photoelectric power systems must be extremely stable for the duration of the measurements of the reference and specimen or set of specimens to be compared against the same reference. There are two advantages of the single-optic system with stage-object switching: 1) it is relatively simple and conveniently attached to nearly all types of microscope, and 2) it has equal optical path for both the reference and specimen.

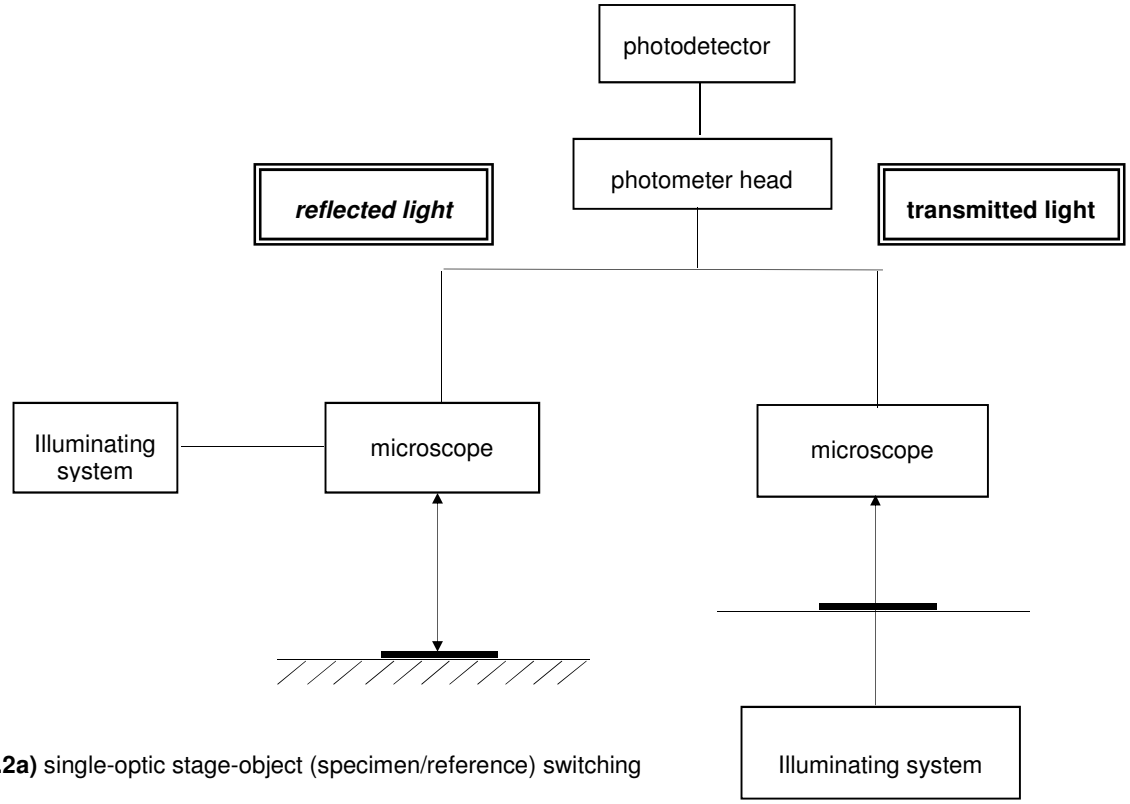

(1.2a) single-optic stage-object (specimen/reference) switching

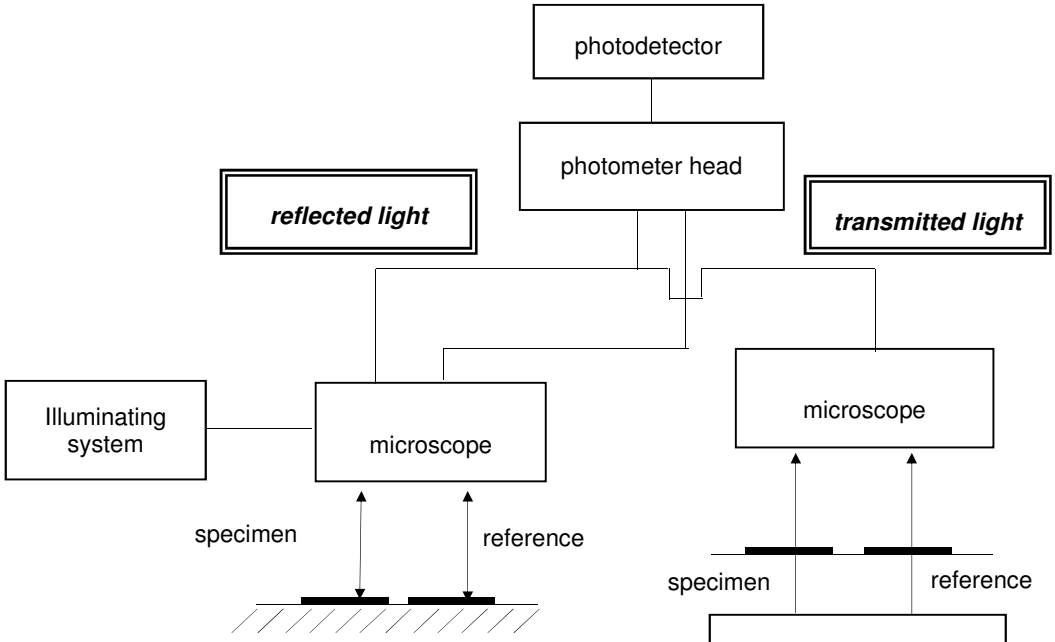

(1.2b) single-optic beam switching

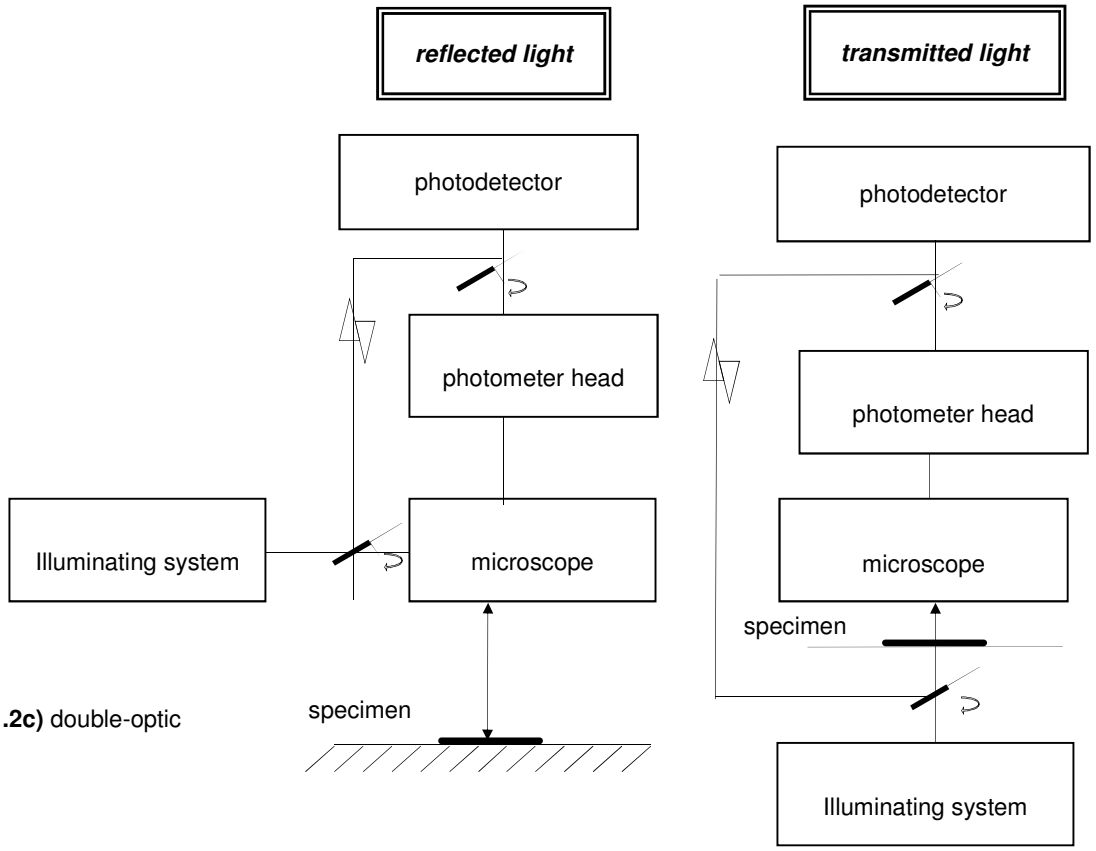

(1.2c) double-optic

Figure 1.2: Three major configurations of microscope photometer systems. (1.2a) single-optic stage-object (specimen/reference) switching, (1.2b) single-optic beam switching, (1.2c) double-optic.

In the second configuration, single-optics with beam switching, which is similar to a double-beam in time with a chopper, the photometric beam path to reach the photodetector must remain unchanged when the measuring spot in the field of view or the stage object field is switched between the reference and the specimen, but note the direction of the photometric beam is changed (Figure 1.2b). Without question, the specimen and reference must be small enough to lie together in the same field of view, since the photometric beam is switched so that the photodetector receives light from one and then the other. The single-optic system with beam switching has two major advantages: 1) fast speed in comparison of pairs of measurements (reference to specimen) with more than 50 measurements possible in one second, and 2) immediate display of variation of comparison results with wavelength by ratioing out instrumental and environment conditions such as temperature.

Lastly, in a double optics system one optical path is described as that of the microscope, and the other optical path is that of the control optical beam (Figure 1.2c). The control optical beam supplies the illumination needed as the reference, but this must first be matched with the reference material. The source illumination optical beam is split before interaction with the specimen and then realigned with the control optical beam immediately preceding the photodetector. A double-optics system requires stringent equality in the two optical systems and equal transmission in the two pathways. This configuration is most demanding on the microscope system but offers a few advantages: 1) fast speed for ratioing pairs of measurements (reference to specimen), 2) immediate display of absolute spectral curves, 3) no restriction to size and position of either the reference or specimen, 4) a less stringent demand on system electrical or power stability, and 5) greatest versatility with respect to computer interfacing or automation.

The first use of a microscope spectrograph may be traced to Henry Clifton Sorby, the father of microscopical metallurgy, in the 1860s when he used a transmission grating eyepiece, Figure 2.1, to view intergranular metal particles known as melt (Walsh, 1958). Similarly, Jelly developed several versions of a spectrograph, Figure 2.2, that employed a transmission grating, collection mirrors and lenses, and a film camera to detect and document observations. Even though the Jelly spectrograph was never commercially available, it inspired many other microscopists to develop microscope spectrophotometers in which the film detector was replaced by a photodetector and electronic recording device (McCrone, 1957).

E. The Microscope as an Optical Bench

Light can be described by propagating, oscillating and orthogonal electric and magnetic fields. It can interact with matter by being scattered, absorbed, or emitted. For radiation in the visible part of the electromagnetic spectrum the interactions are with electrons that have energies comparable to the light. Absorption in condensed matter corresponds to the loss of light when electrons are excited from lower to higher electronic states. Emission is described by the reverse process when a crystal or molecule in an excited electronic state drops back to a lower state, emitting its excess energy in the form of a photon of light. For ordinary light, the light is a wave packet of a very short period of time (approximately 10^{-8} seconds) that propagates in all directions. It is understood that the light is quantized, and often occurs as wave packets resulting from uncertainty in the frequency of the oscillation; an incandescent light source is incoherent; that is there is no synchronization of the phase or orientation of the polarization (electric field) vector of the photons coming from the source even though they overlap in space.

When light travels through an anisotropic specimen such as a polymer fiber or other doubly refracting medium, the optical properties vary with the propagation direction and polarization of the light through the medium. A solid material can have up to three principal refractive indices defined along the material axes.

When the electric and magnetic field vectors are confined in fixed planes the light is considered to be plane polarized. When the electric field rotates as the light propagates, and the electric field vector amplitude in the two directions may or may not be equal and their phase difference is not equal to or equivalent retardation variations of one quarter wavelength, the resultant is known as elliptically polarized light. Circularly polarized light is a special case of elliptically polarized light in which the electric field vector amplitude in the two directions are equal and their phases are related by a quarter wavelength shift. Circularly polarized light may exhibit either a left-hand or right-hand helicity.

Plane polarized light is used to measure the optical properties of anisotropic materials. The optical system of a polarized light microscope starts with a stable light source. In most microscopes the illumination source is a tungsten filament quartz halogen bulb. A polarized light microscope is equipped with a polarizer made of either an absorption film or a double refracting crystal (Glan-Thompson or Nicol prism), a strain-free condenser, a rotating stage, strain-free objectives, a centerable nosepiece, a slot for

a compensator or retardation plate, and a second polarizer (analyzer). In the most flexible systems, the polarizer and analyzer are free to rotate, but when they are positioned 90 degrees to each other the optical field will be dark unless the light goes through an anisotropic material.

In Köhler illumination the lamp filament is conjugate to (imaged on) the aperture iris planes of the microscope so that the specimen plane and its conjugates are uniformly illuminated. Conjugate planes may be explained as those planes in an optical system, in which the first plane is focused on subsequent planes. In a microscope, there are two separate sets of conjugate planes: the illumination set and the image forming (specimen) set. A fundamental knowledge of these conjugate planes is essential to fully understand the correct adjustment of illumination and to understand how and where the image is formed in the microscope. Since the two sets of conjugate planes are separate, they will never appear in any plane of the other set, see Figure 1.3.

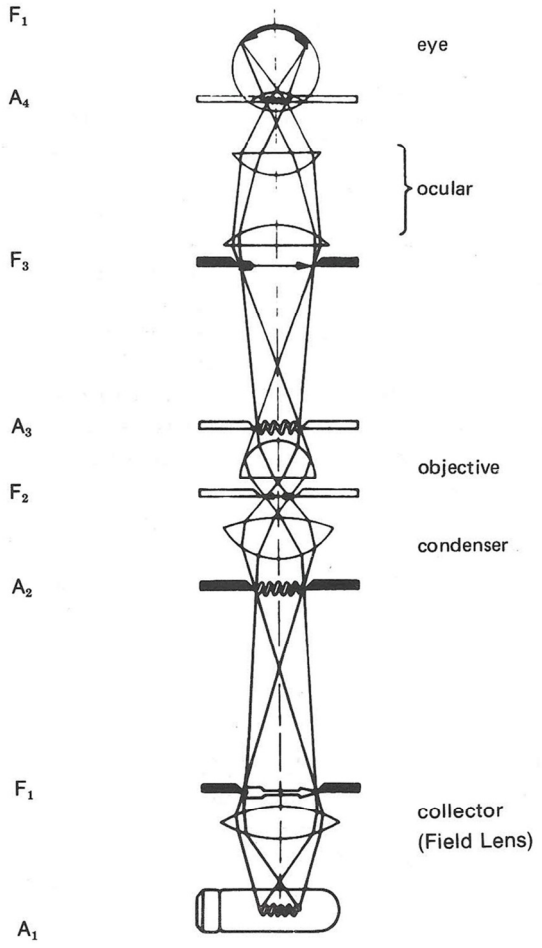

Figure 1.3: Ray paths and conjugate planes in a compound microscope set up for Köhler illumination. Note how field (Fx and aperture stops (Ax) alternate throughout the system. The image forming rays in this diagram diverge from and converge on field stops. The illuminating rays bear a similar relation to the aperture stops. Originally published as Figure 9-10, on page 444, in" Foundations of Forensic Microscopy", Ch. 9, by Peter De Forest, in Saferstein, Richard, Forensic Science Handbook, 1ST Edition, © 1982. Reprinted by permission of Pearson Education, Inc., Upper Saddle River, NJ. Requested drawing appears to be based off of a microscope made by Carl Zeiss Inc.

In the illuminating conjugate planes, the illuminating lamp filament is conjugate with the front focal plane of the substage condenser, which is referred to as the aperture diaphragm. This image of the filament and aperture diaphragm is also conjugate with the back focal plane of the objective and, subsequently, with the exit pupil of the eyepiece or Ramsden disc.

In the specimen conjugate planes, the lamp iris diaphragm or illuminated field diaphragm is conjugate with the specimen plane. The combined image of the specimen and field diaphragm is conjugate with the primary image plane, which is also conjugate with the retina of the eye. Measurement graticules or field masks must be in sharp focus at the same time as the specimen image. In most microscope configurations the measurement graticule is placed in the primary image plane of the eyepiece, which allows for a measurement to be made without introducing the graticule into the video image or photomicrograph. It should be apparent that a measurement graticule may also be placed at the field diaphragm. However, it is most convenient to place the measurement graticule in the primary image plane of the eyepiece. Any graticule must be calibrated for each objective against an accurate ruling scale called a stage micrometer, which is usually a one millimeter scale divided into tenths and hundredths.

Evenly controlled illumination of the specimen is essential for providing even lighting in the specimen plane and for determining the area of the specimen that is imaged. It is desired to restrict the illuminated portion of the specimen in order to reduce glare from scattered light, which tends to reduce the quality of the image. In Köhler illumination this restriction is controlled by reducing the aperture at the front focal plane of the substage condenser to fill 70 – 90 percent of the aperture of the objective. If a significantly smaller aperture is set, then the maximum attainable resolution is reduced, but if too large an aperture is used then the image becomes degraded by stray light.

The objective lens is the most critical element of every microscope. The objective lens controls the magnification, the field of view and resolution, and its quality determines light transmission, contrast and aberrations of the image. The quality of an objective is determined by its design to reduce aberrations, both spherical and chromatic. High quality objectives provide greater resolution and contrast. One of the most important characteristics of an objective is the numerical aperture, $NA = n \sin \alpha$, where n is the index of refraction of the medium between the specimen and the front lens of the

objective and α is the half angle of the cone of light diverging from a point on the specimen to the front objective lens; it describes the angular aperture of the light cone which is a limiting quantity in determining the image quality,. The proper metric for numerical aperture is dependent on the wavelength of the measuring light, λ in a vacuum or λ/*n* in a medium of refractive index *n*. The directions in the specimen space are described by Cartesian coordinates: x, y, and z. The z-direction is typically referred to as being parallel to the major axis direction of the microscope while the perpendicular radial axes are x and y. These quantities are often used to describe the optical units of the specimen.

The two main components affecting image quality are resolution and contrast. Resolution is the intensity pattern observed by a lens at its focal plane. The pattern is called the point-spread-function and defines the resolution element transverse to the optic axis. This pattern is known in microscopy as the Airy disc. The point-spread-function is a function in three dimensions, but usually lenses and apertures are rotationally symmetrical around the optic axis and all distances perpendicular to the optic axis are the same. The typical Airy disc point-spread-function is the diffraction pattern due to a circular aperture, as brought to focus by a lens. The central portion, one resolution element in radius, is the Airy disc. The distance between two adjacent points are just resolved when the center of the Airy discs are separated by resolution distance (d), as explained by Rayleigh when illuminated with a condenser with its numerical aperture matched to that of the objective as:

$$\text{Resolution Distance (d)} = \frac{1.22\lambda}{2NA_{obj}} \qquad \text{Equation 1.5}$$

where λ is the wavelength of illumination in air, and NA_{obj} is the numerical aperture of the objective lens (Born and Wolf, 1975). NA_{obj} is equal to *n* sin θ , where *n* is the refractive index of the medium between the cover glass and the objective lens, and θ is the angle of half the cone of light entering the objective lens. Under this set of conditions then, the resolving power may be expressed as:

$$\text{Resolution Distance (d)} = \frac{0.61\lambda}{NA_{obj}} \qquad \text{Equation 1.6}$$

The underlying concept of numerical aperture and the point-spread-function assumes that the front lens acceptance aperture of the objective limits the light. The point-spread-function is a measure of the resolution because two adjacent luminous points viewed by a microscope are apparent when they are

far enough apart for their Airy discs to be distinct. As determined by Rayleigh, these Airy discs are determined to be separate when the dip between their intensities is about 29% (Born and Wolf, 1975).

The trough between the two resolved points is characterized by its intensity relative to the two adjacent bright peaks. The relative intensity is known as contrast. If the intensity of the bright peaks is called I_1 and the intensity of the trough between the two adjacent bright peaks is called I_2, then contrast may be expressed as (Inoué and Spring, 1997):

$$\text{Contrast} = \frac{I_1 - I_2}{I_1 + I_2} \qquad \text{Equation 1.7}$$

The image is divided into pixels by a solid state detector. These elements are not the same as resolution elements used to describe the point-spread-function employed to describe image formation in optics, but rather they are the divisions of the measurements within the detector device. A charged-couple-device (CCD) divides or pixelates its image because it is an array of photosensitive areas on a silicon chip (Webb and Dorey, 1995). In order for the image to reproduce the object, the detector must acquire at least two pixels per resolution element in every dimension. This is known at the Nyquist criterion. Pixels need to be large enough to smooth the noise, but small enough not to degrade the resolution. The irreducible limit on noise is that due to the random arrival times of photons and is known as quantum noise (Sims, 1994). If the detector gives a quantum-limited signal, then the noise is proportional to the square root of the number of photons; that is, the number of photons impinging on each on each detector element during each integration time. Consequently the noise equals $\sqrt{\text{number of photons}}$. In terms of contrast, the total number of photons I_1 and I_2 are what matters. The signal (S) at the pixel with the maximum signal of the image point that is being resolved is proportional to $I_1 - I_2$, and the noise for that pixel is proportional to $\sqrt{I_1 + I_2}$. Therefore, the contrast signal-to-noise ratio (SNR) is (Inoué and Spring, 1997):

$$\text{SNR} = \frac{(I_1 - I_2)}{\sqrt{I_1 + I_2}} \qquad \text{Equation 1.8}$$

Consequently, the signal depends both on high contrast and a high intensity illumination level, parameters that may be independent under ideal conditions. The number of photons depends on the illuminating power and the efficiency of the microscope collection optics, while contrast is a feature

related mostly to the specimen and of the way the microscope geometry excludes stray light. Stray light is any light that is additive without being a contributing portion of the signal. Once the stray light has been reduced, the full resolution available from the optics may be realized. In microscopy, stray light may be reduced significantly by using a confocal geometry.

A confocal microscope configuration uses only light that comes from the volume of the specimen conjugate to the illumination source and to the detector. A point light source is imaged at the specimen plane so that the illuminated point and the source are confocal, and then the observation optics form an image of the illuminated point on a pinhole mask in an intermediate image plane just prior to the detector or the spectrometer entrance slit. Now there are three points that are all confocal. An object that is not in the focal volume may not be illuminated at all, but if the object is in the illumination beam but out of the focal plane then most of the light it transmits misses the pinhole mask and does not reduce the contrast. So only the portion of the specimen in the volume confocal to the source and pinhole will contribute to the detected light. The most important factor that remains is the dimensions of the confocal volume. In a confocal microscope configuration, the z-direction or the optic axis also has a resolution element (Pawley, 1995):

$$\text{Axial Resolution} = \frac{1.4\,\lambda\,n}{NA^2} \qquad \text{Equation 1.9}$$

The single limiting factor to using a confocal geometry is that most of the specimen is not observable in the field of view of the microscope. Therefore, it is important for the optimum microscope photometer system to have the ability to quickly change between full-view observation of the specimen and confocal pinhole illumination. One important parameter is the size of the pinhole. The bigger the pinhole, the more photons get through to the detector, but also the less efficient the rejection of stray light from outside the focal volume. The roles of the point-spread function and the pin hole need to be clarified. The point-spread-function is determined by the numerical aperture of the objective lens. The image of the pinhole in the specimen plane describes the area from which photons will be collected. A pinhole smaller than the point-spread-function will not improve image resolution; it will only reduce the light intensity. However, it will reduce stray light generated from areas of the sample that act as scattering centers, and this will reduce contrast.

The polarized light microscope could not fulfill its role as an optical magnifier if it were to use collimated light; its very important function is to increase the convergence of light originating from a specimen such that the angle subtended by the image is larger than that angle subtended by the specimen. Consequently, in a microscope photometer, when a circular diaphragm is used as field stop and image mask, the light beam incident on the specimen is conical. The degree of conicity of the illuminating beam is primarily determined by the numerical aperture of the condenser. The larger the aperture, the more conical is the illuminating beam.

F. Fundamental Spectrometer Components:

Systems using microspectroscopic methods for chemical sensing are composed of four basic components: illumination source, sample interface, wavelength selection or separation device, and a photodetector.

1. Illumination Sources:

Illumination in a microscope photometer is best understood using geometric optics to illustrate the interrelationship of lenses and apertures. Conjugate focal planes in the light path are those in which the same image is formed forward or backwards. The specimen may be illuminated by any number of contrast techniques, but the most often used, and possibly the single most important technique, is Köhler illumination (Goldberg, 1980). The primary features of Köhler illumination include 1) the filament of the lamp is imaged into the plane of the condenser aperture diaphragm so that adjustment of the diaphragm controls the aperture angle, which can be reduced below its maximum; 2) the field diaphragm is positioned conjugate to the specimen image so that is may be adjusted to limit the area of illumination on the specimen or on the stage; and 3) as a consequence of these two basic features, it follows that the field is uniformly illuminated and the specimen on the stage outside the illuminated area does not scatter light, while scattering from lens mounts is minimized or greatly reduced.

A diaphragm is a fixed, physical or variable mechanical restriction of an opening; most are constructed of either a set of fixed holes or a continuously adjustable iris that can be adjusted to nearly any required size. In addition to the condenser aperture and field diaphragms mentioned above, there is a third type of diaphragm to consider in a microscope, which consists of a fixed hole and is used to

suppress stray light in the lens mounts and physical body tubes situated between lenses in the imaging and illuminating optical system. The condenser aperture diaphragm controls the effective maximum numerical aperture or the angle of the incident cone of illuminating light incident on the specimen, and on the front surface of the objective. On forming an image most objectives have a fixed aperture diaphragm, but in some high quality objectives a variable iris may be adjusted to control the maximum angle of inclination to the optical axis of the microscope for a marginal ray that may pass through the objective. In contrast to the field diaphragm that controls the area of illumination on the stage in the specimen plane, the ocular or photometer diaphragm controls the area observed or measured on the image of the specimen plane.

In the selection of a light source one should consider the range of wavelength measurement and the intensity requirement. Fluorescence microspectrophotometry normally requires a narrow bandwidth and high intensity source at a wavelength specific to the material, while absorption microspectrophotometry usually requires a broadband source with moderate intensity.

In most modern microscopes, the incandescent light source is a tungsten-halogen lamp. The tungsten flattened coil filament is contained within a quartz bulb, which contains a halide gas. The tungsten filament provides the electrical resistance; heat in the filament causes the filament to become white hot and emit photons according to its black body temperature. Tungsten is an ideal metal filament due to its high melting point (3655 K), its high strength, and ductility. Maximum output is achieved by operating the filament near its melting point, 3450 K. The halide gas in the bulb prolongs the life of the filament through the tungsten halogen cycle. As the filament is in operation, hot tungsten is evaporated from the filament where it combines with the halide gas and circulated within the confines of the bulb. The tungsten eventually redeposits onto the filament and releases the halide components for future cycles (Zukauskas et al., 2002). The tungsten-halogen source has a broadband spectral range between 300 – 2500 nm, is very stable, and is relatively low cost.

Gas discharge lamps are a class of electroluminescent sources, which emit photons by the application of a high voltage across electrodes in a sealed transparent tube or envelope containing a gas or a combination of gases. Characteristically, some of these gas discharge sources contain many

narrowband atomic emission lines across a lower intensity continuum spectrum, with those commonly used being hydrogen, deuterium, mercury, argon, and xenon, or a combination such as mercury/argon.

An additional type of electroluminescent light source is a light emitting diode (LED). LEDs are solid-state semiconductor materials that generate photons, mostly in the visible to infrared wavelength region, and typically have rather narrowband spectral distributions. However, recent developments have seen broadband or white light LEDs that have power outputs close to those of the monochromatic output of a laser (Schubert, 2010). White light contains a broad band of wavelengths (usually thought of as all wavelengths of the visible region between approximately 400-800 nm). However, one must use caution when considering a white light LED and check the spectral output. Many early white light LEDs were comprised of three distinct and separate red, green and blue (RGB) LEDs that did not exhibit a full continuous spectrum.

Laser sources are typically narrowband sources, producing coherent light with high intensity in a spatially narrow beam. Laser is an acronym for light amplification by stimulated emission of radiation. There are several types of lasers, such as gas, solid-state, dye, and semiconductor. Laser type is determined by the lasing medium. Laser diodes are becoming available throughout the visible and infrared regions and are small, inexpensive, and may become the source of choice for high intensity fluorescence microscope spectrophotometry (Zukauskas et al., 2002).

2. Wavelength Separation Devices:

The separation of polychromatic or white light into component wavelengths is known as dispersion. Dispersive devices such as gratings and prisms are used to separate white light into component wavelengths. When white light enters a prism at an angle other than normal to the surface but less than the Brewster angle, the light of different wavelengths traverse the material at different velocities, which separates the light into its spectral components. Dispersion through a prism is nonlinear and requires the exit slit be adjusted according to the dispersion characteristics of the prism in order to maintain a constant bandpass over the wavelength range that is scanned. The synchronization of the dispersion and exit slit width (slit width programming) has been essentially eliminated by the use of a grating, which exhibits near-linear dispersion characteristics over a specified wavelength range. Therefore, the prism has been primarily replaced in spectroscopic instruments by diffraction gratings

whose linear dispersion properties has simplified the instrumental configuration by employing a fixed, but exit slit that may be adjusted to select spectral resolution (Skoog et.al., 2007).

The concept of diffraction applies to constructive and destructive interference of light around a mechanical device such as a slit or aperture. A diffraction grating is composed of many slits or facets and operates by the same principle, whether it is a transmission grating or a reflection grating. The density of the grooves on the grating dictates the dispersion and the wavelength responsivity is a function of the blaze angle or the shape of the groove (Grossman, 1993).

The isolation of narrowband wavelengths may also be achieved using a variety of optical filters. Optical filters function either by absorption of light or by causing constructive and destructive interference of light with broadband or narrowband properties, respectively. Optical filters often exhibit high reflectivity, high transmissitivity or high absorptivity. An absorption filter works on the principles that some materials absorb specific wavelengths of light and convert that light into energy, such as heat. Interference filters reflect or transmit light in a given spectral range while transmitting or reflecting other wavelength ranges with very little to no absorption. Interference filters may have broadband, narrowband, low-pass or high-pass spectral characteristics. Most interference filters are constructed of multiple layers of dielectric or metallic materials. Different low-pass and high-pass filters can be characterized by the slope of the cutoff region.

3. Specimen Interface:

In a microscope spectrophotometer system, the specimen interface is the stage of a microscope. The specimen is typically mounted in a suitable medium between a glass or quartz microscope slide and a cover glass of similar material. The specimen is viewed through the microscope using a visible light source and the area of interest within the specimen is selected and analyzed spectroscopically. The light from the source must interact with the sample to determine the optical and chemical properties of the material. This light interaction may take place and be detected through transmission, reflection or fluorescence modes.

4. Photodetector:

When these rays fall upon the lens of the eye they are brought into focus on the retina to form a real image. For spectrophotometry, the lens of the eye is replaced with a positive optic lens that forms a real image on the entrance slit of a spectrophotometer, which transmits the light to the transducer.

There are several types of optical transducers: 1) photoemissive such as a photomultiplier tube (PMT) as described above, vacuum phototube (PT), p-n junction devices such as photodiode (PD), phototransistors, photoconductive cells, and photovoltaic cells; 2) multichannel detectors such as photographic emulsions, vidicon tubes, photodiode arrays (PDA), charged-couple device (CCD) arrays, and charged-transfer device arrays in the near infrared region such as indium gallium arsenide (InGaAs); and 3) photothermal detectors such as pneumatic, thermocouple, thermistor bolometer, and pyroelectric detectors such as the deuterated triglycine sulfate (DTGS) and the liquid nitrogen cooled mercury, cadmium, telluride (MCT) detectors (Donati, 2000).

The detection of optical radiation is accomplished by converting photon energy into an electrical signal through photosensitive or thermally conductive materials (Ingle and Crouch, 1988). Of these optical detectors, electrical materials typically respond in the 200 – 2500 nm (UV-Vis-NIR) range while the thermal materials typically detect in the 2 – 40 μm (near IR to mid IR) range. Optical radiation detectors contain a photosensitive cathode and a collection anode. In a photomultiplier tube, between the cathode and anode is a series of intermediate electrodes called dynodes that cause a cascade effect of electrons which produces gain. The cathode is negatively biased compared to the anode in order that the anode can collect the photoelectrons. It is a photosensitive material in which an incoming photon causes the emission of a photoelectron. The photoelectron is then attracted to the first dynode which is positively biased by approximately 90 volts, and produces two to five secondary electrons. Each secondary electron is further accelerated to the next dynode by the increased electric field with further amplification. The series of dynodes causes a cascade effect of electrons. This cascade effect essentially multiplies the number of electrons per incoming photon by a factor of approximately 10^4 – 10^7. The specific photoemissive materials of the photodetector determine the sensitivity and spectral wavelength response range.

Photodetector parameters or figures of merit that characterize a specific detector are considered when choosing the appropriate detector for a given application over a wavelength range. These figures of merit include responsivity, quantum efficiency, linearity, and speed of response, wavelength response, and noise. Responsivity is defined as the detector output per unit of input power and is measured in either amperes/watt or volts/watt. Quantum efficiency is defined as the ratio of countable events produced by incident photons on the detector to the actual number of photons. For example, in a PMT where the detector is a photoemissive material that emits electrons, the quantum efficiency is the number of electrons divided by the number of photons. Photodetectors are also characterized by their response that should be linear with incident intensity over a broad range, oftentimes as much as several decades. If the detector output is plotted against the input power, theoretically there should be no change in the slope of the curve. Unfortunately, this is rarely the case and noise will determine the lowest limit of detection while saturation will determine the upper limit of linearity. The response time of the detector must be considered. If a constant source of radiation is instantaneously incident upon a photodetector, it will take a finite amount of time for current to output the device at a constant value. When the same source is then turned off it will take a finite amount of time for the current to decay back to zero. The wavelength range of the detector is the spectral range over which the detector will respond to incident light. The spectral response is plotted as sensitivity vs. wavelength, where sensitivity is the slope of the detector output vs. input power. The variation of detector output with time when the input signal is static is called noise. Noise may be defined as the unwanted fluctuations in the desired signal which interferes with the measurement (Donati, 2000).

The selection of a photodetector will depend on the wavelength range of the selected analysis, the optical system that will deliver the source illumination to the detector, and the parameters of the specimen that will be measured. If, for example, low light level fluorescence in a specimen needs to be measured, then a detector with high sensitivity will be required. In contrast, if the optical signal is relatively high, then a detector with a faster response time may be a better choice.

Ingle and Crouch (1988) outline other figures of merit that characterize sources and detectors, and the microscopist/spectroscopist should be familiar with those most often reported by instrument

manufacturers so as to be able to adequately evaluate performance characteristics for a specific application.

G. Instrument Figures of Merit

The essential instrument qualification parameters that are required to be measured to test the capabilities of an instrument to perform a specified analysis include the following figures of merit. It is critical to instrument verification that standard, certified, or otherwise verified reference materials be used to check instrument performance capabilities. In addition to the following figures of merit, it should be understood that instrument environmental operating conditions must be controlled and may be critically important to obtaining constant, reliable results.

1. Wavelength Accuracy

Wavelength accuracy is the deviation of the average wavelength reading at an absorption or transmission peak maximum from a known wavelength from a reference standard.

2. Wavelength Precision

Wavelength precision is a measure of the ability of a spectrophotometer to reproduce the same position as measured by an absorption or transmission peak of a known wavelength from a reference material. The measure of precision is the standard deviation.

3. Spectral Resolution Dependence on Wavelength

Spectral resolution is determined for a given band; it is usually defined as the full width at half maximum (FWHM) of a measured peak. Many factors in an instrument may influence spectral resolution over the wavelength range capability of the spectrophotometer.

4. Photometric Accuracy

Photometric accuracy is determined using a reference material with known absorbance (optical density) values over a spectral range. Photometric accuracy is required if data is to be transferred or compared from instrument to instrument.

5. Photometric Precision

Photometric precision represents the capability of a spectrophotometer to reproduce the same measurement value over successive determinations. The measure of precision is standard deviation.

6. Photometric Linearity

The photometric linearity is determined over a range of increasing absorbance values. The resultant measurements are plotted with the instrument's measured absorbance values on the ordinate, and the known (referenced) absorbance values on the abscissa. An analytical curve is obtained using linear least squares regression. The range of values over which a straight line is obtained is considered the range over which appropriate calculations may be made.

7. Photometric Noise

Photometric noise is measured on a 100% T (transmittance) line spectrum. For a single beam instrument the 100%T line is obtained by ratioing two successive background (I_0) measurements to produce the transmittance spectrum. Photometric noise is determined by fitting a line to a short spectral region centered on a given wavelength. The region should contain at least eleven data points, but not exceed 2% of the total spectral range. The line is subtracted from the data and the root-mean-square of the residuals is measured and recorded as the RMS noise. The RMS noise should be calculated for the lower, middle and upper wavelength ranges.

8. Short-term Baseline Stability

Short-term baseline stability is monitored over the same spectral ranges used to determine the RMS noise. Deviations of the y-intercept values away from 100%T which were obtained from the fitted line indicate instrument instability and may indicate a spectrometer source or detector malfunction.

H. Instrument Intrinsic Polarization

Intrinsic polarization is an inherent instrument property because dispersive spectrometers generally use a diffraction grating to separate white light into its component wavelengths. It is a result of from significant differences in reflectivity for light polarized normal to and parallel to the grooves of the diffraction grating in the spectrometer. The variation in efficiency with wavelength and diffraction order is an important characteristic of any diffraction grating. For a reflection diffraction grating, efficiency is defined as the intensity of monochromatic light diffracted into the diffraction order under measured, relative to the intensity of the incident radiation (absolute efficiency) or to the intensity of specular reflection (relative efficiency) from a polished mirrored substrate which is coated with the same material

as the reflection grating (Horiba, 2006). A typical efficiency curve is one which plots the absolute or relative diffraction intensity against the diffracted wavelength. For most diffraction gratings the diffracted intensity depends on the polarization of the incident radiation. P-plane polarized light is parallel to the grating grooves, while S-plane polarized light is perpendicular to the grating grooves. For completely unpolarized incident radiation, the efficiency curve is exactly halfway between the P-plane and S-plane efficiency curves (Palmer, 2005)

In order to compensate for the grating's polarization properties, the collection of a background spectrum for each of the two polarization orientations is required. The intrinsic polarization effects of all instruments within this study except the two CRAIC Technologies QDI 2010 systems were measured by using either a rotatable linear polarization substage condenser or a thin film polarizer placed on the specimen stage. In either case the linear polarizer was sequentially rotated five degrees and a corresponding intensity spectrum measured. The intensity values at 550nm were plotted on a polar coordinate graph to illustrate the intrinsic polarization characteristics of the instrument configuration. The intrinsic polarization effects for the two CRAIC Technologies instruments were not measured because the systems use a high intensity high-pressure xenon lamp source that destroys an absorption-type film polarizer and a prism-type polarizer was not available at the time.

I. Processing of Spectral Data

1. Baseline Correction

Spectrometers do not always collect data with a constant baseline. The deciding factor in baseline selection is the reproducibility of the results. Instrument parameters such as source drift, changing environmental conditions like temperature, detector drift, and specimen stability, among other factors, may cause the spectrum baseline to shift. Sometimes these systematic instrument variations may be larger than the specimen signal and thereby dominate the spectral analysis if not removed. The affects may vary from specimen to specimen causing intensity and peak shape variation. An automatic baseline correction function is offered by most instrument control and software platforms. The automatic baseline correction function is one of the more simple processes in which a linear least squares regression is fit to the spectrum over a selected wavelength region. The resulting regression line is

subtracted from the spectrum values in the selected region before plotting the data. Consequently, this correction process may degrade the spectrum more than if no spectral baseline correction were used. Instrument manufacturers have developed more complex baseline correction functions that give the operator more control over the baseline correction processes. These more complex functions involve applying a polynomial approximation to many points on the spectrum which are selected by the operator. A major concern with applying these advanced controlled processes is the subjective nature that relies on visual inspection to assess the best baseline correction. If not applied correctly, then a portion of the chemical or specimen variation will be removed. Some baseline functions use derivatives. When using the derivative function, it is not necessary to select baseline points, but it does not work well in cases where the baseline is only an offset from zero.

Preprocessing to remove noise usually follows baseline correction. Data smoothing reduces the amount of random variation or noise in spectrum. In analytical instrumental analysis, it is assumed that any instrumentally acquired spectrum contains the true specimen signal plus random noise. By applying a data smoothing function, the environmental and digitization noise or errors in analog-to-digital conversion are minimized. The application of a data smoothing function results in the mathematical removal of random noise, while increasing the signal-to-noise ratio. A variety of data smoothing functions is available, but most are variations of a running average, a running median, or a running polynomial. Any of these processes involves applying a mathematical operation to each data point of a spectrum as it relates to a neighboring data point or a selection of data points on either side of the central data point. One of the most commonly known data smoothing functions is the Savitzky-Golay (1964), in which a polynomial best fit curve is fit to the digitized data points. Data smoothing is best applied to data with well-known peak locations, such as with standard samples (Beebe et al, 1998). While baseline correction is applied to correct for specimen and instrument random variation, it does not remove systematic variation. Systematic variation must be removed by spectral normalization prior to comparison. When comparing spectra, the data must be on the same scale which requires an additional preprocessing procedure known as normalization, which will be discussed in greater detail below.

2. Peak-Fitting Function

A natural spectral line shape is Lorentzian (Halliday et. al., 1993). The Lorenztian shape is broadened and altered by molecular collisions, the Doppler effect, interactions of electromagnetic radiation with the specimen. The resultant complex line shape function is called the Voigt line shape (Olivero and Longbothum, 1977, Martin and Puerta, 1981, Saarinen et al., 1995). The Voigt line shape is the true line shape due to interactions associated with most gases. It is a complex and convoluted combination of both Gaussian and Lorentzian line shapes in any varying amount. Consequently, the Voigt line shape is very difficult to solve and most peak-fitting functions are a mathematical approximation of the Voigt function (Martin and Puerta, 1981). One such peak-fitting function applies both Gaussian and Lorentzian functions in the iterative procedure (Losev, 1994). Peaks associated with Lorentzian line shapes are sharp and narrow with most of the intensity located in the tails, which extend to infinity on either side of the peak. A Voigt line shape contributes more area to the tails than a Gaussian line shape, but less than a Lorentzian line shape. As Lorentzian contributions to the peak shape are lessened, the peak shape approaches a Gaussian line shape. As molecules interact and exchange energies in a random process, the broadened peak shape tends to have much smaller tails and greater intensity under the central peak compared to a Lorentzian peak shape. In spectroscopy, these random processes are based on a statistical distribution known as a Gaussian distribution. In this research, the LabSpec (HORIBA Scientific, Edison, NJ) software Gaussian-Lorentzian peak-fitting function was applied to all spectra. The quality of the peak-fitting function was first evaluated using standard spectral low pressure gas lamps (mercury/argon and krypton).

Peak-fitting is useful for determining peak positions, widths, heights, and areas of a set of overlapping peaks, which may result from a multitude of causes, the most important of which in the context of this work is multicomponent fiber dyes. According to the HORIBA Scientific, Inc., LabSpec software version 5.3 used for this research, the peak-fitting function consists of fitting one of any number of possible line shapes to the digitized data spectrum, such as Gaussian, Lorentzian, and a mixed Gaussian-Lorentzian. The peak-fitting function can include a baseline correction using an offset, linear, quadratic or cubic function integrated into the algorithm, thereby eliminating a separate preprocessing

procedure. However, it is sometimes argued that fitting the baseline before band-fitting can often produce better results than fitting them simultaneously (Martin and Puerta, 1981).

The best-fit algorithm continuously iterates until the reduced Chi squared value is minimized, see Equation 1.9 (Grams/AI™, 2013).

$$\chi^2 = \frac{\sum_{i=0}^{n}\left(\frac{Actual_i - Calculated_i}{RMSnoise}\right)}{(n-f)} \qquad \text{Equation 1.10}$$

where n is the number of data points, $Actual_i$ and $Calculated_i$ values are from the original measured and calculated fit data, respectively, *f* is the total number of variables from all the fitted functions, and *n-f* is the number of degrees of freedom in the final fitted curve. In this research, the Gaussian-Lorentzian peak-fitting function was applied to spectra. To this point the selection of optimal preprocessing functions requires knowledge about a known characteristic of the specimen data. In analysis where knowledge about specimen data is not known peak-fitting or curve fitting is the more appropriate preprocessing procedure. The degree of fit was evaluated using standard spectral low pressure gas lamp.

The reduced Chi squared value is a statistical measure of "goodness-of-fit" and it assumes that the uncertainty in the Actual data (RMS noise) is known exactly, however this is not the case. A peak fitting function must then estimate the uncertainty throughout the fitted spectral region. The uncertainty is estimated by first applying a smoothing function (Savitzky-Golay) to the original data and then subsequently subtracting the value of the smoothed function from the original data. The peak-fitting function determines the width of the consecutive data points based on the width of the smallest peak. When the peak fitting function estimates the number of consecutive data points, the presence of a few sharp peaks along with broad peaks, causes it to tend to underestimate the actual uncertainty. This results in an artificially high reduced Chi squared value which may be interpreted as a poor fit when in fact it is a very good fit.

As introduced above, there are several possible line shape functions to best fit the curve to the data. Peak fitting is designed to iteratively fit a series of individual functions simultaneously so as to reach the best fit solution. Since the solutions to the individual functions are interdependent, small changes to one parameter in a single function affects the final results of all of the other individual functions the maximum number of iterations to fit must be defined; but the algorithm may either complete

all iterations defined or stop before the maximum number of iterations if the fit converges to a good fit. During the peak-fitting iterations, the baseline function is calculated and subtracted from each peak. For both linear and higher degree baselines, the line is mathematically fitted using trace values located at endpoints of the fitting region. The linear coefficients are optimized during the iterative process as if they were another peak.

3. Normalization of Data

Normalizing is performed in order to put all spectra on the same scale. Normalization is achieved by dividing each data point by a constant (Grams/AI™, 2013). Several constants may be used to normalize the data, but there are three fundamental ways to normalize spectra: peak height, unit area, and unit length. The first process, peak height, requires that all of the spectra to be compared must contain at least one component that is present in each spectrum. When this requirement is met, then the spectra all contain a peak that may be used "as if" it was an internal standard. All peaks in a spectrum may be compared to that peak. One common function is to divide each spectrum data point value by the common data point value (peak height value of the common peak) to produce a ratio. This ratio is most often less than unity but greater than unity for peaks values larger than the value of the common peak. Another simple normalization function is to divide every data point in the spectrum by the largest data point value. This procedure ensures the ratio is less than unity but assumes all spectra have a sufficient signal-to-noise ratio.

In the second normalization preprocess, unit area, the sum of the absolute values of all data points is determined and then each data point is divided by the sum value. The resulting spectrum contains peaks that are a ratio of unity.

The third preprocess is normalizing to unit length. In this function, each data point is divided by the constant derived by taking the square root of the sum of all of the squared data points.

All normalization functions are designed to remove systematic variation or noise. However, it must be kept in mind that normalization may remove real variations in concentration data. To this point the selection of optimal preprocessing functions require knowledge about known characteristics of a standard reference material. In analysis where knowledge about specimen data is not known peak-fitting is the more appropriate preprocessing procedure.

J. Dichroic Measurements in Forensic Science Procedures

Linearly polarized light provides a powerful tool to investigate the orientation of molecules or the partial orientation of dye molecule assemblies in polymers (Norden, 1978). The microscope photometric determination of linear dichroism (LD) and the dichroic ratio (DR) may be particularly useful in analyzing anisotropic specimens such as dyed fibers with absorption in the ultraviolet and visible range. In the process of light being absorbed by a molecule, the electric field vector of plane polarized light interacts with the transition moments of the molecule responsible for the particular transition, for example, a π to π* transition. The electric dipole transition moment is perhaps the most important transition and the absorption is orientation dependent. Consequently, this leads to an orientational dependence of the absorption of linearly polarized light, which allows for the use of spectroscopy with linearly polarized light to investigate the nature of molecular orientations and partial or complete orientation of moieties (Mickols, 1991).

Microscope spectrophotometry rests on the fundamental premise that the angular distribution of light rays of the measuring beam and the angular distribution of transition moments in a specimen are controlled by two independent processes. The interaction of light with the specimen is restricted to absorption or transmission (as scattered light) such that it does not affect the independence of the two distributions. If this independence holds true and the two variable processes are separable, then several underlying principles may be expressed (Michl and Thulstrup, 1986):

1) The polarization of a photon is an observable quantity described by its two orthogonal polarization states.
2) The polarization of photons in unpolarized light remains unknown until experimentally revealed.
3) A device capable of transmitting polarized light such as a linear polarizer prism, film or wire-grid, can define the mutually orthogonal states of polarization and distribute incoming photons in either one of the two states; one being transmitted and the other being removed from the incoming illumination beam. Therefore, polarizers determine the polarization state of the transmitted photons.
4) A second polarizer (the analyzer) in series is placed 90 degrees to the first polarizer.

5) A specimen (chromophore) capable of undergoing electric dipole moment transitions induced by light, have an analogous effect as a polarizer (analyzer). If an incoming photon makes an angle θ with the chromophore transition moment, the probability for the photon to be absorbed and projected into the parallel state is proportional to the square of the cosine of the angle, $\cos^2 \theta$.
6) Devices incapable of testing polarization are also incapable of changing the state of polarization of photons. Whereas a polarizer or double refracting specimen can change the state of polarization, an unstrained lens or isotropic specimen cannot and the plane of polarization of photons traversing a lens remains unchanged.

When a specimen has an absorbing material distributed inhomogeneously in it, it will exhibit a phenomenon called dichroism. This occurs when there is selected absorption of one of the two orthogonal polarization states of light by optically anisotropic materials. In dichroic specimens light waves with a polarization state perpendicular to the optic axis are absorbed whereas parallel polarization states are transmitted. In addition, a specimen will exhibit dichroism with the selective absorption of specific wavelengths of light by optically anisotropic uniaxial materials. For example, a crystal of tourmaline will show two different colors when illuminated along different axes by plane polarized white light.

In a procedure discussed by Mickols, first the transmission of light is recorded in one polarization orientation and then the polarization was rotated by 90 degrees and the transmission recorded again (Mickols, 1991). By choosing to rotate the polarizer rather than the specimen, uncertainties associated with moving the specimen are reduced. This requires the collection of a background (reference) scan at the two different polarizer positions, and the ratioing of the appropriate background (reference) spectrum with the spectrum collected in the respective position (Mickols, 1991).

Intuitively, the uncertainty associated with moving the polarizer may be greater than the uncertainty of rotating the specimen since the typical Vernier reading of a rotating stage is on the order of 0.1 degree whereas the uncertainty of rotating the polarizer may be as large as ± 1-2 degrees. However, the uncertainty in retaining the optical path or orientation or geometrical centration of a specimen which is being rotated on a stage is dependent on how well the stage is centered and how level (perpendicular)

the stage is to the optic axis of the microscope. Therefore, if the specimen is held in a constant position while the polarizer is rotated, then there is no change in the light path through the specimen.

The determination of the linear dichroism of a specimen is determined using Equation 1.11:

$$\mathrm{LD} = \Delta A = A_0 - A_{90} \qquad \text{Equation 1.11}$$

where A_0 is the intensity of light absorbed with the specimen oriented parallel to the plane polarized light and A_{90} is the intensity of light absorbed with the specimen in the perpendicular orientation with respect to the plane polarized light. Dichroic ratio (polarization ratio) measurements are determined using Equations 1.12, reduced dichroic ratio measurements are determined using Equation 1.13, and modulated dichroic ratio measurements are determined using Equation 1.14 (Norden et al., 2010)

$$\mathrm{DR} = \frac{A_0}{A_{90}} \qquad \text{Equation 1.12}$$

$$\mathrm{RDR} = \frac{\mathrm{LD}}{A_{iso}} = \frac{A_0 - A_{90}}{A_{iso}}, \text{ where } A_{iso} = \frac{[A_0 + 2(A_{90})]}{3} \qquad \text{Equation 1.13}$$

$$\mathrm{MDR} = \frac{A_{diff}}{A_{sum}} \text{ where, } A_{diff} = A_0 - A_{90} \text{ and } A_{sum} = A_0 + A_{90} \qquad \text{Equation 1.14}$$

Absorption in a material is dependent on absorption in all three Cartesian coordinate directions (x, y, z) by $\sqrt[3]{xyz}$ = $(xyz)^{1/3}$. If the specimen is isotropic, then absorption in all three directions is equal so absorption may be determined by $\sqrt[3]{xyz}$ = $(x,x,x)^{1/3}$ = $(x^3)^{1/3}$ = $\frac{3x}{3}$ = x. When measuring an anisotropic, uniaxial specimen the absorption may be determined by $\sqrt[3]{xyz}$ = $(x,y,y)^{1/3}$ = $\frac{x+2y}{3}$ = A_{iso}. Note that this is not the same as the absorbance of an oriented specimen measured with unpolarized light.

The advantage of using either the dichroic ratio (DR) or the reduced dichroic ratio (RDR) instead of LD is that dependence on the concentration of the specimen, the optical path length, and the dipole strength (intensity), μ^2, of the transition has been removed via ratio. Therefore, LD is a function only of the geometric arrangement in space of the transition moments relative to the orientation axis.

A textile fiber is colored by the presence of a dye which is often a planar aromatic molecule. Because the molecules of the textile matrix are usually oriented along the fiber axis, the dye molecules tend to orient along the fiber axis. The environment around the chromophore can cause a shift in the absorption peak maximum, and a change in intensity, as illustrated in Figure 1.4.

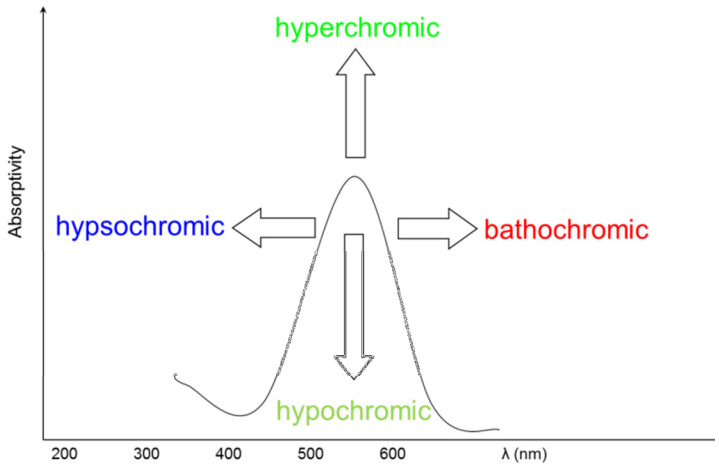

Figure 1.4: Dichroic spectrum effects. A hyperchromic or hypochromic shift is a change in color intensity while a hypsochromic or bathochromic shift is a change in the perceived color due to the shift in the absorption peak.

Because of the orientation of planar molecules, the absorption is different when the light is polarized in the aromatic plane vs. perpendicular to the aromatic plane. In some materials, this dichroic effect varies strongly with the wavelength of light, making the fibers appear to have different colors when viewed with light having different states of linear polarization.

Spectral characteristics (LD, DR, RDR and peak wavelength shifts, Δλ) require using linear polarized light, a rotatable substage polarizer and measurement of spectra in parallel and perpendicular positions relative to the defined specimen orientation, and a rotating stage in order to accurately align the sample parallel and perpendicular to the light polarization. The optimum specimen position will be dependent on the intrinsic instrument polarization characteristics of the microscope photometer being used. Dichroic ratio measurements have the advantage of being independent of uncertainties due to optical path length (sample thickness) and pigment or dye concentration differences. Figure 1.5 illustrates the dichroic spectra of a green color polyester thin film.

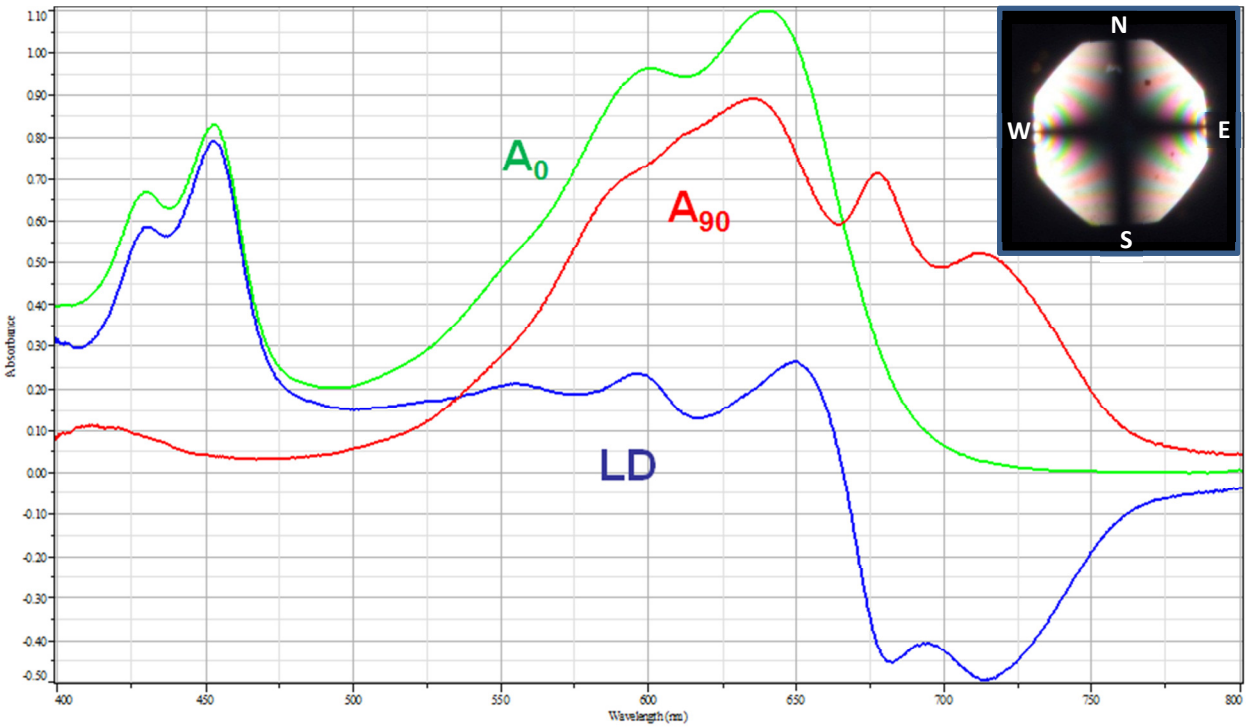

Figure 1.5: Overlay spectra of a dichroic green polyester thin film. The green spectrum was collected with the polarizer in the parallel position, the red spectrum was collected with the polarizer in the perpendicular position, and the blue spectrum is the linear dichroism spectrum. Notice the lower intensity (hypochromic) shift of the red perpendicular spectrum at 450 nm and the longer wavelength (bathochromic) shift of the red spectrum at 700 nm. The resulting linear dichroism spectrum is the blue spectrum which indicates the difference in chromophore excitation based on orientation of the electric field vector of the polarized incident light. Inset image is a conoscopic view of the polyester film at extinction, which is equal to the parallel position (A_0) relative to the EW polarized light.

A training guide published in 2004 by the Scientific Working Group for Materials Analysis (SWGMAT), *A Forensic Fiber Examiner Training Program*, acknowledges that pleochroism / dichroism, the appearance of different colors when the specimen is observed at different angles of plane polarized light, can affect the spectrum obtained: "If a fiber exhibits pleochroism, then taking measurements as the fiber is rotated on the microscope stage will produce spectra that can have considerable wavelength and absorbance differences. When comparing fibers it is generally recommended that the same relative fiber orientation is maintained for each sample" (SWGMAT, 2004). Unfortunately, however, linear dichroism and dichroic ratio measurements are currently not included in the recommended practice in forensic fiber and other microscopical transfer evidence examinations.

K. Possible Spectral Match Criteria

The comparison of measured ultraviolet-visible microspectrophotoscopic data of transfer evidence recovered from crime scenes with representative reference samples collected during the investigation of a crime is well established in forensic investigations. In the United States, the most frequently used statistical methodology is the two-stage approach (Garvin and Koons, 2011). In the two-stage approach, the analyst separates the comparison from a subsequent evaluation of the significance of any matching results. A primary function of the statistical comparison approach is to estimate the false exclusion, a Type 1 error, and false inclusions, a Type 2 error. However, the estimate may be different depending on the type of decision or comparison criteria employed for the statistical comparison. Nearly every method used for a decision criterion begins with defining a test interval encompassing measurements from the known (reference) sample. By convention, the evidence is typically named as coming from a known source (K) or a questioned source (Q). The test interval is that interval obtained by the inter- and intra-sample variation from testing the known sample. The end goal of any comparison is to determine whether two items may have shared a common origin.it. The measurements from recovered evidence of a questioned source are subsequently compared to this test interval to determine whether they “are consistent with” or “could have come from” this known source.

Differences in the use of these decision criteria include the number of K samples analyzed, and the number of measurements made for each K and Q sample, the method of determining the test interval for these many measurements, and the method of combining results when several Q samples are considered. It is common practice in the United States to treat each Q sample independently, because there is no *a priori* assumption that multiple-evidence recovered from a single piece of evidence originated from a common source. Table 1.1 contains several possible match decision criteria to represent variations in absorbance measurements obtained through microscope spectrophotometry.

Possible Match Criteria for UV-Visible Absorption Spectra Comparisons for a Peak Maximum at a Specific Wavelength		
Test No.	Description	Test Criterion
1	1 x SD	$\overline{K} - 1 \text{ x } s_K \leq \bar{Q} \leq \overline{K} + 1 \text{ x } s_K$
2	2 x SD	$\overline{K} - 2 \text{ x } s_K \leq \bar{Q} \leq \overline{K} + 2 \text{ x } s_K$
3	3 X SD	$\overline{K} - 3 \text{ x } s_K \leq \bar{Q} \leq \overline{K} + 3 \text{ x } s_K$
4	$t_{0.05}$ x SD	$\overline{K} - t_{0.05}^{n_k-1} \text{ x } s_K \leq Q \leq \overline{K} + t_{0.05}^{n_k-1} \text{ x } s_K$
5	$t_{0.01}$ x SD	$\overline{K} - t_{0.01}^{n_k-1} \text{ x } s_K \leq Q \leq \overline{K} + t_{0.01}^{n_k-1} \text{ x } s_K$
6	Fixed 0.001 abs units	$\overline{K} - 0.001 \leq \bar{Q} \leq \overline{K} + 0.001$
7	Fixed 0.002 abs units	$\overline{K} - 0.002 \leq \bar{Q} \leq \overline{K} + 0.002$
8	Range	$K_{min} \leq \bar{Q} \leq K_{max}$
9	Range +0.005 abs units	$K_{min} - 0.005 \leq \bar{Q} \leq K_{max} + 0.005$
Where, SD, standard deviation; $\overline{K}$, mean of K measurements; $\bar{Q}$, either single Q measurement or mean of three Q measurements; s_K, standard deviation of K measurements; n_K, number of K measurements (5, 6, 7…..20, 25, 30, or 50 measurements); t, value of t at $n_K - 1$ degrees of freedom and stated two-tailed confidence level; K_{min}, minimum of K measurements; K_{max}, maximum of K measurements.		

Table 1.1: A tabulation of proposed match criteria to differentiate materials that exhibit an absorption spectrum in order to establish whether a questioned specimen may share a common origin with a known reference sample based on absorbance measurements.

Currently, the Scientific Working Group for Materials does not provide guidance to fiber or paint examiners for how to approach match criteria in either type of evidentiary analysis. In light of the National Academy of Sciences, National Research Council (NRC) report (NRC, 2009) examiners must consider exploring research into establishing a set of match criteria for trace evidence examiners in order to estimate Type 1 and Type 2 errors as estimates for error rates associated with the type of examination. Further research with large sample sets along with the application of the test criteria presented in Table 1.1 may help determine a consensus for error rates associated with transfer evidence analyzed by UV-visible microscope spectrophotometry.

L. Contributions to Criminal Justice and Forensic Science

This research contributes to the existing knowledge by identifying optimum instrument features and function characteristics while establishing well defined limitations of the instrumentation and techniques. In addition, this research has developed or delineated fundamental scientific parameters necessary to satisfy the rigorous scientific testing necessary to assess reliability, validity, and ultimately to satisfy the scientific testing required of forensic methods presented in the courts of law. The results of this research may be used to establish good laboratory practice and procedures to collect dichroism absorption measurements for increased specimen discrimination and for inference of source determinations.

CHAPTER 2. REVIEW OF THE LITERATURE

A. Chronology of Development

The first uses of a microscope spectrograph (Figure 2.1) may be traced to the mid 1800s when Glan, Köenigsberger, and Sorby employed the technique to compare the transmission spectrum of light traversing different directions in crystals (Johannsen, 1914). The first microphotometer was developed in 1899 by Hartmann as a means to measure density gradients or the intensity of spectral lines across a photographic emulsion (Walsh, 1958). Since the variation of intensity from point to point may be very rapid, the primary goal was to measure the transmission of an exceedingly small area of the emulsion.

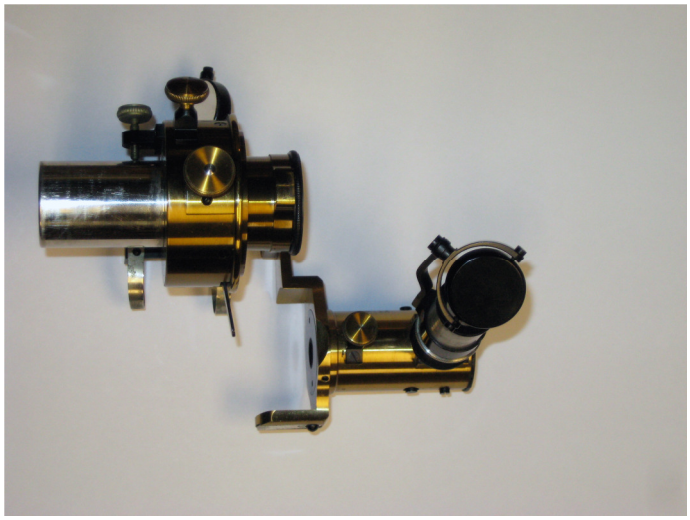

Figure 2.1: Sorby microscope spectrograph. This spectrograph is on display at Microtrace LLC, 790 Fletcher Drive, Suite 106, Elgin, Illinois, 60123.

A photograph of the 1934 Jelly microspectrograph, designed and built by Dr. Edwin E. Jelly, which is on display at McCrone Research Institute is shown in Figure 2.2. It was used to investigate the colors exhibited by pleochroic crystals to determine the birefringence at a given orientation and the dispersion of that birefringence, as well as the dispersion of the optic axis or optic axial angle (McCrone, 1957). Unfortunately, however, the Jelly microspectrograph was never commercially available.

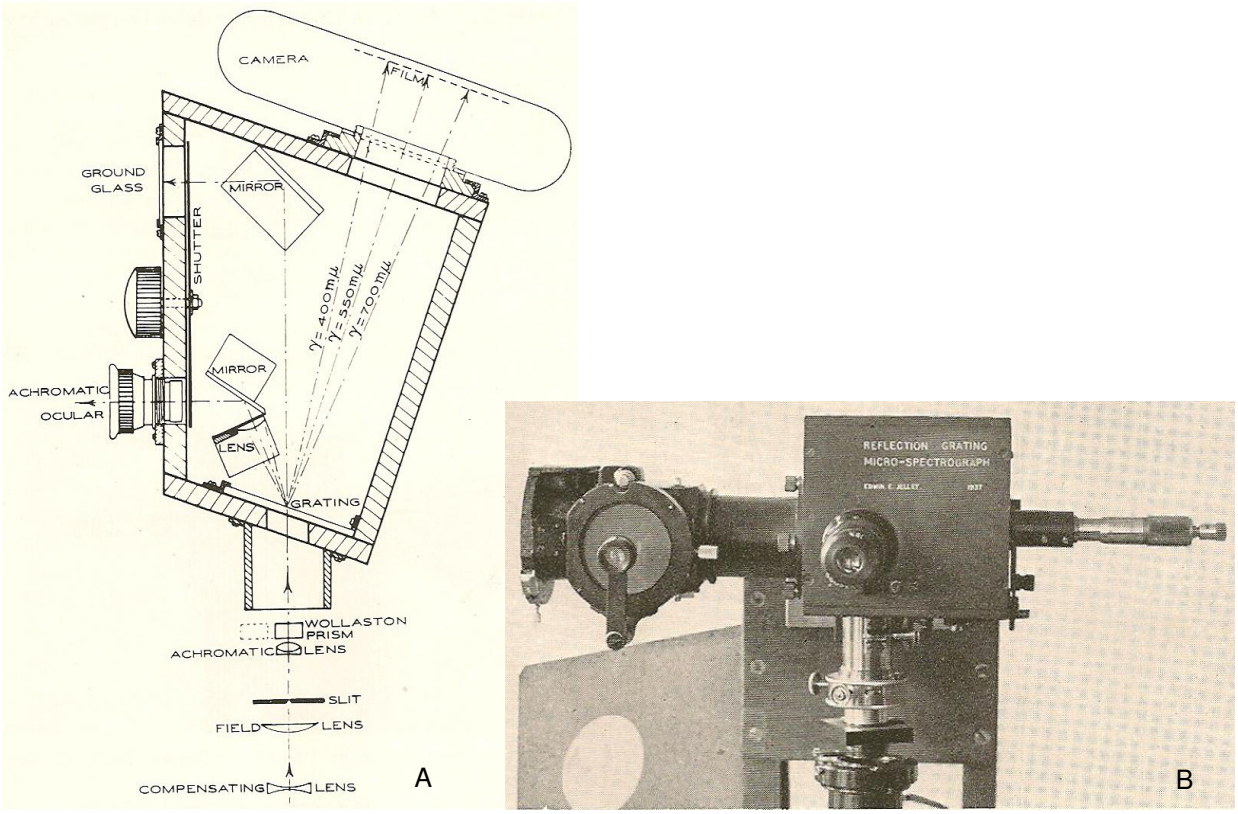

Figure 2.2: Jelly microspectrograph: evolved from Model II (A) to Model IV (B), which was built in 1941. The Jelly spectrograph is capable of imaging a colored object under a microscope with or without polarized light, with either orthoscopic or conoscopic observation, and under brightfield or darkfield illumination. The Model IV spectrograph is on display at McCrone Research Institute. Reprinted with permission from Microscope Publications Division of McCrone Research Institute, 2820 S. Michigan Avenue, Chicago, IL, 60616.

According to Hidehiko Isaka in his monograph *Introduction to Microspectrophotometry: Applications to Biomedical Research* (1972), UV light microscope spectrophotometry of individual cells as a quantitative approach to DNA composition was first reported by Torbjörn Oskar Caspersson in 1936. Since that time several microscope photometer instruments have been constructed by Caspersson (1936, 1940, and 1950), Lison (1950), Caspersson et al. (1951), Franzer and Davidson (1953), and Eaton (1979). Unfortunately these microscope photometers were laboratory-built instruments and not commercially available systems (Isaka, 1972). Table 2.1 contains a partial list of commercially available microscope spectrophotometer systems; some systems are obsolete but have been included for a historical perspective.

Some of the instrumental designs of early microscope spectrophotometers were relatively simple, but a few were elaborate, expensive, and rather difficult to engineer. Consequently, very few laboratories employed such instrumentation. The two-wavelength method of microscope spectrophotometry developed by Patau (1952) to reduce distributional error was systematically evaluated by Mendelsohn (1958a, 1958b, 1958c) and revised by him (1961) such that the results were identical in theory, but the new technique was more suitable for electronic computing. A polarized light microscope spectrophotometer was built in 1974 by Eaton (Eaton and Hofrichter, 1989) while working at the National Institute of Health (NIH) which was constructed around a Leitz Ortholux I polarizing microscope and photometer attachment. This instrument was used to study the spectroscopic properties of hemoglobins using polarized absorption and linear dichroism spectroscopy. Phase modulation microscope spectrophotometry was employed by Taylor et al. to investigate the amyloid-Congo Red complex optical properties such as dispersion of birefringence and linear dichroism superimposed on circular dichroism and optical rotary dispersion (Taylor et al., 1974). A system designed to measure sample birefringence was developed by Allen et al. in which they used a polarized light microscope, a birefringence detection system, and an electronically driven stage to pass the specimen at specific velocities across the image plane of an aperture placed at the field stop and imaged in the specimen plane by the condenser. The detector registered retardations directly as a voltage at a constant deflection sensitivity over a range of approximately 120 angstrom units. Garcia introduced a one-wavelength, two-area method in microscope spectrophotometry, but the method was restricted to biological samples that were amenable to smear preparation, and all tissues had to be fixed and stained simultaneously to reduce differences in stain clumping (Allen et al., 1963, Garcia, 1965).

Make	Model	Era / Date
A.S. & Co. GmbH	SpectraVision	2011
CRAIC Technologies, Inc.	QDI 1000	2000s
	20/20 PV™ UV-Visible-NIR	2010s
	308 PV™	2000s
	MP-2™	2000s
	UVM-1 ™ Ultraviolet Microscope	2000s
Farrand Optical Company, Inc.	Microscope Spectrum Analyzer (MSA)	1976
HORIBA Jobin Yvon	VS140	2000s
J&M Analytick AG	TIDAS MSP 200	2000s
	TIDAS MSP 400	2000s
	TIDAS MSP 800	2000s
JASCO, Inc.	MSV-3000	2000s
LEITZ	MPV	1970s
	MPV SP	1980s
Nanometrics, Inc.	NanoSpec 10S	1970s
	Nano 100UV	1980s
	Nanometrics 210 XP Scanning UV	1990s
Olympus, Inc.	MSP-A-IV	1970s
	DMSP-II	1970s
S.E.E. Inc. now CRAIC Technologies	SEE1000	1990s
	SEE2000	2000s
	SEE2100	2000s
Ocean Optics, Inc.	USB2000+	2010s
Rofin	Micro-Colorite	1990s
Vickers Instrument Inc.	M85	1970s
	M86	1970s
Zeiss	UMSP 1	1960s
	UMSP 50	1970s
	UMSP 80	1970s
	SF attachment	1970s
	MPM 03	1977
	MPM 400 / 800	1990s

Table 2.1: Microscope Photometer Systems.

Microscope photometer instrumental designs have evolved from systems using monochromatic illumination transmitted through the sample and detected by a photodetector to systems employing polychromatic white-light incident upon a sample followed by a non-scanning, fixed position grating spectrometer equipped with a charged-transfer device detector (Si 200-950 nm or InGaAs 850-2300 nm), computerized data acquisition, and signal processing (Donati, 2000). The components of a modern microscope photometer vary depending upon the instrumental design, but most consist of a continuous polychromatic white-light source (i.e., tungsten-halide, or xenon or mercury arc lamp), a compound microscope capable of various contrast techniques such as polarized light, fluorescence, and a

photodetector such as a photomultiplier tube or charge-transfer device, all interfaced with a data acquisition board for computer data collection, processing, and storage

B. Applications

Early literature reported on studies of deoxyribonucleic acid and other biological materials such as normal and abnormal lymphocytes or epithelium, tumorous tissues, polyps of the rectum, malignancy of neoplasms, uterine carcinoma, and liver tissues (Isaka, 1972). Microscope photometric results reported in Belgium by Pasteel and Lison (1950) on cytophotometric measurements were often in disagreement with results of American scientists Ris and Mirsky (1949), Swift (1950), Leuchtenberger *et al.* (1951), and Davidson (1953) who was using an apparatus described by Pollister and Moses (Isaka, 1972, Pollister & Moses, 1949).

In the 1960s, Piller constructed the Zeiss UMSP 1, which was a double-optic system made with fused quartz optics (Piller, 1977). The second generation instrument was the Zeiss MPM 03, which was a single-optic system with a grating monochromator which increased the resolution of the spectrophotometer system. The new system also benefited by using an improved, more stable illumination source and photodetector. The greatest improvement was the ability to interface the instrument to a computer. During this era, several other microscope spectrophotometer systems were commercially available such as the Leitz MPV, the NanoSpec 10S, the Farrand Optical Company Incorporated (FOCI) microscope spectrum analyzer (MSA), and the Australian made Rofin Micro-Colorite. The system developed by Vincent J. Coates at Nanometrics, Inc., the NanoSpec 10S, has had the most profound influence on forensic science applications of microscope spectrophotometry. Forensic science applications of visible microscope spectrophotometry have concentrated on textiles and fiber dyes, automotive and architectural paint, hair color dyes, ball-point pen and gel inks, stained biological specimens, and other types of transfer evidence. Forensic science applications of ultraviolet microscope spectrophotometry have thus far been limited to automobile top coat clear coat analysis.

In 2001, Wiggins reported on the results of a self-reporting survey of 256 forensic science laboratories from mostly the United States (North and South America) and Europe (Asia and Australia). Forty seven percent (103) of the American and eighty-two percent (32) of the European (for a total of 135

laboratories) responded they performed forensic textile fiber analysis (Wiggins, 2001). Of all that responded, twenty-two percent (29) of the laboratories use UV microscope spectrophotometry, forty-seven percent (64) of the laboratories use visible microscope spectrophotometry, and nineteen percent (25) of the laboratories use fluorescence microscope spectrophotometry. Only three percent (3) of the American laboratories routinely use UV microscope spectrophotometry against forty-four percent (14) of the European laboratories, while only thirty-four percent (35) of the American laboratories use visible microscope spectrophotometry against seventy-five percent (24) of the European laboratories, and only three percent (4) of all laboratories use fluorescence microscope spectrophotometry. More importantly, while UV-visible microscope spectrophotometers are almost standard equipment in a European forensic science laboratory, only slightly more than one-third of the American forensic science laboratories were equipped with UV-visible microscope photometers (Wiggins, 2001).

The selected literature review of the applications of UV and visible microscope spectrophotometry that follows is organized by the common types of transfer evidence such as fibers, paint, documents, and miscellaneous materials reported in mostly, but not limited to, the forensic science literature.

1. Textiles and Fibers:

The first forensic analysis of fibers by visible microscope spectrophotometric analysis was conducted by an Examining Magistrate and commercial chemist, Dr. George Popp, during the 1908 homicide investigation of Margarethe Filbert in Bavaria near Rockenhausen, Germany. The victim's body was found in a section of the forest known as Schelmenkopf. Significant evidence against the suspect, Andreas Schiller, a local factory worker and farmer, was dyed light-brown cotton and light-brown and reddish-brown wool fibers. These dyed fibers connected the suspect to the crime scene. Schiller was convicted of murder and sentenced to death. Later, after his sentence was commuted to life imprisonment, Schiller confessed to the crime (Thorwald, 1967).

The discriminating power of microscope photometric characterization of dyes on wool fibers was investigated by Macrae et al. in 1979 in which they used a collection of visually similar dyed wool samples and compared the conclusions with those from comparison microscopy, fluorescence microscopy, visible light microscope spectrophotometry, extracted dye thin-layer chromatography, and extracted dye solution

spectrophotometry. The study included 12 red wools, 12 black wools, and 18 blue wools. Fibers from each group were mounted with XAM (G.T. Gurr, Ltd., UK) on a microscope slide and first compared by white light microscopy and then by fluorescence microscopy with a combination of BG38 and UG1 excitation filters used in conjunction with a K430 barrier filter. The authors were looking for indistinguishable fibers. While make and model of the microscope system employed in this research was not described, they reported that a microscope attachment was placed in the sample beam of a Shimadzu MPS-50L spectrometer. The authors employed a 100 µm substage diaphragm, a 20 µm objective diaphragm, a 25X glass objective, and spectral range between 400 – 700 nm using a tungsten light source. The absorbance values, following background subtraction (reference ratioing), were calculated over 10 nm intervals for each spectrum. The total absorbance of each spectrum (summation of area under the curve) was recorded along with the fractional portion of each 10 nm interval. The combination of these data, for at least two fibers from each sample, was used for data processing. The authors stated that normalizing each spectrum effectively eliminated variations due to fiber thickness and dye uptake. The normalized spectra for otherwise indistinguishable pairs were compared by 1) the difference in wavelength at corresponding peaks (λ_{max}), 2) the sum of the squares of the differences in the absorbance values between corresponding data points, 3) the sum of the absolute differences in gradient at corresponding data points, and 4) the maximum difference between the cumulative absorbance distributions obtained by successive additions of absorbance values across the spectra. The authors reported that when using the λ_{max} values alone the discriminating power for red wools was 0.67 and for blue wools 0.87. They postulated the difference in discriminating power could be attributed to the fact that spectra of blue wools exhibit multiple peaks. The discriminating power of the comparison parameters studied by Macrae et al. is summarized in Table 2.2.

The authors concluded that the discriminating power of microscope spectrophotometry alone is similar to those destructive techniques (i.e., extraction techniques) that require approximately 500 times more sample. The comparison procedure described could be used to assess the evidential value of fiber comparisons when used in conjunction with a suitable database of reference spectra. The authors also stated that microscope photometers are expensive, but they offer advantages over other techniques. They also speculate that it may be advantageous to use a slit aperture instead of a round aperture to

increase light levels and to average out local color variations along the fiber length. The collection of light over a wide angle (high acceptance angle) will be necessary for heavily delustered fibers or fibers with irregular cross section (Macrae et al., 1979).

parameter	[a] red wools	[b] blue wools
λ_{max}	0.67	0.87
cumulative squares of difference	0.89	0.97
cumulative difference in gradients	0.85	0.97
maximum difference in cumulative spectra	0.80	0.87
cumulative squares + λ_{max}	0.94	0.99
cumulative gradients + λ_{max}	0.92	0.99
[a] 66 paired comparisons examined		
[b] 153 paired comparisons examined		

Table 2.2: The discriminating power of microscope spectrophotometry for red and blue wools as measured by using various test parameters. Reprinted, with permission, from the Journal of Forensic Sciences, Vol. 24, No. 1, copyright ASTM International, 100 Barr Harbor Drive, West Conshohocken, PA 19428.

In 1983, Kubic et al. reported that a significant improvement in the characterization of fibers may be achieved by combination of fluorescence microscopy with a microscope photometer. They described a fluorescence microscope photometer system and technique to differentiate colorless fibers in forensic examinations. The equipment employed included an Olympus® BH microscope equipped with a 100W mercury vertical illuminator with a UG-1 excitation filter and ultraviolet dichroic mirrors, a 420 nm barrier filter, Olympus 20X (0.65 NA) planapochromat objective, 10X widefield eyepieces in a trinocular observation head to which is attached a Farrand® Optical Microscope Spectral Analyzer (MSA). The MSA is equipped with a monochromator drive motor that scans at a constant 100 nm/minute, changeable entrance pinhole masks and exit bandpass slits, a photomultiplier tube detector, and a Hitachi model 056 strip chart recorder. All specimens were mounted in Cargille Type A immersion oil and covered with a No.1 cover glass. The authors reported that even though this was a preliminary study using only a few fibers, the technique showed such promise for colorless fibers that were indistinguishable by all other methods and recommended fluorescence microscope spectrophotometry for all forensic science

laboratories. The authors also noted that dichroic ratio analysis using this technique may provide additional information and discrimination power (Kubic et al., 1983).

The measurement of single fiber birefringence using microscope spectrophotometry has been reported by Harshorne and Laing (1984). The authors employed a NanoSpec 10S monochromator and photodetector mounted on the trinocular head of a Leitz Ortholux II microscope fitted with polarizer and analyzer filters, and a calibrated reticule eyepiece to measure fiber thickness. Of particular interest was an explanation of how to interpret the acquired spectrum in order to calculate birefringence. A plot of intensity versus wavelength is obtained by microscope spectrophotometry, which contains a series of peaks. The conditions for reinforcement is $D = k\lambda$ where k is an integer and, therefore, if the spectrum is arbitrarily assigned k values (1,2,3,…) the peak of greatest wavelength being assigned 1, then a plot of k versus $1/\lambda$ should be a gradient straight line. With knowing the thickness of the fiber (d), the birefringence may then be calculated from $\Delta n = D/d$. But, due to dispersion, the plot of k versus $1/\lambda$ produces a curve and not a straight line. A least squares quadratic curve was fit to the data and the corresponding equation obtained. The first differential of the equation provided the gradient value (D) of the curve for each value of $1/\lambda$, which produces the birefringence at that wavelength (λ). The authors concluded that the method described above exhibits several advantages: 1) highly birefringent (polyesters) and thick fibers where birefringence is typically difficult to measure can now easily be examined, 2) the technique provides an indication of dispersion, and 3) colored fibers that may be difficult to analyze are more amenable to analysis. These are minimal compared to the errors in counting fringes or orders in fibers with high birefringence (Hartshorne and Laing, 1984).

Colorimetry is the science of the measurement of an observed color and its translation to a mathematical representation to determine and specify color. A thorough review of the application of colorimetry to fibers may be found in a book chapter written by Adolf and Dunlop titled “Microspectrophotometry/Colour Measurement” in which the authors describe the basic theory of the absorption of radiation with matter, color and psychophysiological fundamentals, colorimetry, a numerical color coding system, the visible comparison using standards (Munsell, Ostwald, or DIN systems), and instrumental methods to determine color, among other useful and interesting topics (Adolf and Dunlop, 1999). In addition, several American Society for Testing and Materials (ASTM) international methods

have been written to standardize color measurements such as the D2244 (1993) method for calculation of color differences from instrumentally measured color coordinates, E1347 (1990) a method for color and color-difference measurement by tristimulus colorimetry, E1345 (1990) standard practice for reducing the effect of variability of color measurement by use of multiple measurements, and E1164 (1993) standard practice for obtaining spectrophotometric data for object-color evaluation.

Several articles have been written that preceded these ASTM guidelines and deserve mention here. In 1986, Laing et al. discussed in detail the application of complementary chromaticity coordinates and error ellipse (uncertainties in both the *x* and *y* directions) as a means of classification of colored fibers. The error ellipse was plotted on the complementary chromaticity diagram, and the values were plotted within the elliptical area around the mean. The size and inclination of the ellipse was calculated. The direction of the ellipse major axis was found as a line dividing the data in two so that the sum of squares of the perpendicular distance from the line to each point was minimized. In a similar way, the minor ellipse axis was positioned to intersect at the average value of x' and y'. Using the distance of points from each axis, the respective standard deviations of points from each axis was determined. A distance of two standard deviations (2σ) was plotted along the respective axes in both directions from the center (where the major and minor axes intersect). Under these statistical parameters, 90% of the chromaticity values should be enclosed in the ellipse. The authors report the problem of variable dye uptake from fiber to fiber may be alleviated, but acknowledge that problems may occur since the complementary system was originally developed to classify solutions, and that deviations from the Beer-Lambert Law, selective uptake of individual dyes from multi-component dyes, and inherent dye colors may all contribute to errors. Importantly, the research reports high specific color codes for single fiber analysis (Laing et al., 1986).

In 1991, Hartshorne and Laing wrote a three part series discussing in great detail the microscope photometric measurements of fluorescent dyes and brighteners on single textile fibers. In part 1, they describe how to adapt a NanoSpec 10S system to be able to measure fluorescence spectra. The system, based on a Leitz Ortholux II microscope, was fitted with a 25X Fluotar objective and a Leitz Ploemopak Fluorescence Illuminator. The excitation source was a Wotan HBO 50W mercury lamp with a multiple-mirror housing. The vertical fluorescence illuminator was equipped with two filter cube

assemblies: A and H2. Cube A had an excitation spectral range between 340 – 380 nm with fluorescence detection above 430 nm. Cube H2 had an excitation spectral range between 390 – 490 nm with fluorescence detection above 515 nm. The authors described the necessity to correct for illumination differences in order to compare to Commission Internationale de l'Eclairage (CIE) Illuminant A, based on color correction for a quartz-halogen source. By comparing the spectral power distribution of the quartz-halogen with the system and comparing the values to those for Illuminant A stored in the SDP-2000 processor, a correction factor over the spectral range was computed. This correction factor could subsequently be stored in the processor memory for the correction of fluorescence spectra acquisition. In addition, the emission spectrum for the mercury lamp was also determined. The authors used a small metal disc with a central hole placed behind the illumination diffuser to attenuate the intensity of the quartz-halogen bulb during correction. The authors concluded that even though the method does not apply to all dyes, it does indicate real value for the discrimination of single textile fibers with fluorescent brighteners, for which no other objective method exists for comparison. They also propose that it may be possible to code fluorescent colors based on a modified CIE system (Hartshorne and Laing, 1991 part 2), and since prolonged exposure to excitation emission cause fluorescence intensity to diminish over time or decay (Hartshorne and Laing, 1991 part 3), it may be possible to use the decay as a means to differentiate single fibers (Hartshorne and Laing, 1991 part 1).

In 1995, Palmer and Turnbull completed a study to investigate the variation in dye batch across different manufacturers and mass produced textile fibers. Their samples included 100 police uniforms obtained from one police force that were supplied by the same company. Fiber samples were all obtained from inside the right tunic pocket. The dyes were analyzed by both a NanoSpec AFT microscope photometer to determine tristimulus values and by thin-layer chromatography. The authors report a significant difference in dye uptake between different fibers and along the length of a single fiber. They also report that the manufacturer of the police uniforms purchases fabric material from four to five suppliers under competitive contract. Each supplier dyes the fabric to a dark navy color determined by a British Standards Institute (BSI) standard. The dye recipe may vary widely and still meet the color standard between suppliers (Palmer and Turnbull, 1995).

In 2001, Suzuki et al. reported on the analysis of single wool fibers dyed with indigo and seven indigo derivatives (see Table 2.3) using UV-visible transmission microscope spectrophotometry. The microscope photometer system was a Zeiss UMSP-80 using quartz objectives, slides and cover slips. The fibers were mounted on the quartz slides using glycerine. Transmission spectra were obtained over the spectral range between 240 -760 nm.

Compound	CI number
Indigo	73000
4,5,4',5'-tetrachoroindigo	73035
5-bromoindigo	73055
5,5'-dibromoindigo	73060
5,7,5',7'-tetrabromoindigo	73065
4,5,7,4',5'-pentabromoindigo	73070
4,5,6,4',5',6'-hexabromoindigo	73075
7,7'-dimethylindigo	73090

Table 2.3: Indigo and its derivatives used in the experiments. Reprinted from Science & Justice, Vol. 41, No. 2, Copyright (2001), with permission from Elsevier.

The authors reported that six positions on each fiber were measured and examined for intra-sample variation, and six different fibers from the same textile for inter-sample variation. The results indicated that intra-sample variation was quite small, and that the spectra were virtually super imposable, but inter-sample transmission variation was relatively large between fibers examined from different locations on the same textile. However, the λ_{max}, λ_{min}, and the shoulder positions were all at the same wavelength. Moreover, there were no differences observed between the peak intensity ratios of the λ_{max} and λ_{min}. The authors state that when analyzing the same wool fiber type with all eight types of dyes, the spectra were all differentiated (Suzuki et al., 2001).

In 2011 De Wael and Vanden Driessche reported on "Dichroism measurements in forensic fibre examination Part 1 – Dyed polyester fibres", in which the authors discuss the results of their analysis of one hundred and twenty dyed polyester fiber samples by plane polarized light visible microspectrophotometry. Linear dichoism was defined as the selective absorption of plane polarized light of different orientation relative to the fiber long axis by the dye-fiber system. They reported that most of

the dispersed dyed polyester fibers exhibited strong dichroism (dichroic ratio, R>1), as well as significant peak shifts, mostly to lower wavelengths (hypsochromic shifts, λ >0). In addition, the authors state that peak shifts responsible for the dichroism effect are related to the orientation of the dye structure with respect to the substrate fiber polymer chain orientation. The data was collected using a combined system of a Zeiss Axioplan 2 polarized light microscope with a J&M Tidas 800 microspectrometer with a diode array detector type MCS 1024, providing a spectral range of 190-1020 nm. Spectra were typically collected with an integration time of 350 ms and 5 accumulations. The measurements targeted the center of the mounted fibers viewed at 400x magnification with an analysis area of 5 x 30 micrometers. Visible light analysis was conducted using a tungsten halogen source. The data acquisition was completed using TidasDaq software and the raw data was exported as CSV files, without ever performing either spectral smoothing or baseline correction. This article is the first of six articles that report on dichroism (De Wael and Vanden Driessche, 2011a).

In Part 2, De Wael and Vanden Driessche (2011b) report on dichroism analysis of dyed polyamide fiber types nylon, wool, and silk. Polyamide polymer fibers are constructed of aliphatic chains with regularly spaced and recurring peptide functional groups (-—CO—NH—). Most nylon fibers encountered in forensic examination are either nylon 6.6 or nylon 6. Fibers that contain peptide functional groups are typically dyed with acid dyes, however dispersive and reactive dyes are sometimes encountered. The authors report that no dichroism was visibly observed for any of the 650 dyed wool fibers in their collection using plane polarized light, but a measurable dichroism was reported using plane polarized light microspectrophotometry. Silk fibers also exhibited small visual dichroism using plane polarized light, but weak dichroism was measured.

In Part 3, De Wael and Lepot (2011) examined “Dyed cotton and viscose fibres” which are cellulosic fibers. The dye classes most commonly used on cellulose include direct, reactive, vat, and sulfur dyes, with a very limited application of basic and Ingrain dyes. Direct dyes are applied under basic conditions, and reactive dyes are also applied under basic conditions but react with the hydroxyl groups. Vat and sulfur dyes require an environment that promotes oxidation to their leuco form in order to promote solubility into the cellulose by a reduction process where they get trapped inside the cellulose. In general, strong dichroism was observed in cellulosic fibers, regardless of the fiber dye class. It is

important to note that the authors state that further research is needed on multi-dye mixtures and the ability to discriminate between samples dyed with similar structures. Lastly, the authors reported on the variation of dichroism due to the measurement position on the cotton where a variation of the dichroic effect is observed on the sample and the selection of area to measure is crucial to obtaining reproducible results.

In Part 4 De Wael (2012) reports on "dyed acrylic and acetate" fibers, all of which exhibit low birefringence. The study included twenty-two acrylic fibers dyed with basic dyes, eighteen acrylic fibers dyed with disperse dyes, and three variations of polyacrylonitrile (PAN) undyed fibers, PAN vinyl acetate (PAN/VA), and PAN methyl methacrylate (PAN/MMA). The cellulose acetate fibers included forty-four triacetate (TrAc) fibers, twenty diacetate (Ac), twenty-five polyester (Pes), and nine (polyamide) fibers. The author reports that dichroism is stronger in dyed polyester than in dyed polyamide, and smaller dichroic effects were observed for acid dyes on polyamide than those of disperse dyes on polyester. However, when comparing different fibers dyed with the same disperse dye, the polyamide fibers exhibit a stronger dichroism. In most acrylic and acetate fibers, the absorption of polarized light is small in both orientations (parallel and perpendicular), and the author states that "measurement of the separate polarization spectra is valid whenever the absorption difference is higher than 0.01." Acrylic fibers dyed with a bright basic dye often result in spectra with strong absorption in the parallel position so care must be practiced when selecting an area to measure, especially if the fiber has a structured cross-section.

In Part 5 De Wael and Lepot (2012) discuss the analysis of eighty "pigmented fibres" consisting of acetate, viscose, polyamide, polyamide imide, acrylic, polyethylene, polyester, and polyethylene terephthalate fiber types. When viewed under plane polarized light, 38 samples exhibited strong dichroism (48%), 16 samples exhibited weak dichroism (20%), while 26 samples exhibited no dichroism (32%). Most of the pigmented fibers were dichroic and measurable using plane polarized light microspectrophotometry. The dichroic behavior of pigmented fibers was the opposite as that observed for the same phthalocyanine structures applied as a direct dye to cotton or as a pigment in man-made fiber. The authors postulate that this effect is the result of the disc-like structure that is oriented perpendicular to the draw direction of the fiber, and that it acts like an E-type polarizer.

In Part 6 De Wael, Lepot, and Lunstroot (2012) discuss method "validation and practical aspects" of plane polarized light microspectrophotometry. The validation parameters included:

a) Repeatability

Intrarun precision – the standard deviation on the complementary chromaticity coordinates (CCC) obtained from five pairs of consecutive measurements with A_0 and A_{90} on the same measurement positions should be less than 1.5×10^{-3}.

Intravariation – the standard deviation on the CCC from five pairs of consecutive measurements on the same fiber should be less than 15×10^{-3}.

Intervariation – the standard deviation on the CCC from five pairs of consecutive measurements on five different fibers should be less than 10×10^{-3}.

b) Reproducibility

The standard deviation on the CCC from five pairs of intermittent measurements with a month interval between measurements should be less than 20×10^{-3}.

c) Robustness

The standard deviation on the CCC from five pairs of measurements using slightly varying parameters should be less than $5.x\ 10^{-3}$. The factors affecting the measurements to the largest degree should be identified and avoided. For example, translational and angular differences in sample position, length of time between collection of the background spectrum and the sample spectrum, which establishes source and instrument stability, among others.

De Wael, Lepot, and Lunstroot also discuss a decision criterion (match criterion) in which they use raw data, data that has not been smoothed or baseline corrected. A number of measurements of the known (N) were used to visualize the variation of the sample. From the spectral data, the linear dichroic spectrum as determined and the variation at each point in the spectrum were calculated using Equation 2.1:

$$LD_{mean}(\lambda) = \sum \frac{A_0(\lambda) - A_{90}(\lambda)}{N} \pm n\ x\ s(\lambda) \qquad \text{Equation 2.1}$$

in which *s* is the standard deviation at each wavelength and *n* is between 1 and 3 in increments of 0.1. The authors report the best results were obtained for values of *n* equal to 2.0 or 2.5.

Sensitivity was reported as the ability to correctly associate a question sample with the known set according to the decision criterion. For a decision criterion of 2.5s limit, the sensitivity is about 95% for samples with a weak-to-strong observed dichroism, and a lower sensitivity would be expected for those samples that exhibit no observed dichroism (R<1.3).

2. Paints and Coatings:

One of the most notable characteristics of an automobile is its paint color. The visual comparison of paint color of a known or reference sample (flake) and a question or suspect sample (flake) is the first test performed in a forensic paint examination. The ability to efficiently perform the visual comparison becomes increasingly difficult the smaller the paint flake. Early attempts were made to color code paint specimens, but these systems were prone to inter-observer errors and, to a lesser degree, intra-observer errors (Fouweather et al., 1976).

In 1980, Laing et al. used a NanoSpec 10S interfaced with a Leitz Ortholux II equipped with Ultropak objectives that have internal annular illuminators for bright-field or dark-field applications. The system was interfaced via an Anaspec Ltd. analog-to-digital converter to a PET 2001 Commodore Business Machines, Inc. microcomputer. The NanoSpec 10S uses a system data processor-SDP 2000 that stores 2000 points of data in memory from a reflectance reference sample. The reflectance colors from a questioned sample are collected and ratioed against the stored memory and the “true” reflectance colors of the question sample are obtained. The resulting spectrum may be processed for CIE values since the microscope photometer meets the specifications for 0º viewing and 45º illumination. A polished opal glass, type MS20, produced by National Physical Laboratory (NPL) was used to calibrate the system at 5 nm intervals over the visible range between 390 – 710 nm. The area under examination was approximately 25 µm x 100 µm using adjustable slits. The tristimulus values (X, Y, Z) and chromaticity coordinates (x, y) were obtained using the NanoSpec 10S system and compared to the values obtained by an independent Hardy system by a Paint Research Association. The values obtained by both systems compared well and the small differences were reported to be within operational variation or experimental error. The authors concluded that the microscope photometer was an acceptable system that offered a

more precise, rapid, and convenient method to measure color differences in small samples that were typically difficult to characterize due to their small size (Laing et al., 1980).

In 1982, Laing et al. investigated the discrimination of small household gloss paint fragments using microscope spectrophotometry to collect comparison reflectance spectra of apparently metameric (specimens that appear to be the same color but have a different spectrum) color matching pairs of paint samples. The authors obtained nine different British Standard colored paints from fifteen different paint manufacturers for comparison. They prepared samples by dipping a microscope slide into the paint, removing the slide and allowing the paint to dry evenly over the surface of the slide. For multilayer paint, they serially dipped the slides into paint, allowing each layer to completely dry before applying the next layer. The paint was cross-sectioned using a razor blade. The paint layers were first categorized by visual color comparison as previously described by Fouwether et al. (1976) and those groups of paint samples were further examined by microscope spectrophotometry for spectral comparison. The authors used the same system as stated above (Laing et al., 1980) and concluded that paint samples smaller than 0.5 mm x 0.5 mm were very difficult to compare visually and differentiate, but the microscope photometer was capable of measuring reflectance spectra of both surface and cross-section samples of small fragments. The typical examination size was on the order of 20 µm x 80 µm. When compared numerically, using a difference calculated as the square root of the integrated squares of the difference in reflectance at 10 nm intervals along the spectral range, the spectra provided a high level of discrimination over the much more subjective appreciation of color (Laing et al., 1982)

The identification and classification of pigments in small paint samples was investigated by Cousins et al., in 1984. The relative mixture of a small number of different pigments may produce a wide range of different colors. Therefore, the forensic scientist would benefit largely from knowledge about the individual pigments commonly used in the manufacture of paint. The authors acquired a number of common blue, green, yellow, orange, red, and white (rutile) pigments from various supply sources. Visible reflectance spectra were acquired using the same type of system as described above by Laing et al. A computer program, written in-house based on Kubelka-Monk theory, was used to predict spectra that would be obtained from different combinations of paint pigments. This program is similar to a computer program used to color match when an automobile is taken to an autobody repair shop for

repainting. The authors concluded that microscope spectrophotometry is a very useful technique to compare small paint fragments and may be useful for identifying pigments in blue and green paints. The yellow, orange, and red pigments were much more difficult to characterize and suggested more work needs to be done to increase discrimination (Cousins et al., 1984).

Suspectless hit-and-run cases add a dynamic to a forensic investigation that requires knowledge of a population of samples for a meaningful comparison or to provide an investigative lead. During the course of the investigation Nowicki and Patten (1986) speculate that the make and model of an automobile may need to be determined. If a suspect automobile is subsequently located, a comparison sample may be directly compared to make an association or eliminate the automobile as a possible source. Direct color comparison is the first step of the comparison process, as previously stated. The feasibility of using microscope spectrophotometry and visible reflectance spectra for paint comparison has already been established (Laing et al., 1982). With the advancement of computer storage, the authors could store up to 172 reference spectra for comparison. The computer comparison was between stored spectra and a sample was made by summing the quantitative spectral differences over a specified wavelength range. The microscope photometer instrument used in this study was the new DocuSpec I (an updated version of the NanoSpec 10S) attached to an Olympus® BHT microscope with brightfield and darkfield optics, quartz-halogen lamps, a holographic grating, and a gallium arsenide PMT. The system was interfaced to a CS-2 computer with 32K RAM and memory for a spectral library. A 20X objective with a fixed sample area mask of 18 µm x 126 µm was used throughout the examination. In this study nine spectra were collected to produce an average spectrum representing each paint sample and stored for reference. The authors concluded that the DocuSpec I is capable of differentiating paint samples that are similar in color based on their visible reflectance spectral characteristics. The computer matching process is capable of matching a suspect paint sample to a stored reference collection that results in identification of the make and model of a suspect automobile. They also recommend that the optional external storage hard disk be added to the system to store the database of over 1000 colors available in the Reference Collection of Auto Paints distributed through Collaborative Testing Services, McLean, Virginia (Nowicki and Patten, 1986).

In 1988 Wilkinson et al. reported the result of a study conducted on thin sections of paint using transmission visible microscope spectrophotometry. Transmission data obtained on edge microtomed paint cross-sections produce good quality spectra from individual layers for comparison. Individual paint sections of 2 µm or 5 µm were selected for examination. The samples were mounted using Cryobloc mounting medium and a cover slip. Visible transmission spectra were collected over the spectral range between 390 – 710 nm using a NanoSpec 10S connected to a Leitz Ortholux II microscope. Five replicate spectra were collected from separate sections and complementary chromaticity coordinates were calculated from the spectra. The authors reported that depending on the concentration of the pigments in the paint, the appropriate thickness sample exhibited a lower absorbance with improved resolution. A thickness reduction from 5 µm to 2 µm exhibited a small change in complementary chromaticity coordinates. Moreover, the authors noted the errors in measurements of transmission of thin microtomed sections are small compared to the errors obtained by replicate measurements from fibers. The authors also indicated that transmission spectra may provide better discrimination than reflection spectra and that a comparison of the two methods was already underway (Wilkinson et al., 1988).

In 1999, Stoeklein and Fujiwara published a paper on UV-absorbers that was previously presented at the First Meeting of the European Academy of Forensic Sciences in Lausanne, Switzerland in 1997. The authors reported that the automobile industry began efforts to stabilize paint against weathering effects around 1987 using UV-absorbers and light stabilizers. The authors introduced three classes of commercially available UV-absorbers: hydroxyphenylbenzotriazole, benzophenone, and oxalanilide. Ultraviolet absorbers must absorb light between 290 – 350 nm since light in this energy range causes the photodegradation of polymers. The most effective UV-absorbers exhibit maximum molar extinction coefficients in this wavelength range, but should not absorb above 400 nm, which would interfere with visual coloration. The instrument used by these researchers was the Zeiss MPM 800 system with infinity corrected quartz optics (Ultrafluar 40/0.6 NA objective and Ultrafluar 0.8 NA condenser) with a spectral range between 240-760 nm, a holographic grating in both the illumination and the imaging monochromator, a spectral bandwidth of 2.5 nm, monochromator scan steps of 2.5 nm, and an extended response S-20 Hamamatsu R928 PMT. The illumination is a voltage stabilized XBO 75 xenon, mercury, and quartz-halogen lamps. The system also employs an A/D and a D/A processor,

which is a link between the photometer and its control, and the computer for data processing. The authors reported on long term artificial weathering effects of various types and concentrations of UV absorbers in 20 µm microtomed thin sections mounted in glycerin on quartz microscope slides and covered with quartz cover slips. Differences in absorption properties of the binder system and the UV absorber can be used to differentiate between clear coats. The authors also illustrated this by using several different thickness sections to trace UV absorber concentrations down to nanogram quantities (Stoecklein and Fujiwara, 1999).

3. Inks, Papers, and Documents:

According to Pfefferli, a paper by Roy Huber presented at the 1968 annual meeting of the American Society of Questioned Documents Examiners (ASQDE) introduced the application of microscope spectrophotometry as a new instrument in the field of questioned documents (Pfefferli, 1983). Reportedly, the early models of microscope photometers were not adequately designed to measure the reflection spectrum of an ink sample of the dimension of a single ink pen stroke of approximately 1mm wide. In this article, he reports using a NanoSpec 10S attached to a Leitz Ortholux II with Ultropak UO.11 objective to record reflectance spectra from an area of less than 10 μm^2 directly on the paper. The instrumental parameters were set to a maximum entrance slit width, spectral range between 380 – 740 nm, a scan speed of 200 nm/ minute. The 12 volt, 50 watt, quartz-halogen illumination was regulated by a Countant ASB 500 stabilized power supply operated at 6.5 V. The significance of this article was the ability to objectively discriminate, via spectral comparison, colored areas too small for effective visual examination or comparison. However, care must be exercised when collecting spectra to avoid high gloss areas and to minimize “bronzing” or the effect of interference colors that causes abnormal reflectance variations in color density. The evaluation of spectra requires a comparison of the overall differences in the number of peaks, the wavelength of the peak maxima, and the relative intensities of the peaks. The author further stated that microscope spectrophotometry is rapid, non-destructive and that it is complementary to, but does not replace chemical analysis of ink (Pfefferli, 1983).

In 1985, Totty et al. reported on a comparison study using visible microspectrophotometry (VM) and high performance thin layer chromatography (HPTLC) of black and blue aqueous inks used in porous

tip and roller ball pens. In their study, a small portion of the ink line, approximately 1 x 5 mm, was removed from the document for analysis. This amount of sample was necessary to complete the HPTLC analysis whereas microscope spectrophotometry required much less sample. The transmission spectra were collected using a NanoSpec 10S attached to a Leitz Ortholux II microscope over the spectral range between 390 – 790 nm. The authors reported a discrimination power of 0.95 (HPTLC) and 0.86 (VM) for black inks and a discrimination power of 0.98 (HPTLC) and 0.84 (VM) for blue inks. The authors concluded that visible microscope spectrophotometry offers less discrimination than high performance thin layer chromatography and noted significant differences of the same ink on different papers (Totty et al., 1985).

In a very detailed study presented by Olson from the Immigration & Naturalization Service Forensic Document Laboratory (INSFDL) (1986), a NanoSpec 10S microscope photometer was used in the examination of inks and dyes on a variety of suspected fraudulent passports, visas, alien registration documents, and other travel or identity documents used to gain access to services in the country. Olsen reported the instrument was connected to a Leitz Orthoplan trinocular microscope with brightfield and darkfield vertical illuminator and both 16X and 32X objectives. The illuminator was a 12V/100W tungsten halogen lamp operated at 11.5 V and a 100W mercury arc lamp for a combined spectral range from 220 – 900 nm. The regulated power supply for the tungsten lamp was a Hewlett Packard 6286A stabilized to 0.1%, while the mercury arc lamp power was regulated by a Leitz 1230 power source. The grating monochromator provided a maximum of 2 nm resolution, depending on the size of the variable entrance slit and the objective used. The photodetector was a gallium arsenide photomultiplier tube. The Nanometrics SDP-2000 Spectral Data Processor controlled the wavelength drive, stored the background spectrum for automatic ratioing of data to a readout as transmittance, reflectance, or absorbance spectra, and to calculate chromaticity coordinates and tristimulus values. The system was equipped with a Hewlett Packard 7015 B x-y recorder and an Axiom EX-801 Microprinter that prints intensity values every 10 nm of a scan. Olsen presented the results of three cases. The first case involved documents using printing inks on two sets of counterfoils (looks like a large postage stamp) at different times. The counterfoils were obvious under visual comparison to be fraudulent, but the question was whether they may have been printed at the same plant. The inks were spectrally indistinguishable. It was later

discovered that the documents were confiscated from the same location. Case number two involved stamping ink on three passports, each with a rubber stamp impression documenting the passport holder's entry and processing status as a resident alien. Under ultraviolet light the colors fluoresced and appeared very similar, but the stamps were on different colored paper. Examination with the microscope photometer demonstrated the inks to be different than genuine ink. In the final case, security fibers, which are introduced into paper during the pulp stage, were shown to be spectrally indistinguishable from fibers adhered to the surface of the paper in the suspected counterfeit passports so the passport could not be ruled out as being genuine without further analysis (Olsen, 1986).

Zeichner et al. (1988) investigated scattering and bronzing (Newton color fringes) interferences that causes possible deviations of Beer-Lambert Law in both transmission and reflection spectra. They concluded that transmission spectra do not involve bronzing interferences. In addition, when a single inked fiber was mounted in a mounting medium, Permount® with refractive index 1.567 versus the refractive index of cellulose of 1.53, the deviation from Beer-Lambert Law was greatly reduced. The study included dark-field (diffuse reflectance) and bright-field (specular reflectance) measurements. These authors reported that bronzing did not occur when spectral reflections were not collected on smooth, glazed paper but was present on regular or non-glazed paper. Bronzing effects were most apparent with highly absorbent inks on tinted fiber paper. The authors cautioned that the opacity of the paper may greatly influence scattering affects in both transmission and reflection modes.

The Kubelka-Munk transform is the most widely used model to quantitatively describe the interactions of light with diffusing media. However, Zeichner et al. (1988) recognized that the Kubelka-Munk model does not consider the effects of specular reflection to the measured reflectance. The Fresnel equation may better describe the interaction since it models specular reflectance and absorbing materials. The maximum specular reflectance as a function of the wavelength occurs near or at the maximum absorption. This effect causes anomalous dispersion due to quickly changing refractive index values near the absorption band, thus the apparent absorption maximum does not generally coincide with the actual absorption maximum. The authors believed this anomalous dispersion results in the recording of complimentary colors which explains the bronzing effect apparent in the spectrum. The authors

concluded, however, that distinct spectral features may be used to discriminate between the inks investigated (Zeichner et al., 1988).

In 1993, Aginsky discussed in a feasibility study consisting of four methods, the possibility of determining the age of ballpoint pen ink; one of which was microscope spectrophotometry. Ballpoint pen inks are composed of complex mixtures containing dyes, synthetic resins, polymers, and volatile organic vehicles that change over time as the inks start to evaporate upon application to the paper. It is believed that the rate of change of these components vary between inks and substrate depending on the environment, the rate of evaporation of the volatile organic components, the rate of oxidation, and the rate of cross-linking of the polymer components. The microscope spectrophotometer system used was a Leitz MPV-SP with a current-stabilized 12V/100W tungsten-halogen light source, a monochromator with a 1200 lines/mm grating and a half bandwidth resolution of 3 nm, a Hamamatsu R928 PMT detector operated at 500V, a dark-field Ultropak condenser and U0-6.5, 0.12NA objective. The spectra were collected over the spectral range from 400 – 700 nm. The spectra were recorded on a Goerz Metrawatt SE-120 chart recorder operating at a chart speed of 1 cm/minute. The procedure was based on monitoring the spectral changes of the volatile organic components over various time intervals using reflectance microscope spectrophotometry. Several variations of the same basic experiment were carried out on paper. One experiment involved treating the ink with a basic solution and monitoring the changes, while another experiment the paper was contained in a chamber under constant flow of an inert gas such as nitrogen or helium, and monitoring the changes in volatile organic components over time. The results were plotted as the rate in change versus age. This curve was used to predict the age of an unknown. The author cautioned against making age determinations based on this study due to the strict, known environmental conditions and the vast unknown environmental conditions of forensic science samples and stated that more work needs to be done before application of this technique to casework samples (Aginsky, 1993).

In 1995, Aginsky reported on an additional proposal using a microscope spectrophotometry method for dating ballpoint pen inks. The method employed the ratio of comparatively unstable and stable dyes on the surface of documents using unpolarized (spectral reflection) and polarized (diffuse reflection) reflectance values. Aginsky reported that distributional errors increase with increasing magnification and recommended the use of a low-power, long working distance objective to prevent the

photodetector from “seeing” the real image of the fine structure of the paper. However, he could not test that hypothesis without access to other power objectives (Aginsky, 1995).

Roux et al., conducted a study in 1999 to investigate the evidentiary value of black and blue ballpoint pen inks using three techniques: filtered light examination (FLE), reflectance visible light microscope spectrophotometry (MSP), and thin-layer chromatography (TLC). The microscope photometer system employed in their study was configured using an Olympus® BH-2 microscope with a Rofin Microcolourite spectrometer. The spectra were collected and displayed the intensity (% reflectance) against wavelength (λ, nm) over the spectral range between 380 – 880 nm. They acquired fifty scans per measurement. Five separate measurements were made and all spectra were averaged to account for variation. A computer comparison was completed using threshold percent match values based on the variability of five replicate measurements of the same specimen. The spectra were matched based on threshold percent:

> “By threshold percent match value it is meant that any percentage match (of any ink with the target ink, between 0 and 100%) which falls below the threshold value, can be said to be discernible from the target ink; alternatively, any percentage match (of any ink with the target ink, between 0 and 100%) which falls above the threshold value, can be said to be undifferentiable from the target ink. The lowest of these values, i.e., that which showed the largest variation among the five measurements of the same ink has been taken as the general threshold value (or error) applied to each ink of the same colour (blue or black).”

Those spectra determined to be undifferentiable were compared visually, side-by-side and were distinguishable. This indicated that the defined match criteria were too conservative to provide a result other than “not discernible” for inks of different batches of the same brand and type, despite obvious spectral differences. The authors reported a discriminating power, DP = number of discriminated pairs / number of possible pairs. Microscope spectrophotometry alone had a DP of 83% for blue inks and 83% for black inks, and when combined with the other techniques, 99% and close to 100%, respectively. Importantly, the computerized comparison worked well for different inks from different brands and from different models of the same brand (Roux et al., 1999).

4. Miscellaneous Materials:

In 1977 a review article was written on the Applications of Luminescence in Forensic Science in which Gibson stated that cathodoluminescence may have application in the analysis of minerals, ceramics, paint, and glass to differentiate amongst container, window, and headlamp samples (Gibson, 1977). More recently, in 2007, Palenik and Buscaglia authored a book chapter titled "Applications of Cathodoluminescence in Forensic Science" in which the authors described in detail the microscope photometer system in which they collected emission spectra with a research grade high-resolution dual-grating spectrometer employing either a PMT or CCD detector that was interfaced via a fiber optic to a Nikon Eclipse 800 polarized light microscope with a stage mounted evacuation chamber containing a cold-cathode electron gun and leaded glass observation windows. The microscope was equipped with long working distance condenser and planachromat objectives. Forensic applications include minerals, glitter particles, duct tape, masking tape, concrete and cement, slag, and glass (Palenik and Buscaglia, 2007).

Ultraviolet-visible microscope spectrophotometry was used to detect microscopic amounts of dried blood on single fibers, without extraction, directly in XAM mounting medium. The authors identified a major absorbance peak at 422 nm and two minor peaks at 454 and 581 nm. The authors go on to say they were successful at collecting excellent spectra from blood crusts as small as 10 – 20 µm. No discrimination was obtained between species (Kotoswki and Grieve, 1986).

Grieve and Deck (1995) introduced a new mounting medium, Phytohistol, used in forensic examinations of textile fibers. Phytohistol is colorless, water-soluble, and miscible with water-glycerine but without the health hazards associated with xylene-based mounting mediums. This new medium exhibits no fluorescence when fresh and does not absorb in the ultraviolet region between 240 – 340 nm. It has a refractive index of 1.497. It exhibited no fading and no leaching of various dyes from cotton, acetate, wool, nylon, acrylic and polyester fibers. Slight background fluorescence was observed when phytohistol was dried. Phytohistol was adopted for use in the authors' laboratory for all fiber examinations (Grieve and Deck, 1995).

In 2008, microscope spectrophotometry was used in the examination of tape lifts used to collect small particles from garments (De Wael et al., 2008). Small particles of suspected blood were examined

using a Tidas 800 coupled to a Zeiss Axioplan 2 microscope with a diode array detector type MCS 1024 with a spectral range between 190 – 1020 nm. The absorption spectra were obtained directly from specimens attached to tape on a microscope slide using an integration time of 350 ms and 5 accumulations. The measurements were made at 400X magnification through a 5 µm x 30 µm field. TidasDaq™ acquisition software was used to collect the data and export as CSV files, without data smoothing or processing. The method was used to confirm the presence of blood but no species differentiation could be made between human, feline and canine (De Wael et al., 2008).

In 2002, Aerneke investigated the potential of hematoporphyrin fluorescence by microscope spectrophotometry as a confirmatory test for blood. As part of his Master's thesis, Aerneke successfully interfaced an analog Farrand® Optical Company, Incorporated (FOCI) Microscope Spectrum Analyzer™ (MSA) through a National Instruments PCI-1200™ digital acquisition board to a Dell Optiplex computer for data collection, formatting, conversion, and processing for display in Grams 32© AI v.6 software. The Farrand® MSA monochromator was operated with a 2 mm entrance slit and a 1 mm exit slit to a Hamamatsu R818 PMT (near infrared sensitive) to detect the fluorescence emission spectral range. The monochromator was configured with a 14,000 lines/inch diffraction grating with a spectral range between 325 – 708 nm. The grating is rotated at a constant speed motor calibrated to 50 nm/minute. Fluorescence studies were carried out using an Olympus® Microscope model BH-RFL Vertical Illuminator with a 100 W high pressure mercury burner through four excitation cube and numerous barrier filter options. Research indicated that three methods were investigated to generate fluorescence: 1) sulfuric acid, 2) Ju-Hwa and Chu, and 3) Dotzauer and Keding. The sulfuric acid test was recommended because it was the least labor-intensive and produced the highest level of fluorescence. However, the reagent was destructive to the substrate fibers on which the blood was tested (Aerneke, 2002).

In 1991, the results of a collaboration amongst six Home Office Forensic Science Laboratories in the United Kingdom were published in the Journal of Forensic Sciences (Kotowski and Grieve, 1991). The collaboration examined color matching using a colored glass standard developed in house in an effort to standardize all instruments employed by the six laboratories. Each laboratory was equipped with the NanoSpec 10S attached to a Leitz Ortholux II microscope with either Ultropak U011 or Fluotar objectives. The Home Office Fiber Database required the valid comparison of color measurements from

all six instruments. The standardized sample was also employed as a check sample to monitor instrument performance (Hartshorne and Laing, 1991). As of this writing, no other article has been identified that reports a collaborative effort for a forensic certified reference material to compare colors between different microscope photometer systems.

A microscope photometric comparison of lipstick smears on paper or fabric was reported by Choudhry in 1991. The author reported that microscope spectrophotometry was capable of differentiating minute amounts of lipstick of apparently similar shades, from a single manufacturer (Choudhry, 1991). However, it was not apparent from this article whether the analysis consisted of intra-sample or inter-sample variation.

In 1996, Griffin et al. reported that cellophane is chemically similar to rayon since it is made from regenerated cellulose. The colorants used in the manufacture of cellophane may be classified as inorganic pigments, organic pigments, and dyes. Therefore, the dyes were analyzed using ultraviolet-visible spectroscopy. A Nanometrics NanoSpec 10S microscope photometer was used for data collection for samples too small to be extracted for macrospectroscopy. The small samples were mounted on a microscope slide using XAM mounting medium and the absorbance measured from 390 – 700 nm. The resulting spectra were comparable to the macrospectroscopy results, and complementary chromaticity coordinates were obtained (Griffin et al., 1996).

In 2007, Parsons and Mountain described the analysis of visually similar beige color polyurethane foam using a Zeiss MSP to collect spectra from 380 – 760 nm and Spectralys™ software to process a 1st derivative spectrum, using the Savitzky-Golay algorithm. The authors reported that inter-sample variation using 1st derivative spectra was minimal and that 1st derivative spectra were used to differentiate samples of different origin that were visually and microscopically indistinguishable. A significant, but not surprising finding in this article was that microscope spectrophotometry was able to differentiate several beige color polyurethane foam samples when the FT-IR spectra were indistinguishable (Parsons & Mountain, 2007).

The forensic discrimination of dyed hair was reported in 2010 using a CRAIC QDI 2000© microscope photometer. The reported instrument parameters were a spectral range between 200 - 700 nm, 150X magnification, 25 total scans (5 scans x 5 hairs), 10 scan averages, sampling time between 100 - 300 ms, and a resolution factor of 2. A total of 55 red hair dyes were analyzed. Reported data

analysis consisted of importing data into Microsoft Excel© and each spectrum was baseline corrected and normalized, and each group of 25 spectra were averaged. The authors used the spectral range between 200 – 210 nm as the baseline reference. Normalization of each baseline-corrected spectrum was based on the "sum of squares" approach. An average spectrum was calculated from these 25 spectra, and used for comparison. The authors also reported that the original hair color had a large effect on the overall spectra. However, the presence of a dye peak in the dyed hair samples reduced intra-sample variation while providing a spectral feature for sample differentiation. Spectral comparisons of replicate samples that represent each dye indicated that sample outliers may occur (Barrett et al., 2010). Multivariate statistical analysis on the same data set was reported using agglomerative hierarchical clustering (AHC), principal component analysis (PCA), and discriminant analysis (DA). A cross validation resulted in an accuracy assessment of 89% for averaged spectra representing each type of dye, and an accuracy of 81% for hair-by-hair analysis was reported. The authors reported the hair analysis was not capable of individualizing either natural undyed hair or dyed hair samples. However, the results support a need for further research to optimize the method for validation (Barrett et al., 2011).

CHAPTER 3. RESEARCH DESIGN

Accurate spectrophotometric measurements through a microscope involve many interrelated factors that affect the quality of the light passing through the microscope optical system, through the specimen, and through the wavelength selection devise to the detector. Assuming proper use of the instrumentation, the instrumental parameters responsible for accurate measurements using a microscope spectrophotometer include a stabilized radiant energy source, the proper alignment of all microscope optical elements, the optical properties of the specimen, the spectrophotometric linearity, and the spectrometer resolution. It is commonly believed that modern microscope spectrophotometric systems are capable of more accuracy than most analysts obtain and that most problems arise in the proper selection of important parameters and the proper use of the instrumentation (ASTM E275, 2008). In order to ensure proper instrument operation, good laboratory practice should consist of an ongoing and living evaluation of instrument parameters that control the quality of the results. These instrument figures of merit are wavelength accuracy and precision, photometric accuracy and precision, photometric linearity, photometric noise, short-term baseline stability, and wavelength dependence on spectral bandwidth. Unsatisfactory results for measuring any of these parameters may indicate improper instrumentation or improper use of the instrumentation. Therefore, as many of these parameters as applicable were monitored for each of the instruments evaluated in this research. A record of operating conditions was kept for each instrument. Reference to manufacturer's recommendations was followed as necessary.

A. Microscope Spectrophotometer Instruments

Six microscope spectrophotometer systems located in five laboratories were selected for evaluation. These instruments were selected based on their fundamental design differences in microscope optical configuration, ancillary components, and spectrometer components and design. This research design incorporates inter-laboratory and inter-instrument aspects for the comparison of analytical results:

1. **CRAIC Technologies, Inc., QDI 2010 System #1**

Figure 3.1: CRAIC Technologies, Inc., QDI 2010 System 1. This image was obtained by Dale K. Purcell during performance evaluation on July 18, 2012

The instrument was configured for UV-visible transmission, reflection, and fluorescence measurements. General specifications include (QDI 2010 user's manual, 2009):

CRAIC Technologies, Inc., QDI 2010 system 1			
Axio microscope	100 – 127 volts input	50 – 60 Hz	Six fixed measuring field apertures: ~1 μm^2 to 8 mm^2, translated to the specimen plane
	Infinity corrected optics Zeiss Ultrafluar	10x, 40x objectives	HBO 100 mercury arc, ± 0.3 %, XBO 75 xenon arc, ± 0.3 %
Spectrophotometer	16 bit A/D	1000:1 SNR	3 count RMS dark noise
	Pixels: 1044 x 64	Pixel size: 24.5 μm^2	Thermoelectric cooled, ±0.1 ˚C of set temperature in <2 minutes
Imaging	Video: 1280 x 960 at 7.7 – 3.75 fps	Dynamic range: A/D 10 bits (1024 cnts)	SNR: A/D 9 bits at (512 cnts) at 25 ˚C, gain 0 dB

Table 3.1: Summary table of components for CRAIC Technologies, Inc., QDI 2010 system #1.

2. CRAIC Technologies, Inc. QDI 2010 System #2

Figure 3.2: CRAIC Technologies, Inc., QDI 2010 System 2. This image was obtained by Dale K. Purcell during performance evaluation on July 18, 2012.

The instrument was configured for ultraviolet-visible transmission measurements only. General specifications include (QDI 2010 user's manual, 2009):

CRAIC Technologies, Inc., QDI 2010 system 2			
Axio microscope	100 – 127 volts input	50 – 60 Hz	Six fixed measuring field apertures: ~1 μm^2 to 8 mm^2, translated to the specimen plane
	Infinity corrected optics Zeiss Neofluar	10x, 50x objectives	HBO 100 mercury arc, ± 0.3 %, XBO 75 xenon arc, ± 0.3 %
Spectrophotometer	16 bit A/D	1000:1 SNR	3 count RMS dark noise
	Pixels: 1044 x 64	Pixel size: 24.5 μm^2	Thermoelectric cooled, ±0.1 ˚C of set temperature in <2 minutes
Imaging	Video: 1280 x 960 at 7.7 – 3.75 fps	Dynamic range: A/D 10 bits (cnts)	SNR: A/D 9 bits at (512 cnts) at 25 ˚C, gain 0 dB

Table 3.2: Summary table of components for CRAIC Technologies, Inc., QDI 2010 system #2.

3. Zeiss MPM400-MSP65 System

Figure 3.3: Zeiss MPM400-MSP65 Visible Microscope Photometer and Microscope System Processor. This original image was obtained by Dale K. Purcell during performance evaluation on June 19, 2012.

The instrument was configured for reflection and fluorescence measurements. General specifications include (MPM400 user's manual, 1990):

ZEISS MPM400-MSP65			
Axioskop microscope	110 – 120 volts input	50 60 Hz	HAL 100, halogen 12 V, 100 W, ± 0.1 % HBO 100 mercury arc, ± 0.3 %
	Infinity corrected optics: 10x, 20x, 40x Zeiss Epi-Plan Neofluar objectives	20x, condenser objective	Measuring field diaphragm, 0.5 micrometers to 8 millimeters diameter, translated to the specimen plane Luminous field diaphragm, 1.0 micrometer to 8 millimeters diameter, translated to the specimen plane
Spectrophotometer	12 bit A/D	R 928 PMT	Dynamic range, ~10^5
	Linearity, ~0.1% Accuracy, ~0.2% A/D	Voltage: 310 – 1200V	Gain factors: 1x, 10x, 100x, 1000x, auto-ranging
	Scanning monochromator 380 – 750 nm	Wavelength accuracy ± 0.5 nm	Minimum increments, 0.2 nm
	Holographic concave grating 1208 grooves/mm	Blaze wavelength 500 nm	Spectral bandwidths, 1, 2.5, 5, 10, 20 nm

Table 3.3 Summary table of components for Zeiss MPM400-MSP65

4. Custom Built Horiba JY XploRA Raman-Visible Polarized Light Microscope System

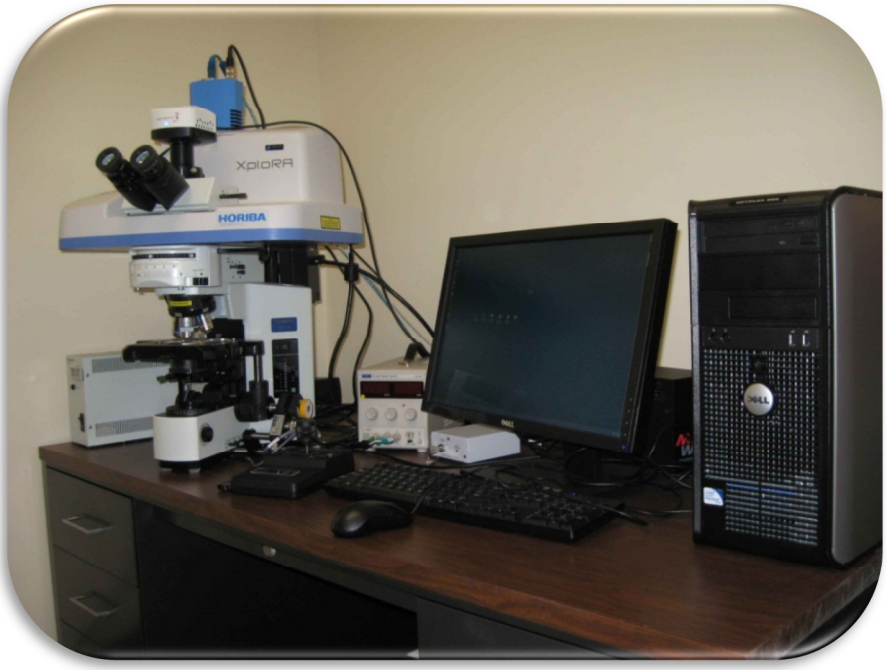

Figure 3.4: Custom Built Horiba XploRA Raman-Visible Spectrophotometer. This original image was obtained by Dale K. Purcell on March 4, 2011 at John Jay College of Criminal Justice.

The instrument was equipped for transmission, reflection, and fluorescence measurements (XploRA Raman-Visible user's manual, 2011):

Custom Built HORIBA XploRA Raman-Visible Microspectrophotometer				
BX51TRF microscope	110 – 120 volts input	50 – 60 Hz	HAL 100, halogen 12 V, 100 W, ± 0.1 % HBO 100 mercury arc, ± 0.3 %, 532 nm laser 785 nm laser	
	Infinity corrected optics: 10x, 50x LWD, 50x, 100x	Variable aperture polarized light condenser	100, 300, 500 µm selectable measuring field pin-hole apertures	
	Fluorescence cube	Excitation filter, nm	Dichroic mirror, nm	Barrier filter, nm
	U-MWU2	330-385	400	Removed
	Bright field cube		400	
Spectrophotometer	16 bit A/D	1000:1 SNR	3 count RMS dark noise	
	CCD Pixels: 1044 x 64	Spectral range, 400 – 800 nm	Communication, USB 2.0	
	Acquisition: 10 ms – 65 s Programmable to acquire consecutive data over hours	Holographic gratings: 300 grooves/mm 600 grooves/mm 1200 grooves/mm 1800 grooves/mm	100, 200, 300 µm selectable spectrometer entrance slits	
Imaging	Infinity video camera	5.0 MP	16 bit color 2572 x 1956 resolution 13 fps maximum	

Table 3.4: Summary table of components for custom built HORIBA XploRA Raman-Visible microspectrometer.

5. Custom Built Olympus BX51TRF Polarized Light Microscope System

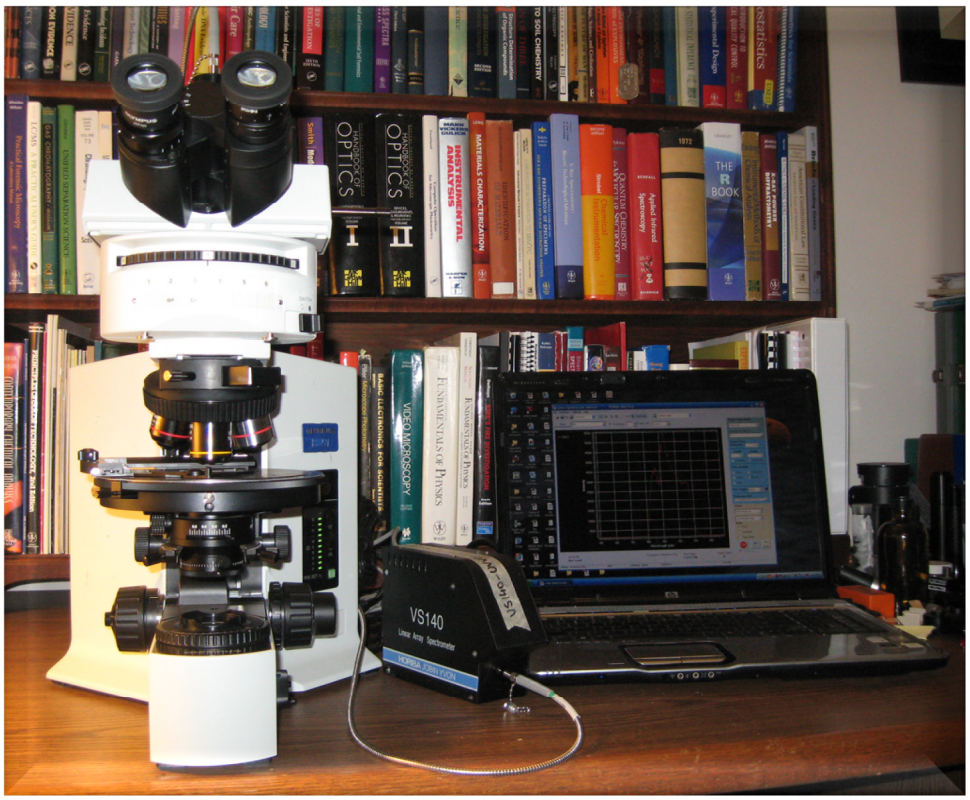

Figure 3.5: Custom built microscope photometer configured on an Olympus BX51TRF microscope with an HORIBA VS140 fiber optic spectrometer. The system was assembled by Dale K. Purcell on January 4, 2013.

The instrument was based on an infinity corrected optical microscope system equipped with a fiber optic Horiba VS140™ spectrograph configuration. The system equipped for transmission, reflection, and fluorescence ultraviolet-visible measurements (VS140™ user's manual, 2008):

Olympus BX51TRF polarized light microscope with Horiba VS140 fiber optic spectrometer				
BX51TRF microscope	110 – 120 volts input	50 – 60 Hz	HAL 100, halogen 12 V, 100 W, ± 0.1 % HBO 100 mercury arc, ± 0.3 %, XBO 75 xenon arc, ± 0.3 %	
	Infinity corrected epi-illumination optics: 5x, 10x, 20x, 40x, All Reflecting Objective (ARO), 10x	Variable aperture polarized light condenser	115 µm diameter, 0.2 NA, SMA fiber optic, ~2.5 µm diameter to 25 µm diameter measuring field aperture, translated to the specimen plane	
	Fluorescence cube	Excitation filter, nm	Dichroic mirror, nm	Barrier filter, nm
	U-MWU2	330-385	400	420
	U-MWB2	460-490	500	520
	Bright field cube		400	
	Dark field cube		400	
Spectrophotometer	16 bit A/D	1000:1 SNR	3 count RMS dark noise	
	CCD Pixels: 3864 Size: 8 x 200 µm	Spectral range, 190 – 900 nm	Communication, USB 2.0	
	Acquisition: 10 ms – 65 s	Grating: aberration corrected holographic concave	Blaze wavelength, 250 nm Dispersion, 24.2 nm/mm Spectral Resolution, 2.3 nm with 100 µm diameter core fiber optic	
Imaging	Tuscan video camera	5.0 MP	16 bit color 2572 x 1956 resolution 13 fps maximum	

Table 3.5: Summary table of components for custom built Olympus BX51TRF polarized light and fluorescence microscope with fiber optic HORIBA VS140 spectrometer.

6. Custom Built Olympus BH-BHA-RFA Polarized Light Microscope System

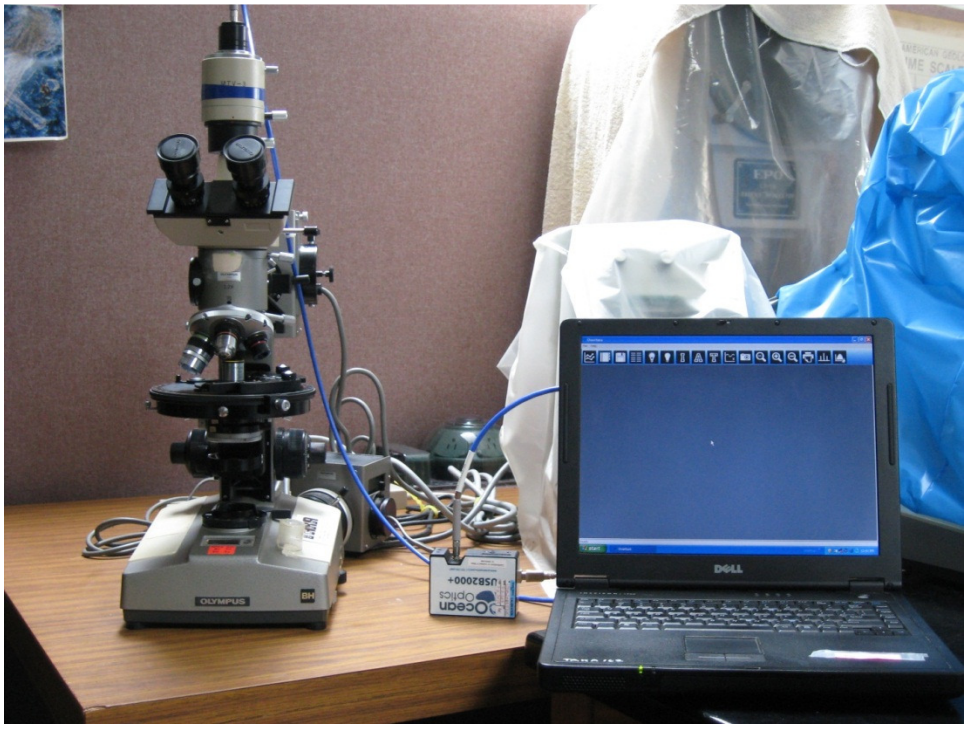

Figure 3.6: Custom built Olympus BH-BHA-RFA polarized light transmission and fluorescence microscope with an Ocean Optics® USB-2000+™ UV-visible fiber optic spectrometer. The system was assembled by Dale K. Purcell on January 8, 2013.

The instrument was based on a finite corrected (160 mm) optical microscope equipped with a fiber optic Ocean Optics® USB2000+™ spectrometer. The system was set up to make transmission, reflection, and fluorescence measurements (USB2000+™ user's manual, 2011):

Olympus BH-BHA-RFA polarized light microscope with Ocean Optics® USB2000+™ spectrometer				
BH-BHA-RFA microscope	110 – 120 volts input	50 – 60 Hz	Halogen 6 V, 25 W, ± 0.1 % HBO 100 mercury arc, ± 0.3 %,	
	160 mm tube length optics: 4x, 10x, 20x, 40x,	Variable aperture polarized light condenser	600 µm diameter, 0.2 NA, SMA fiber optic, ~10 µm diameter to 100 µm diameter measuring field aperture, translated to the specimen plane	
	Fluorescence cube	Various selection of excitation filter, nm	Various selection of dichroic mirror, nm	Various selection of barrier filter, nm
Spectrophotometer	16 bit A/D	1300:1 SNR	~50 count RMS dark noise	
	CCD Pixels: 2048 Size: 8 x 200 µm	Spectral range, 200 – 850 nm	Communication, USB 2.0	
	Acquisition: 10 ms – 65 s	Grating: 600 grooves/mm	Blaze wavelength, 400 nm Dispersion, 24.2 nm/mm Spectral Resolution, 1.2 nm FWHM with 25 µm slit	

Table 3.6: Table 3.5: Summary table of components for custom built Olympus BH-BHA-RFA polarized light and fluorescence microscope with fiber optic Ocean Optics® USB2000+™ spectrometer.

When appropriate, consensus or commercially available standard reference materials, certified reference materials, or verified reference materials were used for the purpose of instrument qualification, calibration or validation. In addition, when appropriate, and if available, a standard practice or consensus method of measurements was followed according to those available from American Society for Testing and Materials (ASTM) International, British Standards Institution or National Physics Laboratory (NPL), and the German Institute for Standardization known as Deutsches Institut für Normung (DIN). Refer to Tables 3.7 for published methods, and for standard, certified or validated reference materials.

Parameter	SRM/CRM and Reference Materials	Published Practice
Wavelength accuracy	SRM 2034, CAL-2000, KR-1	E925, E275
Wavelength precision	SRM 2034, CAL-2000, KR-1	E925, E275
Wavelength resolution	CAL-2000, KR-1	
Spectrophotometric accuracy	SRM 930, 1930, metal on glass	E925, E275
Spectrophotometric precision	SRM 930, 1930, metal on glass	E925, E275
Spectrophotometric linearity	SRM 935a, metal on glass	E169
Spectrophotometric noise	SRM2017, 100%T	E1866
Short-term baseline stability	y-intercept of 100%T line	E1866
Spectral resolution	FWHM	E958
Dichroism / pleochroism	SRM 1866, fibers, chemicals, films	

Table 3.7: Summary table of system figures of merit, standard or certified or verified reference materials, and ASTM International consensus practices for describing and evaluating performance parameters for ultraviolet-visible spectrophotometer.

B. Verification of Standard, Certified or Validated Reference Materials

Ultraviolet-visible microscope spectrophotometry has been generally available since the mid-1970s, when it became possible with manual photoelectric spectrophotometers interfaced with a microscope to make quantitative measurements of the amount of energy absorbed by a specimen as a function of the wavelength of the incident radiation. Even though the evolution of commercially available instrumentation has increased the efficiency of time loss necessary to collect experimental data, there is no compelling evidence to indicate that the reproducibility and accuracy of measurements between instruments or laboratories approaches that from within a given instrument or laboratory. What follows are the fundamental factors that must be considered to obtain the greatest precision and accuracy from a microscope spectrophotometer to collect a high quality spectrum. In some cases the instrument design will dictate the quality of the spectrum but in others the analyst can have a direct influence on the quality of the results.

This research includes the scientific evaluation of several Standard Reference Materials (SRMs) from the National Institute of Standards and Technology (NIST), Certified Reference Materials (CRMs) or otherwise validated reference materials, and microscope supplies were made available to me by Thomas A. Kubic and Associates, Inc., or purchased from commercial supply houses by John Jay College of Criminal Justice.

1. Photometric Accuracy and Precision Standards

There are two types of neutral density or optical density filters: absorptive and reflective. A metal-on-silica stepped optical density slide was purchased from Edmund Optics® (Part No.A64-384). This slide has eleven steps of increasing optical density values. The reported optical density range is from 0.04 to 3.0. The slide was used to measure spectrophotometric accuracy, spectrophotometric precision, and spectrophotometric linearity in the visible light spectral region. Five to ten absorbance spectral measurements over the visible range for each instrument were collected and plotted as an overlay spectrum. The average and standard deviation for each step was calculated. The data was tabulated for each instrument and may be found in the "Instrument Qualification and Summary Report", which accompanies the discussion of each instrument in the Results chapter. Figure 3.7 represents the theoretical optical density step increases at each step. Figure 3.8 illustrates the actual measurements obtained for verification using a Shimadzu UV-2450 bench top spectrophotometer located at John Jay College of Criminal Justice.

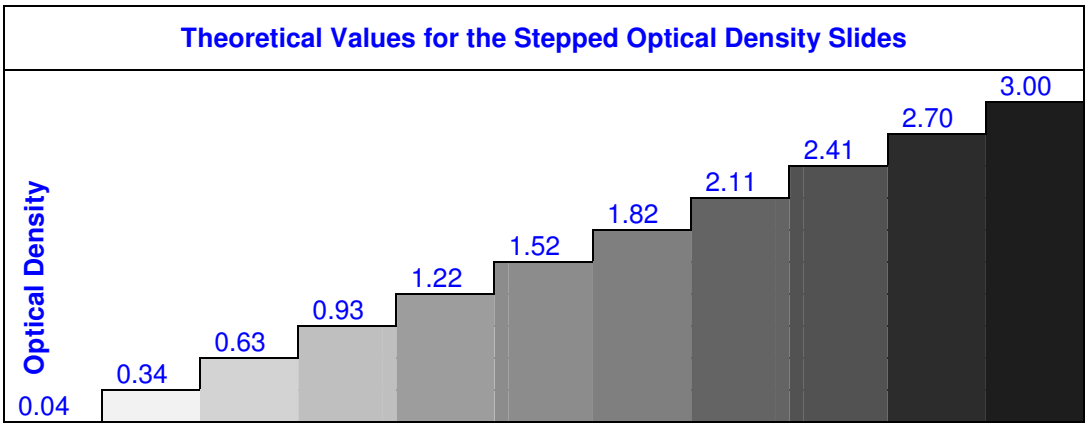

Figure 3.7: Theoretical representation of the optical density values for each of the eleven steps of the Edmund Optics® (Part No. A64-384) stepped optical density slide. Each step increases equally by 0.296 optical density ± 5% between 400 – 700 nm.

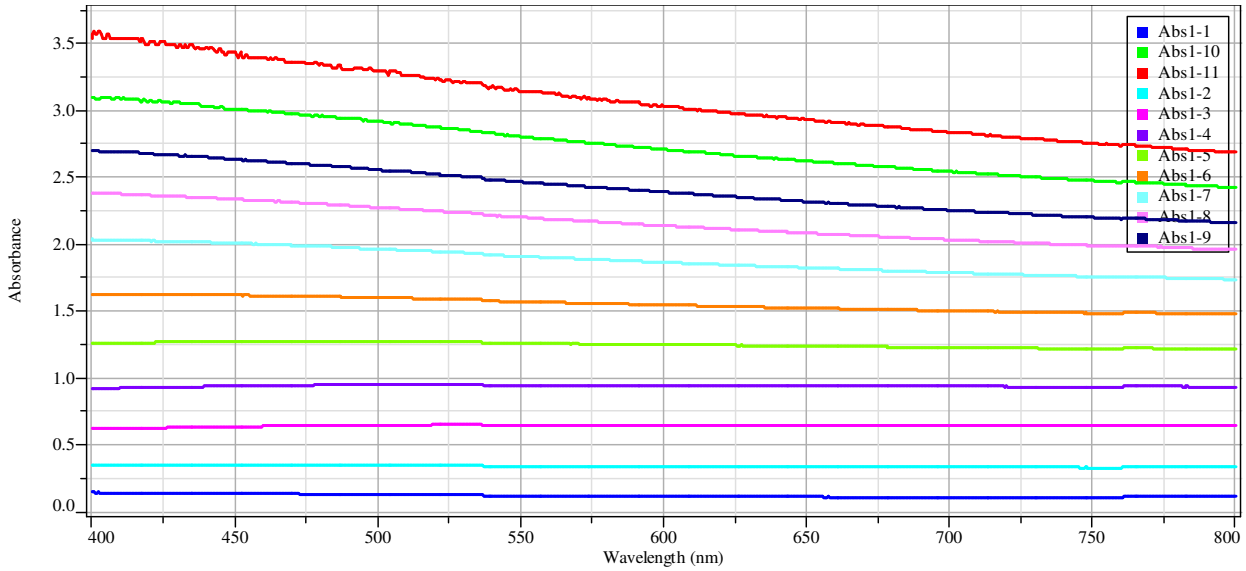

Figure 3.8: Overlay of spectra of Edmund Optics® stepped optical density slide #1 collected on a Shimadzu UV-2450 bench top spectrophotometer located at John Jay College of Criminal Justice. Instrument spectral collection and measurement parameters: wavelength range, 400-800 nm; scan speed, slow; sampling interval, 0.2 nm; slit width, 0.1 nm bandwidth.

2. Dichroism Standards: Chemicals, Thin-Ffilms, and Fibers

A standard test slide was prepared for each of the following: 1) cuprous acetate, 2) dyed polyester films, 2) nine different color dyed polyester fibers. Each standard was mounted on a microscope slide in a refractive index liquid at or near one of the refractive indices for the specimen. The standards were used to develop and qualify a methodology to measure specimen dichroism.

3. Wavelength Calibration Standards

a. Low-Pressure Gas Discharge Lamps

The most generally accepted and accurate wavelength calibration method is to employ a low pressure discharge lamp at the specimen plane using a fiber optic with deep-ultraviolet transmission interfaced with a calibration line source. Accurate values for the wavelengths of these lines can be obtained from reference sources, but it should be understood that these values have usually been measured in a vacuum and the lines from a normal, commercially available lamp source may vary by approximately 0.1 nm from the reported literature values (Burgess and Frost, 1999). At ultraviolet wavelengths, the mercury lines at 253.6 and 184.9 nm are the primary calibration lines while the 435.8

and 546.1 nm lines in the visible light region are useful lines for calibration from a low pressure gas discharge lamp, as illustrated in Figure 3.9. Argon has useful lines in the upper visible light region located at wavelengths 763.5, 811.6, and 912.3 nm. In addition, as illustrated in Figure 3.10, krypton lines at wavelengths 557.0, 587.1, 760.1, and 810.4 nm are useful to verify the calibration of the mercury-argon wavelength lines. Alternatively, a deuterium lamp may be used with emission calibration lines located at 486.0 and 656.1 nm (ASTM E275, 2008).

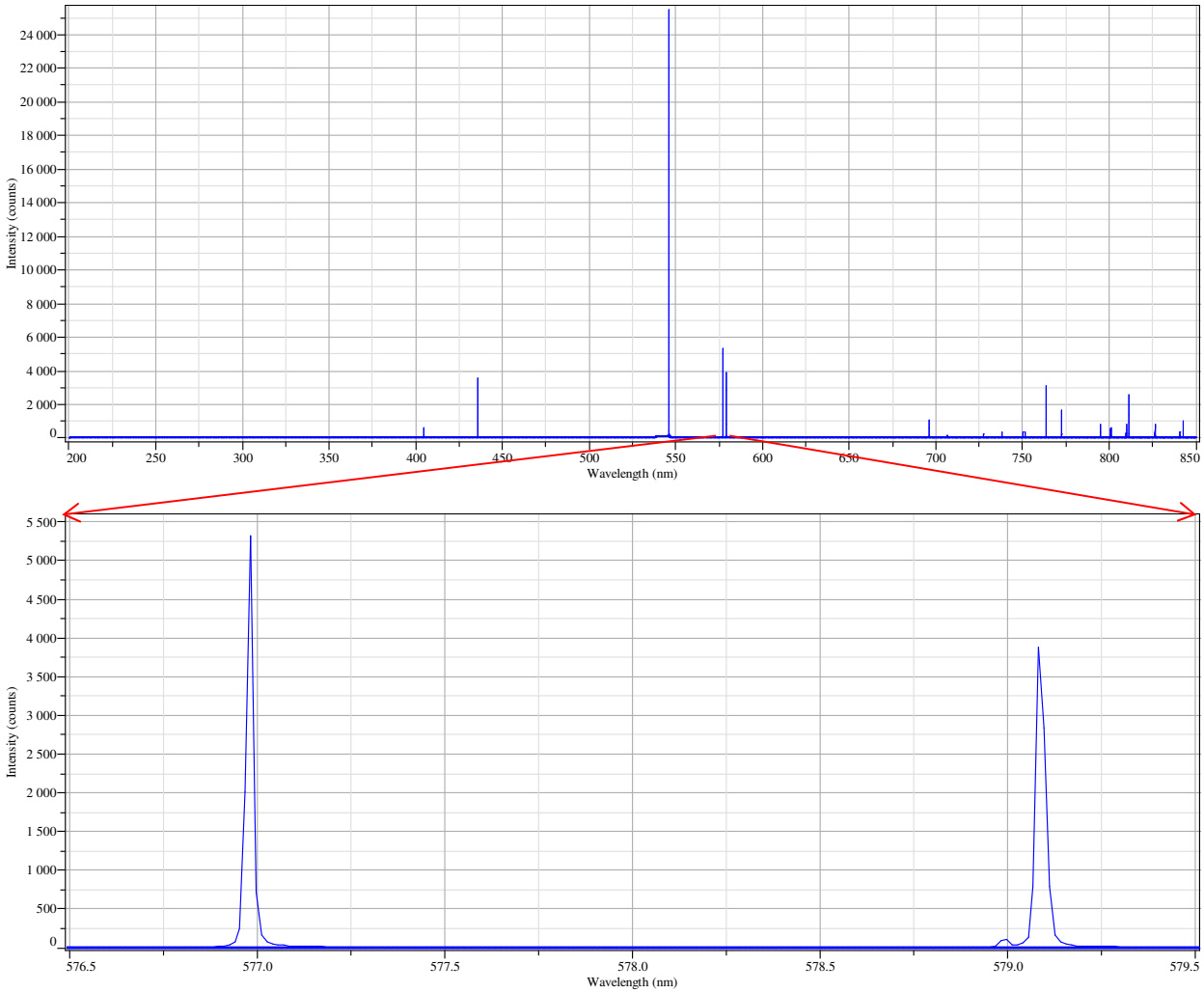

Figure 3.9: Single-beam intensity spectrum of Ocean Optics® CAL-2000™, mercury-argon low-pressure gas discharge lamp collected with a Horiba Scientific LabRAM HR Evolution Raman Spectrometer located at Horiba Scientific, Edison, New Jersey. Instrument spectral collection and measurement parameters: grating, 1800 grooves/mm; wavelength range, 200-850 nm; data acquisition rate, 0.05 seconds, accumulations, 16; hole, 25 micrometer.

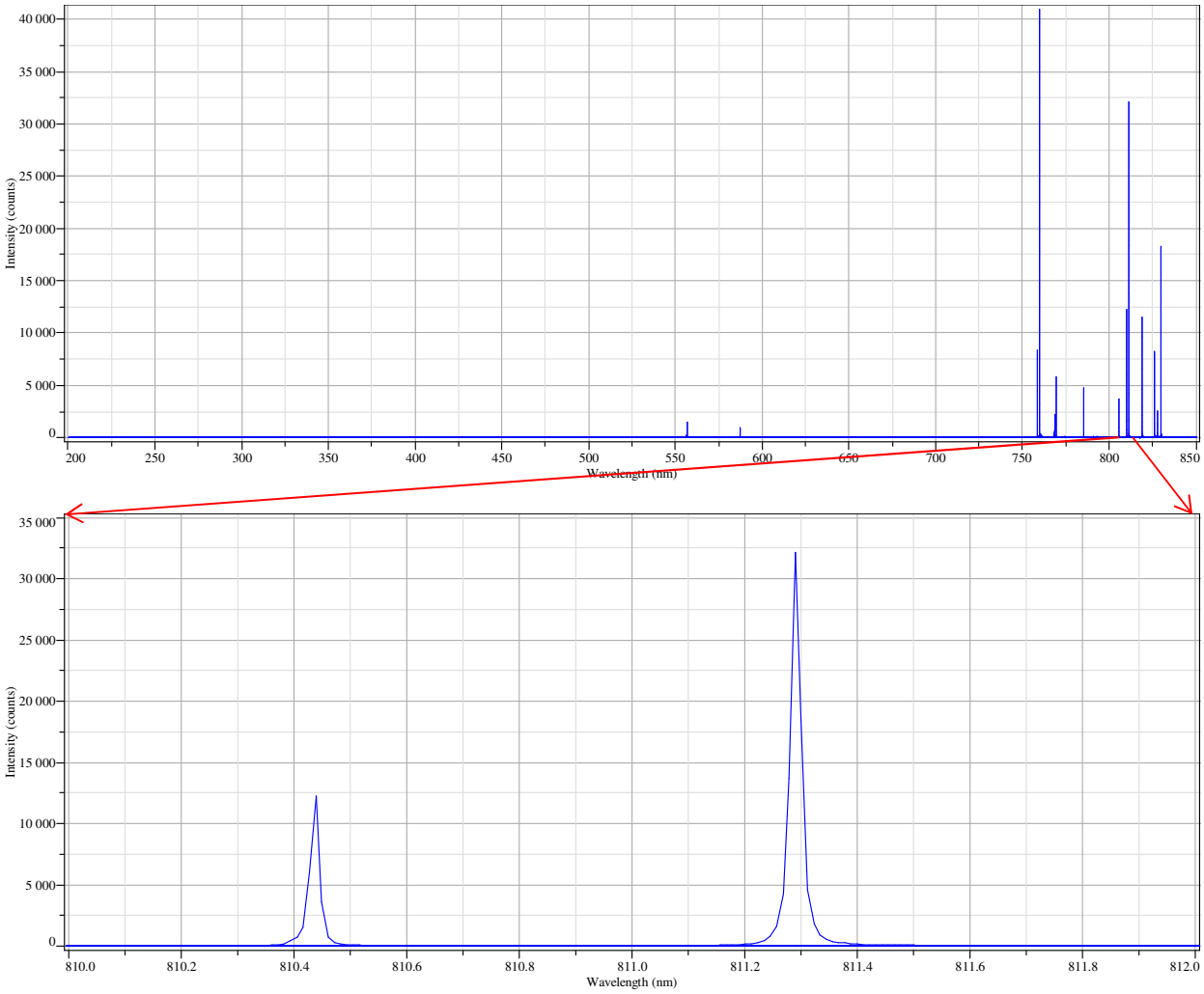

Figure 3.10: Single-beam intensity spectrum from Ocean Optics® KR-1™, krypton low-pressure gas discharge lamp collected with a Horiba Scientific LabRAM HR Evolution Raman Spectrometer located at Horiba Scientific, Edison, New Jersey. Instrument spectral collection and measurement parameters: grating, 1800 grooves/mm; wavelength range, 200-850 nm; data acquisition rate, 0.05 seconds, accumulations, 16; hole, 25 micrometer.

b. Absorption Glass Standards

Rare-earth element containing glasses, holmium oxide and didymium (a mixture of neodymium and praesodymium) are often used and sold as calibration standards by the instrument manufacturers. Absorbance spectra of each are shown in Figure3.11 and 3.12, respectively. Relative to spectral lines obtained by low-pressure gas discharge lamps, these glass standards have broad absorption bands and their wavelength positions are sensitive to slit widths. These glass standards are only useful with

relatively wide-band instruments that have spectral bandwidths larger than 5 nm (Burgess and Frost, 1999). However they may be useful to monitor wavelength precision and accuracy after instrument calibration is achieved with a low-pressure discharge lamp.

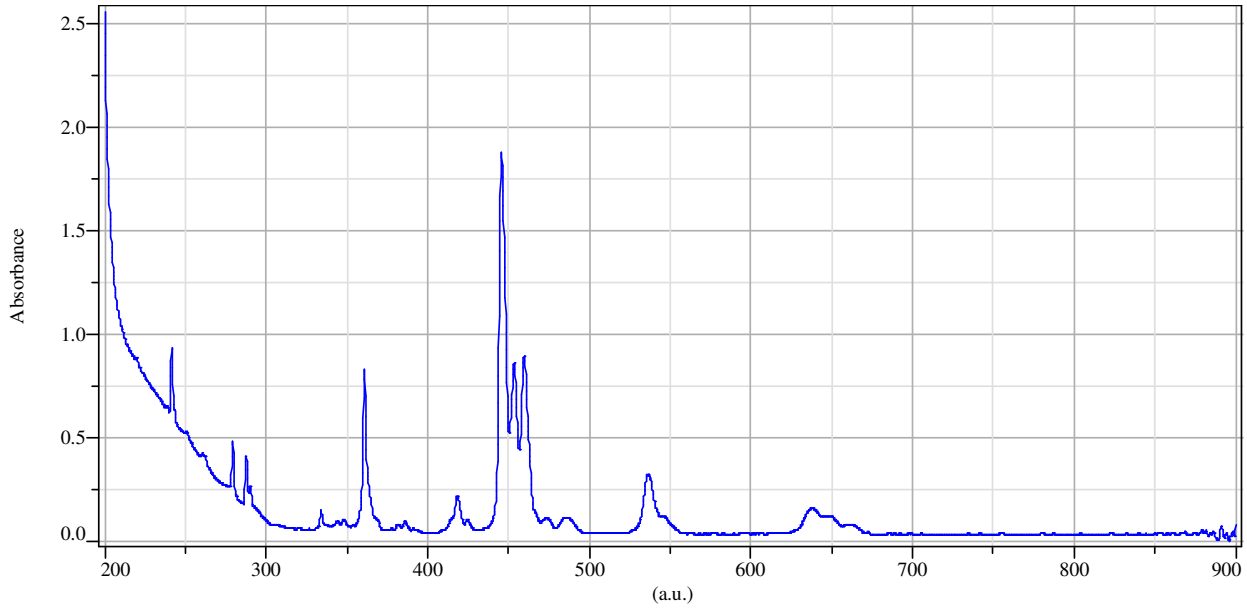

Figure 3.11: An absorbance spectrum of Starna® RM-HG, holmium oxide glass collected with a Shimadzu UV-2450 bench top spectrophotometer located at John Jay College of Criminal Justice. Instrument spectral collection and measurement parameters: wavelength range, 400-800 nm; scan speed, slow; sampling interval, 0.2 nm; slit width, 0.1 nm bandwidth.

A spectral bandwidth that largely exceeds the natural bandwidth of the line being measured will lead to a wavelength shift from the true value. Therefore, the proper selection of a calibration standard depends on the resolving power of the instrument being calibrated, and emission lines from low-pressure discharge lamps are required for instruments that operate at spectral bandwidths of less than 5.0 nm.

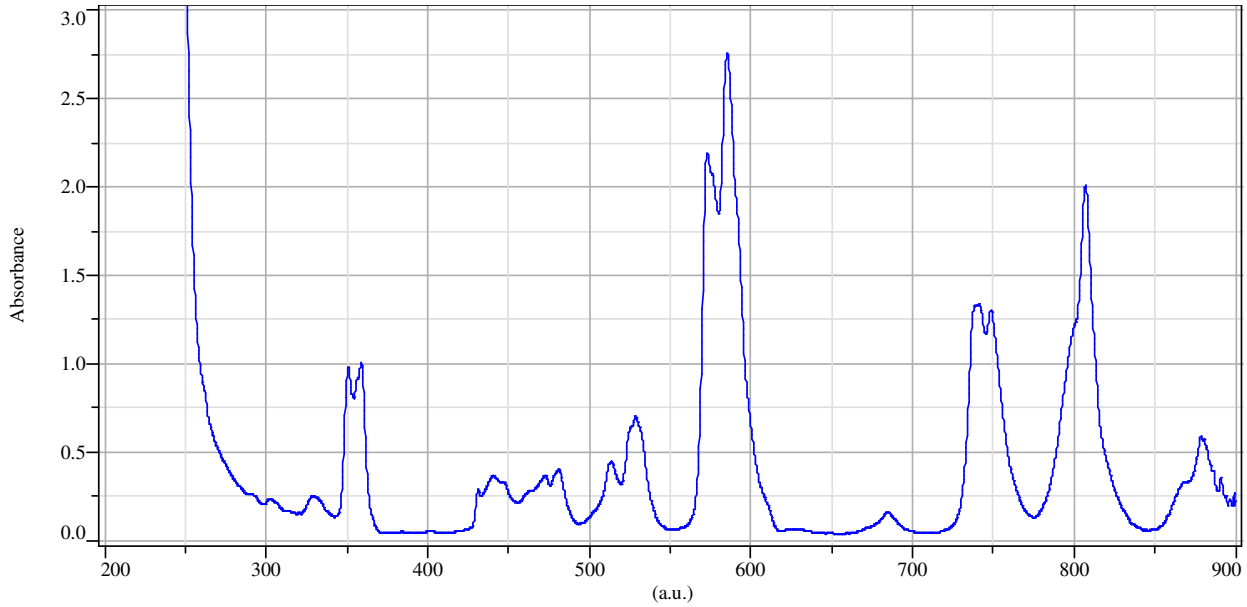

Figure 3.12: An absorption spectrum of the Starna® RM-DG, didymium glass wavelength accuracy standard collected with a Shimadzu UV-2450 bench top spectrophotometer located at John Jay College of Criminal Justice. Instrument spectral collection and measurement parameters: wavelength range, 400-800 nm; scan speed, slow; sampling interval, 0.2 nm; slit width, 0.1 nm bandwidth.

4. **Microscopy Supplies and Materials**

In microscope photometry, the specimen is mounted on a microscope slide in a clear, transparent medium and protected with a cover slip. When performing examinations in the ultraviolet region the slide material must be of sufficient quality to allow transmission throughout the region of interest. A variety of slide and cover slip materials are available through commercial supply houses, and their transmission characteristics must be verified prior to analysis of a specimen. Ultraviolet grade synthetic fused silica (amorphous silicon dioxide) is produced by chemical combination of silicon and oxygen, and it is an ideal material for most ultraviolet applications (Corning Inc., 2003). It is transparent over a wide spectral range from 180 to 2000 nm (2.0 µm), it has a low coefficient of thermal expansion, and it is quite resistant to scratching and thermal shock. Corning 7980 synthetic fused silica materials are manufactured by flame hydrolysis in which tetrachlorosilane is decomposed in an oxyhydrogen flame. The resultant material is colorless and non-crystalline, and it has an impurity content of approximately one part per million (µg/ml). In addition, it has very low fluorescence levels at approximately 0.1% that of fused natural quartz when excited at 254 nm (Corning Inc., 2003).

a. Ultraviolet Grade Synthetic Fused Silica Micro Flow Cells

A matched set of one-hundred micrometer path length (Part No. 48-Q-0.1) and a matched set of ten micrometer path length (Part No. 48-Q-0.01) micro flow cells were obtained from Starna® Cells, Inc. (Atascadero, CA). Both sets of are constructed from Spectrosil® Quartz, which has a spectral transmission range of 170 to 2700 nm. Spectrosil® Quartz is recommended for fluorescence measurements because it does not exhibit background fluorescence. The matched sets were purchased from Starna® Cells, Inc. have a matched tolerance of approximately 1.5%, with a path length tolerance of approximately ± 0.002 µm, and with a window thickness of 1.25 mm. The approximate volume for 48-Q-0.1 cells is 30 microliters and for 48-Q-0.01 cells is 3 microliters. The exterior dimensions are 12.5 (w) x 2.6 (l) x 45 (h) mm and the interior dimensions are 8 (w) x 0.01 (l) or 0.1 (l) x 38 (h) mm (Starna® Cells Inc. Catalog, 2011). An example of an absorbance spectrum for a Spectrosil® Quartz flow cell is illustrated in Figure 3.13. The inset photograph is an original image to illustrate the configuration of the flow cells: top, side view of the flow cell, bottom, top-view of the flow cell.

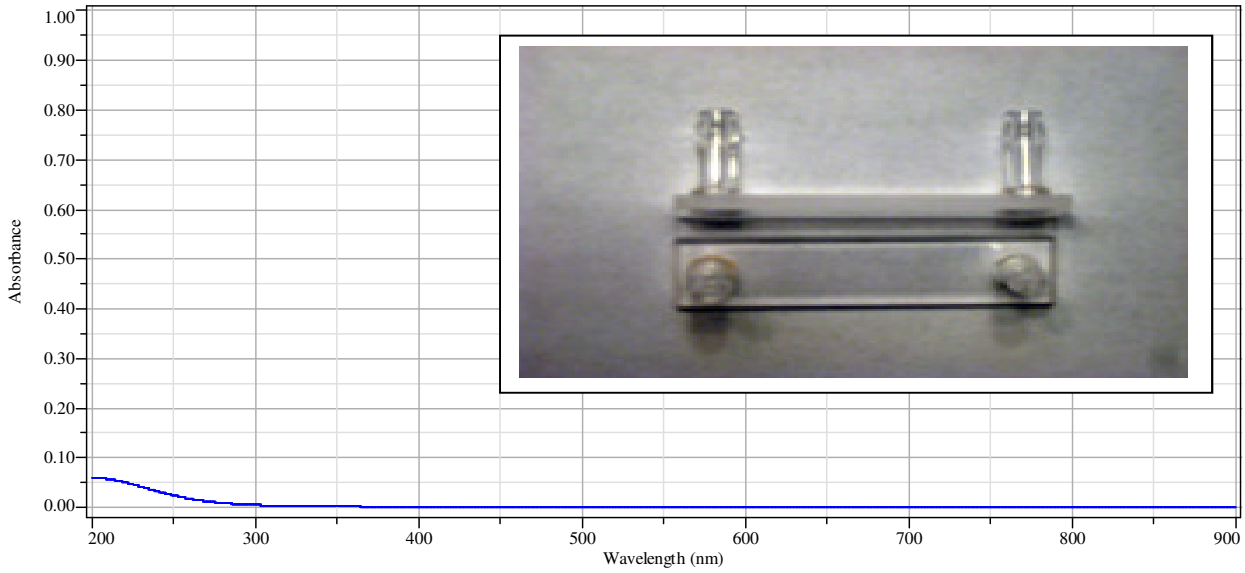

Figure 3.13: An absorbance spectrum of the Starna® 48-Q-0.01, fused-silica quartz flow cell, 0.01 mm path length collected with a Shimadzu UV-2450 bench top spectrophotometer located at John Jay College of Criminal Justice. The flow cell was empty and referenced against air. The inset is an original image to illustrate the actual configuration of the flow cells: top, side view of the flow cell, bottom, top-view of the flow cell. Instrument spectral collection and measurement parameters: wavelength range, 400-800 nm; scan speed, slow; sampling interval, 0.2 nm; slit width, 0.1 nm bandwidth.

b. Ultraviolet Grade Synthetic Fused Silica and Fused Quartz Microscope Slides and Cover Slips

A collection of fused silica, fused quartz or quartz microscope slides and cover slips were analyzed for absorption characteristics. The transmission wavelength range of fused silica is dependent upon the manufacturing process and the materials used. Microscope slides were purchased from several commercial supply companies or acquired from scientists from industry or from university professors. A list of manufacturers and the model numbers and lot numbers, if available, are listed in Table 3.8. The spectrum for each microscope slide and cover slip may be found in Appendix A: Spectral Database.

Synthetic Fused Silica, Fused Quartz or Quartz Slides and Cover Slips				
Manufacturer / Size	**Material**	**Model number**	**Lot number**	**Wavelength Cut-off (nm)**
SPI, Inc. 1 x 25.4 mm disc	Corning 7980 fused silica	1001-AB	1170223	<200
SPI, Inc. 25.4 x 25.4 x 1 mm	Corning 7980 fused silica	1003-AB	1170223	<200
SPI, Inc. 25.4 x 25.4 x 0.2 mm	Fused quartz Cover slip	1015	1120917	<200
SPI, Inc. 25.4 x 25.4 x 1 mm	Fused quartz	1016	1130128	<200
SPI, Inc. 25 x 76 x 1 mm	Fused quartz	1018-AB	1140630	<200
SPI, Inc. #2, 25.4 mm diameter	Fused quartz Cover slip	1019-AB	1140611	<200
Perkin Elmer 16 x 20 x 1 mm	Quartz			325
CRAIC Technologies 25.4 x 25.4 mm	Quartz Cover slip	OC-015		225
CRAIC Technologies 25 x 76 x 1 mm	Quartz Slide	OC-005		225
ChemGlass 25 x 25 x 1 mm	Quartz	CGQ-0640-03	060322	<200

Table 3.8: Summary table containing manufacturer's information and wavelength cut-off values for fused-silica, fused-quartz or quartz slides and cover slips. The spectrum for each component may be found in Appendix 1.

5. Optical Filters

a) Absorbance Wide Bandwidth Filters

Absorption color filters are often used to restrict wave length ranges. An example spectrum for an orange color broad-band absorption filter is illustrated in Figure 3.14. The spectrum for each bandwidth filter may be found in Appendix 1.

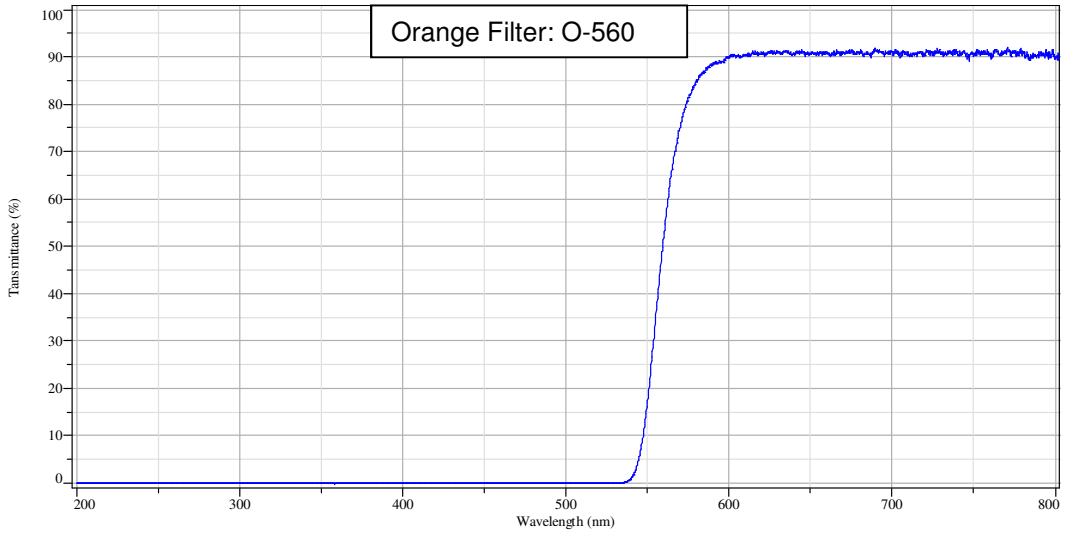

Figure 3.14: Example spectrum for an orange color broad-band absorption filter. The spectrum was collected on a Shimadzu UV-2450 bench top spectrophotometer located at John Jay College of Criminal Justice. Instrument spectral collection and measurement parameters: wavelength range, 400-800 nm; scan speed, slow; sampling interval, 0.2 nm; slit width, 0.1 nm bandwidth.

b) Narrow Bandwidth Interference Filters

Narrow bandwidth interference filters are used to provide either a narrow excitation spectral range or a narrow emission spectral range for emission. An example spectrum for a 10 nm bandwidth interference filter with a spectral range from 360-370 nm is illustrated in Figure 3.15. The spectrum for each narrow bandwidth interference filter is in Appendix 1.

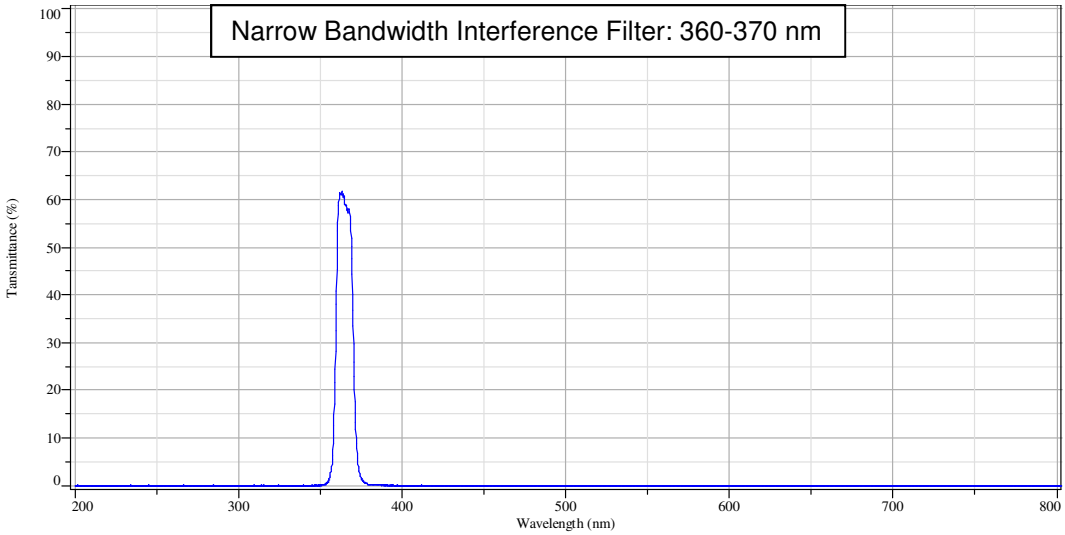

Figure 3.15: An example spectrum for a 10 nm bandwidth interference filter with a spectral range from 360-370 nm. The spectrum was collected on a Shimadzu UV-2450 bench top spectrophotometer located at John Jay College of Criminal Justice. Instrument spectral collection and measurement parameters: wavelength range, 400-800 nm; scan speed, slow; sampling interval, 0.2 nm; slit width, 0.1 nm bandwidth.

c) Fluorescence Cube Dichroic Mirrors

A fluorescence cube dichroic mirror (a.k.a., dichromatic beamsplitter) has surface coatings that are designed to be highly transmissive for longer wavelengths and highly reflective for shorter wavelengths. The dichroic mirror is oriented at a 45 degree angle to the optical path of the excitation light entering a fluorescence cube through the reflected light vertical illuminator. Its primary function is to direct the selected short wavelength excitation light through the objective and onto the specimen, while it passed the longer wavelength light through to the barrier filter and on to the spectrometer, and reflecting any scattered short wavelength excitation light back to the excitation source. The spectrum of a 500 nm dichroic mirror is illustrated in Figure 3.16. The spectrum for each dichroic mirror is in Appendix 1.

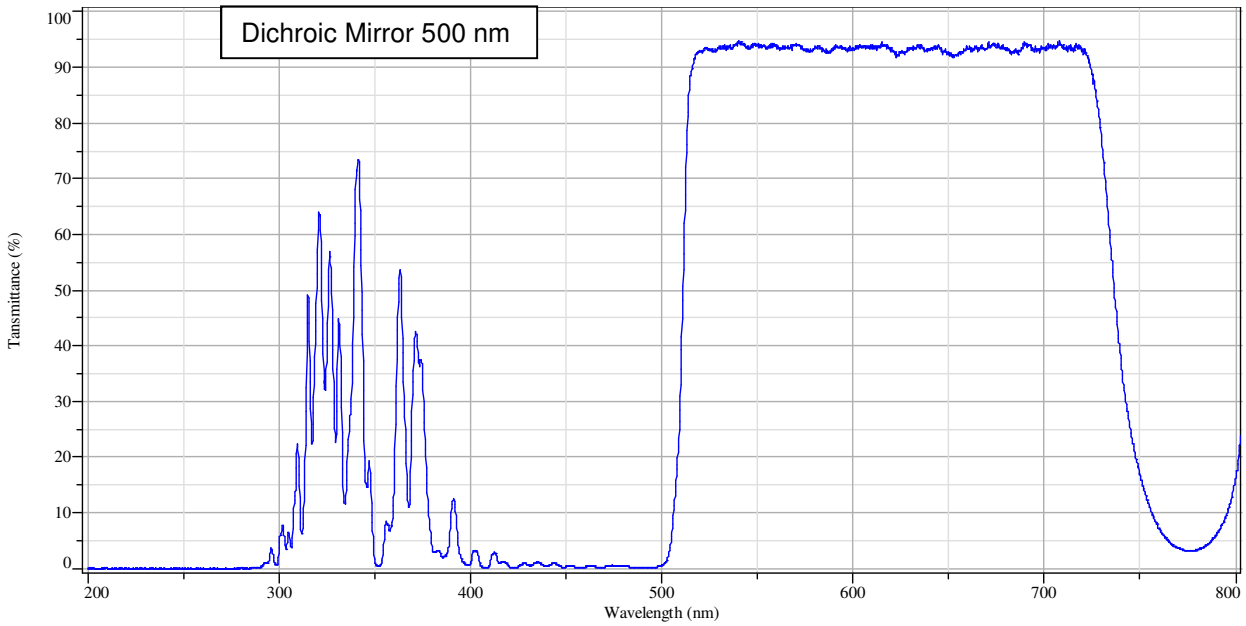

Figure 3.16: A spectrum of a 500 nm broad band spectral range dichroic mirror used in a fluorescence cube. The spectrum was collected on a Shimadzu UV-2450 bench top spectrophotometer located at John Jay College of Criminal Justice. Instrument spectral collection and measurement parameters: wavelength range, 400-800 nm; scan speed, slow; sampling interval, 0.2 nm; slit width, 0.1 nm bandwidth.

6. Reflection Standards

a. Avian Technologies LLC, WCR-UVvis-02c, Reflection Standard

The reference material is intended for use to check the calibration of the reflectance scale for reflectance instruments at UV-visible wavelengths. WCR-UVvis-02c is holmium oxide diffuse reflectance material used to monitor wavelength accuracy and precision from 250 – 850 nm, with a precision of better than 0.2 nm. A copy of the certificate of analysis is located in Appendix VII.

b. NIST SRM 2017 Multi-Angle White Reflection Standard

This standard reference material is intended for use in calibrating the reflectance factor scale of multi-angle reflectance instruments for an illumination angle of 45 degrees and aspecular angles of 15, 25, 45, 75, and 110 degrees at visible wavelengths. This SRM is a polished white Russian opal glass with a diameter of 44 millimeters, mounted in a protective holder. The mark on the holder indicated the direction of illumination. The serial number for this SRM is 2017-02-8. Refer to the certificate of analysis located in Appendix VII for more information.

C. Procedures Used to Measure Instrument Figures of Merit

This research includes the scientific evaluation of six instruments total with two systems being currently available commercially, one commercial instrument is a discontinued system, and four custom built microscope spectrophotometer systems. These systems encompass transmission, reflection, and fluorescence microscope photometry. In practice, the instrument manufacturer specifies recommendations for instrument operating conditions and performance, which may vary between manufacturers. The scientific evaluation of these systems consists of measurements as outlined in ASTM E275 (2008), E387 (2004), E925 (2002), E958 (2005), and E1866 (2007) for the following eight figures of merit:

1. Wavelength Accuracy

Wavelength accuracy was evaluated by the deviation of the average measured wavelength peaks in the spectrum of either a mercury-argon or krypton low-pressure discharge lamp, or a holmium oxide or didymium glass standard certified reference material. When possible three peaks were monitored depending on the reference material and these peaks were selected to cover the upper, middle, and lower third of the reference's spectral range. For example, Figure 3.17 illustrates the spectrum of the Ocean Optics® CAL-2000™ mercury-argon low pressure gas discharge lamp. The spectrum was baseline corrected and peak-fitted; the procedures for which are described in detail below. Data collected from 8 to 10 spectra were tabulated to determine the mean measured peak wavelength value, the standard deviation, and the deviation of the maximum intensity's mean peak wavelength value from the standard reference value. The data was tabulated for each instrument and may be found in the "Instrument Qualification and Summary Report", which accompanies the discussion of each instrument in the Results chapter, and an example of the data is illustrated in Table 3.9

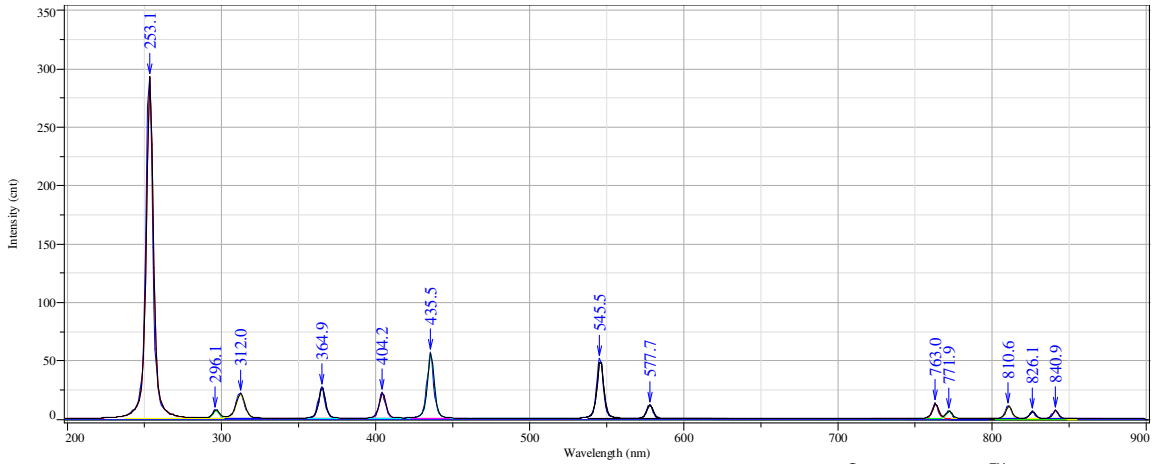

Figure 3.17: Example of a spectrum obtained from the Ocean Optics® CAL-2000™ mercury-argon low-pressure gas discharge calibration lamp collected on CRAIC Technologies, Inc., QDI 2010 system #1. The spectrum was baseline corrected and peak-fitted. Instrument spectral collection and measurement parameters: wavelength range, 200-900 nm; integration time, 10 ms, accumulations, 10; sample mask #4, objective, 10X.

2. Wavelength Precision

Wavelength precision is a measure of the ability of a spectrometer to return to the same spectral position as measured by an absorption wavelength or fluorescence wavelength when the instrument is reset to read absorbance or fluorescence at a known wavelength. The index of precision is the standard deviation of the maximum intensity's mean peak wavelength value. When possible three peaks were monitored, depending on the reference material, and selected to cover the upper, middle, and lower third of the standard's spectral range. Table 3.9 illustrated the data tabulated to determine the wavelength precision.

Wavelength Accuracy and Wavelength Precision Data													
*λ (nm)	1	2	3	4	5	6	7	8	9	10	Ave. λ	stdev	*λ – Ave.λ
253.65	252.2	252.2	252.2	252.2	252.2	252.2	252.2	252.2	252.2	252.2	252.2	3.0E-14	1.45
296.72	295.1	295.1	295.1	295.1	295.1	295.1	295.1	295.1	295.1	295.1	295.1	6.1E-14	1.62
312.57	311.5	311.5	311.5	311.5	311.5	311.5	311.5	311.5	311.5	311.5	311.5	0.0E+00	1.07
365.02	363.9	363.9	363.9	363.9	363.9	363.9	363.9	363.9	363.9	363.9	363.9	6.1E-14	1.12
404.66	403.4	403.4	403.4	403.4	403.4	403.4	403.4	403.4	403.4	403.4	403.4	6.1E-14	1.26
435.93	434.5	434.5	434.5	434.5	434.5	434.5	434.5	434.5	434.5	434.5	434.5	0.0E+00	1.43
546.07	544.6	544.6	544.6	544.6	544.6	544.6	544.6	544.6	544.6	544.6	544.6	0.0E+00	1.47
578.01	576.6	576.6	576.6	576.6	576.6	576.6	576.6	576.6	576.6	576.6	576.6	0.0E+00	1.41
763.51	761.8	761.8	761.8	761.8	761.8	761.8	761.8	761.8	761.8	761.8	761.8	1.2E-13	1.71
772.42	770.7	770.7	770.7	770.7	770.7	770.4	770.7	770.7	770.7	770.7	770.7	1.1E-01	1.72
811.53	809.4	809.4	809.4	809.4	809.4	809.4	809.4	809.4	809.4	809.5	809.4	1.2E-13	2.13

Table 3.9: Example of a summary table containing wavelength accuracy, precision, and deviation data calculated from ten independent measurements of Ocean Optics® CAL-2000™ mercury-argon calibration low-pressure gas discharge calibration lamp. *Standard spectral data wavelength values were obtained from ASTM E275 (2008).

a. precision calculation **–** the wavelength precision was measured using the equation for standard deviation (*S*):

$$S = \sqrt{\frac{\Sigma(\lambda_{ave} - \lambda_i)_n^2}{n-1}} \qquad \text{Equation 3.1}$$

where λ_i is the individual observed wavelength, λ_{ave} is the averaged observed wavelength, and n is the number of observations.

3. Spectral Resolution Dependence on Wavelength

Wavelength dependence on spectral resolution was monitored by measuring the bandwidth at full-width of half-peak-maximum (FWHM) of several peaks in the spectrum of either a mercury-argon or krypton low-pressure gas discharge lamp, or a holmium oxide or didymium glass standard certified reference material. When possible three peaks were monitored, depending on the reference material, and selected to cover the upper, middle, and lower third of the standard's spectral range. For example, the procedure to measure the spectral resolution is illustrated in Figure 3.18.

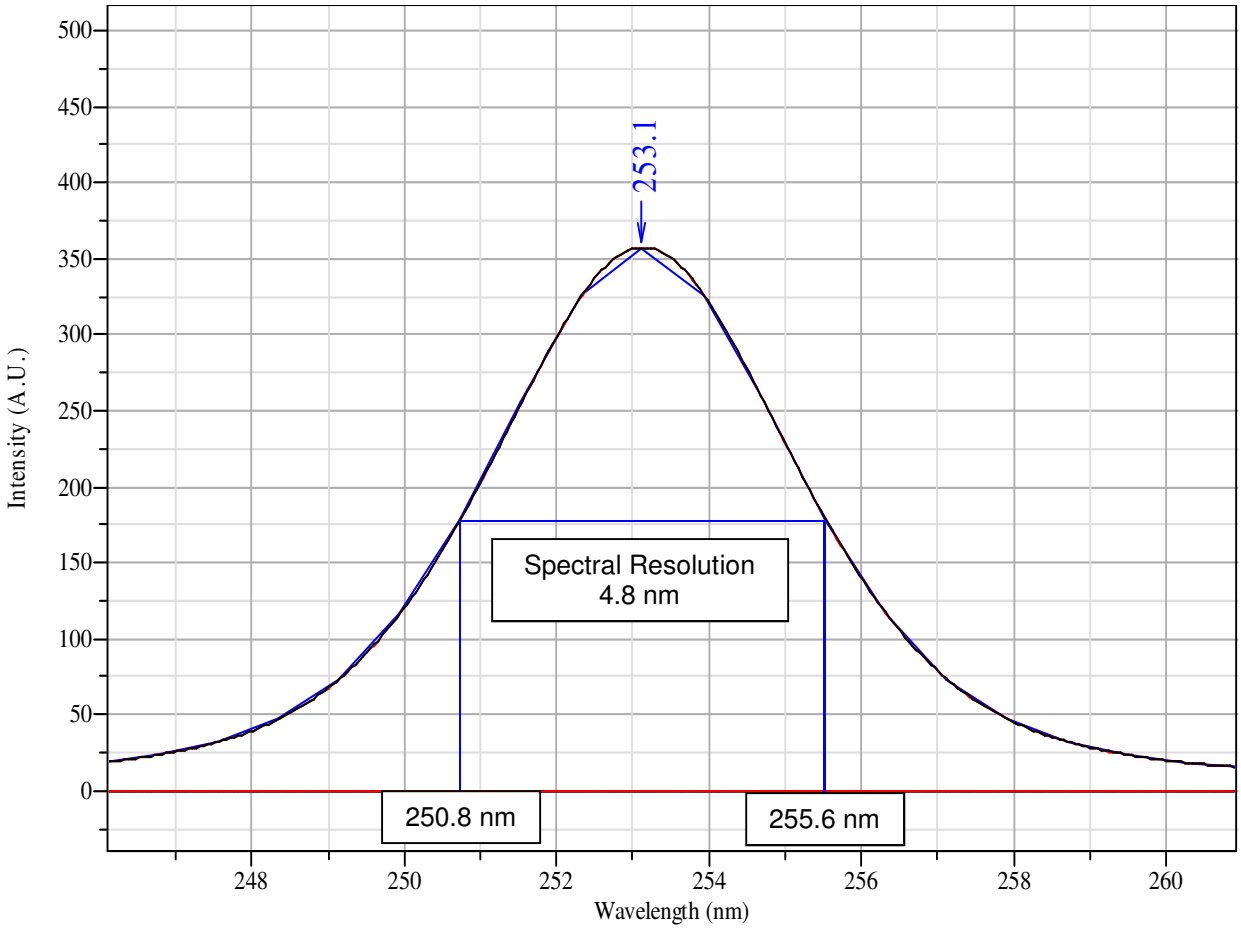

Figure 3.18: An example of how to measure the spectral resolution at a wavelength by using the full-width at half-maximum (FWHM) for the 253.6 nm mercury line from the Ocean Optics® CAL-2000™ as illustrated in Figure 3.13. The blue "curve" is the digitized raw data and the black curve is the peak-fitted curve.

4. Spectrophotometric Accuracy

To evaluate spectrophotometric accuracy, the absorbance or transmittance value is compared to a standard or certified reference material of known absorbance or transmittance. Spectrophotometric accuracy in the visible region was determined by using stepped optical density stepped slides, refer to Figure 3.7. Data collected from 5 to 10 spectra were tabulated to determine the mean absorbance value, the standard deviation, and the deviation of the mean absorbance from the standard reference value. The data was tabulated for each instrument and may be found in the "Instrument Qualification and Summary Report", which accompanies the discussion of each instrument in the Results chapter. An

example of the data is illustrated in Table 3.10. The red-color horizontal data was used to determine spectrophotometric accuracy and precision.

5. Spectrophotometric Precision

Spectrophotometric precision is the capability of a spectrophotometer to reproduce the same absorbance or transmittance value in successive determinations. The spectrophotometric precision was determined by taking the average and standard deviation of up to ten individual measurements The precision was measured using either the Equation 3.2 or Equation 3.3:

$$S = \sqrt{\frac{\Sigma\left(A_{ave} - A_i\right)_n^2}{n-1}} \qquad \text{Equation 3.2}$$

$$S = \sqrt{\frac{\Sigma\left(T_{ave} - T_i\right)_n^2}{n-1}} \quad , \qquad \text{Equation 3.3}$$

where A_i and T_i is the individual absorbance or transmittance value, A_{ave} and T_{ave} is the average absorbance or transmittance value, and n is the number of observations.

Reference Material: Edmund Optics® Stepped Optical Density Slide #1								
Optical Density (*True) - Step	OD @ 400 nm		OD @ 500 nm		OD @ 600 nm		OD @ 700 nm	
	Mean	St Dev	Mean	St Dev	Mean	St Dev	Mean	St Dev
(0.04) – step 1	0.06	0.012	0.06	0.009	0.06	0.005	0.06	0.005
(0.34) – step 2	0.24	0.005	0.25	0.004	0.26	0.004	0.26	0.004
(0.63) – step 3	0.54	0.012	0.57	0.011	0.59	0.010	0.59	0.009
(0.93) – step 4	0.85	0.004	0.89	0.006	0.89	0.006	0.89	0.006
(1.22) – step 5	1.15	0.008	1.19	0.008	1.18	0.008	1.16	0.008
(1.52) – step 6	1.47	0.015	1.51	0.022	1.47	0.026	1.43	0.028
(1.82) – step 7	1.78	0.004	1.87	0.006	1.79	0.006	1.72	0.007
(2.11) – step 8	1.95	0.006	2.13	0.008	2.04	0.007	1.95	0.008

Table 3.10: Example of a summary table containing spectrophotometric accuracy and spectrophotometric precision data for an Edmund Optics® stepped optical density slide. Values represent mean and standard deviation of five measurements. Red-color horizontal data was used to determine spectrophotometric accuracy and precision, while the red-colored vertical data was used to determine spectrophotometric linearity found in the "Instrument Qualification and Summary Report", which accompanies the discussion of each instrument in the Results chapter. *The true value was obtained from the documents supplied with the stepped optical density slides.

6. Spectrophotometric Linearity

Spectrophotometric linearity is the ability of a spectrophotometric system to yield a linear relationship between radiant power incident on its detector and some measurable quantity provided by the system. In practice, it is necessary to determine the linearity at a specified wavelength, such as 500nm. Data collected from 5 to 10 spectra were tabulated to determine the mean absorbance value at consecutive increasing optical density values from a stepped optical density slide. The data was tabulated for each instrument and may be found in the "Instrument Qualification and Summary Report", which accompanies the discussion of each instrument in the Results chapter. An example of a linearity plot is found in Figure 3.19. The red-color data in the vertical column at 500 nm from Table 3.10 was used to determine linearity by the least-squares method.

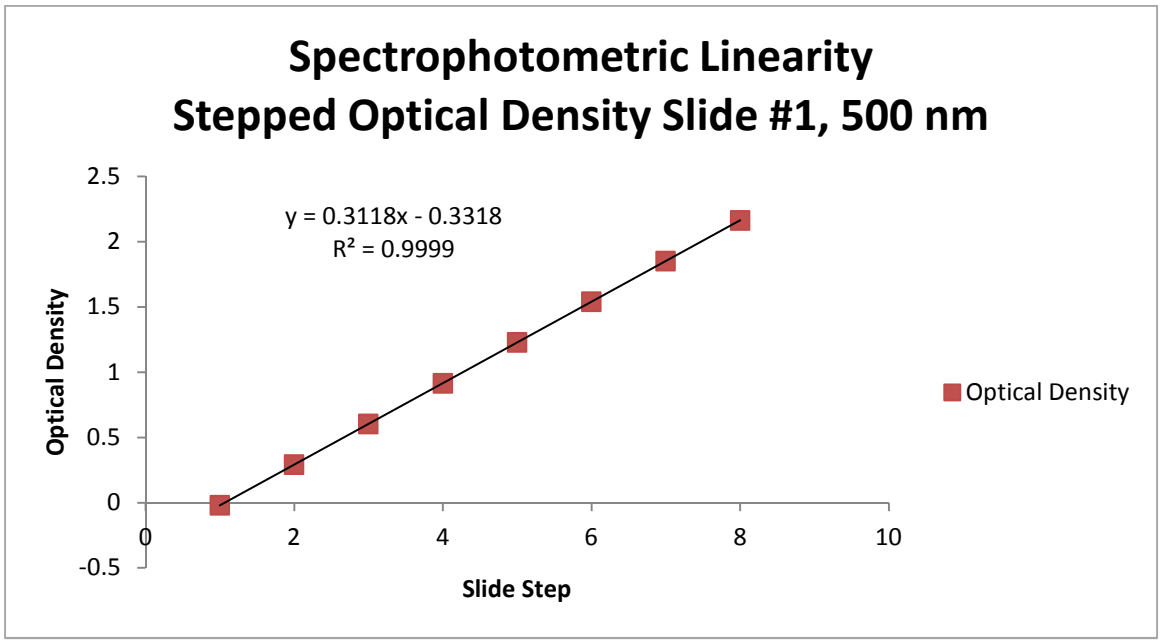

Figure 3.19: Spectrophotometric linearity plot illustrating linearity of optical density measured at 500 nm. The column containing the red-color vertical data from Table 3.4 was used to produce this linearity plot.

a. An alternative method to monitor spectrophotometric linearity was to measure changes to linearity. In this method, the absorbance values of two or more peaks in the absorbance spectrum were baseline corrected, and the ratio of the absorbance values of the two peaks was calculated. This ratio

value iss used to monitor changes in spectrophotometric linearity, but not to establish the absolute spectrophotometric linearity.

7. Spectrophotometric Noise

Spectrophotometric noise was determined using the 100% Transmittance line spectrum. For single optic beam spectrophotometer systems where the background and specimen spectra are measured at different times, a 100% Transmittance spectrum was obtained by ratioing two successive background (I_0) measurements to obtain a transmittance measurement. Spectrophotometric noise was measured by fitting a line to the 100% Transmittance spectrum over a short range of wavelengths centered on a test wavelength, using a least squares approach. This region should contain at least 11 data points or more, but should not exceed 2% of the total points that define the spectral range. An example of a 100% Transmittance spectrum is illustrated in Figure 3.20.

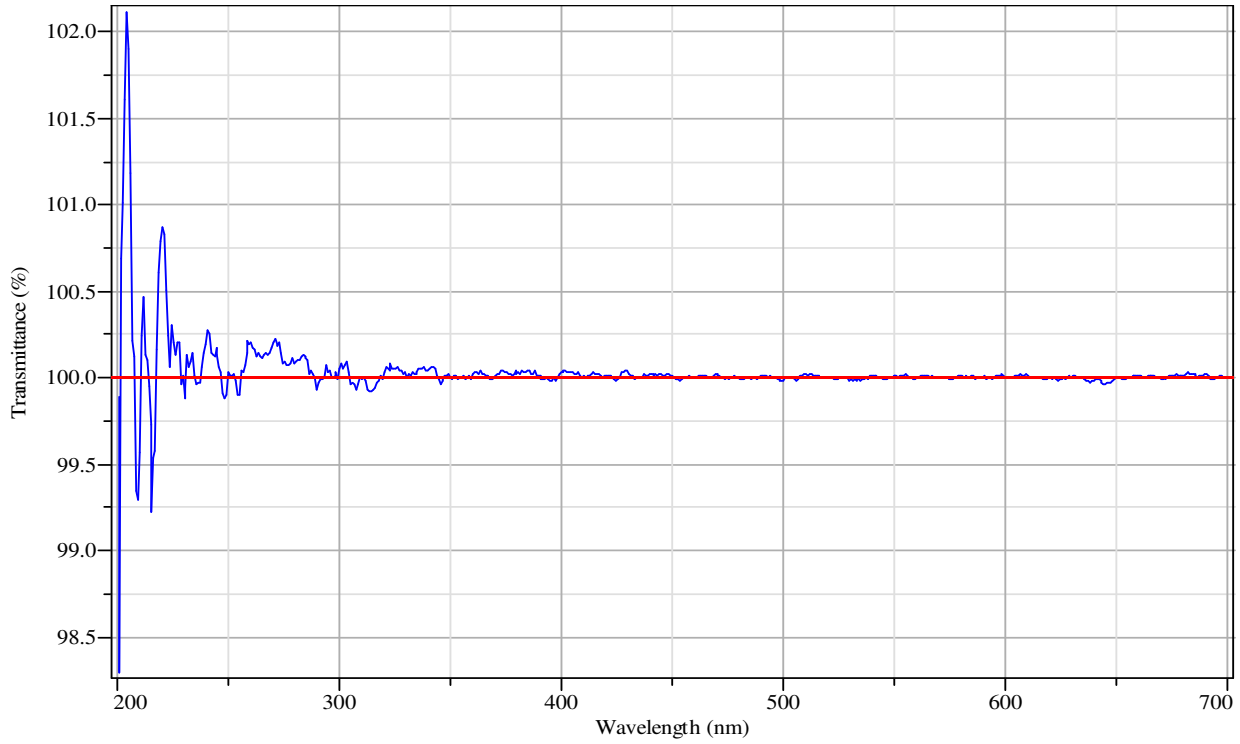

Figure 3.20: An example of a 100% Transmittance spectrum used to calculate the RMS noise. Data was collected on CRAIC Technologies, Inc., QDI 2010 system #1. Instrument spectral collection and measurement parameters: wavelength range, 200-900 nm; integration time, 10 ms, accumulations, 10; sample mask #4, objective, 10X; fused silica microscope slide.

λ	Slope	y-intercept	RMS Noise, 100%T
300	-1.30^{-03}	100.4	4.22×10^{-02}
400	1.93^{-03}	99.2	1.62×10^{-02}
500	-1.37^{-04}	100.1	1.09×10^{-02}
600	8.07^{-04}	99.5	6.58×10^{-03}

Table 3.11: An example of data obtained when determining the RMS noise calculated from Figure 3.20.

The line is subtracted from the spectral data, and the RMS noise is calculated as the square root of the mean square residual. An increase in the spectrophotometric noise can indicate a misalignment of the microscope optics, a malfunction with the source, or a malfunction in the detector electronics. This procedure measures the root-mean-square (RMS) noise as follows:

$$Noise_{RMS} = \sqrt{\frac{\Sigma\left(T_i - \left(mi + b\right)\right)^2}{n-2}} \qquad \text{Equation 3.4}$$

where $m = \dfrac{n\Sigma iT_i - \Sigma T_i \Sigma i}{n\Sigma i^2 - \left(\Sigma i\right)^2}$ Equation 3.5

and $b = \dfrac{\Sigma i^2 T_i - \Sigma i \Sigma i T_i}{n\Sigma i^2 - \left(\Sigma i\right)^2}$ Equation 3.6

The data was tabulated for each instrument and may be found in the "Instrument Qualification and Summary Report", which accompanies the discussion of each instrument in the Results chapter.

8. Short-Term Baseline Stability

The short-term baseline stability is monitored using the y-intercept value obtained in the spectrophotometric RMS noise calculations and it represents the transmittance averaged over a specified number of data points centered on a test wavelength. Deviation from 100% Transmittance is an indication of instability. Short-term baseline stability was monitored from the data recorded in the spectrophotometric noise test, as found in Table 3.12.

λ	y-intercept	Deviation, 100% T
300	100.4	0.4
400	99.2	-0.8
500	100.1	0.9
600	99.5	-0.5

Table 3.12: Summary table containing short-term baseline stability data where deviations from 100% Transmittance is an indication of short term baseline instability and may indicate a malfunction of the microscope spectrophotometer.

D. Procedures Used to Measure Instrument Intrinsic Polarization

The intrinsic polarization effects were measured by using either a substage condenser with a rotatable linear polarizer or a thin film polarizer placed on the specimen stage. In either case the linear polarizer was sequentially rotated five degrees and a corresponding intensity spectrum measured. The intensity values at 550 nm were plotted as a polar coordinate graph to illustrate the intrinsic polarization characteristics of the instrument configuration. Figure 3.21 illustrates the polarization effects of a 300 groove/mm grating. The polarization for the two CRAIC Technologies, Inc., instruments was not measured because both systems use a high intensity high-pressure xenon lamp source that destroys a thin-film absorption polarizer and a Glan-Thompson or other prism-type polarizer was not available at the time.

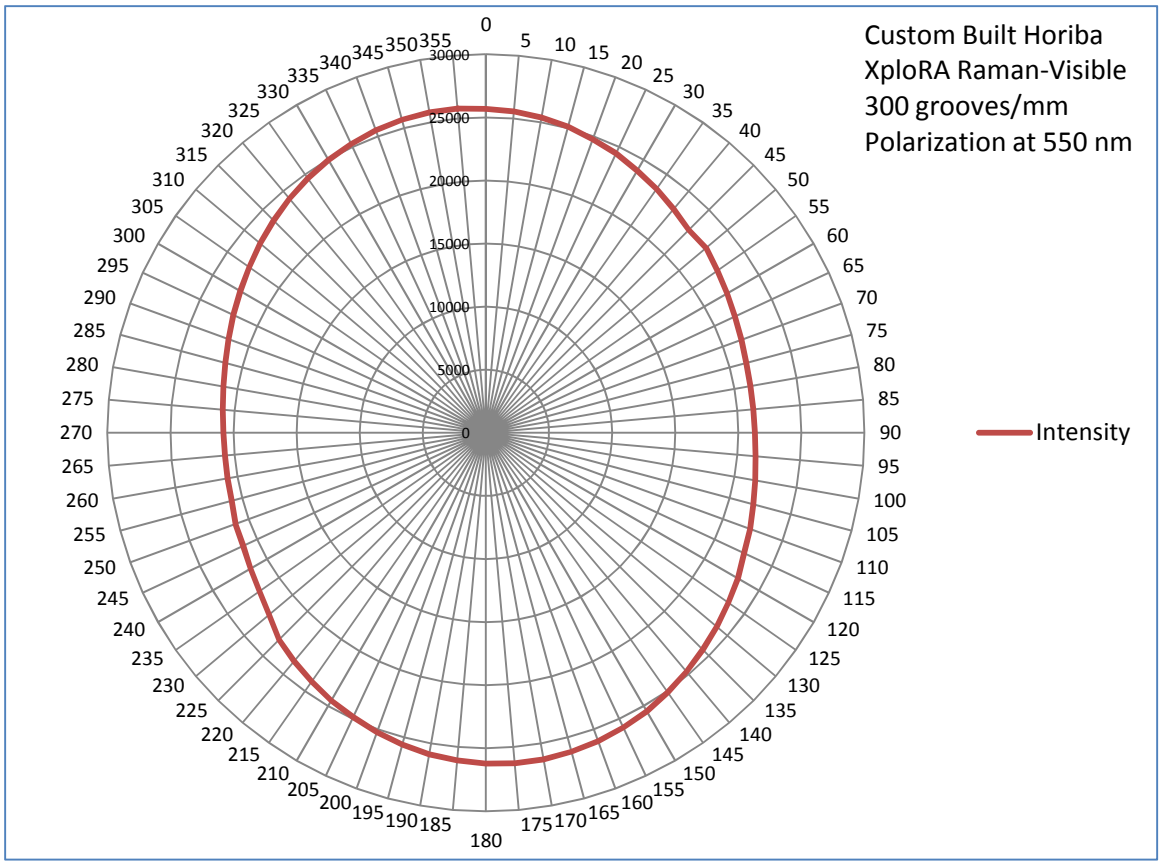

Figure 3.21: A polar plot of the intensity versus degree of orientation of the linear polarizer. The zero (0) position is equal to the polarizer being positioned in the east-west (EW) position. The polarization ration of the grating is determined by dividing the long axis by the short axis. The polarization ratio for this grating is approximately 1.3:1.

E. Procedures Used for Spectral Processing

The Bouguer-Beer-Lambert Law states that both a linear and direct relationship exists between a specimen's pathlength or thickness, its concentration, and its absorbance of electromagnetic radiation at a particular wavelength. In reality, it is not always possible to collect spectra from forensically significant specimens at a constant pathlength. For example, the thickness of a naturally occurring fiber may vary by a few tens of micrometers along its length, while man-made polymeric fibers extruded under very controlled conditions may vary in thickness by a several micrometers along its length. These changes in pathlength present themselves in ultraviolet-visible spectra as changes in detector response that are not related to concentration. Several spectrum preprocessing techniques have been developed to account

for instrumental and specimen variations. These techniques include baseline correction, peak-fitting, normalization, assessment of spectral quality, and spectral match criteria.

1. Baseline Correction

The spectra in this research were baseline corrected as a function of peak-fitting. Peak-fitting is described in more detail next.

2. Peak-Fitting Function

Mixed Gaussian-Lorentzian peak-fitting was used to determine peak positions, widths, heights, and areas of a set of overlapping peaks, which may result from multi-component fiber dyes. The peak-fitting function also applied a baseline correction thereby eliminating a separate procedure.

3. Normalization

Normalizing by either peak area or peak height was performed in order to put all spectra on the same scale.

4. Assessment of Spectral Quality

Data acquisition parameters and instrument conditions were recorded and included with the spectrum for comparison and valid interpretation.

F. Procedures Used to Measure Dichroism

If the specimen was a fiber, the fiber was aligned east-west (EW) on the microscope stage and the polarizer was aligned parallel to the fiber's long axis in the EW direction. A background ($I_{0\text{-parallel}}$) single-beam spectrum was collected next to the fiber. The fiber was moved into place for analysis. A parallel (I-para) single-beam spectrum of the fiber was collected. The polarizer was rotated 90 degrees. A perpendicular (I-perp) single-beam spectrum of the fiber was collected. The fiber was moved and a background ($I_{0\text{-perpendicular}}$) single-beam spectrum was collected. The parallel absorbance spectrum (A_0)

was calculated. The perpendicular absorbance spectrum (A_{90}) was calculated. The LD was calculated in accordance with Equation 1.11 and the DR was calculated in accordance with Equation 1.12.

G. Match Criteria for Comparing Spectra

An evaluation of a possible match criterion was conducted on the reference set of color dyed polyester fibers using the average of multiple measurements with a one standard deviation envelope over the spectral range. Figure 3.22 illustrates an average and one standard deviation envelope for the spectral range of a polyester fiber measured at 10 locations along one fiber.

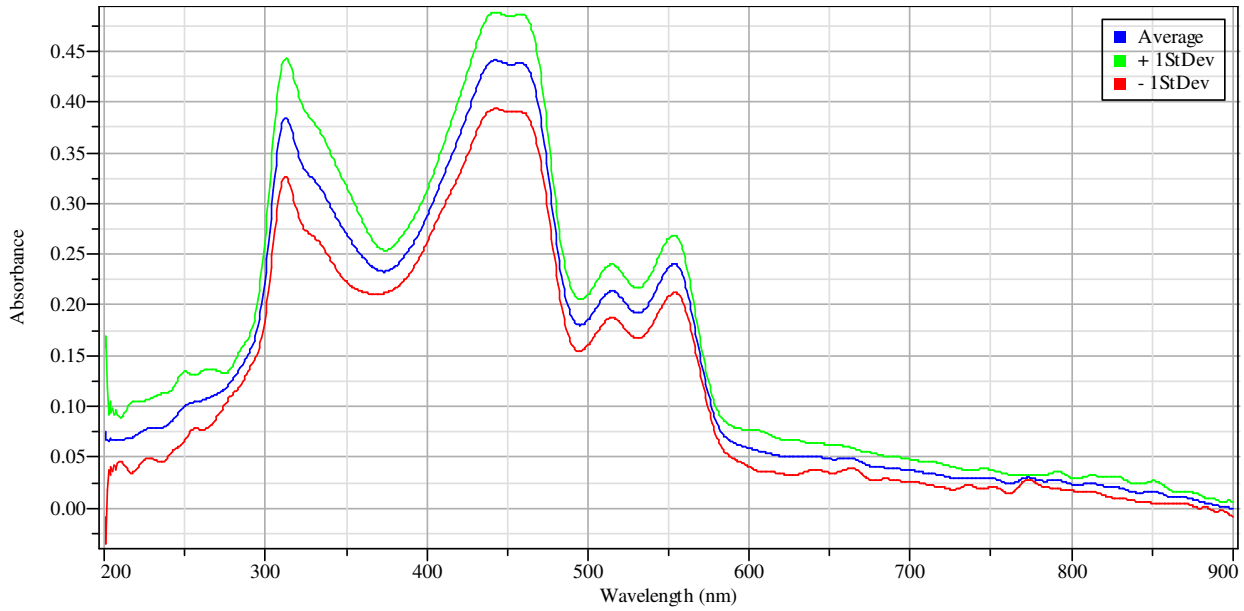

Figure 3.22: Plot illustrating the spectral match criteria using the average (blue trace) and +1 standard deviation (green trace) and –1 standard deviation (red trace) envelope, over the complete spectral range of 200 – 900 nanometers.

The

CHAPTER 4. RESULTS

A. Microscope Photometer Systems and Instrument Qualifications and Summary Reports

1. CRAIC Technologies, Inc., QDI 2010 System 1

Instrument Qualification and Summary Report

Instrument Description

Manufacturer: CRAIC Technologies, Inc.	Serial Number: 20090630 UA3
Model: QDI 2010, system 1	Illumination: Xenon, XB0 75
Beam Geometry: Single	Monochromator / Spectrometer: Post Specimen

Instrument Performance

Reference Material Used:	**Reference Material Used:**
Ocean Optics® CAL2000™ Hg-Ar	**Edmund Optics®, OD stepped slide**
Certificate Number (Date): **33057-33085 (23 Feb 2011)**	**Certificate Number and Date:**

Wavelength Accuracy & Precision (N=8)

Reference λ, (nm)	Mean (nm)	Difference (nm)	Standard Deviation
253.65	253.0	0.6	0.280
435.93	435.5	0.4	0.000
546.07	545.5	0.5	0.000
763.51	763.0	0.5	0.000

Photometric Accuracy & Precision (N=5)

Reference Abs	Mean, Abs	Difference Abs	Standard Deviation
400 nm, 0.93	0.81	0.12	0.031
500 nm, 0.93	0.87	0.06	0.026
600 nm, 0.93	0.88	0.05	0.022
700 nm, 0.93	0.88	0.05	0.017

Short-term Baseline Stability, 100% T (N=12)

Wavelength	Value	Deviation
300 nm	99.9	-0.1
400 nm	99.9	-0.1
500 nm	100.2	0.2
600 nm	100.1	0.1

Photometric Noise (RMS) at 100% T (N=12)

Wavelength	RMS noise
300 nm	1.15×10^{-2}
400 nm	1.60×10^{-3}
500 nm	2.64×10^{-3}
600 nm	2.71×10^{-3}

Spectral Resolution Dependence on Wavelength

Reference Material		**Photometric Linearity**				
		Step	**Reference**	**500 nm**	**600 nm**	**700 nm**
Measured Value, FWHM		1	0.04	0.04	0.00	0.06
Wavelength	Resolution	2	0.34	0.29	0.26	0.26
253.65 nm	4.7 nm	3	0.63	0.58	0.59	0.59
546.07 nm	3.5 nm	4	0.93	0.87	0.89	0.89
760.15 nm	3.9 nm	5	1.22	1.19	1.18	1.16
		6	1.52	1.52	1.47	1.43
		7	1.82	1.89	1.79	1.72
		8	2.11	2.19	2.04	1.95

Table 4.1: Summary table containing instrument performance and qualification data for a CRAIC Technologies, Inc., QDI 2010 System 1. See Appendix I for supporting spectra and data tables.

2. CRAIC Technologies QDI 2010 System 2

Instrument Qualification and Summary Report

Instrument Description

Manufacturer: CRAIC Technologies, Inc.	Serial Number: 20081016 UA3
Model: QDI 2010, system 2	Illumination: Xenon, XB0 75
Beam Geometry: Single	Monochromator / Spectrometer: Post Specimen

Instrument Performance

Reference Material Used:	**Reference Material Used:**
Ocean Optics® CAL2000™ Hg-Ar	**Edmund Optics®, OD stepped slide #1, step #4**
Certificate Number (Date): **33057-33085 (23 Feb 2011)**	**Certificate Number and Date:**

Wavelength Accuracy & Precision (N=9)				**Photometric Accuracy & Precision (N=5)**			
Reference λ, (nm)	Mean (nm)	Difference (nm)	Standard Deviation	Reference Abs	Mean, Abs	Difference Abs	Standard Deviation
253.65	252.2	1.46	0.000	400 nm, 0.93	0.85	0.08	0.004
435.93	434.5	1.4	0.000	500 nm, 0.93	0.89	0.04	0.006
546.07	544.6	1.4	0.000	600 nm, 0.93	0.89	0.04	0.006
763.51	761.8	1.7	0.000	700 nm, 0.93	0.89	0.04	0.006

Short-term Baseline Stability, 100% T, (N=10)			**Photometric Noise (RMS) at 100% T (N=10)**	
Wavelength	Value	Deviation	Wavelength	RMS noise
400 nm	100.4	0.4	400 nm	3.97×10^{-03}
500 nm	100.2	0.2	500 nm	5.19×10^{-03}
600 nm	99.8	-0.2	600 nm	1.60×10^{-03}
700 nm	100.9	0.9	700 nm	7.15×10^{-03}

Spectral Resolution Dependence on Wavelength		**Photometric Linearity**				
Reference Material		**Step**	**Reference**	**500 nm**	**600 nm**	**700 nm**
Measured Value, FWHM		1	0.04	0.06	0.06	0.06
Wavelength	Resolution	2	0.34	0.29	0.25	0.26
253.65 nm	6.2 nm	3	0.63	0.58	0.59	0.59
546.07 nm	3.8 nm	4	0.93	0.87	0.90	0.90
760.15 nm	4.8 nm	5	1.22	1.19	1.18	1.16
		6	1.52	1.52	1.47	1.43
		7	1.82	1.89	1.79	1.72
		8	2.11	2.19	2.04	1.95

Table 4.2: Summary table containing instrument performance and qualification data for a CRAIC Technologies, Inc. QDI 2010 System 2. See Appendix II for supporting spectra and data tables.

3. Zeiss MPM400-MSP65 System

Instrument Qualification and Summary Report

Instrument Description

Manufacturer: ZEISS	Serial Number: 454328-000
Model: MPM400-MSP65	Illumination: Tungsten, 100W, Quartz Halogen Mercury, HBO100 W/2
Beam Geometry: Single	Monochromator / Spectrometer: Post Specimen

Instrument Performance

Reference Material Used:				**Reference Material Used:**			
Ocean Optics® CAL2000™ Hg-Ar				**Edmund Optics®, OD stepped slide**			
Certificate Number (Date): **33057-33085 (23 Feb 2011)**				**Certificate Number and Date:**			
Wavelength Accuracy & Precision (N=8)				**Photometric Accuracy & Precision (N=5)**			
Reference λ, (nm)	Mean (nm)	Difference (nm)	Standard Deviation	Reference Abs	Mean, Abs	Difference Abs	Standard Deviation
435.93	435.5	0.4	0.000				
546.07	545.5	0.5	0.000				
763.51	763.0	0.5	0.000				

Short-term Baseline Stability, 100% T (N=6)			**Photometric Noise (RMS) at 100% T (N=6)**	
Wavelength	Value	Deviation	Wavelength	RMS noise
400 nm	110.7	10.7	400 nm	0.9453
500 nm	102.5	2.5	500 nm	0.3181
600 nm	88.1	11.9	600 nm	0.2021
700 nm	89.7	11.3	700 nm	0.3804

Spectral Resolution Dependence on Wavelength		**Photometric Linearity**				
Reference Material		**Step**	**Reference**	**500 nm**	**600 nm**	**700 nm**
Measured Value, FWHM		1	0.04			
Wavelength	Resolution	2	0.34			
253.65 nm	4.7 nm	3	0.63			
546.07 nm	3.8 nm	4	0.93			
579.07 nm	2.1 nm	5	1.22			
		6	1.52			
		7	1.89			
		8	2.19			

Table 4.3: Summary table containing instrument performance and qualification data for a Zeiss MPM400-MSP65 visible light microscope photometer system. See Appendix III for supporting spectra and data tables.

4. Custom Built HORIBA XploRA Raman-Visible Microspectrometer

Instrument Qualification and Summary Report

Instrument Description

Manufacturer: HORIBA	Serial Number: X/7/80 2010,October
Model: XploRA	Illumination: Tungsten, 100W, Quartz Halogen, Mercury, HBO 100 W/25
Beam Geometry: Single	Monochromator / Spectrometer: Post Specimen

Instrument Performance

Reference Material Used:	**Reference Material Used:**
Ocean Optics® CAL2000™ Hg-Ar	**Edmund Optics®, OD stepped slide**
Certificate Number (Date): **33057-33085 (23 Feb 2011)**	**Certificate Number and Date:**

Wavelength Accuracy & Precision (N=10)				**Photometric Accuracy & Precision (N=10)**			
Reference λ, (nm)	Mean (nm)	Difference (nm)	Standard Deviation	Reference Abs	Mean, Abs	Difference Abs	Standard Deviation
435.93	438.0	2.1	0.000	400 nm, 0.93	0.89	0.04	0.047
546.07	548.2	2.1	0.000	500 nm, 0.93	0.86	0.07	0.026
763.51	765.9	2.3	0.000	600 nm, 0.93	0.87	0.06	0.022
772.42	774.8	2.2	0.000	700 nm, 0.93	0.87	0.06	0.018

Short-term Baseline Stability, 100% T (N=10)			**Photometric Noise (RMS) at 100% T (N=10)**	
Wavelength	Value	Deviation	Wavelength	RMS noise
500 nm	99.1	-0.9	500 nm	4.03×10^{-02}
600 nm	100.2	0.2	600 nm	2.38×10^{-02}
700 nm	100.3	0.2	700 nm	5.34×10^{-02}

Spectral Resolution Dependence on Wavelength		**Photometric Linearity**				
Reference Material		**Step**	**Reference**	**500 nm**	**600 nm**	**700 nm**
Measured Value, FWHM		1	0.04	0.03	0.03	0.03
Wavelength	Resolution	2	0.34	0.27	0.27	0.27
435.93 nm	0.6 nm	3	0.63	0.57	0.57	0.58
546.07 nm	0.9 nm	4	0.93	0.86	0.87	0.87
763.51 nm	0.6 nm	5	1.22	1.18	1.17	1.16
		6	1.52	1.50	1.46	1.42

Table 4.4: Summary table containing instrument performance and qualification data for a HORIBA XploRA Raman-visible microspectrometer. See Appendix IV for supporting spectra and data tables.

5. Custom Built Olympus BX51TRF Polarized Light and Fluorescence Microscope with a HORIBA VS140™ UV-Visible Fiber Optic Spectrometer.

Instrument Qualification and Summary Report

Instrument Description

Manufacturer: HORIBA	Serial Number: VS140 – DEM 03
Model: VS140	Illumination: Tungsten, 12V/100W, Quartz Halogen, Mercury HBO 100 2/W
Beam Geometry: Single	Monochromator / Spectrometer: Post Specimen

Instrument Performance

Reference Material Used:	**Reference Material Used:**
Ocean Optics® CAL2000™ Hg-Ar	**Edmund Optics®, OD stepped slide**
Certificate Number (Date): **33057-33085 (23 Feb 2011)**	**Certificate Number and Date:**

Wavelength Accuracy & Precision (N=8)				**Photometric Accuracy & Precision (N=5)**			
Reference λ, (nm)	Mean (nm)	Difference (nm)	Standard Deviation	Reference Abs	Mean, Abs	Difference Abs	Standard Deviation
253.65	253.0	0.6	0.000	400 nm, 0.93	0.93	0.12	0.031
435.93	435.5	0.4	0.000	500 nm, 0.93	0.87	0.06	0.026
546.07	545.5	0.5	0.000	600 nm, 0.93	0.88	0.05	0.022
763.51	763.0	0.5	0.000	700 nm, 0.93	0.88	0.05	0.017

Short-term Baseline Stability, 100% T			**Photometric Noise (RMS) at 100% T**	
Wavelength	Value	Deviation	Wavelength	RMS noise
300 nm	100.4	0.4	300 nm	0.0422
400 nm	99.0	-0.8	400 nm	0.0162
500 nm	100.1	0.1	500 nm	0.0109
600 nm	99.5	-0.5	600 nm	0.0066

Spectral Resolution Dependence on Wavelength		**Photometric Linearity**				
Reference Material		**Step**	**Reference**	**500 nm**	**600 nm**	**700 nm**
Measured Value, FWHM		1	0.04	0.04		
Wavelength	Resolution	2	0.34	0.29		
253.65 nm	1.8 nm	3	0.63	0.58		
546.07 nm	1.7 nm	4	0.93	0.87		
760.15 nm	1.9 nm	5	1.22	1.19		
		6	1.52	1.52		
		7	1.89	1.89		
		8	2.19	2.19		

Table 4.5: Summary table containing instrument performance and qualification data for an Olympus BX51TRF polarized light transmission, refection, and fluorescence microscope with an HORIBA VS140 UV-visible fiber optic spectrometer. See Appendix V for supporting spectra and data tables.

6. Custom Built Olympus BH-BHA-RFA Polarized Light Transmission and Fluorescence Microscope with an Ocean Optics® USB2000+™ UV-Visible Fiber Optic Spectrometer.

Instrument Qualification and Summary Report

Instrument Description

Manufacturer: Ocean Optics, Inc	Serial Number: 20090630 UA3
Model: USB-2000+	Illumination: Tungsten, 50W, Quartz Halogen
Beam Geometry: Single	Monochromator / Spectrometer: Post Specimen

Instrument Performance

Reference Material Used:	**Reference Material Used:**
Ocean Optics® CAL2000™ Hg-Ar	**Edmund Optics®, OD stepped slide**
Certificate Number (Date): **33057-33085 (23 Feb 2011)**	**Certificate Number and Date:**

Wavelength Accuracy & Precision (N=10)				**Photometric Accuracy & Precision (N=10)**			
Reference λ, (nm)	Mean (nm)	Difference (nm)	Standard Deviation	Reference Abs	Mean, Abs	Difference Abs	Standard Deviation
365.02	364.7	0.3	0.000	500 nm, 0.93	0.90	0.03	0.017
404.66	404.1	0.5	0.000	600 nm, 0.93	0.94	0.01	0.013
546.07	545.2	0.8	0.000	700 nm, 0.93	0.97	0.04	0.040
763.51	762.3	1.2	0.000				

Short-term Baseline Stability, 100% T (N=10)			**Photometric Noise (RMS) at 100% T (N=10)**	
Wavelength	Value	Deviation	Wavelength	RMS noise
500 nm	108.7	8.7	500 nm	0.2259
600 nm	90.4	-9.6	600 nm	0.1704
700 nm	104.3	4.3	700 nm	0.2426

Spectral Resolution Dependence on Wavelength		**Photometric Linearity**				
Reference Material		**Step**	**Reference**	**500 nm**	**600 nm**	**700 nm**
Measured Value, FWHM		1	0.04			
Wavelength	Resolution	2	0.34	0.33	0.35	0.39
253.65 nm	4.7 nm	3	0.63	0.57	0.60	0.64
546.07 nm	3.8 nm	4	0.93	0.90	0.94	0.97
		5	1.22	1.23	1.26	1.29
		6	1.52	1.56	1.56	1.59
		7	1.89	1.92	1.88	1.91
		8	2.19			

Table 4.6: Summary table containing instrument performance and qualification data for an Olympus BH-BHA-RFA polarized light and fluorescence microscope with an Ocean Optics® USB-2000+™ UV-visible fiber optic spectrometer. See Appendix VI for supporting spectra and data tables.

Figures of Merit Results for all Six Microscope Spectrophotometer Systems						
	1	**2**	**3**	**4**	**5**	**6**
Spectrometer wavelength (λ) range (nm)	**200 – 900**	**200 – 900**	**380 – 750**	**425 – 800**	**190 – 800**	**200 – 850**
Wavelength (λ) accuracy (nm), average value	**(N=8)** **0.5**	**(N=8)** **1.5**	**(N=8)** **1.4**	**(N=10)** **2.1**	**(N=10)** **1.1**	**(N=10)** **0.7**
Wavelength (λ) precision (nm), average value	**0.000**	**0.000**	**0.000**	**0.000**	**0.000**	**0.000**
Photometric accuracy (abs), average value	**(N=5)** **0.07**	**(N=5)** **0.05**		**(N=10)** **0.05**	**(N=10)** **0.04**	**(N=10)** **0.02**
Photometric precision (abs), average	**0.024**	**0.005**		**0.028**	**0.009**	**0.023**
Short –term stability, 100%T, average value	**(N=12)** **0.1**	**(N=10)** **0.3**	**(N=6)** **9.1**	**(N=10)** **0.5**	**(N=10)** **0.4**	**(N=10)** **3.4**
RMS Noise, 100%T, average value	**(N=12)** **0.189**	**(N=10)** **0.449**	**(N=6)** **0.461**	**(N=10)** **0.117**	**(N=10)** **0.121**	**(N=10)** **0.212**
Spectral resolution dependence on wavelength (λ) **Measured FWHM (nm)**	**253.65 = 4.7 nm** **546.07 = 3.5 nm** **760.15 = 3.9 nm**	**253.65 = 6.2 nm** **546.07 = 3.8 nm** **760.15 = 4.8 nm**	**435.85 = 4.7 nm** **546.07 = 3.8 nm** **579.07 = 2.1 nm**	**435.93 = 0.6 nm** **546.07= 0.9 nm** **763.51 = 0.6 nm**	**253.65 = 1.8 nm** **546.07 = 1.7 nm** **760.15 = 1.9 nm**	**435.93 = 1.2 nm** **546.07 = 1.2 nm** **810.43 = 1.4 nm**

Table 4.7: Summary table containing results of the figures of merit data for all six microscope spectrophotometer systems.

B. Microscope Configurations for Specimen Masking

1. Specimen Masking with Mirror Beamsplitter in the Primary Image Plane

An intuitive and convenient fixed-position measurement masking system was developed by Vincent J. Coates, founder of Nanometrics, Incorporated, 1975. The system used a stationary mirror with a non-mirrored section placed in the illumination path that acts as a beamsplitter to send the reflected image to a video camera and a portion equal to the non-mirrored area transmitted to the spectrophotometer for analysis. This system design is very robust in that the fixed-hole mirror is stationary, but adjustable to allow optimum alignment of the optical system. Figure 4.1 illustrate the selector knob on the CRAIC Technologies Incorporated, QDI 2010 system in which the operator uses it to select the desired measuring mask mirror. Not all commercial microscope photometer systems available on the market today use a mirror beamsplitter mask. These instruments will be discussed in the next two sections.

Figure 4.1: Selection knob located on the right side of the CRAIC Technologies Inc., QDI 2010 microspectrophotomer used to position one of six fixed-diaphragm mirrored specimen image mask.

Figure 4.2 illustrates each of the six fixed-diaphragm mirrors used in the CRAIC Technologies Inc., QDI 2010 microspectrophotometer of which the operator must select one as a specimen mask.

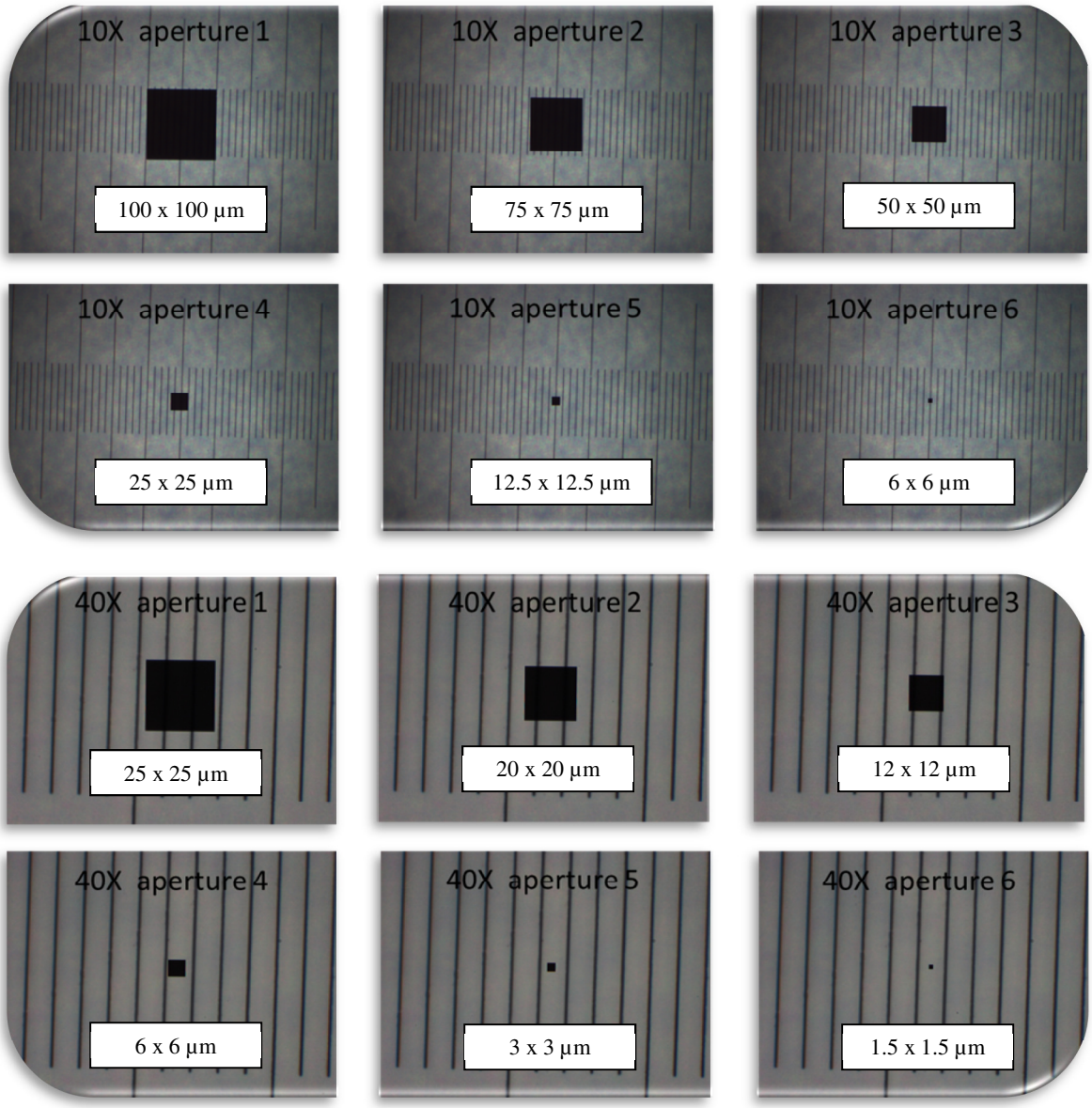

Figure 4.2: Fixed-size mirror diphragms used in CRAIC Technologies Incorporated, QDI 2010 microspectrophotometer. The set of images on the top are representative of the actual collection size using a 10x objective while the images on the bottom illustrate the collection size using a 40x objective. The parallel vertical lines in each image are from a stage micrometer used to calibrate the gratiducle in the ocular in order to make optical measurements. Each line increment reperesent 10 micrometers.

The development of the mirrored diaphragm was a technological advancement that allowed visualization of the area being analyzed while providing a useful way to document the specific area on a specimen that was analyzed. This design greatly improved photomircrograph documentation in forensic science applications. The only drawback to this system is that the dark area present in the image which

is selected for analysis is permanently present in the image. Wherease, with other configurations, the photomicrographic image does not have the permanent obscuration. Other commerically available instruments such as the J & M Analytik AG, Tidas MSP 400/800 series microspectrometer systems, uses a computer software calibrated digital imaging to virtually meaure the visualized region of interest for analysis (Kubin, personal communication). In the two custom designed fiber optic instruments, a fiber optic with a fixed diameter was positioned at the intermediate image plane, which effectively defines the image mask or area of analysis based on the fiber core diameter and the objective maginfication.

2. Specimen Masking with Fiber Optic Apertures in the Intermediate Image Plane

The first fiber optic instrument was the custom built Olympus BX51TRF polarized light and fluorescence microscope with a HORIBA VS140 UV-visible fiber optic spectrometer. The fiber optic employed is an Ocean Optics® extreme solarization-resistant (part #: QP115-2-XSR), 115 micrometer diameter, single core, two meters long, and has SMA connectors. This fiber optic links the HORIBA VS140 UV-visible spectrometer to the trinocular head phototube attachment that was modified to accept an SMA fiber optic adapter. This adapter and configuration is illustrated in Figure 4.3.

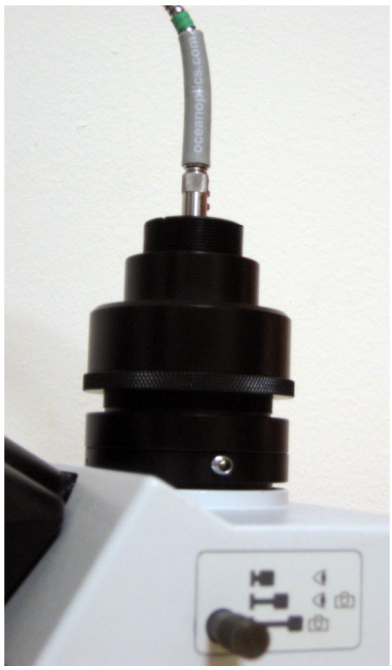

Figure 4.3: Fiber optic connection via trinocular head phototube adapter with an SMA connector. The adapter is capable of being vertically adjusted (and locked into position) in order to bring the tip of the fiber optic into sharp focus in the intermediate image plane, which is conjugate to the specimen plane.

The spot size of the specimen mask is determined by the magnification of the objective lens and the diameter of the fiber optic cable. Figure 4.4 illustrates the effective mask size for the 115 micrometer diameter fiber optic image mask, which was centered about a cross-hair reticule in the eyepiece.

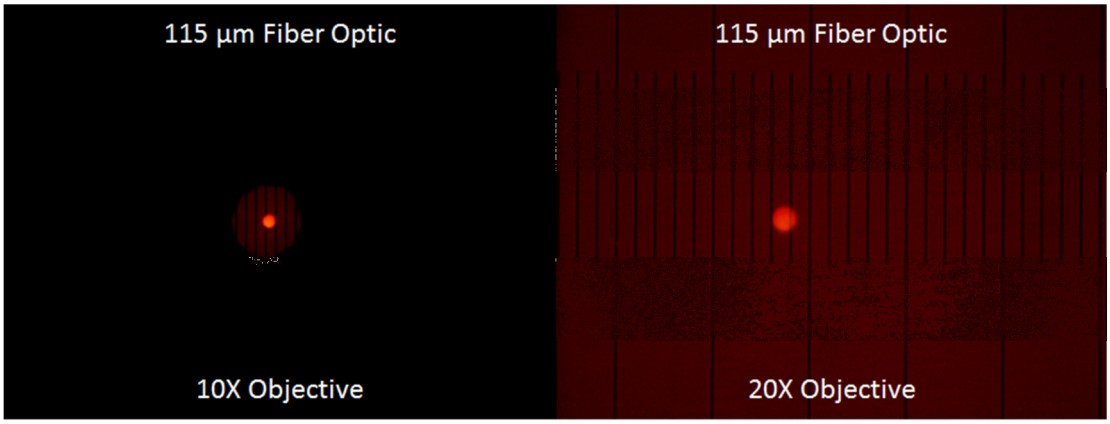

Figure 4.4: The effective analysis specimen mask spot size obtained using an Ocean Optics® extreme solarization-resistant, 115 micrometer diameter, single core, fiber optic in the conjugate intermediate image plane. The image on the left was collected with a 10x objective and with the filed diaphragm closed. The image on the right was collected using a 20x objective with the field diaphragm open. The parallel vertical lines in each image are from a stage micrometer used to calibrate the gratiducle in the ocular in order to make optical measurements. Each line increment reperesent 10 micrometers intervals.

The spot size was made visible by back-illuminating the fiber optic using a quartz-halogen lamp, while the red background color was obtained using a 656 nm interference filter placed over the transmission field lens and field diaphragm. The dimension of the field measuring diaphragm was determined by dividing the diameter of the fiber optic by the magnification of the objective. Therefore, the effective spot sizes for the 10x and 20x objectives are 11.5 and 5.75 micrometers, respectively. The only drawback to this configuration is that the measuring field mask is not visible as with the mirror mask configuration. The analyst must know the spot size associated with each objective being employed for a measurement so as to effectively select the correct measuring mask size.

The second fiber optic instrument was custom built Olympus BH-BHA-RFA polarized light and fluorescence microscope interfaced with an Ocean Optics® USB2000+™ UV-visible fiber optic spectrometer. The connection was accomplished using an Ocean Optics® solarization-resistant, 600 micrometer diameter, single core, two meter long fiber optic (part #: QP600-2-UV-VIS) with a SMA connector. The spectrometer functions were computer controlled using SpectraSuite™ software. Figure

4.5 illustrates the fiber optic SMA connector interface to the c-mount of the MTV-3 adaptor using a 3.3x NFK photo relay on top of an Olympus BH-2 series trinocular head.

Figure 4.5: Fiber optic SMA connection via an Olympus MTV-3 with a 3.3x NFK photo relay lens connected to an Olympus BH-2 series trinocular head. The SMA adapter is capable of being vertically adjusted inside of the outer black ring order to bring the tip of the fiber optic into sharp focus in the intermediate image plane, which is confocal to the specimen plane.

The spot size of the specimen mask was determined as outlined above. Figure 4.6 illustrates the effective mask size of the 600 micrometer diameter fiber optic specimen mask, which was centered about a cross-hair reticule in the right eyepiece. The images in Figure 4.6 were collected using a Nikon Coolpix 995 digital camera fixed in position at the Ramsden circle of the right ocular containing a linear graticule at the primary image plane.

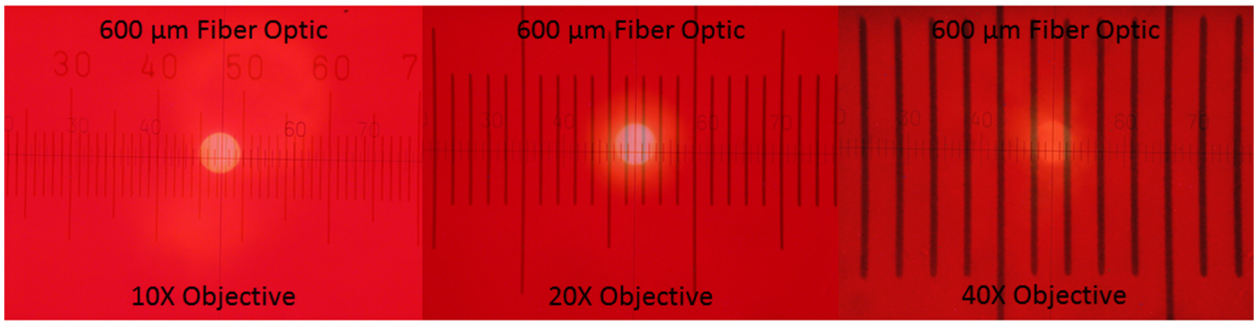

Figure 4.6: The effective analysis specimen mask spot size obtained using an Ocean Optics® two meter long, 600 micrometer diameter, single core, fiber optic in the conjugate intermediate image plane of the trinocular head. The image on the left was collected with a 10X objective, the center image was collected using a 20X objective, and the right image was collected using a 40X objective. All three images have two sets of parallel vertical lines. The first set, which appears the same size in all three images is the contribution from the graticule located at the primary image plane of the ocular. The second set, which appears increasing larger with increasing magnification is the contribution from the stage micrometer. Each stage micrometer increment reperesent 10 micrometers.

3. Specimen Masking with Variable Diaphragm in Intermediate Image Plane

The Zeiss MPM400-MSP65 microscope spectrophotometer system produces an image in the intermediate image plane, which is conjugate with the measuring field diaphragm illustrated in Figure 4.7. This intermediate image plane is conjugate to the specimen plane located at the stage of the microscope. The measuring area of interest was defined by using the variable measuring diaphragm to establish an area for analysis. During observation and system setup, the variable measuring diaphragm was reflected directly onto the specimen plane by inserting a pilot light behind the measuring diaphragm, as illustrated in Figure 4.8. The image of the measuring diaphragm was superimposed into the specimen plane, along with the conjugate field diaphragm from the illumination of the microscope. During spectrophotometric data collection, the pilot light was removed from the field and turned off to eliminate light scatter.

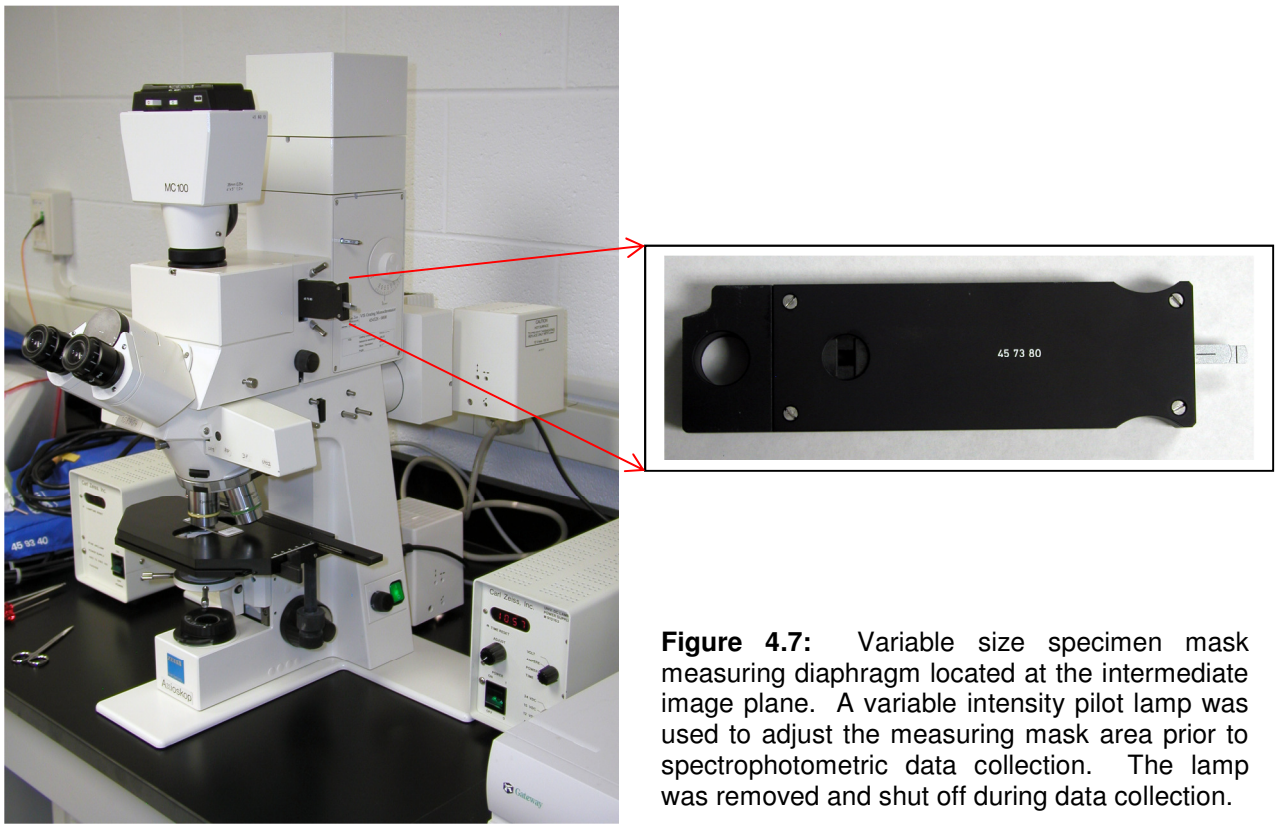

Figure 4.7: Variable size specimen mask measuring diaphragm located at the intermediate image plane. A variable intensity pilot lamp was used to adjust the measuring mask area prior to spectrophotometric data collection. The lamp was removed and shut off during data collection.

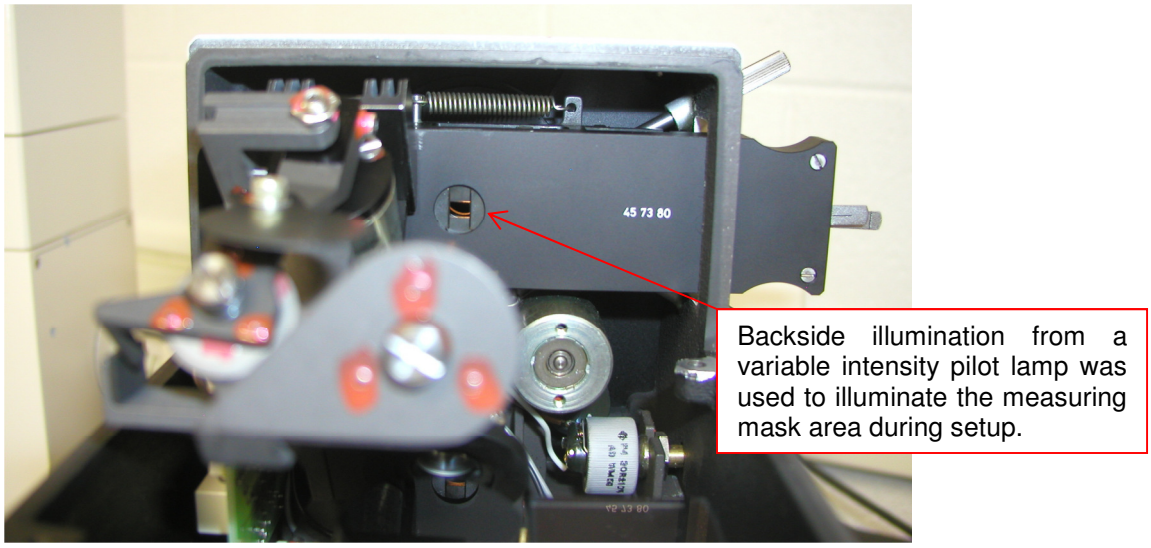

Figure 4.8: A variable intensity pilot lamp was used to adjust the measuring mask area prior to spectrophotometric data collection. The lamp was removed and shut off during data collection.

Many instruments (J&M Analytik and A.S. & Co.) use an adjustable, variable rectangular mask or variable round pinhole mask located in the intermediate image plane to select an area on the specimen from which to collect spectroscopic data. These instruments use back-illumination to image the variable mask onto the specimen prior to data collection.

4. Monorchromator Spectral Resolution

Spectrophotometric measurements are made using a post-specimen monochromator with a concave holographic grating. Monochromator spectral resolution was controlled using coupled entrance and exit slits, which are manually selected for 1 nm, 2.5 nm, 5 nm, 10 nm, and 20 nm spectral bandwidths. An image of the coupled spectral bandwidth selection lever is illustrated in Figure 4.9.

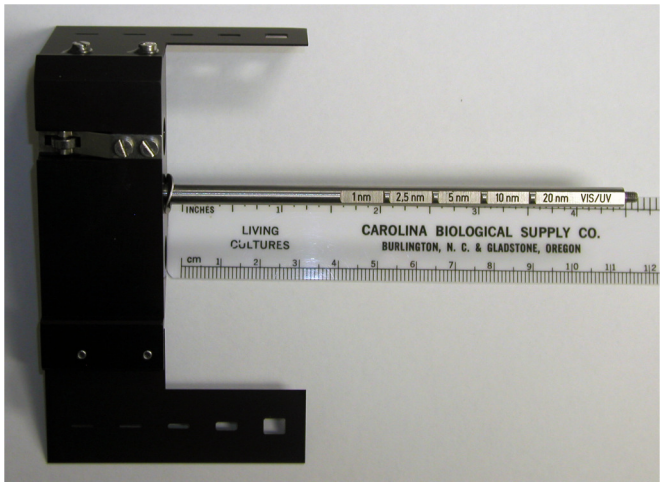

Figure 4.9: An image to illustrate the coupled fixed-size entrance and exit slits used in the monochromator. The slits at the bottom of the image are the entrance slits that allow light into the monochromator, while the slits at the top of the image are the exit slits that provide light image onto the entrance slit of the photomultiplier tube detector.

5. Variable Fixed-Size Illumination Field Masking

Under properly adjusted Köhler illuminator in the microscope images the lamp filament in the condenser entrance pupil or aperture diaphragm and the luminous field diaphragm in specimen plane at the stage. A rotating field diaphragm selector, as illustrated in Figure 4.10, is positioned in the field lens housing, and the operator selects from an open position, a 0.4 mm pinhole, a 0.25 mm pinhole, and a 0.1 mm pinhole.

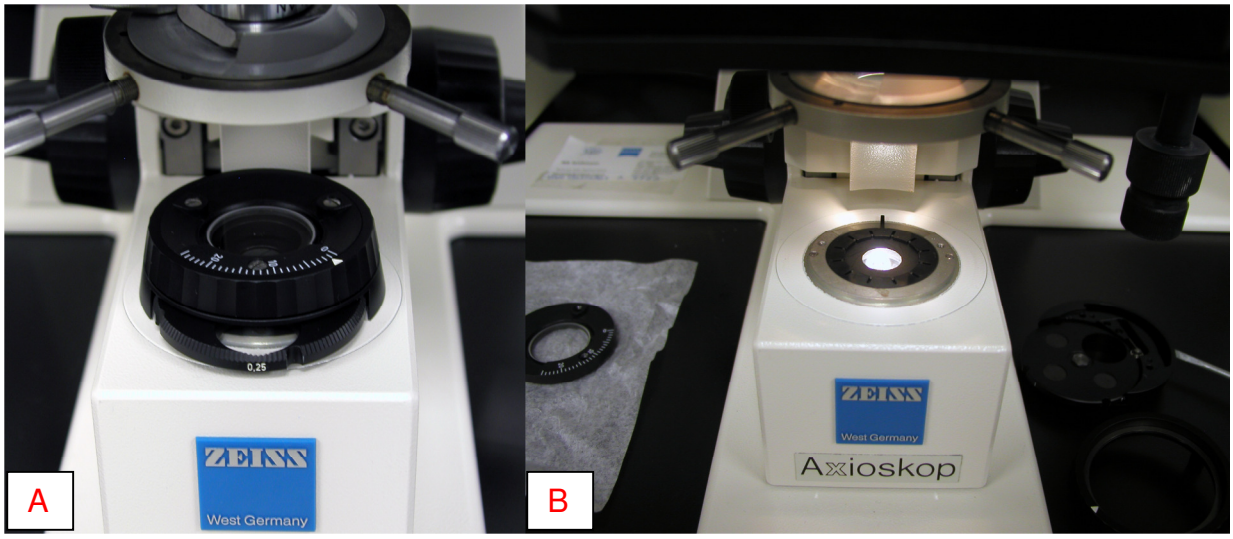

Figure 4.10: An image of the assembled (A) field diaphragm lens with manual selection of variable and fixed-size field diaphragm sizes, and an image of a disassembled (B) field diaphragm lens to illustrate the selection of luminous-field diaphragms which delimit the specimen field to be measured. As a luminous field diaphragm, they clearly limit the field size and reduce stray light in the specimen field to be illuminated and thereby make measurements of low contrast specimens possible.

Attributed mainly to internal reflections in the magnifying optical system, the light passing through the adjacent area of the minute specimen area may cause stray light that is added to the image of the specimen under examination, so that the measured spectrophotometric value of the transmittance is larger than the real transmittance value. This effect, which is especially large when the transmittance of the minute specimen area is small compared to the surrounding illuminating area; this is known as the Schwarzchild-Villiger effect (Naora, 1951). In order to reduce this effect, it is necessary to use a field masks that restrict the transmitted light to illuminate only the specimen under examination. Images of the actual field mask sizes are illustrated in Figure 4.11, while Figure 4.12 illustrates the effect of reducing the luminous field mask size on the quality of absorbance data obtained even though the measuring field diaphragm was fully open.

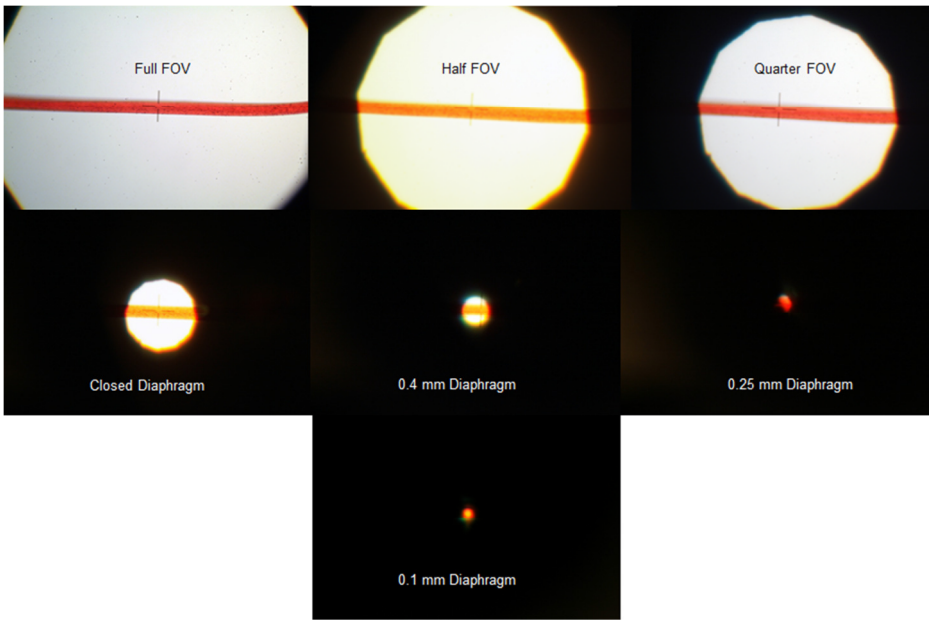

Figure 4.11: Images illustrating the variable and fixed-diameter luminous-field masks used in the Zeiss MPM400-MSP65 microscope spectrophotometer system.

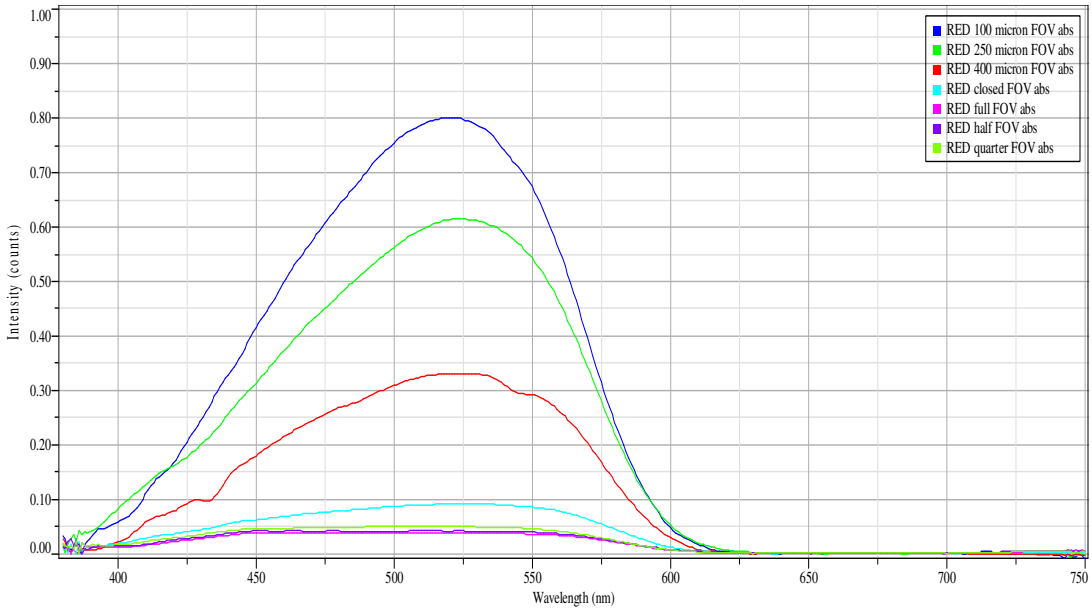

Figure 4.12: Overlay spectra of the red polyester fiber illustrated in Figure 4.11 collected using different luminous field mask sizes. Notice the increase absorbance peak intensity as the field diaphragm diameter becomes smaller, and fully encompasses the specimen. Note: the image measuring mask was fully open and was not a factor in the collection of this spectral data.

C. Instrument Intrinsic Polarization

An important an under-appreciated aspect of absorption of light by molecules lay in the fact that the chromophore has directional absorption characteristics. If a color dyed fiber is not randomly oriented, then the absorption of polarized light by the fiber dye may not be the same in all orientations relative to polarization direction. If the molecular transition dipole moment is parallel to the electric field vector of the plane of polarization of the light, then absorption will be maximal, while if the transition dipole moment is perpendicular to the electric field vector of the plane of polarization of the light then no absorption will occur (Michl and Thurstrup, 1986). This difference in absorption of light in a specimen with respect to the two perpendicular planes of polarization is known as linear dichroism.

Prior to the collection of dichroic spectra, it is necessary to determine the intrinsic polarization effects of the microscope photometer. All grating based spectrometers disperse a continuum spectrum based on a reflection-type diffraction grating. Diffraction gratings exhibit different polarizations due to the grating reflectivity efficiency differences for the two polarization directions: E_0 (E-parallel) and E_{90} (E-perpendicular), and depend on whether the electric field vector of the income light is either parallel to or

perpendicular to the grooves of the grating. The orientation may strongly effect the relative spectral intensity profiles of the spectra recorded. A grating's reflectivity efficiency profile is determined by the number of grooves per unit length (groove density, usually reported as grooves per millimeter) and the geometrical shape of the groove. The resulting reflectively efficiency profile spectrum is completely related to the grating physics. One contributing factor is the process used to make the grating which is a replica grating of a ruled grating or a holographically ruled grating produced by an etching process. The polarization response for any grating consists of two spectral curves: 1) the intensity parallel and 2) the intensity perpendicular. Sometimes a third curve is present with the polarization measurements equal to the average of the two polarization curves.

With this information known, if the intent is to measure orientation effects by measuring absorption differences (dichroism is discussed in more detail in Section D, below) of a forensically significant specimen, then being cognizant of the intrinsic polarization effects it is extremely important to minimize or eliminate these artifacts in the spectral measurements. These intrinsic polarization effects can be minimized by keeping the polarization characteristics fixed by using plane polarized illumination and by collecting a background (reference) intensity spectrum in each of the polarization positions which must then be ratioed with the corresponding specimen intensity spectrum in the same polarization direction. Therefore, two background spectra and two specimen spectra are required for each position being analyzed on the specimen.

The following data are single-beam intensity spectra to illustrate the grating reflectivity efficiency as a function of polarization direction for each specified microscope spectrophotometer. Corresponding polar plots illustrating reflectivity efficiency at 550 nm were selected to illustrate intrinsic instrument polarization artifacts at the wavelength at which the human eye is most efficient and most sensitive (Edisbury, 1967).

1. Zeiss MPM400-MSP65

The Zeiss MPM400-MSP65 system was equipped with a long working distance Achroplan, 20X/0.40 NA, infinity corrected objective. The system was not equipped to conduct polarized light measurements. To facilitate collection of intrinsic instrument polarization, a polar plot printed on a sheet

of white copy paper was centered and fixed to the microscope stage. A sheet linear polarizer was positioned on the microscope stage for data collection. The linear polarizer was rotated in 5 degree increments and a corresponding single beam intensity spectrum collected. A total of 72 spectra were collected and plotted in Figure 4.13.

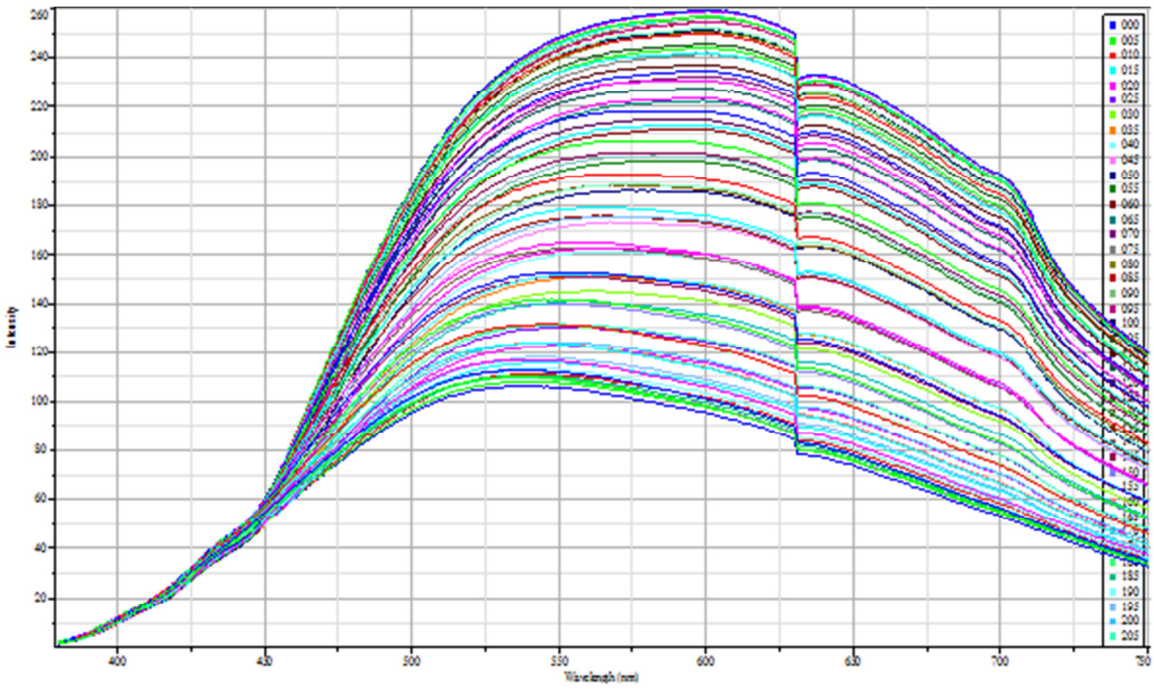

Figure 4.13: Zeiss MPM400-MSP65 - overlay of all seventy two individual single-beam reflectivity efficiency intensity spectra measured at 5 degree intervals from 0 to 355 degrees for the 1208 groves/mm grating.

A plot of the intensity values at 550 nm for each of the 72 polarization positions was produced as a polar plot. The polar plot illustrates the variation in reflectivity efficiency at a given wavelength. The polarization extremes are visually expressed by the intensity at a given polarization angle. The maximum intensities for the Zeiss MPM400-MSP65 1208 groove per millimeter grading is evident at 85 degrees and 265 degrees, while the minimum intensities are evident at 175 degrees and 355 degrees, respectively. The polarization ratio for this grating may be calculated by taking the average of the intensities along the long axis divide by the average of the intensities along the short axes. The polarization ratio for the grating at 550 nm, as illustrated in Figure 4.14, is approximately 2.5:1.

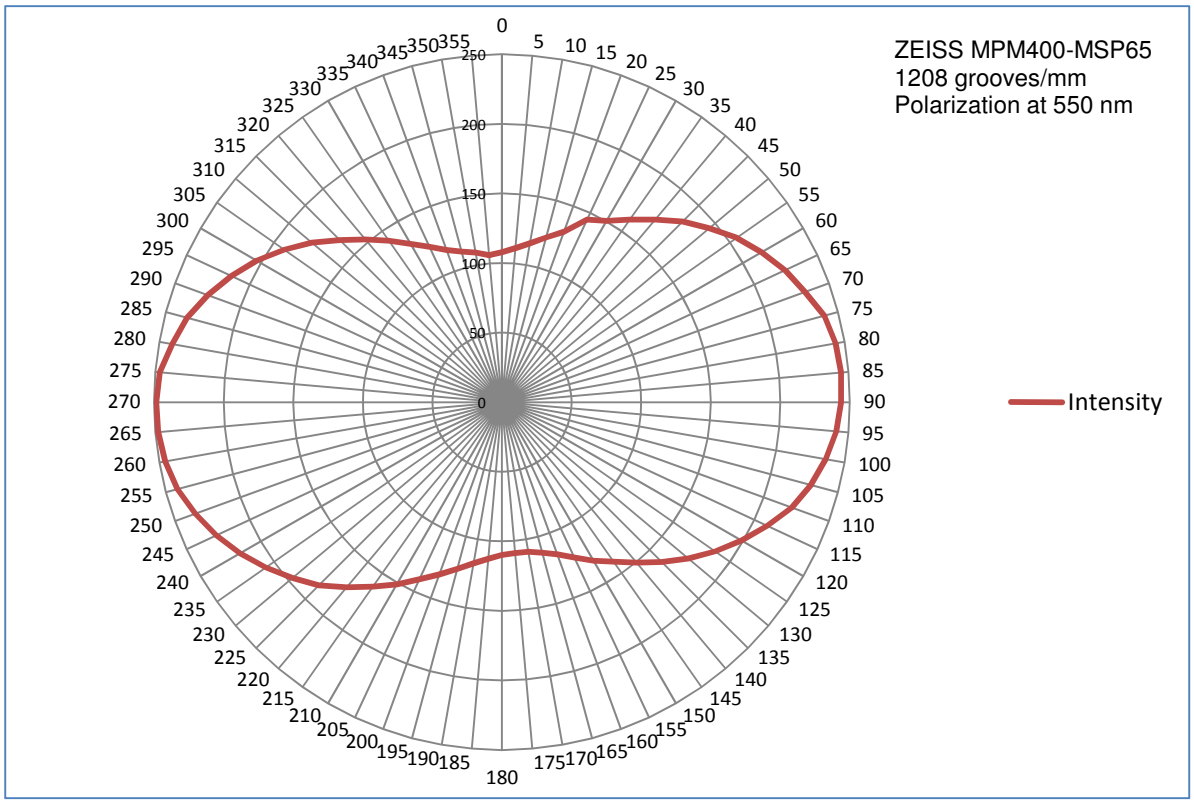

Figure 4.14: Zeiss MPM400-MSP65 - polar plot illustration of the polarization characteristics at 550nm for the 1208 grooves/mm grating.

2. Custom Built HORIBA XploRA Raman-Visible Microspectrometer

The custom built HORIBA XplorRA Raman-Visible microspectrometer was based on an Olympus BX51TFR polarized light, fluorescence, and reflectance microscope. Intrinsic instrument polarization measurements were facilitated using a polarized light condenser, which contained a rotatable polarizer. The linear polarizer was rotated in 5 degree increments and a corresponding single beam intensity spectrum collected for each of the four gratings: 1) 300 g/mm, 2) 600 g/mm, 3) 1200 g/mm, and 4) 1800 g/mm. A total of 72 spectra were collected and plotted for each grating, Figures 4.15, 4.17, 4.19, and 4.21. Notice the relatively small differences in reflectivity efficiency of the 300 groove per millimeter grating as compared to grating with higher groove density (more grooves per millimeter) as illustrated in Figure 4.13 and Figure 4.19. In addition, a polar plot was generated for each of the four gratings and may be viewed in Figures 4.16, 4.18, 4.20, and 4.21.

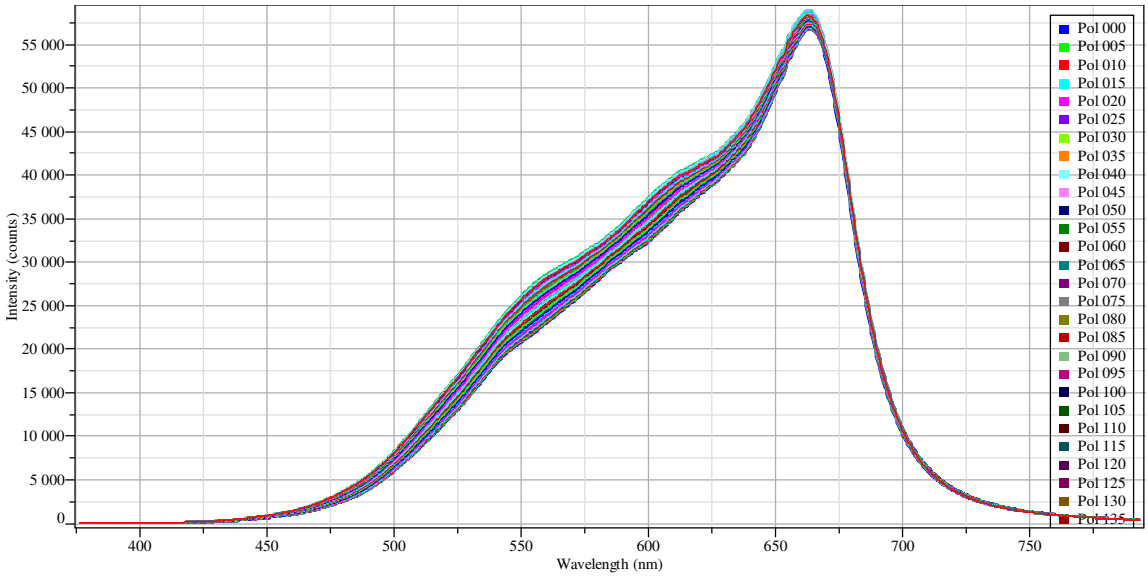

Figure 4.15: Custom built HORIBA XploRA Raman-Visible spectrometer - overlay of all seventy two individual single-beam reflectivity efficiency intensity spectra measured at 5 degree intervals from 0 to 355 degrees for the 300 groves/mm grating.

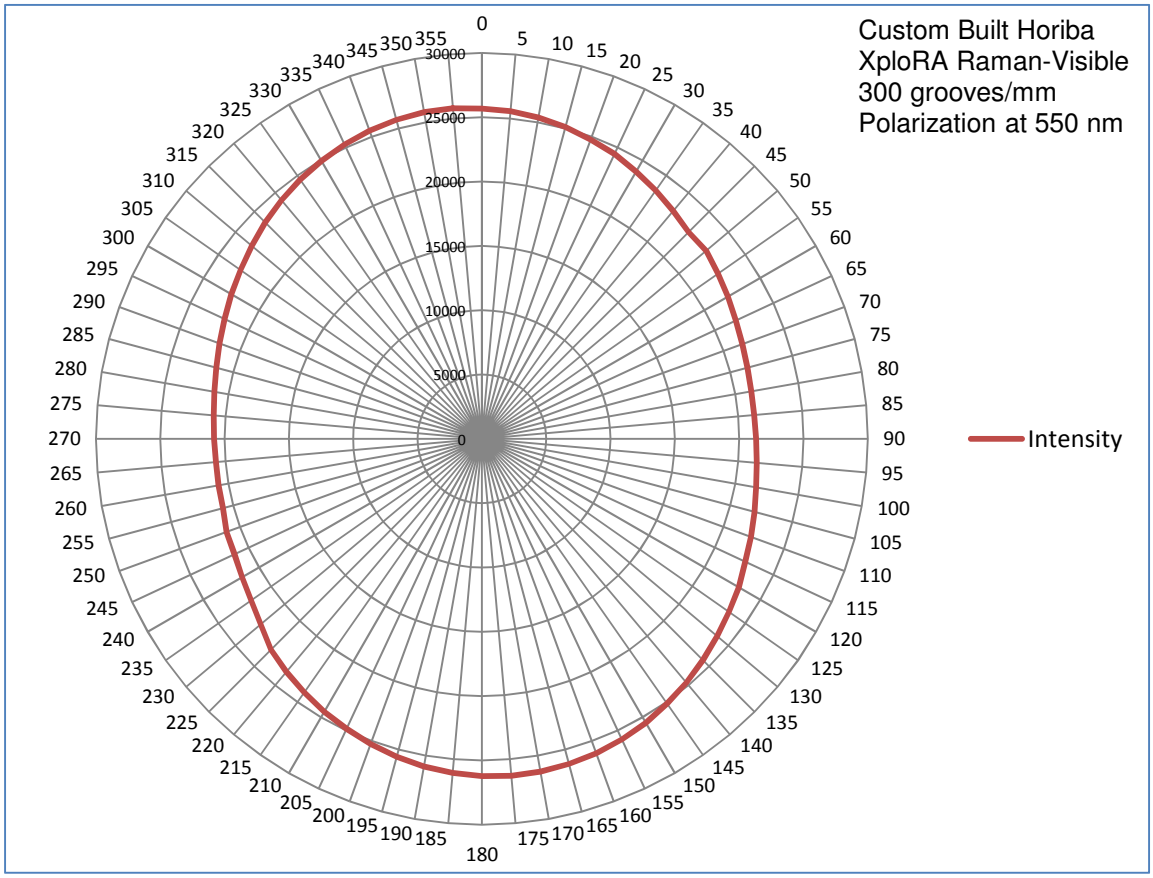

Figure 4.16: Custom built HORIBA XploRA Raman-Visible - polar plot illustration of the polarization characteristics at 550nm of the 300 grooves/mm grating.

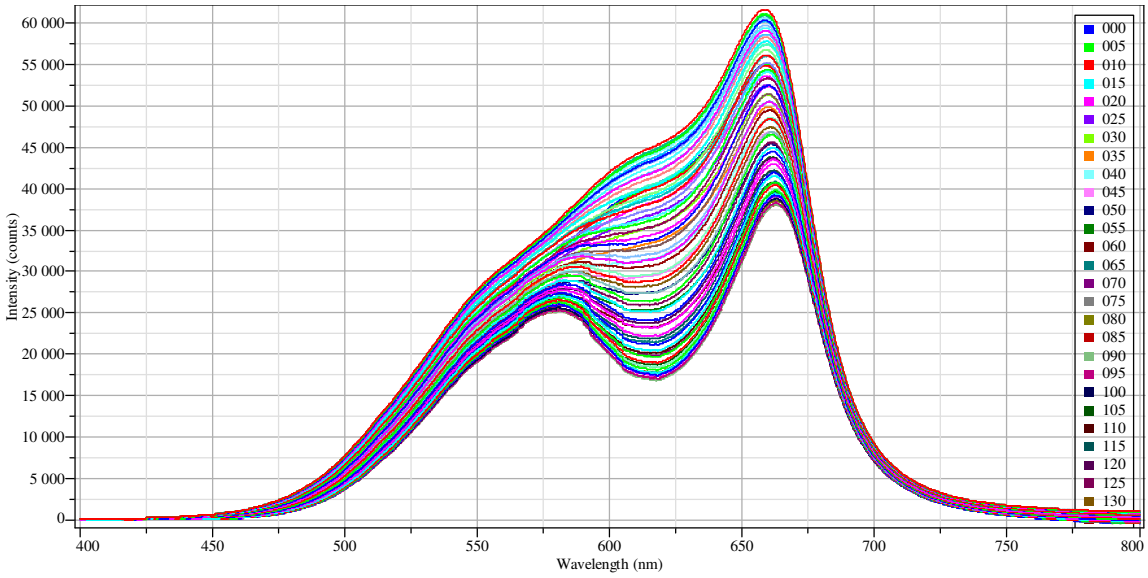

Figure 4.17: Custom built HORIBA XploRA Raman-Visible - overlay of all seventy two individual single-beam reflectivity efficiency intensity spectra measured at 5 degree intervals from 0 to 355 degrees for the 600 groves/mm grating.

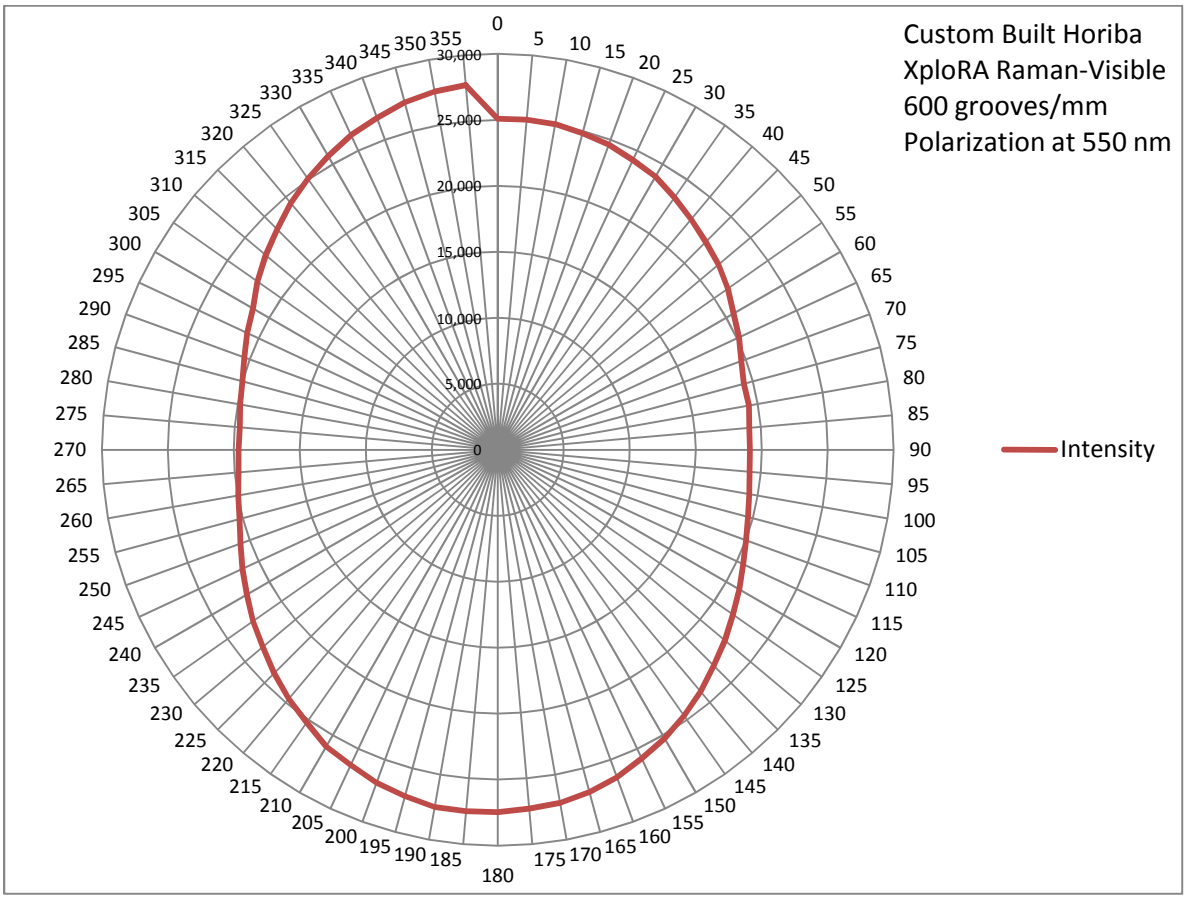

Figure 4.18: Custom built HORIBA XploRA Raman-Visible - polar plot illustration of the polarization characteristics at 550nm of the 600 grooves/mm grating.

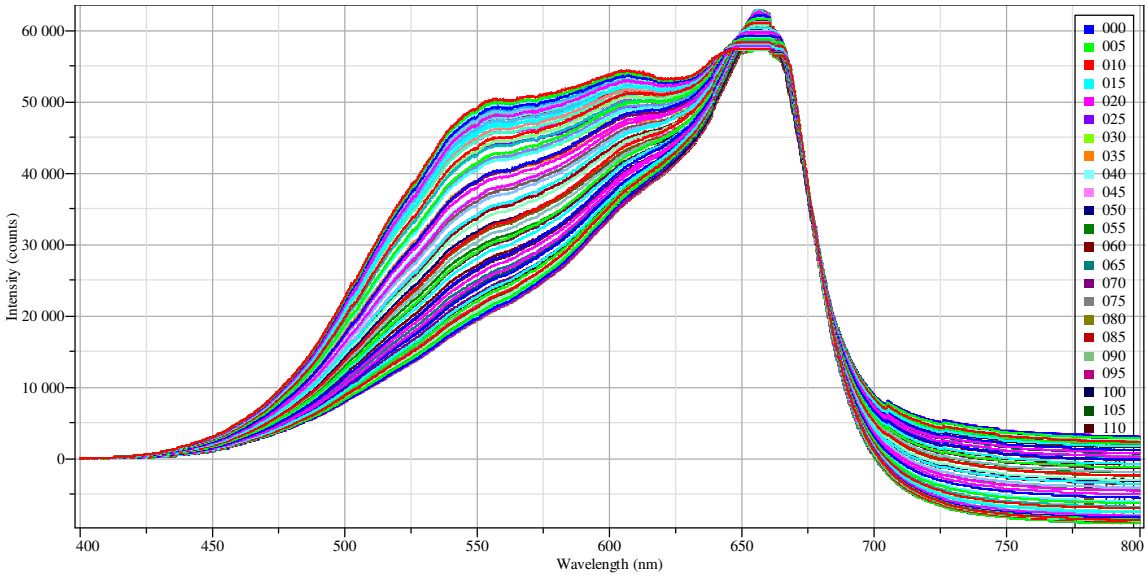

Figure 4.19: Custom built HORIBA XploRA Raman-Visible - overlay of all seventy two individual single-beam reflectivity efficiency intensity spectra measured at 5 degree intervals from 0 to 355 degrees for the 1200 groves/mm grating.

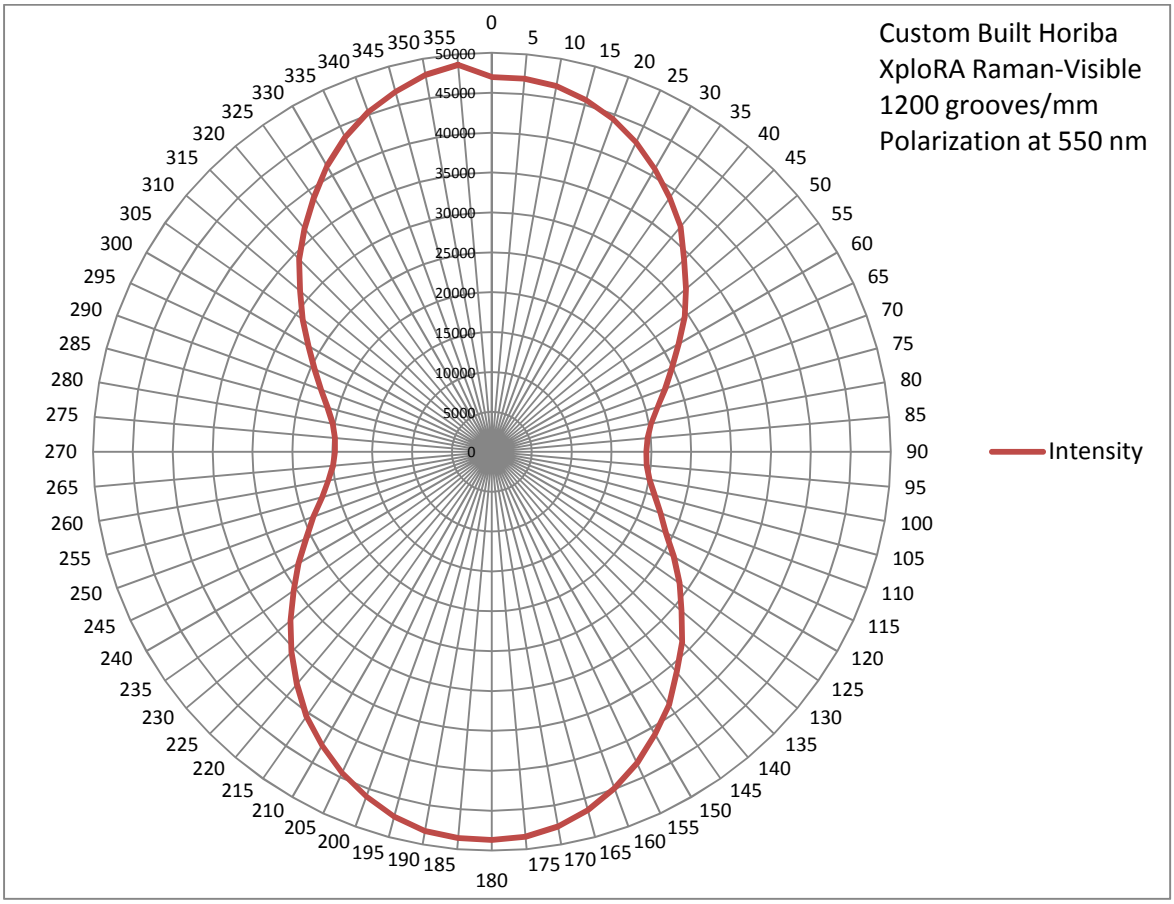

Figure 4.20: Custom built HORIBA XploRA Raman-Visible - polar plot illustration of the polarization characteristics at 550nm of the 1200 grooves/mm grating.

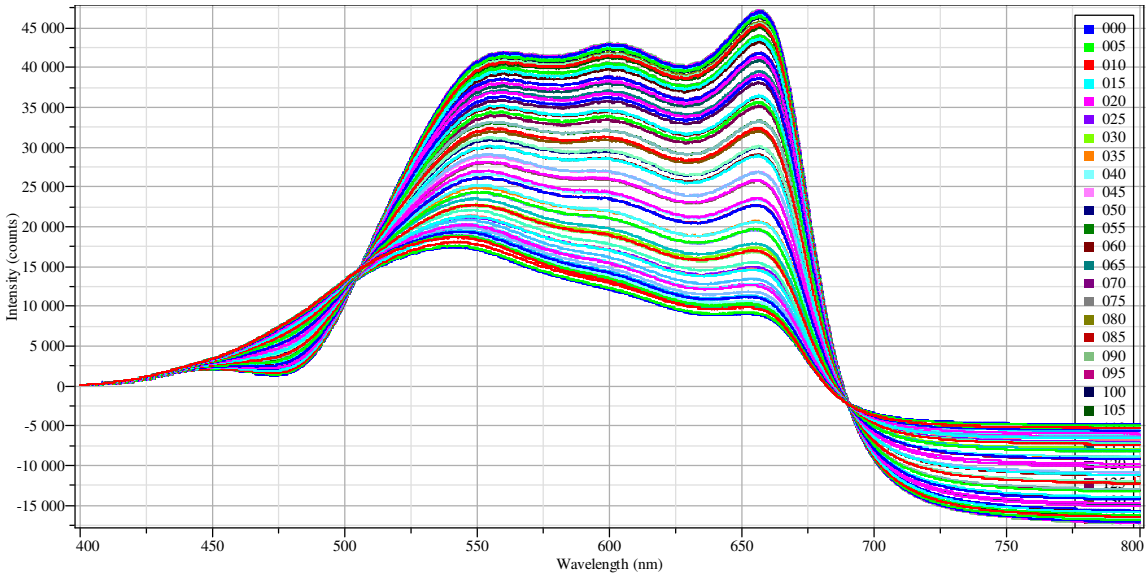

Figure 4.21: Custom built HORIBA XploRA Raman-Visible - overlay of all seventy two individual single-beam reflectivity efficiency intensity spectra measured at 5 degree intervals from 0 to 355 degrees for the 1800 groves/mm grating.

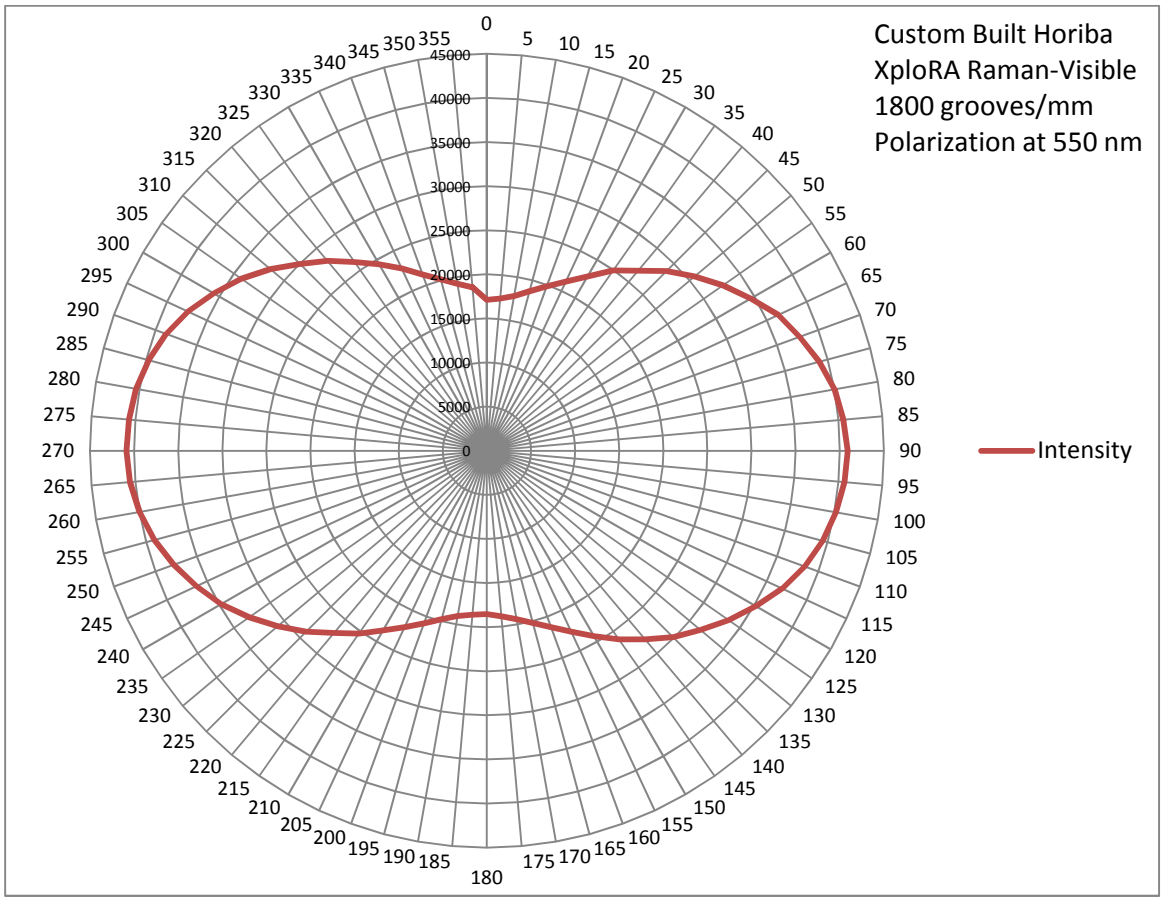

Figure 4.22: Custom built HORIBA XploRA Raman-Visible - polar plot illustration of the polarization characteristics at 550nm of the 1800 grooves/mm grating.

3. Custom Built Olympus BX51TRF Polarized Light, Reflectance, and Fluorescence Microscope with a Fiber Optic HORIBA VS140 Spectrometer

The custom built Olympus BX51TRF polarized light, reflectance, and fluorescence microscope with a fiber optic HORIBA VS140 spectrometer has an intrinsic polarization characteristic as illustrated in Figures 4.23. The characteristic intrinsic polarization has a unique feather which is illustrated in Figures 4.24 and 4.25, which are zoomed in regions of Figure 23. Note the hypsochromic (a blue shift toward shorter wavelengths) and bathochromic (a red shift toward longer wavelengths) shifts as well as hyperchromic (increase of intensity) and hypsochromic (degrease of intensity) shifts in peak positions. These spectral intensity shifts and dichroic effects are quite profound with greater than 20 nm shifts relative to a 10 – 15 degrees rotation in polarization.

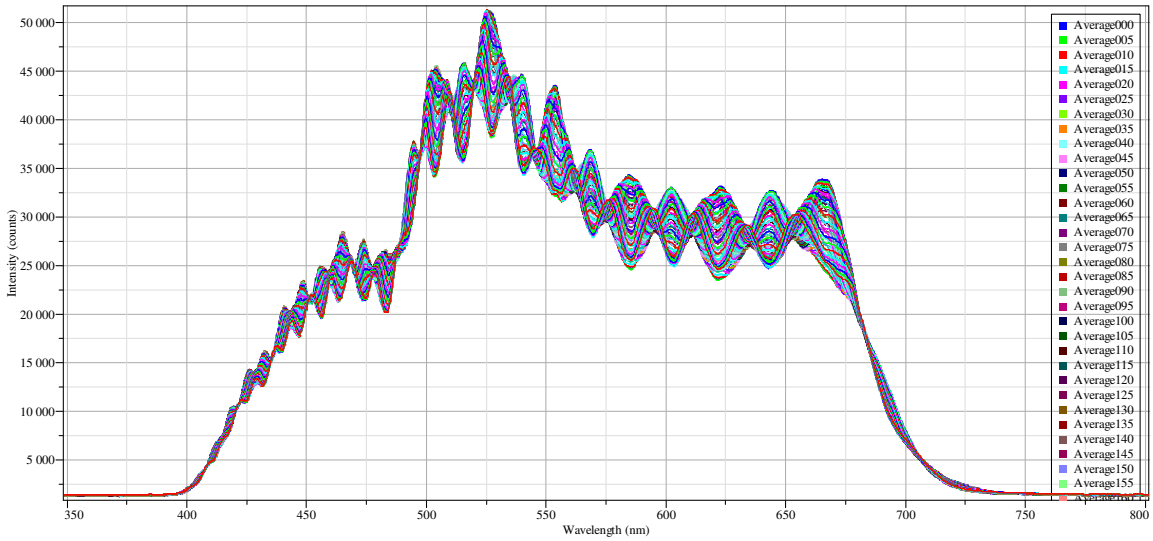

Figure 4.23: Custom built Olympus BX51TRF polarized light and fluorescence microscope - overlay of all seventy two individual polarization spectra measured at 5 degree intervals from 0 to 355 degrees. The groove density is not known.

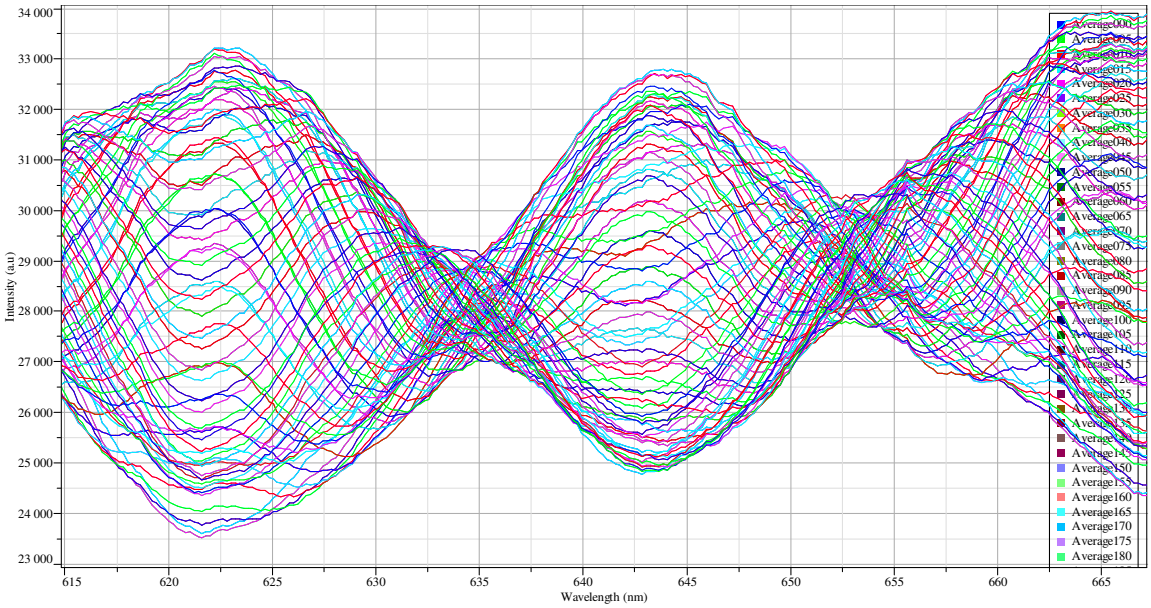

Figure 4.24: Custom built Olympus BX51TRF polarized light and fluorescence microscope - overlay of all seventy two individual polarization spectra measured at 5 degree intervals from 0 to 355 degrees. Zoomed in view from 615 to 667 nm.

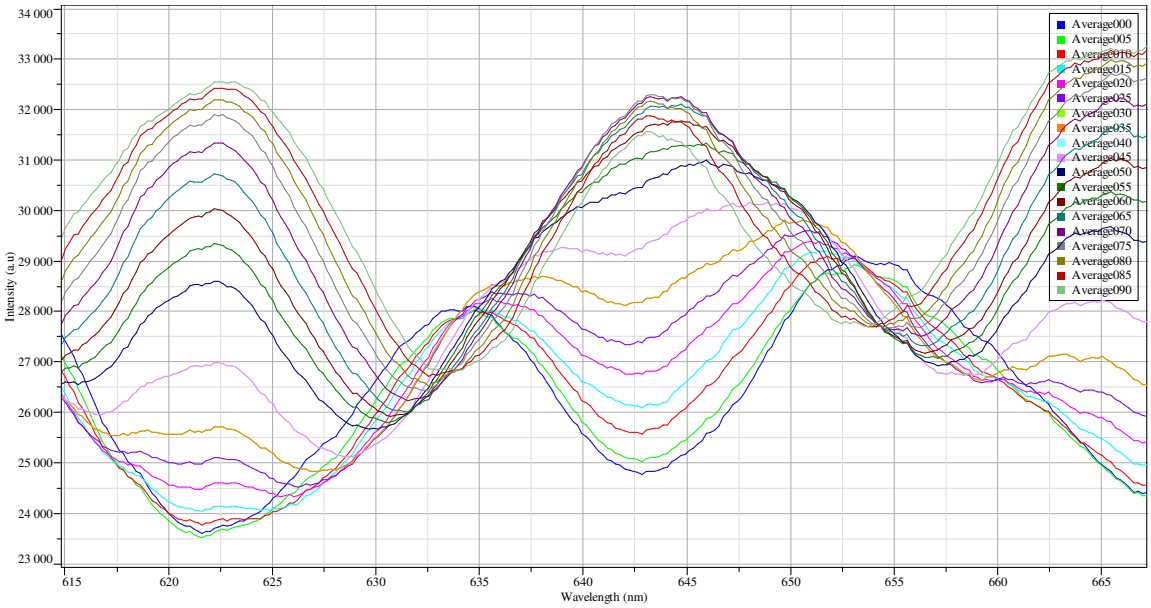

Figure 4.25: Custom built Olympus BX51TRF polarized light and fluorescence microscope - overlay of all nineteen individual polarization spectra measured at 5 degree intervals from 0 to 90 degrees. Zoomed in view from 615 to 667 nm.

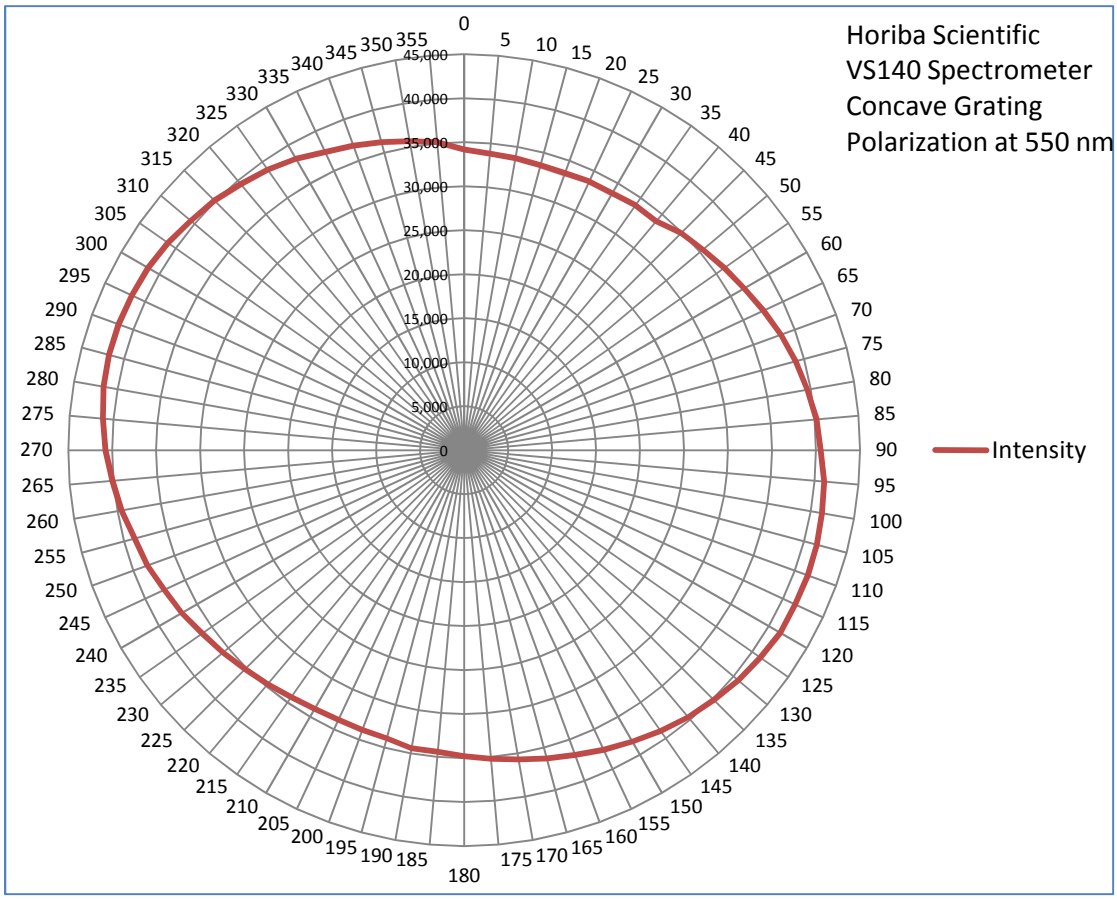

Figure 4.26: Custom built Olympus BX51TRF polarized light and fluorescence microscope - polar plot illustration of the polarization characteristics at 550nm of the HORIBA VS-140 concave grating.

4. Custom Built BH-BHA-RFA Polarized Ffluorescence Ffiber Optic Ocean Optics® USB2000+™ Spectrometer

The custom built Olympus BH-BHA-RFA polarized light and fluorescence microscope with a fiber optic Ocean Optics® USB2000+™ spectrometer exhibits minimal intrinsic polarization as illustrated in Figures 4.27 and 4.28. The reflectivity efficiency profile exhibits very small changes with respect to polarization direction. The characteristic intrinsic polarization is nearly constant at any polarization angle, which is illustrated most clearly in the intensity profile of the polar plot, Figure 4.28.

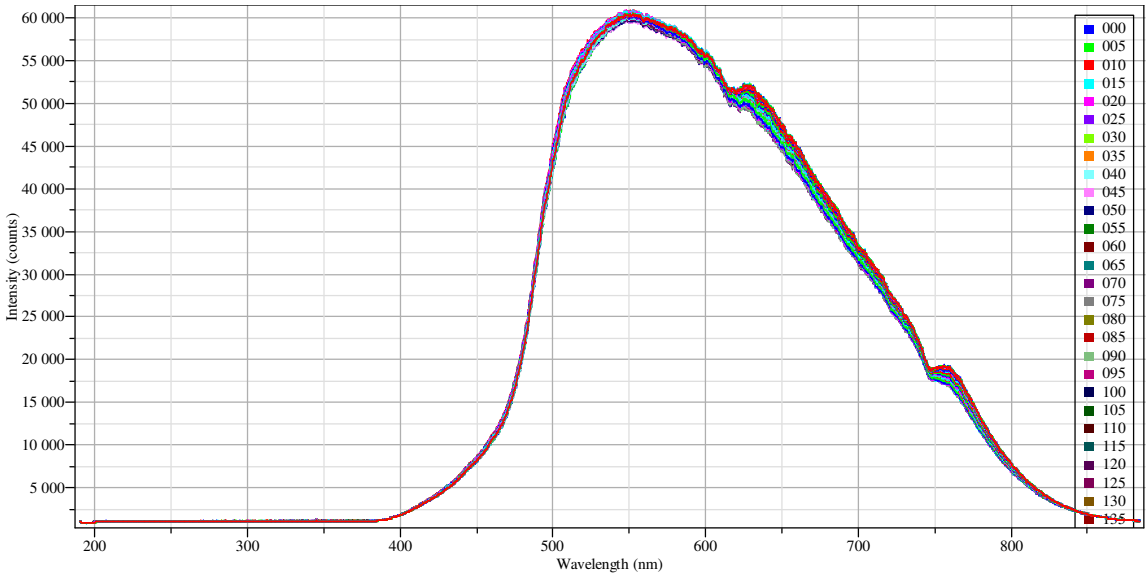

Figure 4.27: Custom built Olympus BH-BHA-RFA polarized light and fluorescence microscope - overlay of all seventy two individual single-beam reflectivity efficiency intensity spectra measured at 5 degree intervals from 0 to 355 degrees for the 600 groves/mm grating.

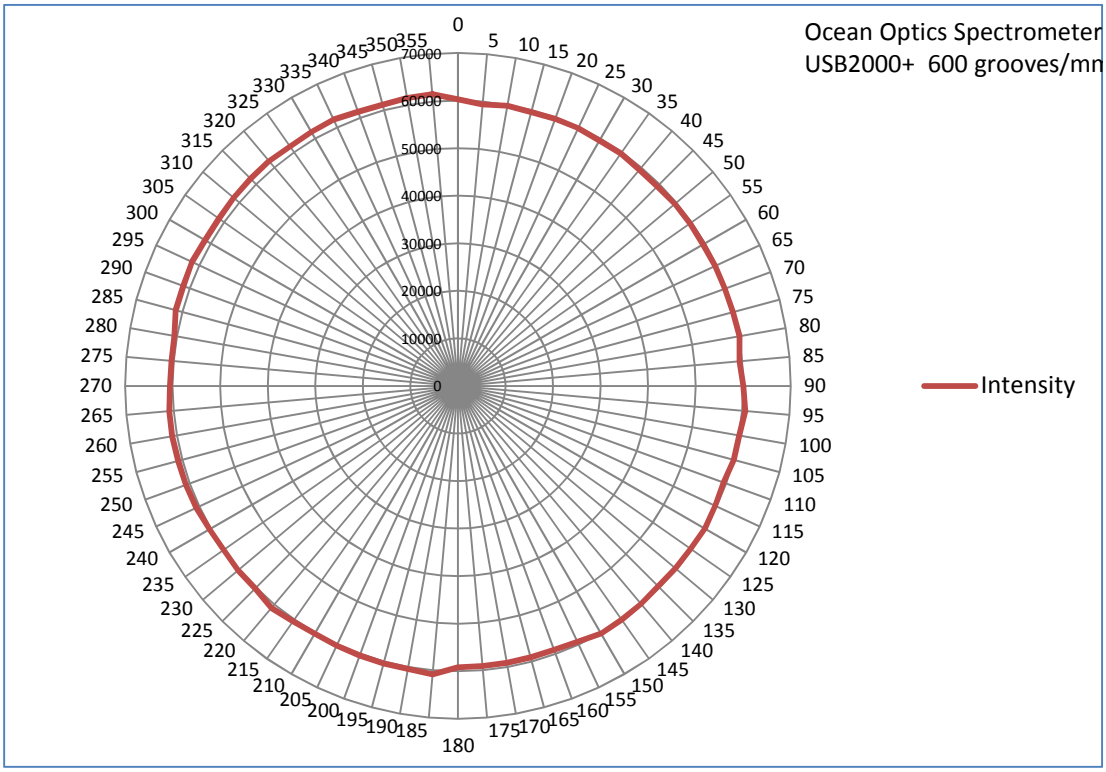

Figure 4.28: Custom built Olympus BH-BHA-RFA polarized light and fluorescence microscope - polar plot illustration of the polarization characteristics at 550nm of the Ocean Optics® USB2000+™ 600 grooves/mm grating.

D. Dichroism Measurements and Spectra of Fibers, Thin-Films, and Cupric Acetate

Forensic scientists continually search for analysis methods that are rapid at obtaining analytical results, are non-destructive to the evidence, and have a high power of discrimination. The polarized light microscope has a rich history in forensic science as the tool of choice to measure the optical properties of specimens which help to determine its chemical composition (De Forest, 1982). A polarized light microscope must be used to visualize and measure dichroism in specimens that are molecularly oriented. A polarizer aligned parallel or perpendicular to an anisotropic fiber's long axis allows the forensic scientist to either observe or measure any differences in color when the electric field vector of the polarized light is aligned with respect to the two fiber orientations.

Because most fibers and films are oriented during their manufacture, they become optically anisotropic. When a colorant is added, it may also exhibit preferred orientation and exhibit different colors when carefully observed with linearly polarized radiation at different orientations of the electric field vector.

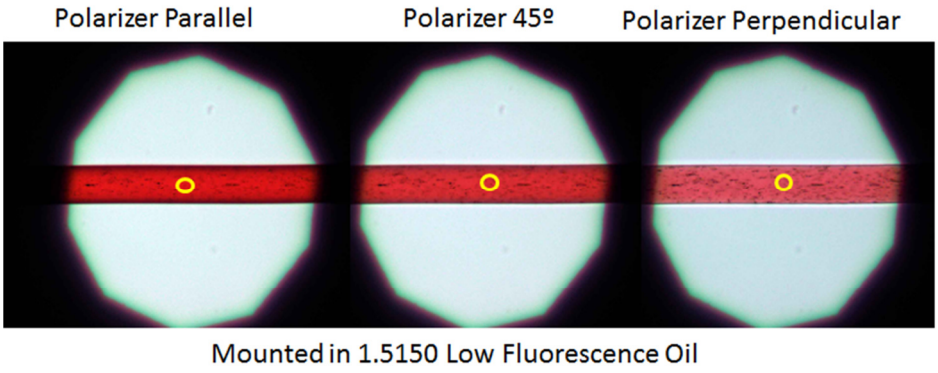

Figure 4.29: Red polyester fiber oriented EW on the microscope stage.

The left image was obtained with the polarizer positioned parallel to the fiber's long axis, the middle image was obtained with the polarizer positioned forty-five degrees to the fiber's long axis, and the right image was obtained with the polarizer positioned perpendicular to the fiber's long axis.

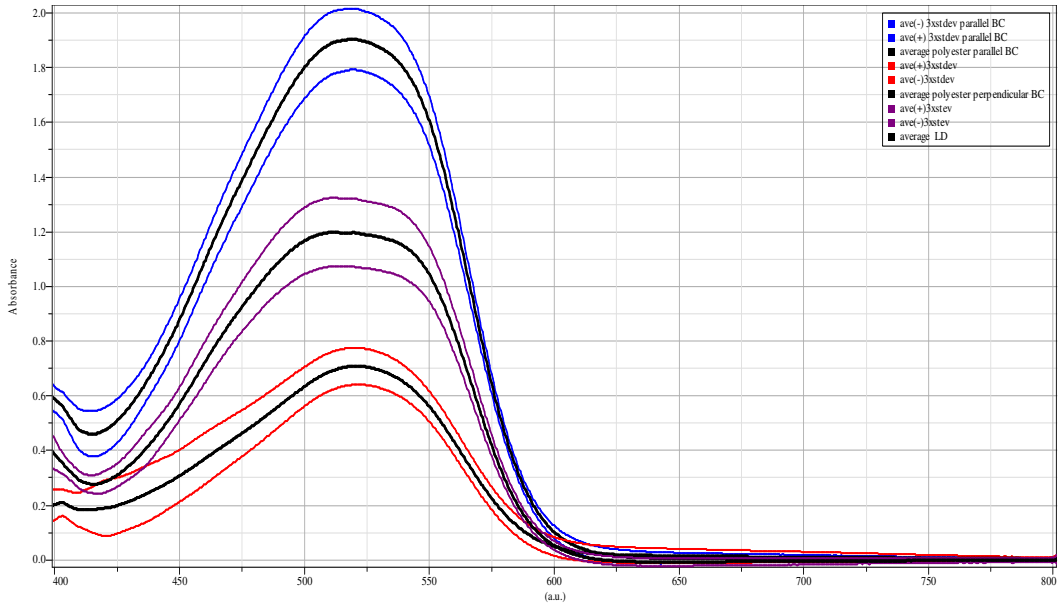

Figure 4.30: Overlay dichroic spectra obtained from the red polyester fiber illustrated in Figure 4.29.

The top absorbance spectrum (black & blue envelope) consists of the average of ten measurements with the polarizer parallel (EW) to the fiber's long axis along with a three standard deviation envelope in blue. The bottom absorbance spectrum (black & red envelop) is the average and three standard deviation with the polarizer positioned perpendicular (NS) to the fiber's long axis (EW). The middle absorbance spectrum (black & purple) is the average and three standard deviation envelope of the linear dichroic spectrum.

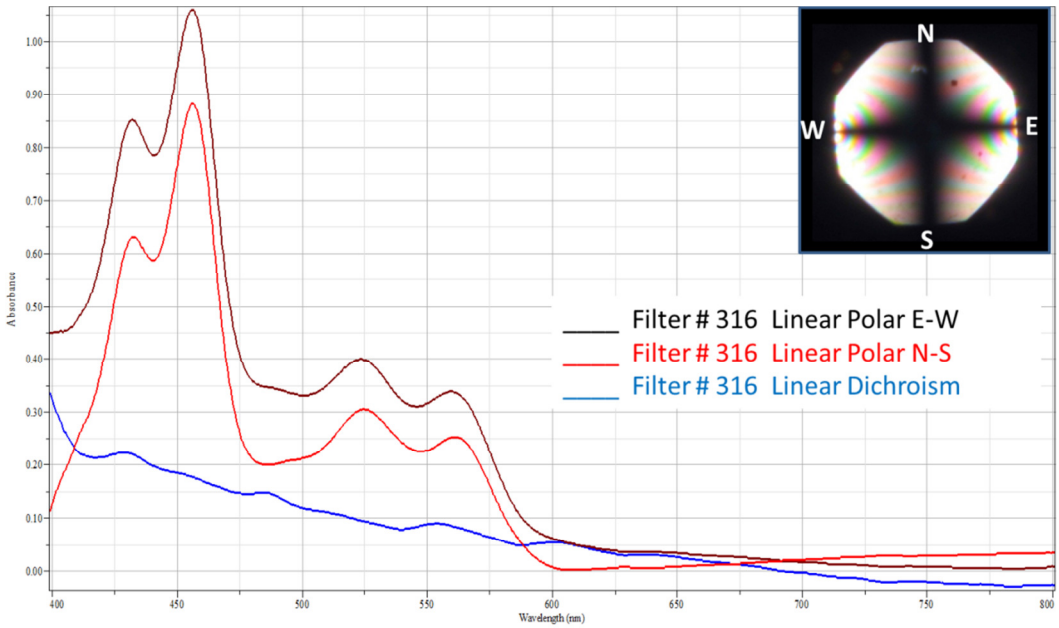

Figure 4.31: Overlay dichroic absorbance spectra from an orange color polyester thin film polyester, ROSCO 316.

The two ROSCO polyester films, Figures 4.31 and 4.32, exhibit biaxial anisotropy so when the film is placed in the extinction position, the polarized light is oriented parallel to the polyester film.

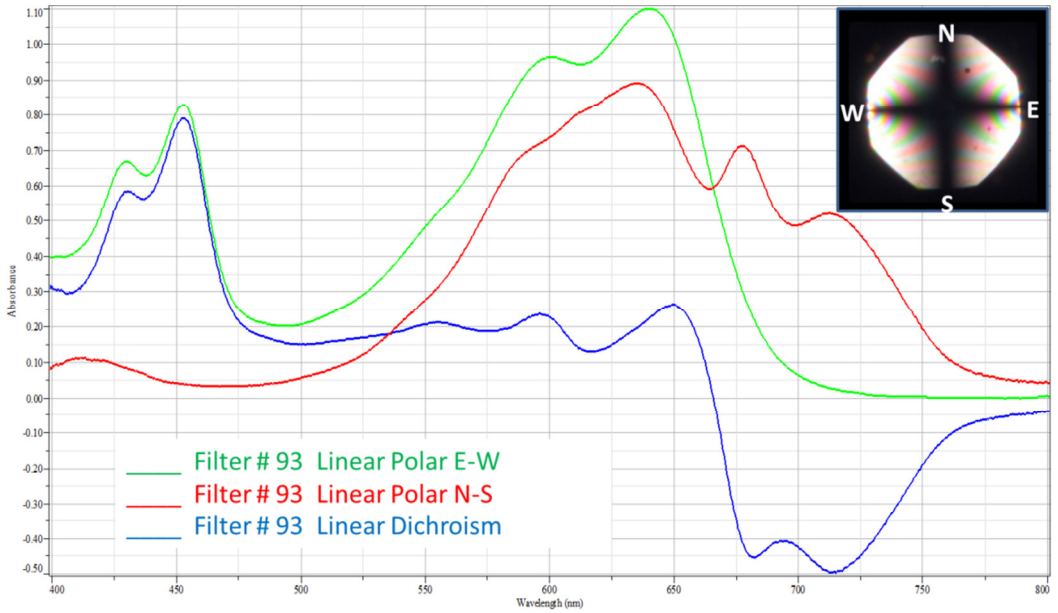

Figure 4.32: Overlay of dichroic absorbance spectra from a Green color polyester thin film polyester ROSCO 93.

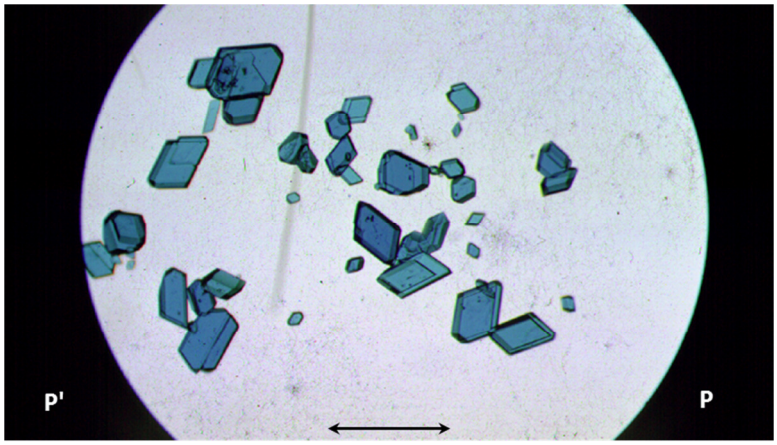

Figure 4.33: Photomicrograph of cupric acetate.

Thin plates of cupric acetate exhibit biaxial anisotropy so when the plate is oriented at the extinction position, the polarized light is parallel to the cupric acetate. The dichroic spectra are illustrated in Figure 4.34.

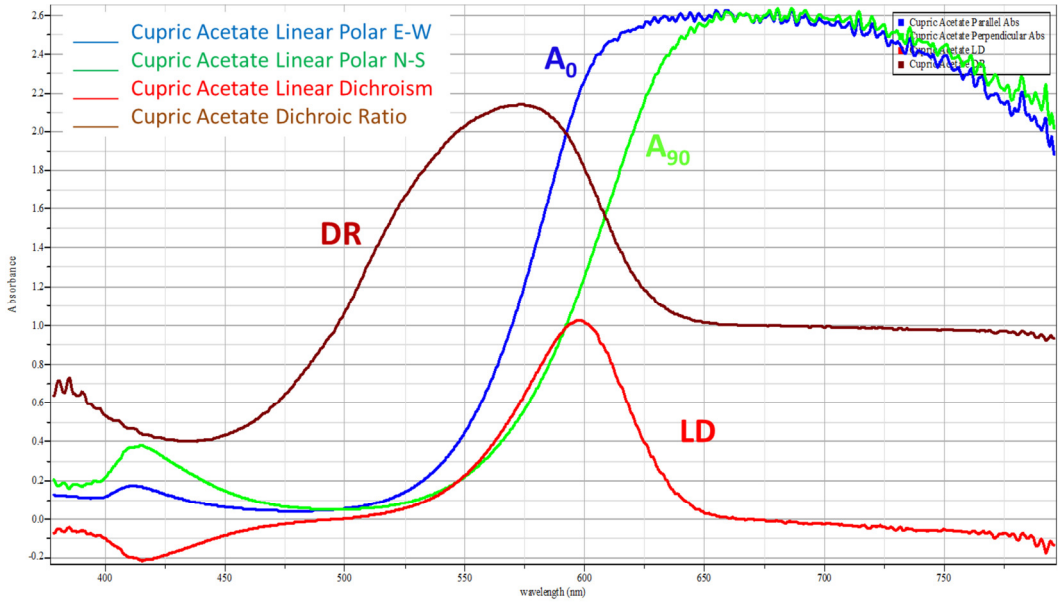

Figure 4.34: Overlay of dichroic absorbance spectra from cupric acetate.

CHAPTER 5. DISCUSSION

In microscope spectrophotometry, the absorption law (Bouguer-Beer-Lambert Law) is the fundamental, governing principle for UV-visible spectrophotometric analysis of microscopically small specimens. The microscope plays a critical role in the controlling how light is supplied to the specimen, transmitted through the specimen, and collected from the specimen to form an image that is analyzed by the spectrophotometer. The following discussion has been divided into two sections. In part A, the discussion will concentrate on the underlying principles, characteristics, and configurations of a light microscope optical system that affect the spectral quality of data. Part B, will concentrate the discussion on microscopical absorption measurements, intrinsic instrument polarization effects, and dichroism measurements for an increase in discrimination power for forensic analysis.

A. A Polarized Light Microscope as the Optical Bench

In order to properly operate a polarized light microscope, the operator must first and foremost be thoroughly familiar with the basic principles of microscopy. The operator must understand the concept of conjugate image planes and illumination planes, Köhler illumination, and how to set up a polarized light microscope for optimum image quality. For example, the field diaphragm must be in focus in the image plane, both of which are confocal with the specimen plane, and the condenser aperture set so that the illumination almost fills the back focal plane of the objective. The operator must understand how the phenomenon of diffraction (Airy disc) acts to place the fundamental limitation on the spatial resolution that an optical system may reach. The next task is to produce a high quality image of the specimen. This image is formed under full field of view, and then the operator will insert an illumination field mask (pinhole) and an image field mask (pinhole) for high quality spectrophotometric measurements to be made.

The polarized light microscope stand provides the sturdy and stable foundation on which the optical components are attached and adjusted. In order to minimize vibrations, the base should be constructed with a rigid material that is equipped with two sets of focus knobs one for course focus adjustment and the other for fine focus. In most modern microscope bases, the focus knob either raises

or lowers the microscope stage with respect to the fixed position objective. The specimen mounted on a microscope slide should be placed on a circular and rotatable stage equipped with a mechanical specimen holder that is translational in both the x – y directions, using Vernier micrometers. A substage condenser that has a rotatable polarizer and the condenser must be capable of being moved up and down the microscope primary axis. The condenser must contain an aperture diaphragm that can be open and closed. The condenser aperture diaphragm controls the angular aperture of the cone of light emerging from the condenser that impinges on the specimen. These characteristics of the condenser are critical to producing good illumination and controlling the contrast of the image.

Specimen illumination should be bright, free from glare, and evenly distributed over the entire field of view. The illumination lamp filament or bulb must be pre-centered or centerable. It is imperative that the illumination field diaphragm be adjustable because it needs to limit the area being illuminated on the specimen during spectrophotometric analysis. The areas chosen for spectrophotometric analysis must be illuminated by either a “pinhole” or other geometrically shaped mask of various sizes to restrict the area of interest for spectrophotometric analysis in order to reduce or eliminate scattered light, as demonstrated in Chapter 4, section B.5. The use of image and luminous field masks will be discussed in more detail below.

The specimen stage should be circular and rotatable to facilitate sample positioning and rotation. The use of a mechanical stage attachment will provide a means for recording the location of features observed in different areas of the slide mounted specimen. This allows for the analyst to screen the entire slide visually before selecting specific locations for spectrophotometric analysis.

The polarized light microscope must accommodate a variety of objectives. The objective is the most critical optical element for producing a clear image with high resolution. If the objective is of poor quality and uncorrected or aberrations, then the image it will produce will be of poor quality and low resolution. Aberrations are primarily of two types: spherical and chromatic (longitudinal or axial, and lateral). Spherical aberrations are variations in focal length with distance from the lens axis, which produces an out-of-focus, fuzzy image. Chromatic aberrations result from the dispersion of wavelengths of white light upon refraction through a transparent medium. Since all transparent and refractive materials disperse light to some degree, when the dispersion is along the principal microscope axis, then

this is called axial or longitudinal chromatic aberration. Since refractive index normally increases as the wavelength decreases, then an uncorrected objective focuses shorter wavelength light closer to itself and toward the axis for lateral chromatic aberration. Chromatic aberrations cause the image to have out of focus color fringes around objects. Therefore, objectives that have been corrected for both spherical and chromatic aberrations produce higher resolution images, and with a smaller depth of focus (axial range in the image that is in focus).

The primary image formed by the objective is located at the focal plane of the eyepiece. This image, a real image, is magnified by the eyepiece and observed as a virtual image through the microscope. The real primary image is further transmitted by the eyepiece to form a real image on the retina of the observer's eye. Alternatively, an intermediate image may be formed at an intermediate image plane that is transmitted to the spectrometer for photometric measurement. In order to obtain the highest quality microscope spectrophotometric measurements a few functional changes need to be made to the microscope base.

Specimen preparation is dependent upon the type of transfer evidence under investigation. Most fibers may be simply placed into a drop of mounting medium on either a glass or fused-silica slide and covered with the appropriate material cover glass, depending on whether analysis will involve visible light or UV-visible light microscope spectrophotometry. The mounting medium must also carefully be chosen to reduce relief between the medium and the specimen, and whether ultraviolet, visible or fluorescence microscope spectrophotometry will be used.

All wide field or full field of view images are composed of light from both in-focus (within the focal plane or depth of field) and out-of-focus planes while confocal images consist of light only from only in-focus planes. A confocal arrangement revolves around quantum efficiency and dynamic range of detectors used, which are typically thermally electrically cooled CCD or PDA, or high-voltage PMT detectors (Pawley, 1995). The CRAIC Technologies Inc., QDI 2010 systems use a mirrored beam-splitter mask in the primary image plane that transmits a "square" portion of the image to the spectrophotometer, see Figure 4.2. Similarly, the two fiber optic based microscope photometers use the fiber entrance as an image mask as illustrated in Figures 4.4 and 4.6. In this configuration, light from out-of-focus planes in the specimen as well as scattered light from around the region of interest on the specimen will be

transmitted to the detector. This will produce an incorrect and higher value of transmission for the selected region of interest (area) for analysis. Another way to think of this is to consider the light being transmitted solely by the specimen area of interest as the signal and the area around the specimen as noise, so therefore the signal will be lost in the noise.

Conversely, if only the area being illuminated is restricted to just the area of the specimen, then the signal-to-noise ratio will be greatly enhanced. This premise was experimentally tested and the overlay spectral results are presented in Figure 4.12, which correspond to the illumination field masks illustrated in Figure 4.11. It should be reiterated that the image field mask was fully open, so these results indicate the effects of limiting the luminous field mask sizes only.

B. Measurement of Transmittance or Absorbance of Microscopic Specimens

Transmittance = I/I_0, for ideal conditions when all conditions of the Bouguer-Beer-Lambert Law are satisfied. As a result, the absorbance is complicated by and made nonlinear by factors such as polychromatic light interacting with the sample, which may induce fluorescence in the visible light region. The visible light fluorescence may go unnoticed, unless the transmittance exceeds 100% T. In addition, the absorbance measurement is complicated by conditions cause deviations from the absorption law: 1) the specimen is typically not homogeneous; 2) the optical path length through the sample varies with the conicity of the illumination; and 3) the specimen is a solid with varying degrees of orientation and systematic structure. These solid specimens are typically anisotropic which causes the incoming light to be separated into at least two principle directions that are orthogonally oriented in space with opposite states of polarization, and have different velocities. This change in velocity imparts a phase shift between the two mutually perpendicular light rays. In addition to these specimen induced polarization changes, there are intrinsic polarization effects due mostly to orientation dependence on the diffraction grating in the spectrophotometer.

Typical grating efficiency curves are a plot of either absolute or relative diffracted efficiency vs. diffracted wavelength. However when the grating is integrated into a microscope spectrophotometer system, the reflectivity (polarization) curves are only close approximations to the actual grating efficiency curves since the spectral emissivity of the illumination source and the spectral response of the detector

contribute to the total grating efficiency curves. In each of the following grating efficiency curves, the blue curve is the average between the two polarization states: P-polarization (parallel) and S-polarization (perpendicular). For unpolarized light, the efficiency curve falls exactly halfway between the two polarization states, the average spectrum, see Figures 5.1 thru 5.7. The efficiency curves for a grating depends on the distance between the grooves, the number of grooves, the groove shape, and any material that may coat the grating surface.

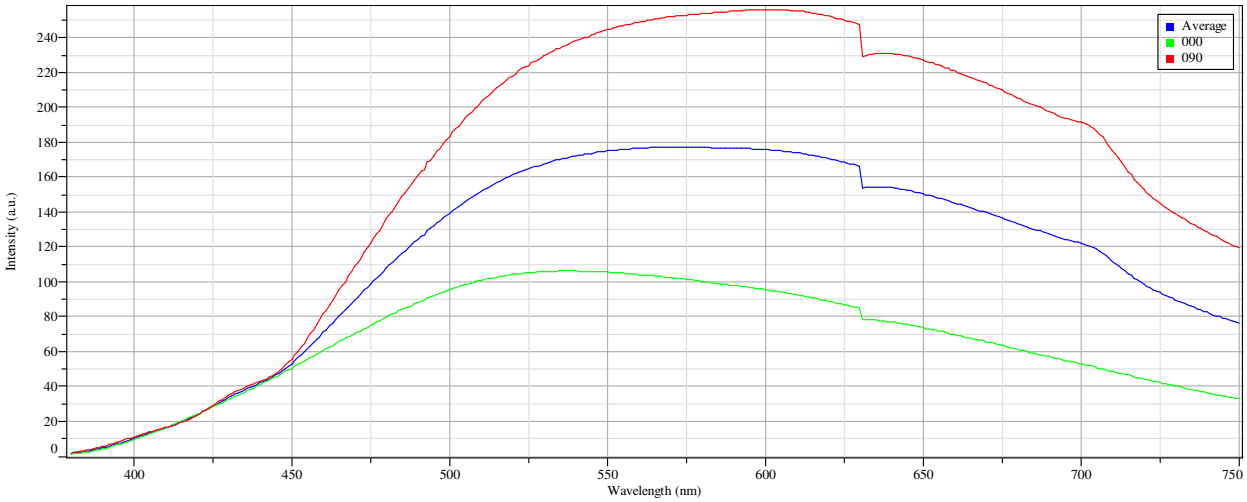

Figure 5.1: Grating reflectivity efficiency and polarization curves for Zeiss MPM400-MSP65 1208 grooves/mm. The red curve (090) is the intensity curve when the polarizer is placed in the NS orientation. The Green curve (000) is the intensity curve when the polarizer is placed in the EW orientation. The blue curve is the average of the two curves, which represents the intensity curve of unpolarized light.

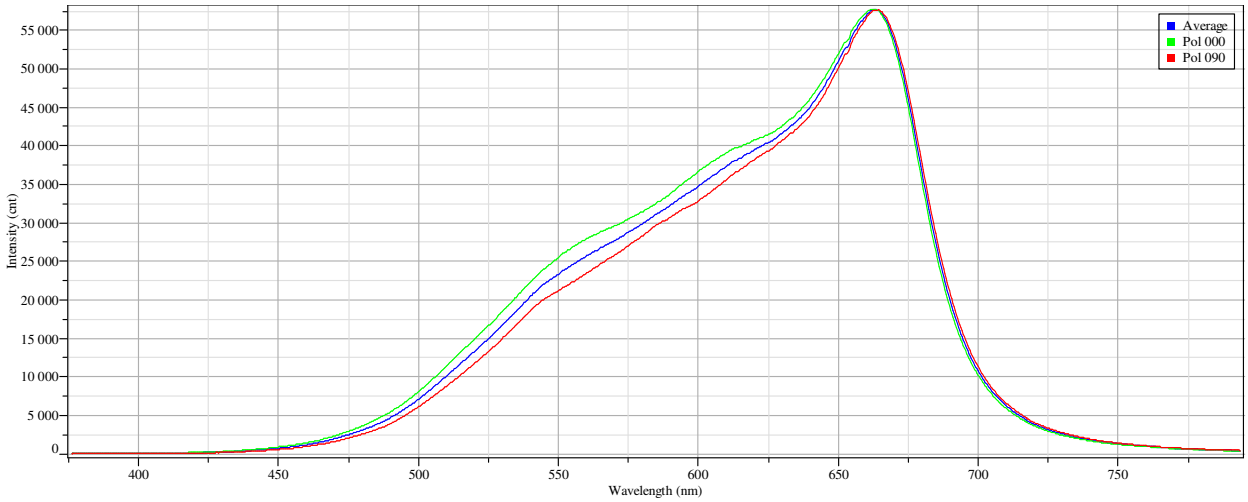

Figure 5.2: Grating reflectively efficiency and polarization curves for HORIBA XploRA 300 grooves/mm. The red curve (090) is the intensity curve when the polarizer is placed in the NS orientation. The Green curve (000) is the intensity curve when the polarizer is placed in the EW orientation. The blue curve is the average of the two curves, which represents the intensity curve of unpolarized light.

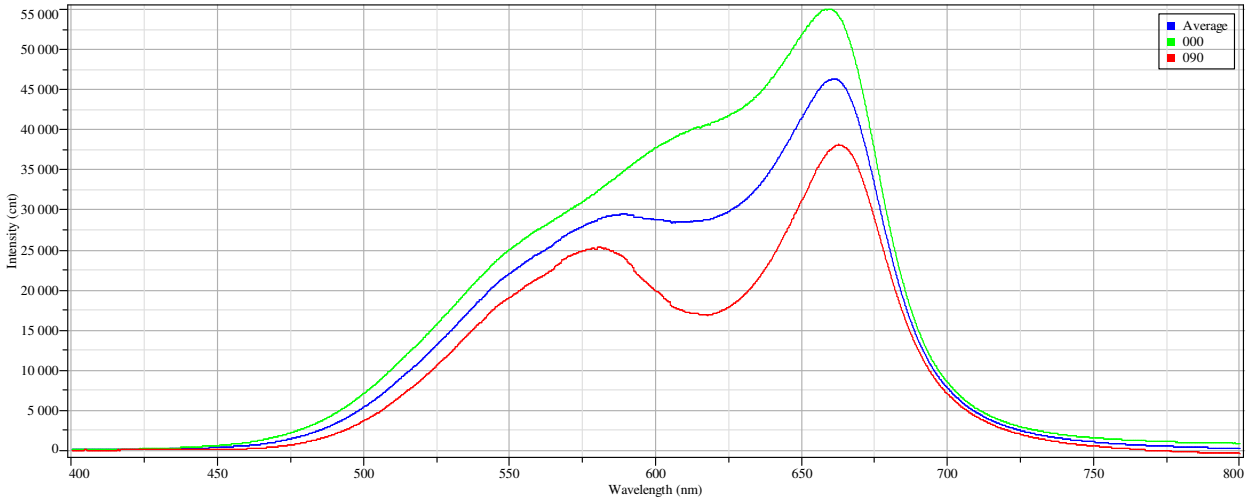

Figure 5.3: Grating reflectivity efficiency and polarization curves for HORIBA XploRA 600 grooves/mm. The red curve (090) is the intensity curve when the polarizer is placed in the NS orientation. The Green curve (000) is the intensity curve when the polarizer is placed in the EW orientation. The blue curve is the average of the two curves, which represents the intensity curve of unpolarized light.

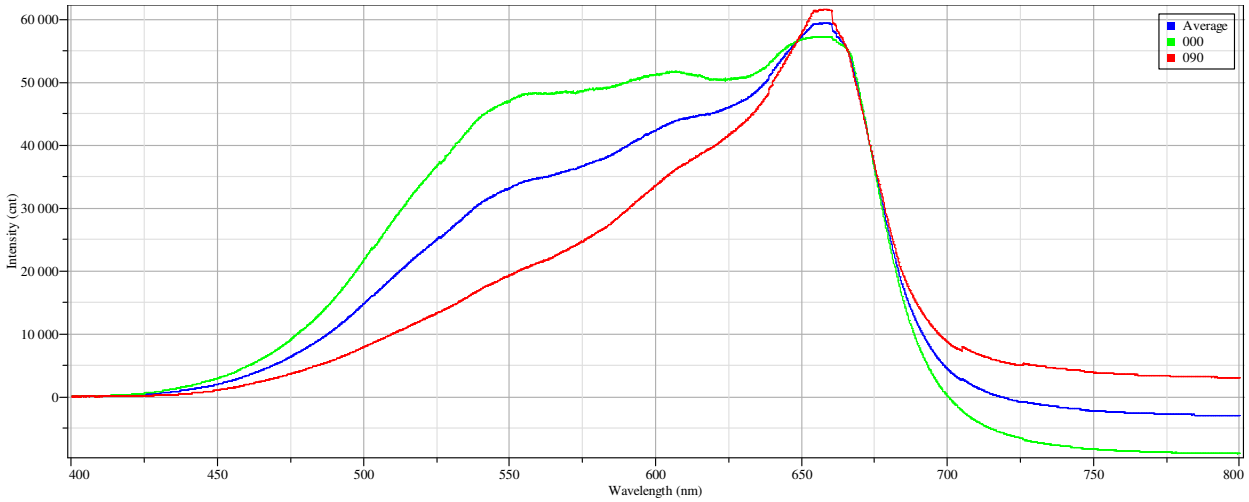

Figure 5.4: Grating reflectivity efficiency and polarization curves for HORIBA XploRA 1200 grooves/mm. The red curve (090) is the intensity curve when the polarizer is placed in the NS orientation. The Green curve (000) is the intensity curve when the polarizer is placed in the EW orientation. The blue curve is the average of the two curves, which represents the intensity curve of unpolarized light.

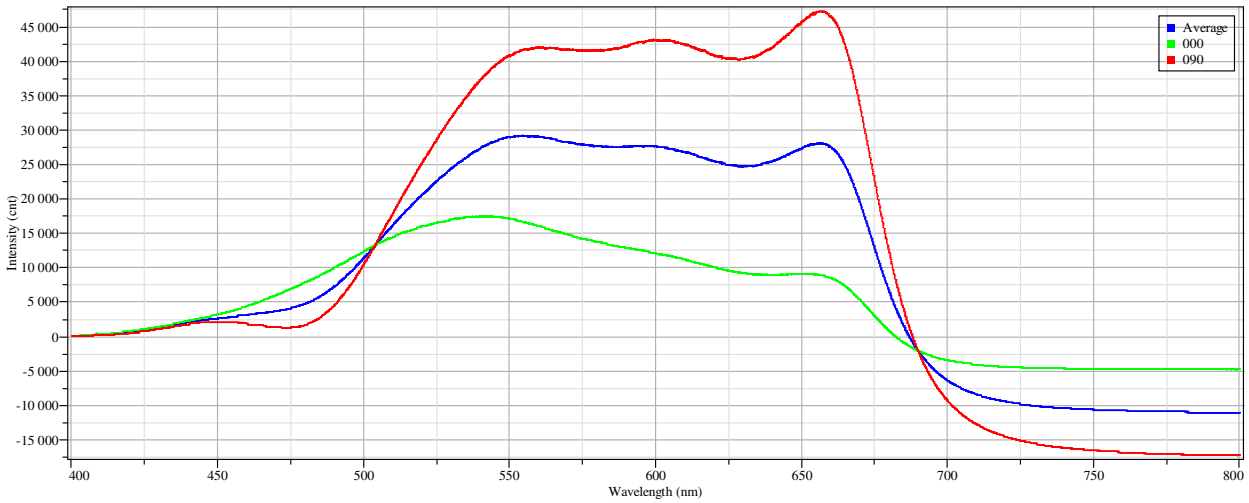

Figure 5.5: Grating reflectivity efficiency and polarization curves for HORIBA XploRA 1800 grooves/mm. The red curve (090) is the intensity curve when the polarizer is placed in the NS orientation. The Green curve (000) is the intensity curve when the polarizer is placed in the EW orientation. The blue curve is the average of the two curves, which represents the intensity curve of unpolarized light.

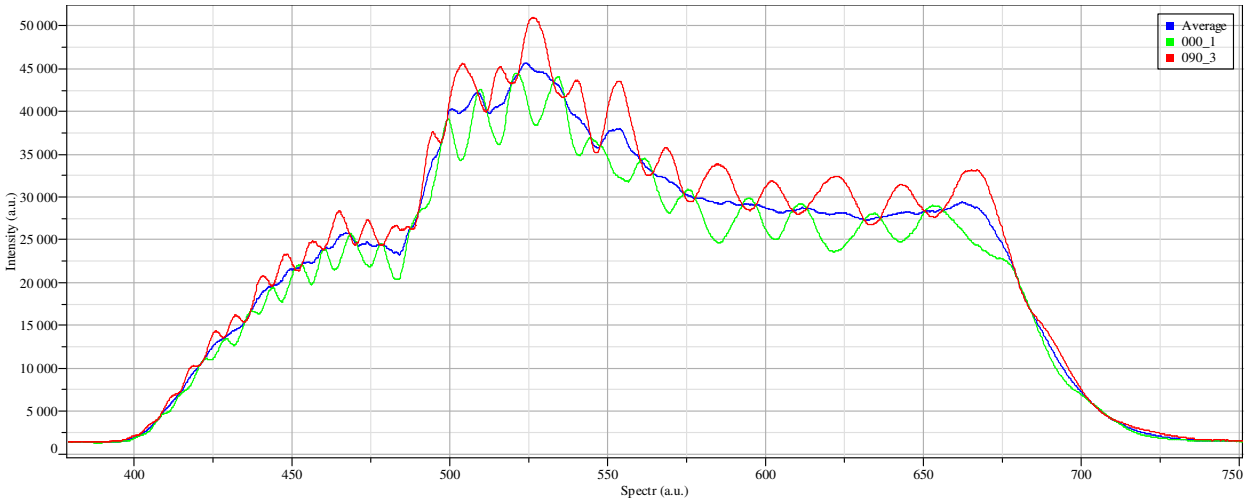

Figure 5.6: Grating reflectivity efficiency and polarization curves for HORIBA VS140. The red curve (090) is the intensity curve when the polarizer is placed in the NS orientation. The Green curve (000) is the intensity curve when the polarizer is placed in the EW orientation. The blue curve is the average of the two curves, which represents the intensity curve of unpolarized light.

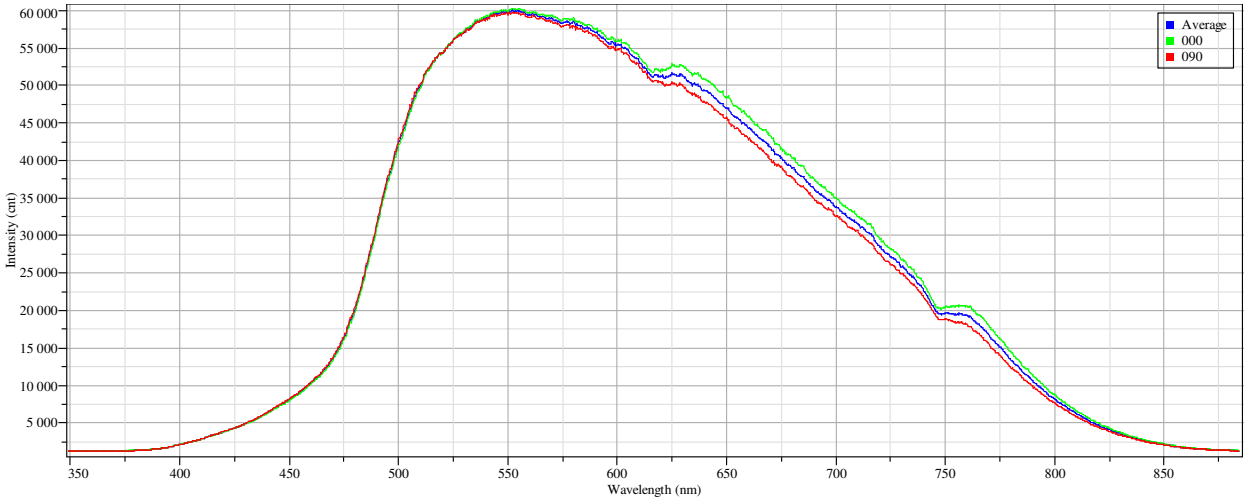

Figure 5.7: Grating reflectivity efficiency and polarization curves for Ocean Optics® USB2000+™ 600 grooves/mm. The red curve (090) is the intensity curve when the polarizer is placed in the NS orientation. The Green curve (000) is the intensity curve when the polarizer is placed in the EW orientation. The blue curve is the average of the two curves, which represents the intensity curve of unpolarized light.

What should be very obvious by this point is that when analyzing anisotropic specimens, proper specimen orientation and background (reference) spectral ratioing becomes extremely important. Improper control of either specimen orientation or polarization effects, or the proper collection and ratioing of the appropriate polarized light background (reference) spectrum, will have a profound effect on the spectral data collected, which if not appreciated by the analyst can lead to an erroneous interpretation of

the data. Figure 5.8 demonstrates this exact proposition by illustrating the absorbance spectra of a single red polyester fiber as the fiber was rotated in 5 degree increments over a ninety degree range. The range of absorbance values may lead the analyst to determine that these spectra were obtained from specimens that originate from different sources, which would be a Type 2 error.

It should be pointed out here that the data in Figure 5.8 were collected with a 300 g/mm grating that exhibits very little polarization effects, refer to Figure 5.2, so it would be expected that data collected on this fiber with a grating with a higher groove density (greater polarization effect) would produce a more profound difference in spectral data quality.

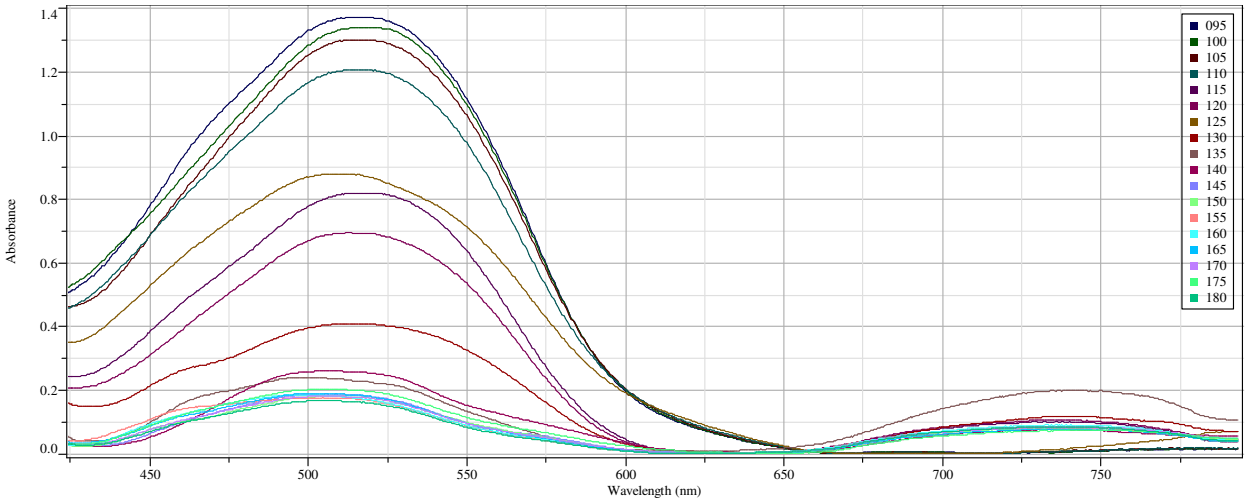

Figure 5.8: Overlay absorbance spectra of a red polyester fiber collected using unpolarized light. Each spectrum was collected at 5 degree increments between 95 – 180 degrees. Spectra were baseline corrected only. All data were collected using the custom built HORIBA XploRA Raman-visible microspectrometer with the following parameters: integration time, 50 ms; accumulations, 128, confocal hole, 100 micrometer; spectrometer entrance slit, 50 micrometer; objective, 50X LWD, grating, 300 g/mm.

Since the instrument polarization response may be very different at different specimen orientations which themselves effect polarization, it is extremely important to eliminate intrinsic instrument polarization artifacts caused by the grating properties. This may be accomplished by keeping the fiber or other specimen in a stationary position throughout all measurements. Uniaxial fibers should be positioned with the fiber long axis horizontal or EW on the microscope stage. Orient the electric field vector of linear polarized light along the fiber long axis. Thus, if the fiber is aligned EW on the microscope stage and the polarizer is aligned in the EW direction when the degree scale on the rotatable polarizer is

set to zero, then the polarizer is oriented parallel to the fiber's long axis. A dichroic spectrum requires two absorbance measurements to be collected at the same point on the specimen. In some materials, the dichroic effect varies strongly with the wavelength of light, making them appear to have different colors when viewed with light having differing linear polarization states. Linear dichroism is a quantitative measure of the difference in absorption at a given wavelength over a spectral range, and requires two measurements: A_0, which is the absorbance parallel to the fiber's long axis when oriented EW, and A_{90}, which is the absorbance perpendicular to the fiber's long axis when oriented EW. The advantage of using either the dichroic ratio or the reduced dichroic ratio (RDR) instead of LD is that dependence on the concentration of the specimen, the optical path length, and the dipole strength (intensity) of the transition has been removed via ratio. These ratio formulae have been derived so as to minimize or elimination errors which arise when dividing by zero.

CHAPTER 6. CONCLUSIONS

In microscope spectrophotometry, absorption of light by a specimen is measured as the relationship expressed in Equation 1.3. The fundamental process of the measurement in microscope spectrophotometry is based on transmittance of light through a specimen. The basic steps for this method are to collect a dark-scan, a background (reference) scan, and a specimen (sample) scan. A dark-scan collects a spectrum of the "background" noise of the system. A background (reference) scan collects a spectrum of the microscope slide, the mounting medium, the cover glass, and the instrument response. A specimen scan collects a spectrum of the specimen, the microscope slide, the mounding medium, the cover glass and the instrument response. The transmittance represents the ratio of the specimen (sample) scan minus the dark-scan to the background (reference) scan minus the dark-scan. The resulting spectrum represents the transmittance of light through the specimen or the light that was absorbed by the specimen.

The Bouguer-Beer-Lambert Law, or the Absorption law, explains the relationships of interactions of light with a specimen in terms of absorption of light by the specimen. In this complex absorption process chromophores of molecules in the specimen are excited and energy is absorbed. The amount of energy absorbed depends on the total number of absorbing species in the specimen that interact with the beam of light. This amount of absorption depends on the thickness of the specimen and the concentration of absorbing species. Several assumptions are made in applying the Absorption law:

1) The incident light is monochromatic
2) The absorbing species act independently of each other
3) The incident light consists of parallel rays, perpendicular to the absorbing species
4) The optical pathlength traversed is uniform over the cross-section of the light beam (all light rays travel the same distance through the specimen)
5) The specimen is homogeneous and does not scatter the light
6) The incident light flux is not too large as to cause saturation effects

The magnitude of absorption is directly proportional to and depends on the wavelength of light, the nature of the absorber, and the concentration of the absorber. Therefore, the optimum instrument design must

control those parameters (assumptions) as effectively and efficiently as possible in order to obtain the highest quality spectral data.

Traditional UV-visible spectrophotometers were designed with the broadband white light source directed into a scanning monochromator that selected a narrow bandpass of light to be transmitted through the specimen and detected by a photomultiplier tube. With the development of multichannel solid-state detectors, as discussed in detail in Chapter 1, section F.4., the fundamental shift in instrument design placed the wavelength selection device after the specimen and all wavelengths of light were collected on the linear array of detector elements. This shift in instrument design reduced sample collection times from minutes to a few milliseconds. However, this fundamental shift in design violates the first assumption of the Absorption law. In addition, when a specimen absorbs energy of a given wavelength and then emits the energy at a longer wavelength, this process is called fluorescence. Traditional instruments were designed to measure the transmittance over a relatively narrow bandpass, which could be less than one nanometer sequentially and the fluorescence was not detectable in the absorbance measurement. Conversely, in instruments that use broadband (white light) sources to illuminate the specimen with all wavelengths simultaneously, fluorescence may be introduced into the absorbance spectrum without being noticed. The analyst may recognize fluorescence when the transmittance exceeds 100% T, but cannot identify fluorescence that results in a transmittance less than 100%T. In forensic analysis, textile treatments such as optical brighteners may cause fluorescence in the visible light region that may go undetected, but be interpreted as transmittance.

Several early microscope spectrometer manufacturers offered as an accessory to their system a monochromator before the specimen such as the Farrand MSP, the Zeiss USMP I, and the Olympus DMSP II systems. These systems were quite expensive in the early 1970s and they were neither computer operated nor did they collect a digitized spectrum for computer software processing. Their data output was recorded on a strip chart recorder and evaluated directly by visual comparison. Later models of the Zeiss MPM400/800 series systems continued to offer as an accessory a monochromator illuminating system. These systems were configured as computer controlled systems with a PMT detector. These systems were also offered on the commercial market as fluorescence systems that only required a monochromator after the specimen because they were not being employed to perform

transmittance measurements. The evolution of these systems to be employed for transmission measurements lead to the replacement of a scanning monochromator and a PMT with a spectrophotometer with a multi-channel array detector. The following recommendations consider the optical characteristics of the microscope, the specimen, and the spectrophotometer.

I recommend the following features as essential for a high performance ultraviolet-visible microscope spectrophotometer are: 1) a polarized light microscope; 2) the ability to switch between a broad-band white-light illumination source to obtain a high quality image and a quick-scan monochromator positioned before the specimen for spectrophotometric analysis; 3) the ability to quickly insert the appropriate size illumination field mask to illuminate only a selected area of the specimen; 4) the ability to quickly insert the corresponding size mask for measuring the selected area of the specimen; 5) the ability select a single channel photosensitive detector for transmission and reflection measurements; 6) the ability to select a multi-channel detector for fluorescence measurements; 7) video camera for photo documentation, and 8) a computer system interface for collecting spectral data, and computer software for data processing and data storage.

I recommend a research based polarized light microscope because it provides an excellent optical bench for mounting illuminators, a rotating circular stage with mechanical *x-y* translation, objectives, eyepieces, and deflecting optics necessary for imaging, observing, and making photometric spectral measurements on microscopically small specimens. The microscope base should also be equipped to accept a mounted and rotatable polarizer and analyzer, illumination and image field masks, and accessory wave plates, compensators, and filters, in such a manner that they may be easily inserted and removed from the optical path. I also recommended these accessories have their position in the microscope optical path as reproducible as possible with the ability to make fine adjustments to their optical alignment.

I recommend the user to have the ability to conveniently switch between white light, for sample orientation and conventional microscopic analysis, and a monochromator for spectrophotometric measurements. This may be accomplished by using a retractable mirror in the microscope base to direct the white light onto the sample when necessary during sample preparation and orientation. In preparation for a spectrophotometric measurement, the analyst should select the appropriate size mask

for measuring the selected area on the specimen from which to collect a spectrum. This is followed by selecting the appropriate size illumination field mask to minimize stray light. The proper selection of these masks is critical to the collection of reliable spectroscopic measurements on a microscopic sample.

The condenser should be on a height adjustable precision mechanism for moving the condenser axially to focus the field aperture or mask onto the specimen plane. The condenser should have an iris diaphragm to control the angle of light rays illuminating the specimen. Reducing the condenser iris diaphragm reduces image resolution but increases image contrast. For UV-visible measurements, I recommend an all-reflecting objective be used as a condenser to focus and transmit deep ultraviolet (down to 190 nm) and visible polarized light onto the specimen.

The specimen should be mounted on microscope slide for visible light measurements or on a Spectrosil™ microscope slide, for UV light measurements, with a clear transmission mounting medium and then protected with an appropriate material cover slip. The mounting medium should be selected to match as closely as possible the refractive index of the specimen. By matching the refractive indices of the specimen and mounting medium, the stray light is minimized at the interface between the specimen and mounting medium. Care must be practiced when positioning the specimen parallel to the preferred direction of the plane polarized light. If the specimen is an elongated fiber, then the long axis of the fiber is to be positioned in the EW position if the plane polarized light has its preferred direction positioned EW

The objective should be an all reflecting objective in order to collect the transmitted deep UV-visible transmitted polarized light to the single element photodetector or to a multichannel spectrometer. The all-reflecting objective is free of chromatic aberration necessary for proper focus of all wavelengths into the image plane to be transmitted through the measuring field mask. Light that is out of focus will be rejected by the image mask from reaching the detector.

The analyst must be cognizant of the effects of changing the polarization direction of the illumination on the transmission intensity of due to intrinsic polarization of the spectrophotometer. The intrinsic polarization may have dramatic effects on the quality of the spectral data measured. Small shifts in sample positioning around the microscope principal axis may produce a dichroic shift in the spectrum by tens of nanometers. These dichroic shifts may lead to an incorrect interpretation of the spectral data

and a misclassification of spectral data. Consequently, it is critical to ensure proper control of intrinsic polarization.

I recommend a stabilized 12 volt, 100 watt quartz halogen be used for visible range transmittance and reflection measurements, while a stabilized high-pressure deuterium lamp would be preferred for ultraviolet measurements. A deuterium lamp is ideal for supplying a particularly intensive continuous spectrum in the spectral range 180 – 360 nm. For fluorescence measurements, however, I recommend a stabilized HBO 100 2/W high-pressure mercury lamp be used because its intensity is much greater than that of a deuterium lamp. I also recommend the high-pressure mercury lamp be used for fluorescence because all commercially available fluorescence cube assemblies used for numerous and various applications are designed to be used with a high-pressure mercury source.

I recommend a high-speed variable wavelength and scanning monochromator be used to select and scan specific wavelengths from the continuous light source. This makes it possible to precisely select the exciting energy of the light for specific transmittance, reflectance or fluorescence measurements. In addition, it is useful to make high-speed full spectrum scanned ultraviolet measurements which ensures excellent specimen protection from continuous broadband ultraviolet illumination. Dual-lamp housings may be used to mount both the tungsten-halogen and the deuterium or mercury lamps to the base for transmission measurements or to the vertical illuminator for reflectance and/or fluorescence measurements. The light projected into the illumination train of the microscope may be directed toward the specimen using aluminum mirrors or aluminum coated all reflecting objectives. Many of the current commercially available instruments employ a stabilized high-intensity, high-pressure, continuous broadband xenon that exposes the specimen to all wavelengths from approximately 200 – 1100 nm. This high intensity source may lead to photobleaching of certain forensically important specimens. In most case, photobleaching is a permanent change that cannot be restored.

If deep UV measurements are not required, then I recommend using quartz objective of sufficient magnification and sufficiently corrected for chromatic and spherical aberrations. Most commercially available quartz objective transmit light to approximately 240 nm, such as the Zeiss Ultrafluar series. . I further recommend the analyst to have available a selection of objectives ranging from 10x to 100x magnification, depending on the specific application.

My future research will investigate using aluminum nanowire grid polarizers on a fused silica substrate in place of the absorption-type film polarizers to be used in the deep UV region. Current UV polarization is achieved by using a crystal-type polarizer down to approximately 240 nm. The application of deep UV polarized light absorption measurements on samples of forensic evidence has not been reported in the literature. It is my opinion that there is application of deep-UV polarized light for classification and discrimination ultraviolet absorbers used in the manufacture of many textile fibers and polymers often encountered as transfer evidence.

These recommendations would be incomplete without optimum parameters of the spectrometer. The spectrometer should be equipped with a variable entrance slit and a selection of diffraction gratings in order to control spectral resolution. Most modern spectrometers are designed with fixed position multi-element multichannel solid state detectors. When choosing a spectrometer, the analyst should consider the choice of solid state detector. The detector should be chosen upon considering the type of measurements being made and the level of sensitivity required. In general, a charged couple device array detector is more sensitive than a photodiode array detector, but the photodiode array detector has a higher dynamic range for highly absorbing specimens.

I also recommend the analyst select a computer software packages that allows for setting data acquisition times ranging from a very fast data collection rate of a few milliseconds, in order to collect kinetic reaction data, to a few minutes to collect data on low light emitting fluorescence specimens. The spectrometer software should be able to average a large number of data scans in order increase signal-to-noise and obtain high quality data.

In closing, I recommend that every analyst assemble a set of fibers, thin-films, polymer coatings, and other types of transfer evidence to analyze on several different microscope spectrophotometers. Become familiar with its intrinsic polarization and learn how to control the possible adverse effects. It is extremely important to the collection of high quality data and to make a correct interpretation of the spectral data. It is extremely important to become a proficient and efficient microscopist. It is just as important to become a proficient and efficient spectroscopist. Lastly, I encourage research to include the application of the proposed match criteria presented in Table 1.1 to help determine proper estimates for error rates. This would require a very large set of fibers, thin-films, and other transfer evidence.

CHAPTER 7. CONTRIBUTIONS TO CRIMINAL JUSTICE AND FORENSIC SCIENCE

At the time of this writing, an extensive literature review revealed that no references have been identified which discuss a comprehensive scientific evaluation of the performance characteristics for a high performance ultraviolet-visible forensic microscope spectrophotometer. This research provides the basis for establishing these design characteristics through the scientific evaluation of spectrometer performance which result from measuring system parameters on several different available microscope spectrophotometer systems. There are important implications for practical and therefore administration of criminal justice to the application of forensic science. The acceptance of microscope spectrophotometry by the forensic science community as an analytical methodology necessitates that it is capable of satisfying the standards for admissibility of scientific evidence in the justice system by being both reliable and relevant. Currently the quality of scientific results from microscope spectrophotometry may vary between instruments manufacturers. The outcome of this research should serve as a model for evaluating ultraviolet-visible microscope spectrophotometer performance and critical instrument parameters for determining the information content of data, and the quality of spectral results. These should assist forensic scientists with assessing instrument validity and the reliability of measurements. Furthermore, these criteria should assist the court with questions of reliability and admissibility.

The Circuit court of the District of Columbia established an admissibility standard in *Frye v. United States,* 293 F. 1013 (D.C. Cir. 1923) in which the admissibility of novel scientific evidence was dependent on it being "generally accepted in the field in which it belongs." This standard was held in federal and state courts for approximately sixty years, until the Supreme Court's decision in *Daubert v. Merrell Dow Pharmaceuticals, Inc.*, 509 U.S. 579 (1993). The Federal Rules of Evidence (FRE) were passed into law in 1975 to assist federal judges and attorneys with questions of admissibility of scientific evidence and expert testimony. The *Daubert* court (1993) ruled the FRE supersede *Frye* and offered guidelines for a trial judge to evaluate the reliability of novel scientific evidence. The *Daubert* court (1993) offered guidelines that are neither all-inclusive nor dispositive in nature, but designed to assist the trial judge as the "gatekeeper" of reliable scientific evidence. This "gatekeeper" role does not guarantee that the trial judge neither correctly determines the admission of valid scientific evidence nor prevents the admission of

"junk science", perhaps because most judges lack sufficient scientific education and training to adequately perform a judicial review (NRC, 2009). In contrast to the National Research Council (NRC) 2009 report, and in part, Justice Blackmun delivered the *Daubert* opinion of the Court:

> "[T]he trial judge must determine at the outset, pursuant to [FRE] Rule 104(a), whether the expert is proposing to testify to (1) scientific knowledge that (2) will assist the trier of fact to understand or determine a fact in issue. This entails a preliminary assessment of whether the reasoning or methodology underlying the testimony is scientifically valid and of whether that reasoning or methodology properly can be applied to the facts in issue. We are confident that federal judges possess the capacity to undertake this review. Many factors will bear on the inquiry, and we do not presume to set out a definitive checklist or test. But some general observations are appropriate." (Daubert, 1993)

While the adversarial process is not necessarily well-equipped for finding scientific truth, the admission or exclusion of scientific evidence via the *Daubert* guidelines provide several factors for the trial judge to consider: (1) whether a theory or technique has been tested, (2) whether the theory or technique has been subjected to peer review and publication, (3) the known or potential rate of error of a particular scientific technique, (4) the existence and maintenance of standards controlling the technique's operation, and (5) a scientific technique's degree of acceptance within a relevant scientific community.

Most importantly, these *Daubert* guidelines were never intended to be used as a definitive checklist, and they are neither mandatory nor exclusive. Many microspectroscopical methodologies are accepted by the relevant scientific community and United States courts recognize these microanalytical techniques as being reliable and valid. Reliable may be thought of as the extent to which an observation or measurement procedure produces the same results on repeated trials, while validity may signify the extent to which the instrument measures what it purports to measure. With these factors in mind, it is incumbent upon the forensic science discipline to ensure it achieves the highest degree of reliability in order to serve the goals of justice.

In the opening summary of the National Academy of Sciences, Strengthening Forensic Science in the United States: A Path Forward,

> "[O]fficials and the members of society they serve need to be assured that forensic techniques are *reliable*. Therefore, we must limit the risk of having the reliability of certain forensic science methodologies judicially certified before the techniques have been properly studied and their accuracy verified by the forensic science community. "[T]here is no evident reason why ['rigorous, systematic'] research would be infeasible." However, some courts appear to be loath to insist on such research as a

> condition of admitting forensic science evidence in criminal cases, perhaps because to do so would likely "demand more by way of validation than the disciplines can presently offer." (NRC, 2009).
> *(Note: emphasis in the original.)*

This quote is quite profound. We, as forensic scientists, must ensure our methodologies and interpretations are based on good science. Scientific facts are established when the validity is expressed or explained to the satisfaction of a prudent and reasonable mind, whereas legal facts are not based on the scientific method, but rather by the adversarial legal system. The role of scientific evidence in the administration of both criminal and civil justice may be summarized as providing the legal system with valid and reliable facts, where the law decides which facts appear most attributive by applying selection criteria that may have absolutely nothing to do with science. A better understanding of microscope spectrophotometry will impact the justice system through better characterization and more accurate comparison of naturally colored or dyed microscopical transfer evidence, which may lead to an increase in significance and usefulness of an association based on transfer evidence examinations and interpretations.

In an ongoing study of random fibers obtained from dryer lint collected from local laundry wash and dry facilities from New York, New Jersey, and Connecticut, approximately 80% of the 3000 fibers examined under plane polarized light exhibited visible dichroism (Prichard and Reffner, personal communication, 2013). These preliminary data indicate the need for instrumentation to not only observe the dichroism, but also a reliable methodology to measure and interpret the spectral data. The acquisition of dichroic spectra to calculate linear dichroism and dichroic ratios is a straight forward process. The added level of discrimination supports the premise that all microscope spectrophotometry measurements should be made using plane polarized light.

The intrinsic polarization studies reported here illustrate the importance of determining the impact that polarization effects may have on the interpretation of spectral data collected on any microscope photometric instrument. The data indicates that polarized light illumination must be used to more closely control these polarization effects, which may plague microscope spectrophotometer systems that use unpolarized light illumination. It is absolutely necessary to determine the degree of polarization in each instrument before making any spectral measurements on specimens of forensic interest (evidence) which may be subjected to spectral comparison to establish inference of common origin. Failing to determine

microscope spectrophotometric instrument intrinsic polarization and properly controlling for dichroic shifts may have a direct negative impact on the reliability of spectral results.

Instruments that use unpolarized light illumination are not immune to intrinsic polarization because an anisotropic specimen splits the light into two orthogonal polarization states, which propagates to the grating and exhibits the same effects as demonstrated using a linear polarizer. Inadequate control of polarization and intrinsic polarization will directly impact the likelihood for a dichroic shift to occur. This may result in an erroneous spectrum that could lead to an error in the interpretation. The interpretation may be either a false positive or a false negative association.

This research contributes to the existing knowledge by identifying optimum instrument features and function characteristics while establishing well defined limitations of the instrumentation and techniques. In addition, this research has developed or delineated fundamental scientific parameters necessary to satisfy the rigorous scientific testing necessary to assess reliability, validity, and to ultimately satisfy the scientific testing required of forensic methods presented in the courts of law. The results of this research may be used to establish a model to identify the optimum instrumental parameters and functions, supported by thorough scientific evaluation, in order to assure the most reliable, and defendable results.

APPENDIX I. SPECTRAL DATA FOR CRAIC TECHNOLOGIES QDI 2010 SYSTEM 1

WAVELENGTH ACCURACY AND PRECISION

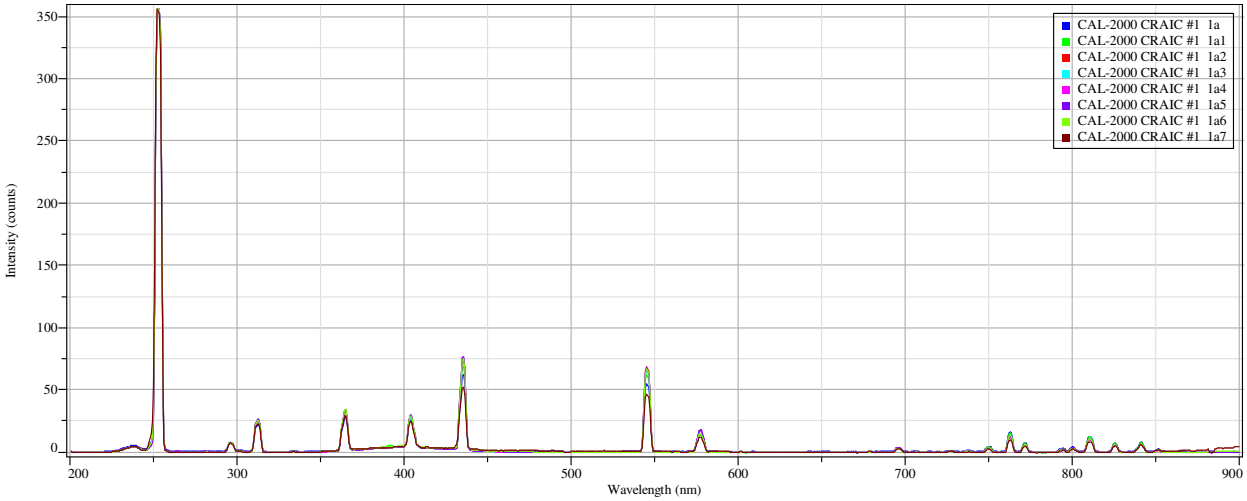

Figure A1.1: Example of an overlay spectrum consisting of eight measurements of a CAL-2000 calibration lamp.

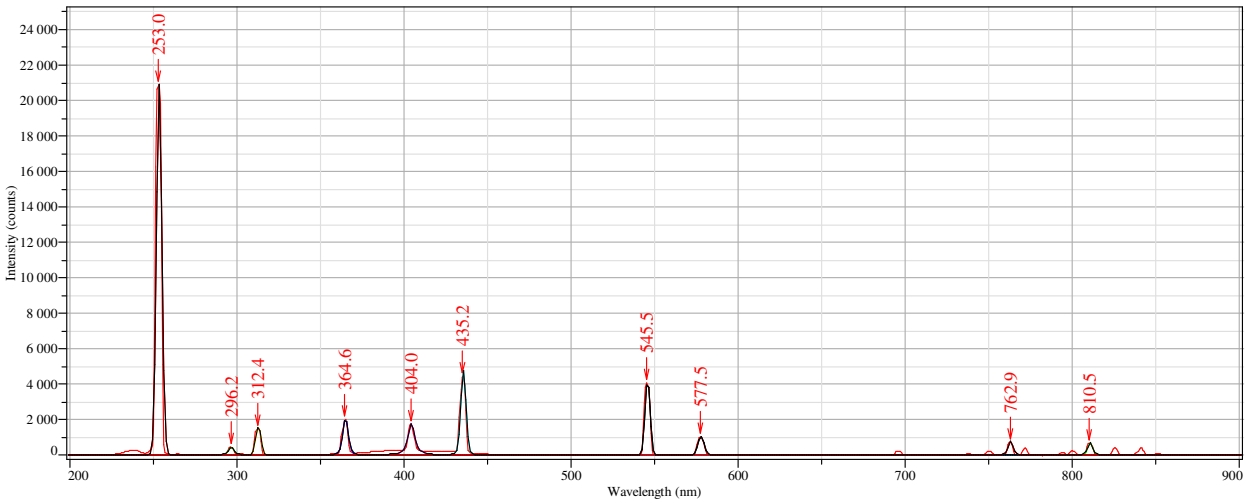

Figure A1.2: Example of a CAL-2000 calibration lamp spectrum that has undergone preprocessing functions for peak-fitting with baseline correction. Wavelength values at peak maximums for several peaks across the spectral range were tabulated and used to determine wavelength accuracy and precision, or wavelength dependence on spectral resolution. The results of which are located in the Instrument Qualification and Summary Report.

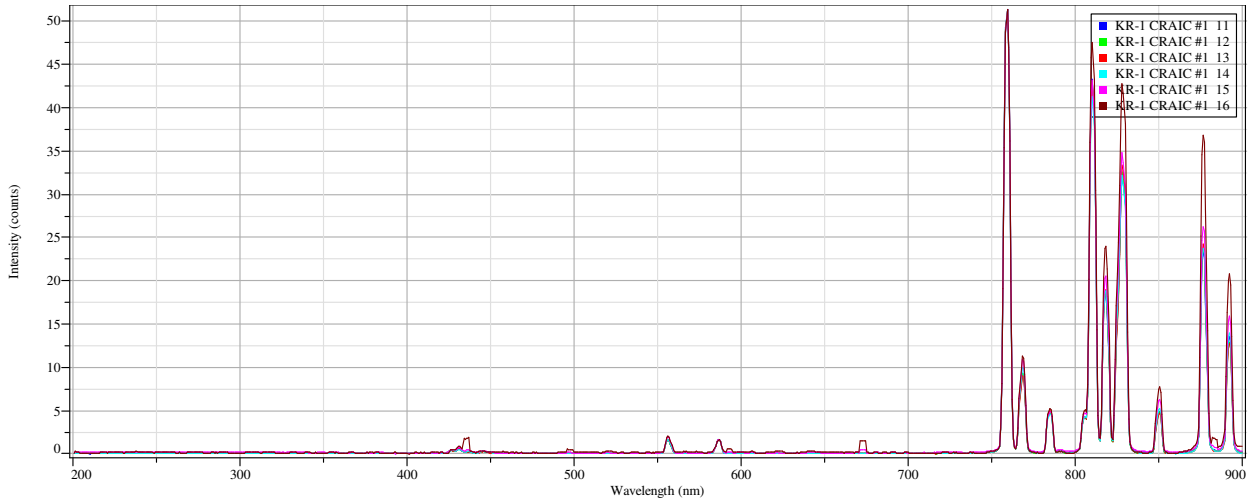

Figure A1.3: Example of an overlay spectrum consisting of six measurements of a KR-1 calibration lamp.

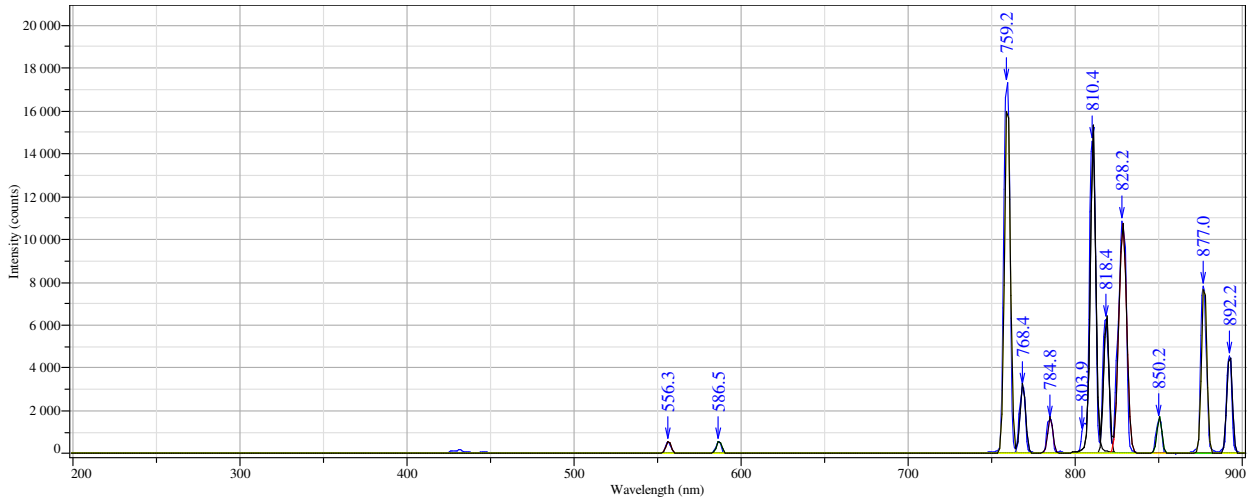

Figure A1.4: Example of a KR-1 calibration lamp spectrum that has undergone preprocessing functions for peak-fitting with baseline correction. Wavelength values at peak maximums for several peaks across the spectral range were tabulated and used to determine wavelength accuracy and precision, or wavelength dependence on spectral resolution. The results of which are located in the Instrument Qualification and Summary Report.

Wavelength Accuracy and Wavelength Precision Data													
*λ (nm)	1	2	3	4	5	6	7	8	9	10	Ave. λ	stdev	*λ – Ave.λ
253.65	252.2	252.2	252.2	252.2	252.2	252.2	252.2	252.2	252.2	252.2	252.2	3.0E-14	1.45
296.72	295.1	295.1	295.1	295.1	295.1	295.1	295.1	295.1	295.1	295.1	295.1	6.1E-14	1.62
312.57	311.5	311.5	311.5	311.5	311.5	311.5	311.5	311.5	311.5	311.5	311.5	0.0E+00	1.07
365.02	363.9	363.9	363.9	363.9	363.9	363.9	363.9	363.9	363.9	363.9	363.9	6.1E-14	1.12
404.66	403.4	403.4	403.4	403.4	403.4	403.4	403.4	403.4	403.4	403.4	403.4	6.1E-14	1.26
435.93	434.5	434.5	434.5	434.5	434.5	434.5	434.5	434.5	434.5	434.5	434.5	0.0E+00	1.43
546.07	544.6	544.6	544.6	544.6	544.6	544.6	544.6	544.6	544.6	544.6	544.6	0.0E+00	1.47
578.01	576.6	576.6	576.6	576.6	576.6	576.6	576.6	576.6	576.6	576.6	576.6	0.0E+00	1.41
763.51	761.8	761.8	761.8	761.8	761.8	761.8	761.8	761.8	761.8	761.8	761.8	1.2E-13	1.71
772.42	770.7	770.7	770.7	770.7	770.7	770.4	770.7	770.7	770.7	770.7	770.7	1.1E-01	1.72
811.53	809.4	809.4	809.4	809.4	809.4	809.4	809.4	809.4	809.4	809.5	809.4	1.2E-13	2.13

Table A1.1: Summary table containing wavelength accuracy, precision, and deviation data calculated from ten independent measurements of Ocean Optics® CAL-2000™ mercury-argon calibration low-pressure gas discharge calibration lamp. *Standard spectral data wavelength values were obtained from ASTM E275-08.

PHOTOMETRIC ACCURACY, PRECISION AND LINEARITY

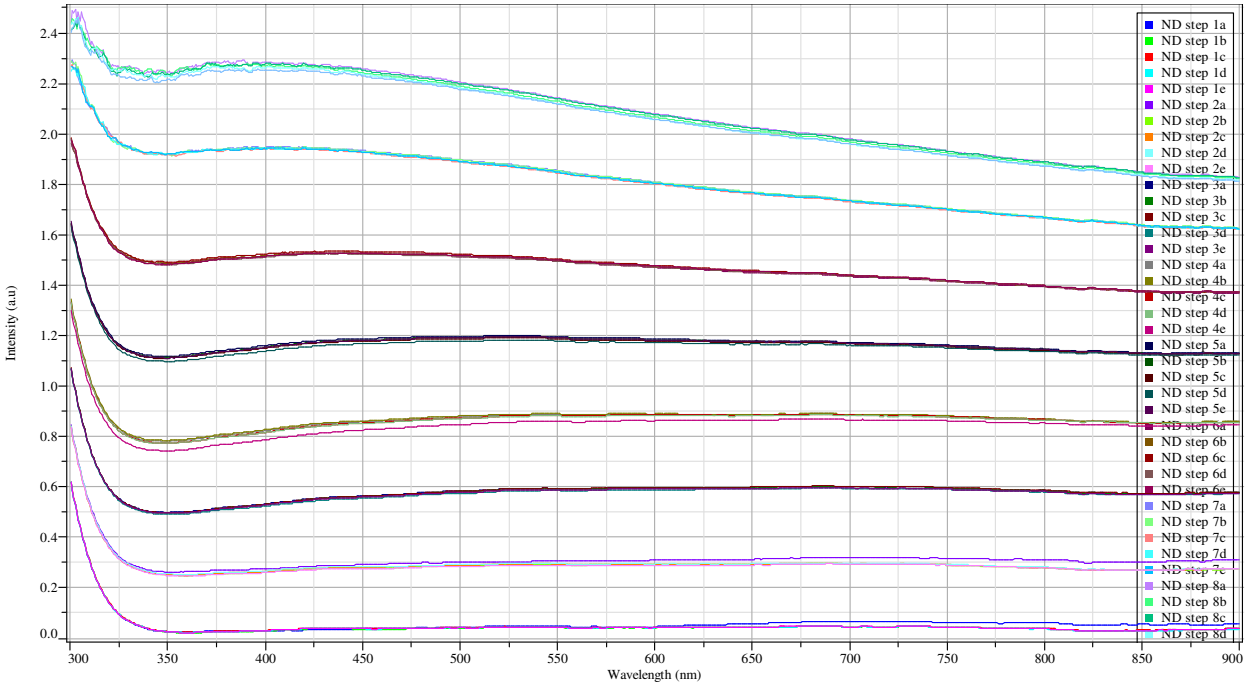

Figure A1.5: Overlay spectra of five measurements at each of eight steps on Edmund Optics® stepped optical density slide #1.

Reference Material: Edmund Optics® Stepped Optical Density Slide #1								
Optical Density (*True) - Step	400 nm		500 nm		600 nm		700 nm	
	Mean	St Dev	Mean	St Dev	Mean	St Dev	Mean	St Dev
(0.04) – step 1	0.06	0.012	0.06	0.009	0.06	0.005	0.06	0.005
(0.34) – step 2	0.24	0.005	0.25	0.004	0.26	0.004	0.26	0.004
(0.63) – step 3	0.54	0.012	0.57	0.011	0.59	0.010	0.59	0.009
(0.93) – step 4	0.85	0.004	0.89	0.006	0.89	0.006	0.89	0.006
(1.22) – step 5	1.15	0.008	1.19	0.008	1.18	0.008	1.16	0.008
(1.52) – step 6	1.47	0.015	1.51	0.022	1.47	0.026	1.43	0.028
(1.82) – step 7	1.78	0.004	1.87	0.006	1.79	0.006	1.72	0.007
(2.11) – step 8	1.95	0.006	2.13	0.008	2.04	0.007	1.95	0.008

Table A1.2: Summary table containing photometric accuracy and photometric precision data for an Edmund Optics® stepped optical density slide. Values represent mean and standard deviation of five measurements. Red-color horizontal data was used to determine photometric accuracy and precision, while the red-colored vertical data was used to determine photometric linearity found in the "Instrument Qualification and Summary Report", which accompanies the discussion of each instrument in the Results chapter. *The true value was obtained from the documented stepped optical density slides.

PHOTOMETRIC NOISE

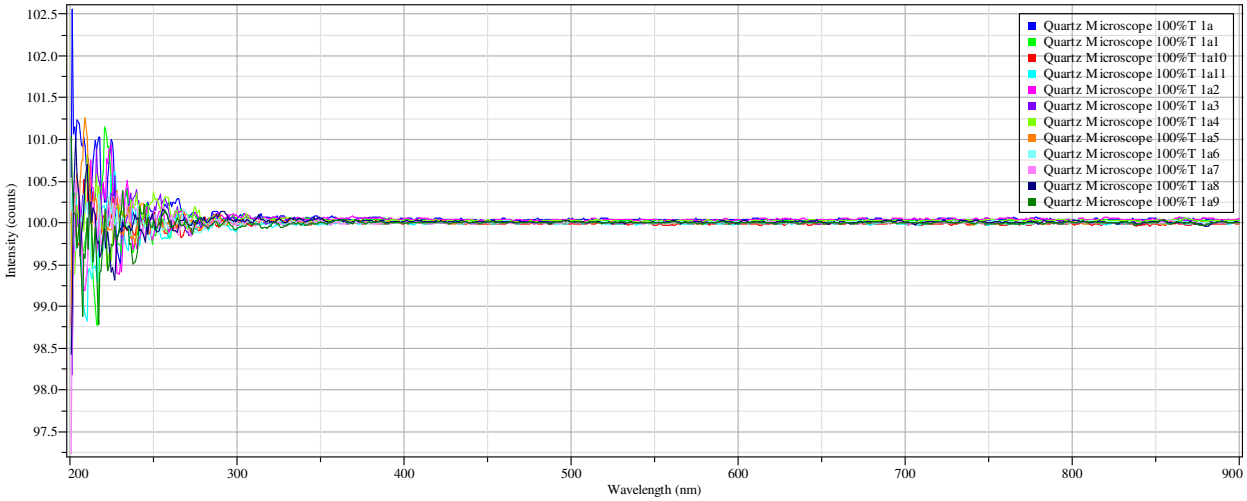

Figure A1.6: Overlay of twelve 100% Transmittance spectra used to calculate the RMS noise and short-term instrument stability

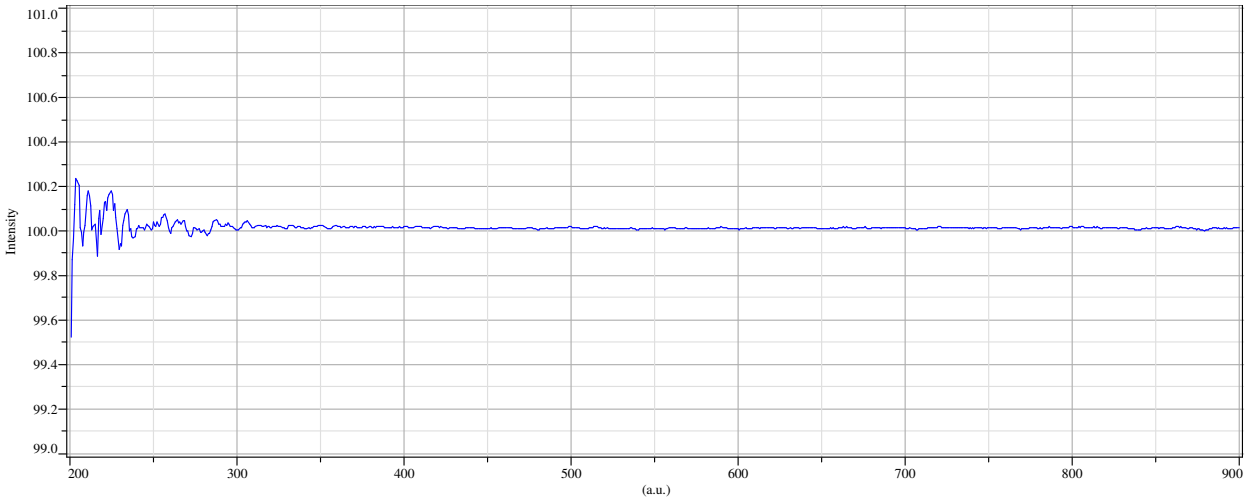

Figure A1.7: RMS Noise, mean spectrum

RMS Noise Data, 100%T			
λ	Slope	y-intercept	RMS Noise
300	3.85E-04	99.90757	1.15E-02
400	2.34E-04	99.9249	1.60E-03
500	-2.79E-04	100.1537	2.64E-03
600	-1.94E-04	100.1281	2.71E-03
700	-5.61E-04	100.4058	1.36E-03

Table A1.3: Summary Tabulation of RMS noise data.

λ	y-intercept	deviation
300	99.9	-0.1
400	99.9	-0.1
500	100.1	0.1
600	100.1	0.1
700	100.4	0.4

Table A1.4: Summary table containing short-term baseline stability data where deviations from 100%T is an indication of short term baseline instability and may indicate a malfunction of the microscope spectrophotometer.

SPECTRAL RESOLUTION DEPENDENCE ON WAVELENGTH

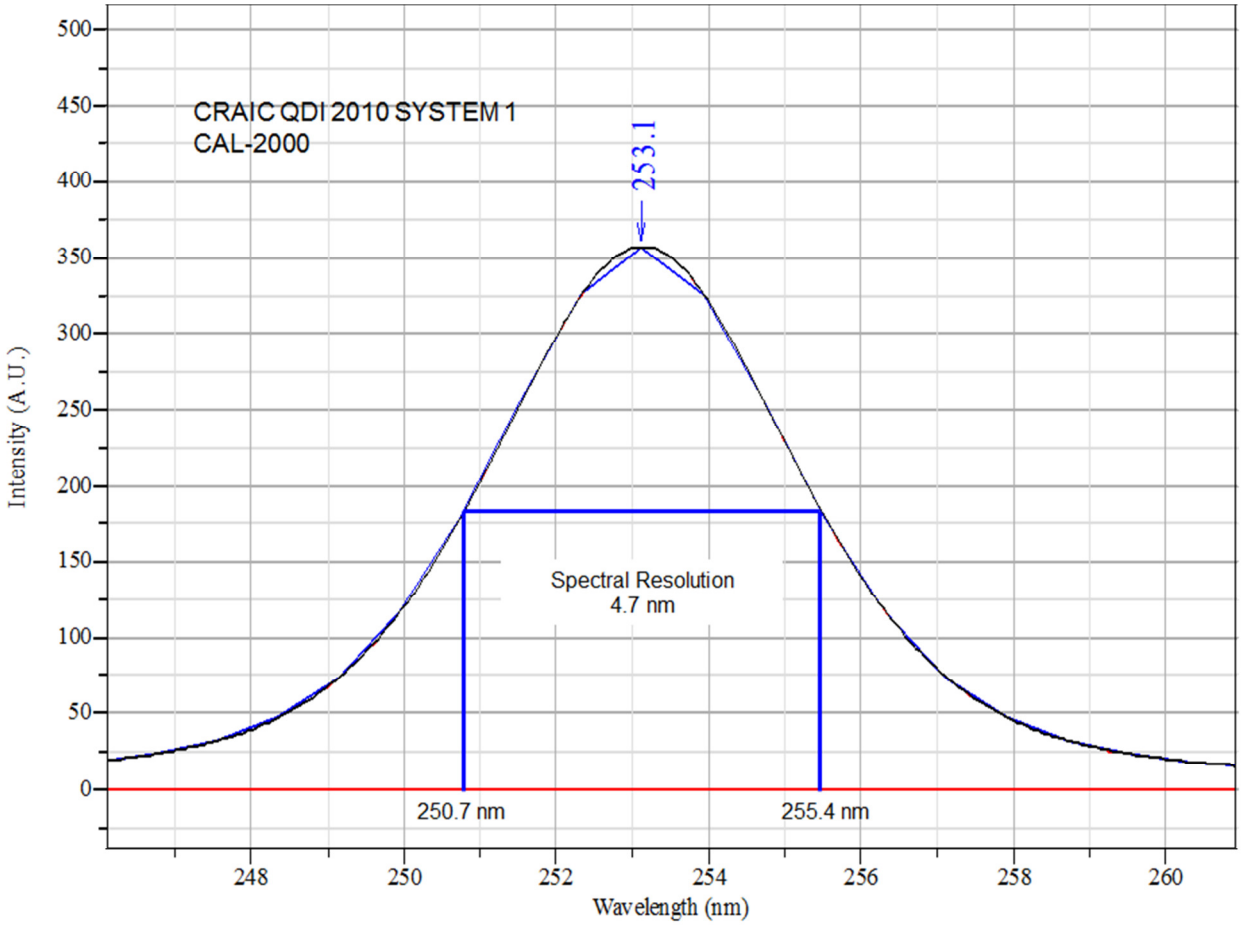

Figure A1.8: Spectral resolution of 4.7 nm at central wavelength 253.1 nm.

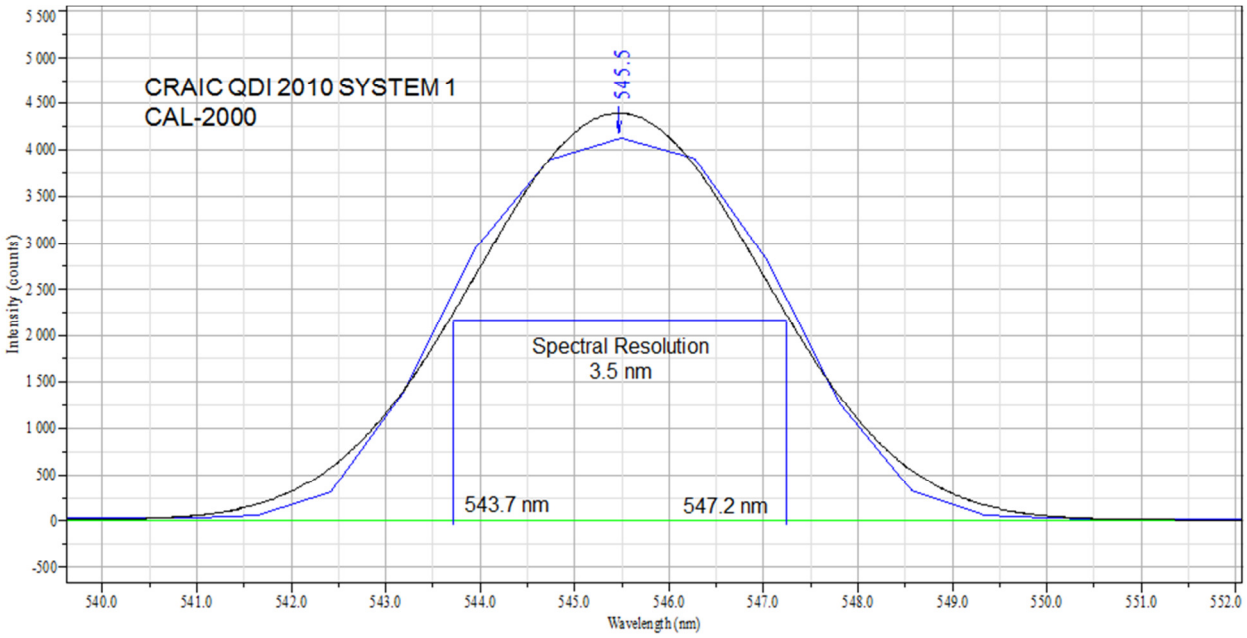

Figure A1.9: Spectral resolution of 3.5 nm at central wavelength 545.5 nm.

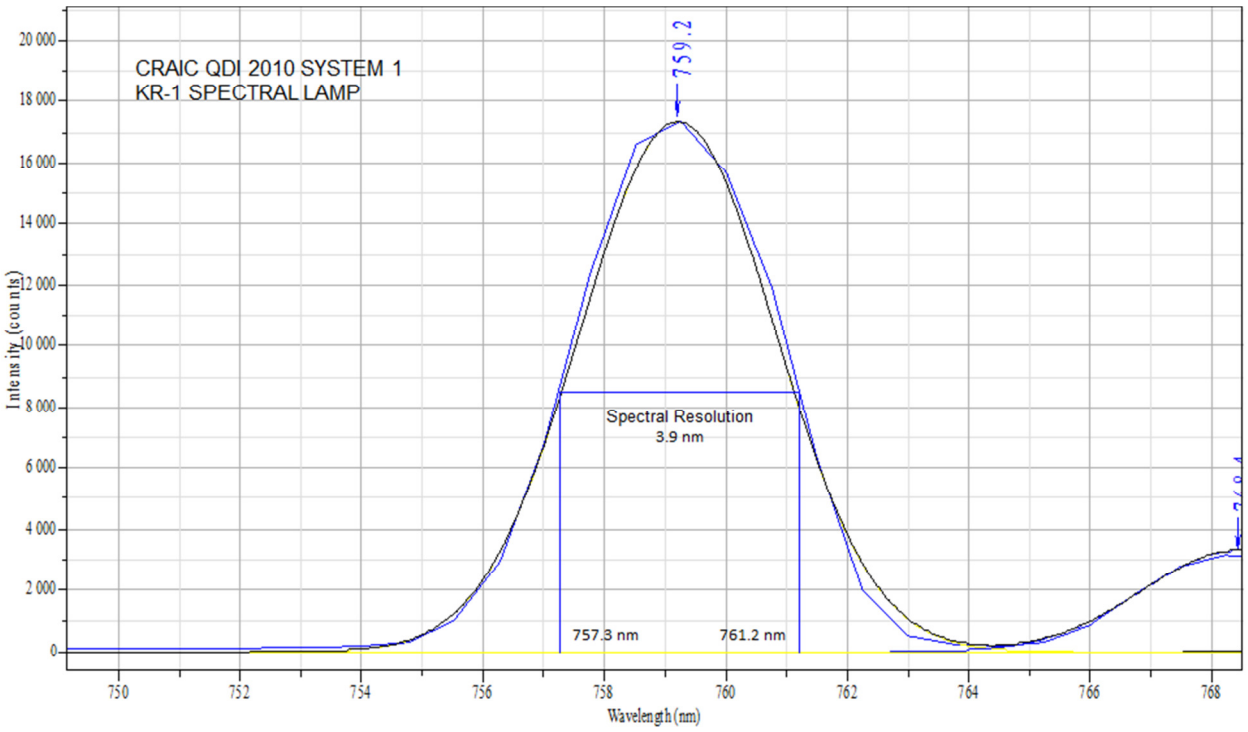

Figure A1.10: Spectral resolution at 760.15 nm.

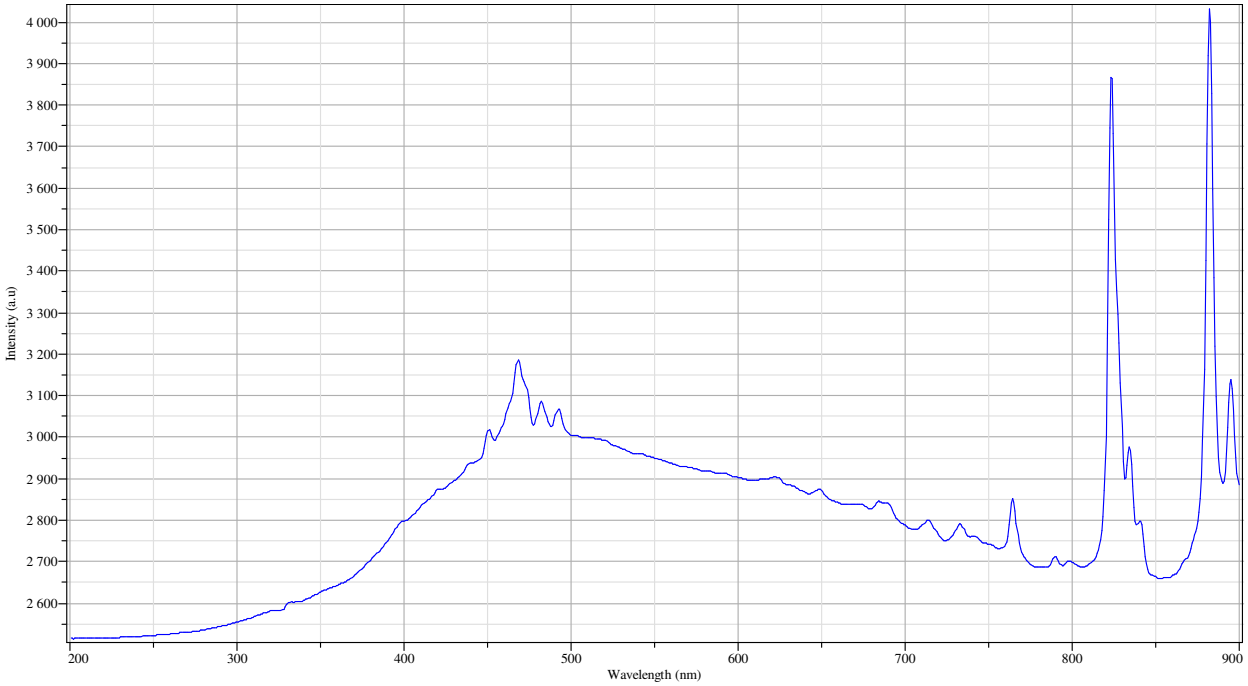

Figure A1.11: Single-beam reflection spectrum of Xenon high-pressure discharge lamp reflected off SRM2017 mulitangle white reflection standard.

APPENDIXI II. SPECTRAL DATA FOR CRAIC TECHNOLOGIES QDI 2010 SYSTEM 2

WAVELENGTH ACCURACY AND PRECISION

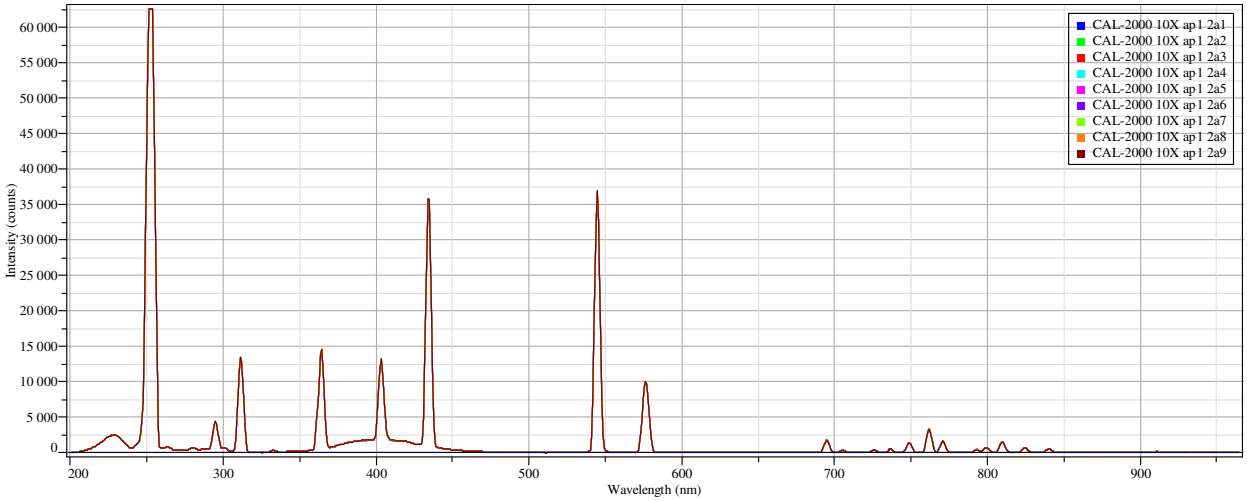

Figure A2.1: Example of an overlay spectrum consisting of nine measurements of a CAL-2000 calibration lamp.

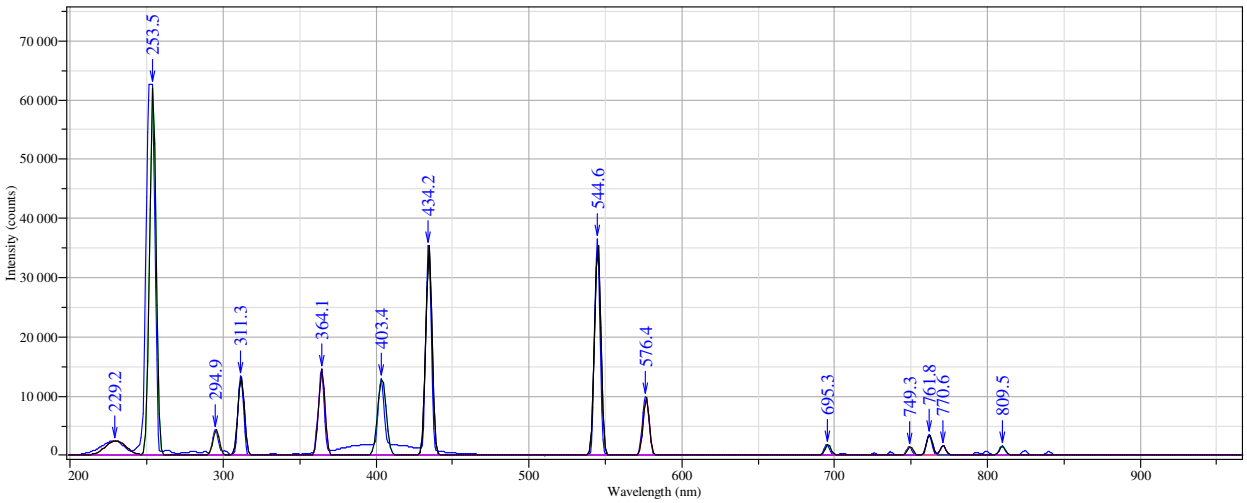

Figure A2.2: Example of a CAL-2000 calibration lamp spectrum that has undergone preprocessing functions for peak-fitting with baseline correction. Wavelength values at peak maximums for several peaks across the spectral range were tabulated and used to determine wavelength accuracy and precision, or wavelength dependence on spectral resolution. The results of which are located in the Instrument Qualification and Summary Report.

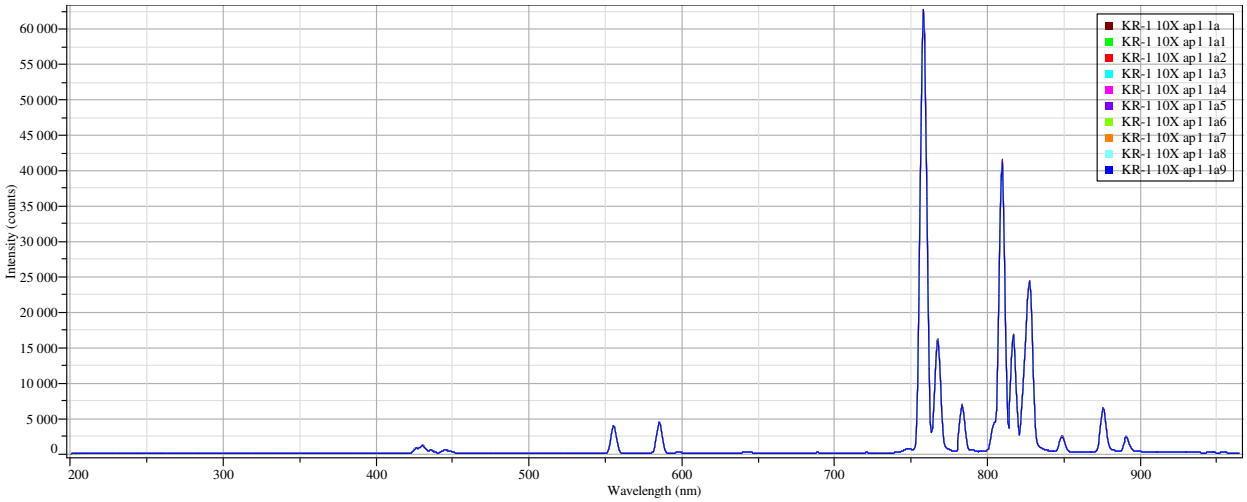

Figure A2.3: Example of an overlay spectrum consisting of nine measurements of a KR-1 calibration lamp.

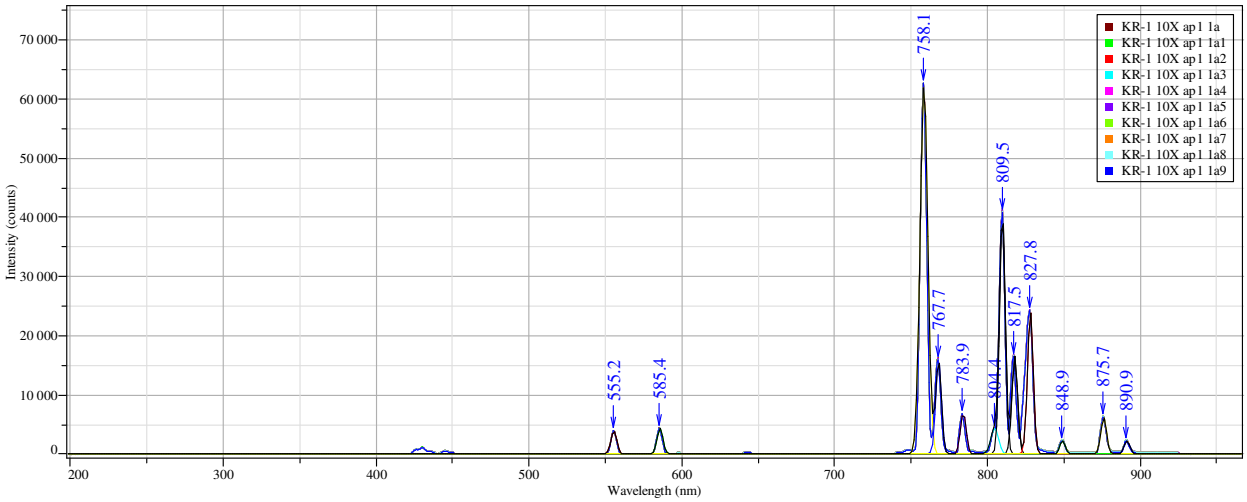

Figure A2.4: Example of a KR-1 calibration lamp spectrum that has undergone preprocessing functions for peak-fitting with baseline correction. Wavelength values at peak maximums for several peaks across the spectral range were tabulated and used to determine wavelength accuracy and precision, or wavelength dependence on spectral resolution. The results of which are located in the Instrument Qualification and Summary Report.

Wavelength Accuracy and Wavelength Precision Data													
*λ (nm)	1	2	3	4	5	6	7	8	9	10	Ave. λ	stdev	*λ – Ave.λ
253.65	252.2	252.2	252.2	252.2	252.2	252.2	252.2	252.2	252.2	252.2	252.2		1.45
296.72	295.1	295.1	295.1	295.1	295.1	295.1	295.1	295.1	295.1	295.1	295.1		1.62
312.57	311.5	311.5	311.5	311.5	311.5	311.5	311.5	311.5	311.5	311.5	311.5		1.07
365.02	363.9	363.9	363.9	363.9	363.9	363.9	363.9	363.9	363.9	363.9	363.9		1.12
404.66	403.4	403.4	403.4	403.4	403.4	403.4	403.4	403.4	403.4	403.4	403.4		1.26
435.93	434.5	434.5	434.5	434.5	434.5	434.5	434.5	434.5	434.5	434.5	434.5		1.43
546.07	544.6	544.6	544.6	544.6	544.6	544.6	544.6	544.6	544.6	544.6	544.6		1.47
578.01	576.6	576.6	576.6	576.6	576.6	576.6	576.6	576.6	576.6	576.6	576.6		1.41
763.51	761.8	761.8	761.8	761.8	761.8	761.8	761.8	761.8	761.8	761.8	761.8		1.71
772.42	770.7	770.7	770.7	770.7	770.7	770.7	770.7	770.7	770.7	770.7	770.7		1.72
811.53	809.4	809.4	809.4	809.4	809.4	809.4	809.4	809.4	809.4	809.5	809.4		2.13

Table A2.1: Summary table containing wavelength accuracy, precision, and deviation data calculated from ten independent measurements of Ocean Optics® CAL-2000™ mercury-argon calibration low-pressure gas discharge calibration lamp. *Standard spectral data wavelength values were obtained from ASTM E275-08.

PHOTOMETRIC ACCURACY, PRECISION AND LINEARITY

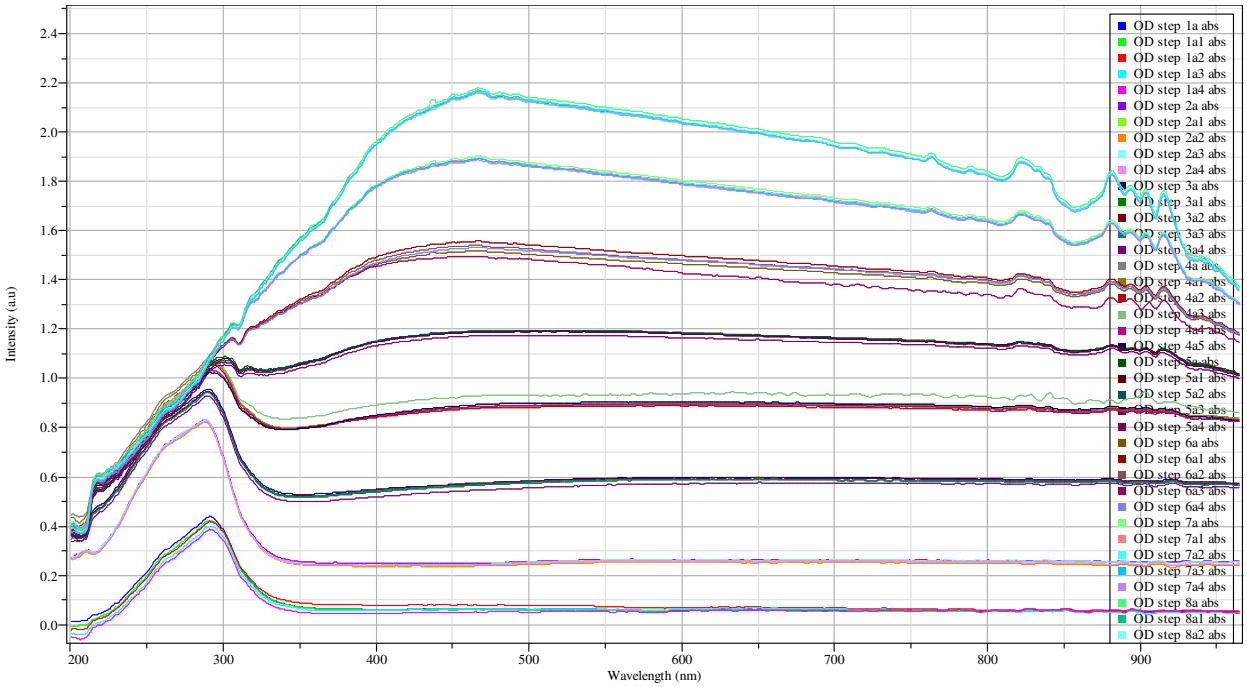

Figure A2.5: Overlay spectra of five measurements at each of eight steps on Edmund Optics® stepped optical density slide #1.

Reference Material: Edmund Optics® Optical Density Stepped Slide #1								
Optical Density (*True) - Step	400 nm		500 nm		600 nm		700 nm	
	Mean	St Dev	Mean	St Dev	Mean	St Dev	Mean	St Dev
(0.04) – step 1	0.06	0.012	0.06	0.009	0.06	0.005	0.06	0.005
(0.34) – step 2	0.24	0.005	0.25	0.004	0.26	0.004	0.26	0.004
(0.63) – step 3	0.54	0.012	0.57	0.011	0.59	0.010	0.59	0.009
(0.93) – step 4	0.85	0.004	0.89	0.006	0.89	0.006	0.89	0.006
(1.22) – step 5	1.15	0.008	1.19	0.008	1.18	0.008	1.16	0.008
(1.52) – step 6	1.47	0.015	1.51	0.022	1.47	0.026	1.43	0.028
(1.82) – step 7	1.78	0.004	1.87	0.006	1.79	0.006	1.72	0.007
(2.11) – step 8	1.95	0.006	2.13	0.008	2.04	0.007	1.95	0.008

Table A2.2: Summary table containing photometric accuracy and photometric precision data for an Edmund Optics® stepped optical density slide. Values represent mean and standard deviation of five measurements. Red-color horizontal data was used to determine photometric accuracy and precision, while the red-colored vertical data was used to determine photometric linearity found in the "Instrument Qualification and Summary Report", which accompanies the discussion of each instrument in the Results chapter. *The true value was obtained from the documented stepped optical density slides.

PHOTOMETRIC NOISE

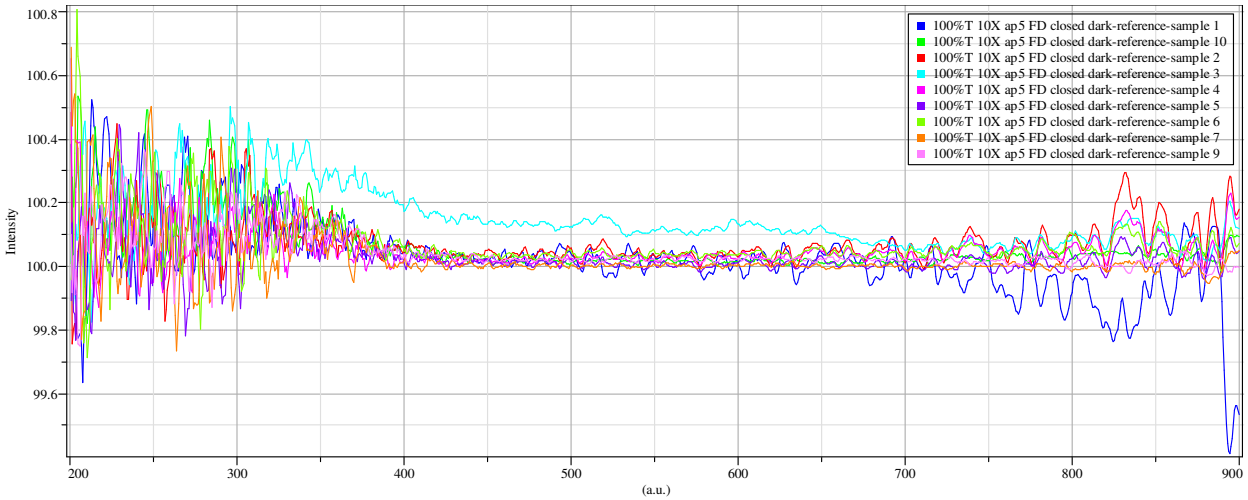

Figure A2.6: Overlay of ten 100% Transmittance spectra used to calculate the RMS noise and short-term instrument stability

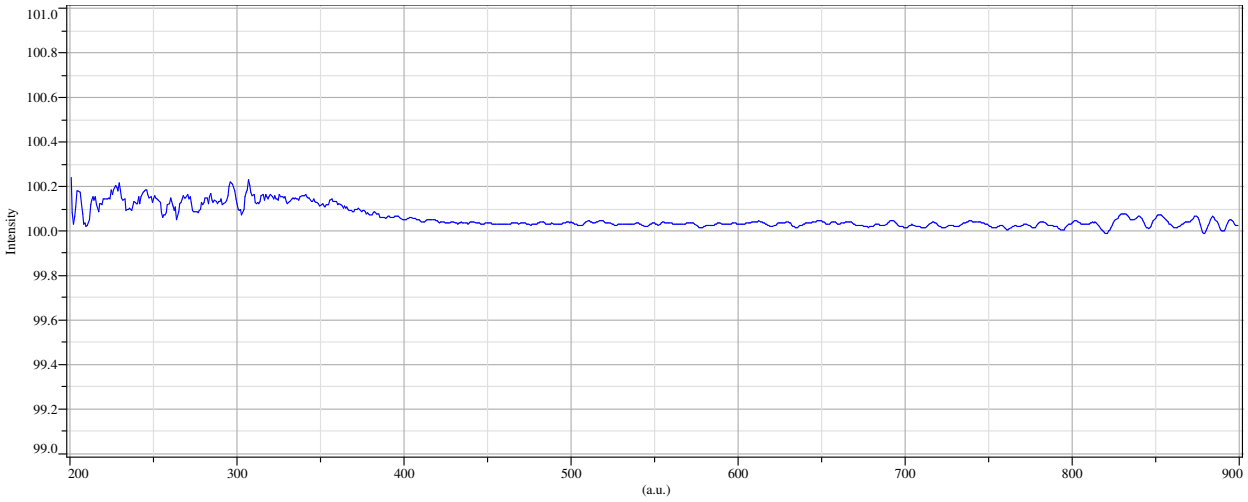

Figure A2.7: RMS Noise, mean spectrum

Photometric RMS noise, 100 %T			
λ	slope	y-intercept	%T RMS noise
300	9.78E-04	99.86134	4.55×10^{-02}
400	-7.72E-04	100.3669	3.97×10^{-03}
500	-2.68E-04	100.167	5.19×10^{-03}
600	3.17E-04	99.84373	1.60×10^{-03}
700	-1.24E-03	100.8959	7.15×10^{-03}

Table A2.3: Summary Tabulation of RMS noise data.

λ	y-intercept	deviation
300	99.8	-0.2
400	100.3	0.3
500	100.1	0.1
600	99.8	-0.2
700	100.8	0.8

Table A2.4: Summary table containing short-term baseline stability data where deviations from 100%T is an indication of short term baseline instability and may indicate a malfunction of the microscope spectrophotometer.

SPECTRAL RESOLUTION DEPENDENCE ON WAVELENGTH

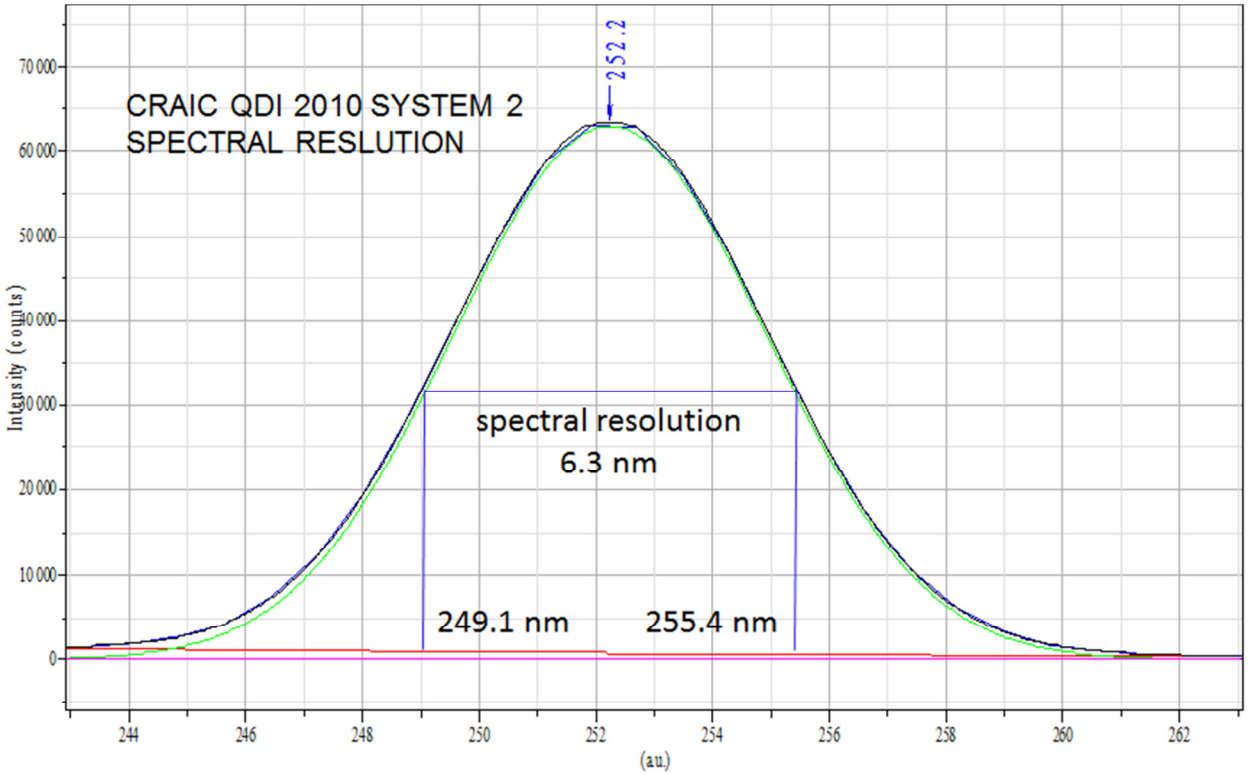

Figure A2.8: Spectral resolution of 6.3 nm at central wavelength 252.2 nm.

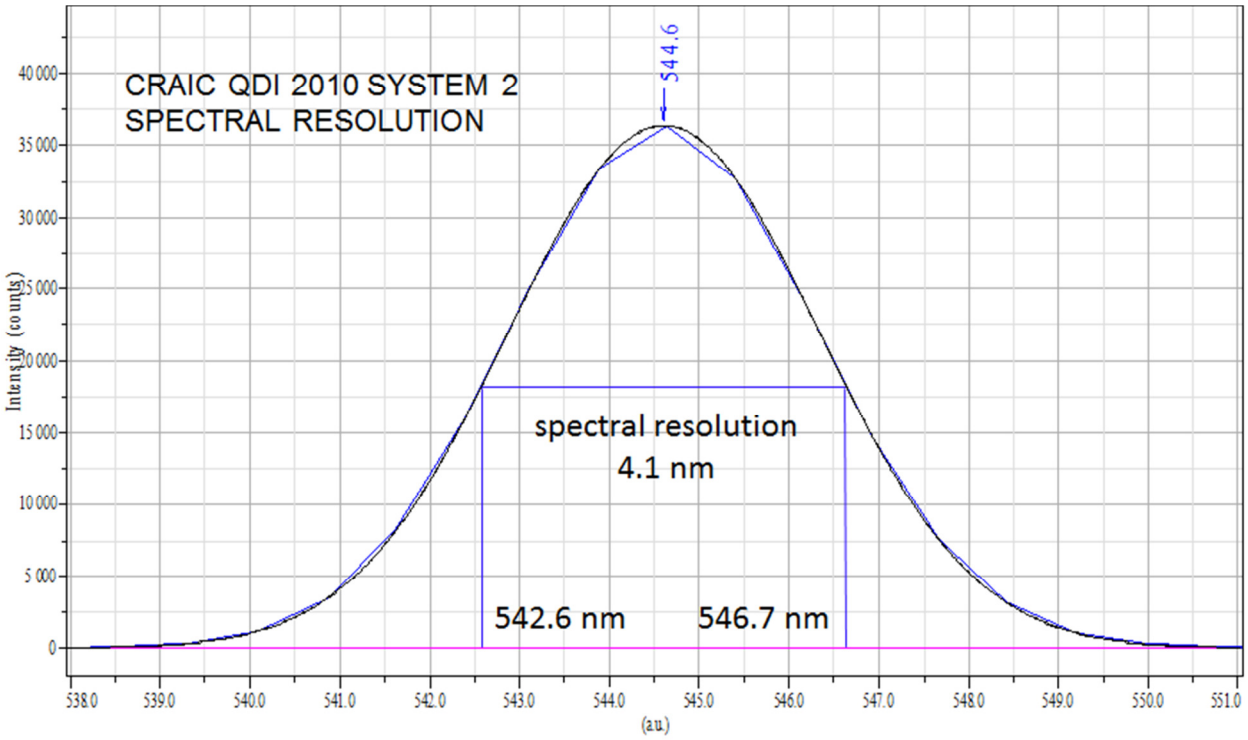

Figure A2.9: Spectral resolution of 4.1 nm at central wavelength 544.6 nm.

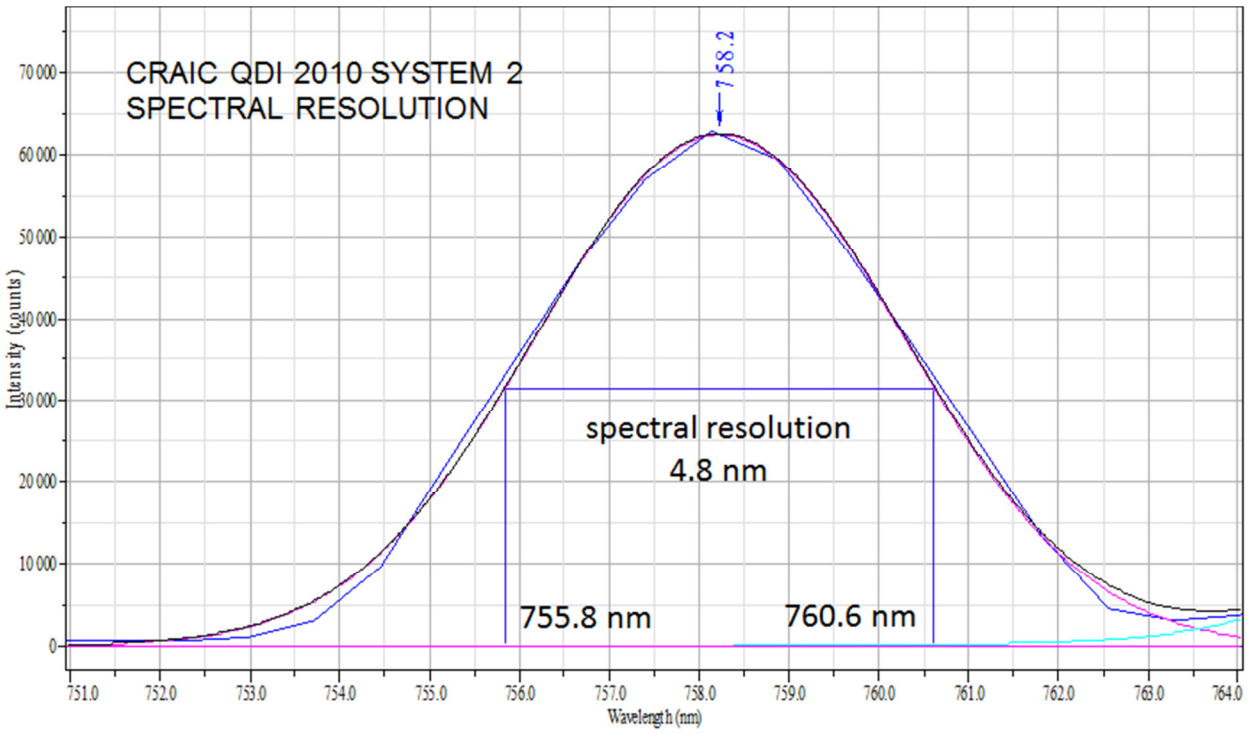

Figure A2.10: Spectral resolution of 4.8 nm at central wavelength 758.2 nm.

APPENDIX III. SPECTRAL DATA FOR ZEISS MPM400-MSP65

WAVELENGTH ACCURACY AND PRECISION

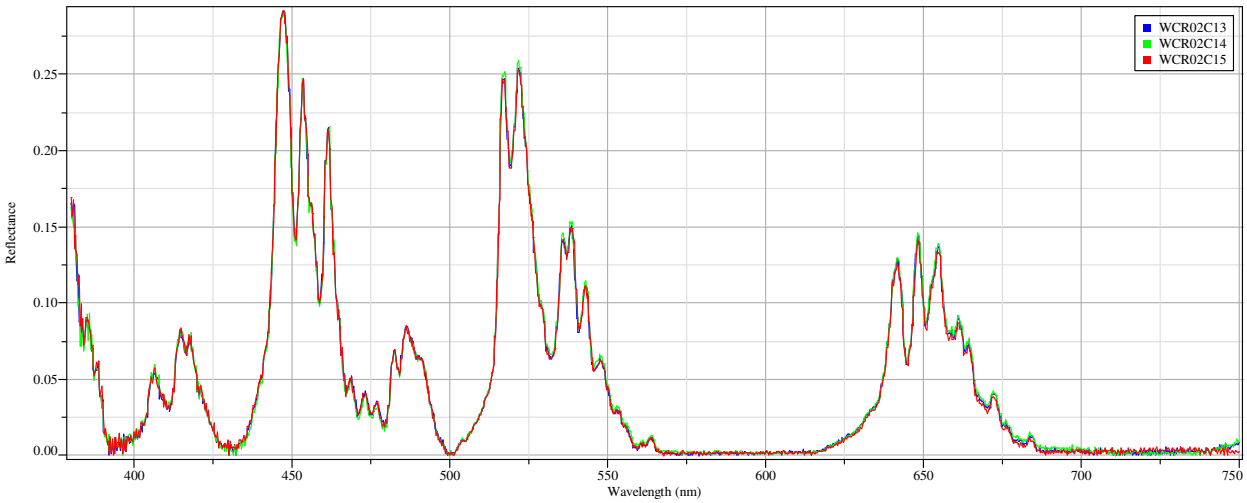

Figure A3.1: Example of an overlay spectrum consisting of three measurements of a FW-WC-UVVis-02c, holmium oxide reflection reference material.

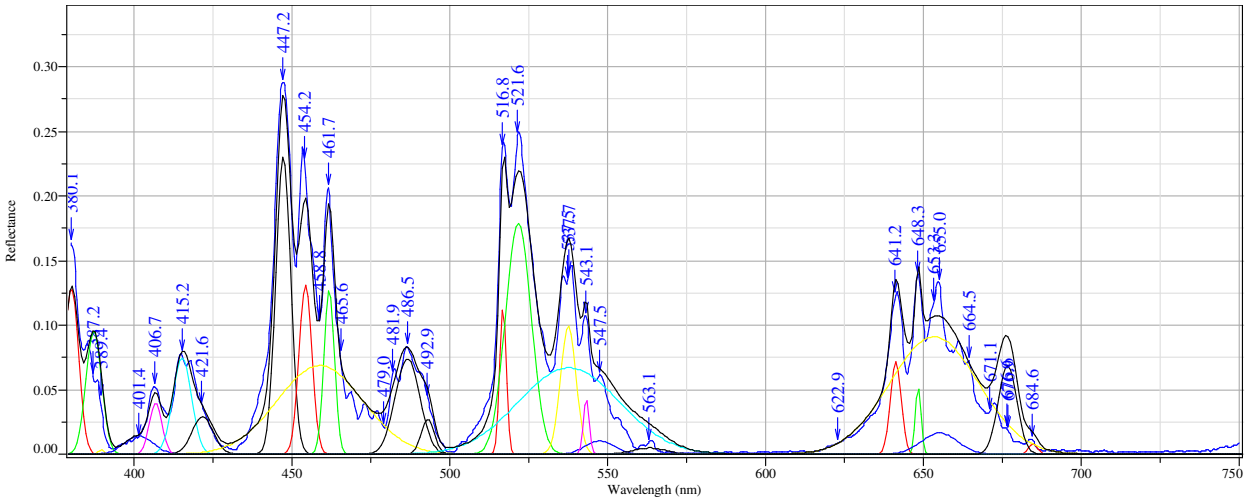

Figure A3.2: Example of a FW-WC-UVVis-02c, holmium oxide reflection reference material spectrum that has undergone preprocessing functions for peak-fitting with baseline correction. Wavelength values at peak maximums for several peaks across the spectral range were tabulated and used to determine wavelength accuracy and precision, or wavelength dependence on spectral resolution. The results of which are located in the Instrument Qualification and Summary Report.

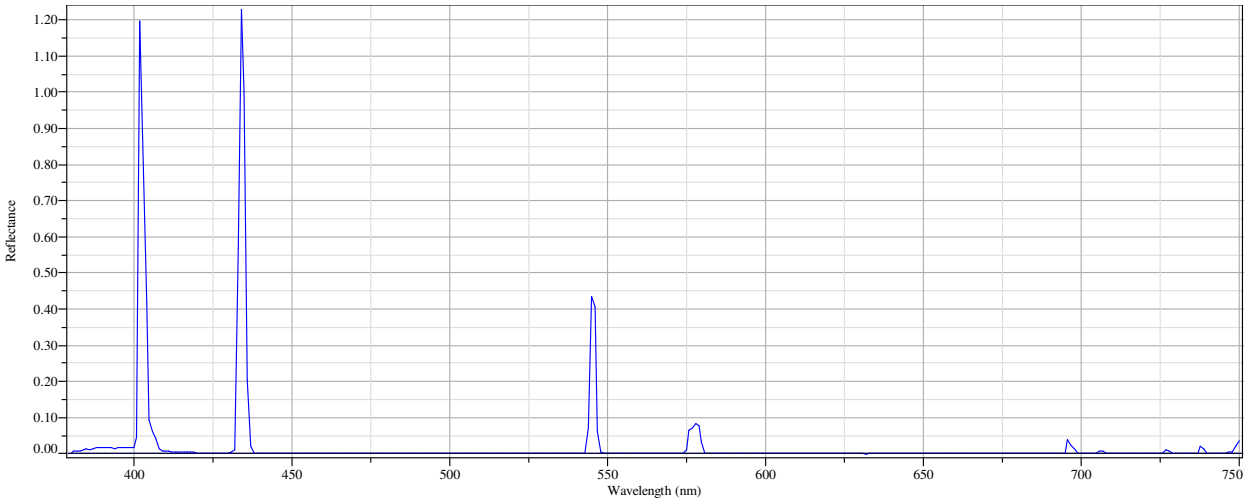

Figure A3.3: Example of a spectrum of a CAL-2000 calibration lamp.

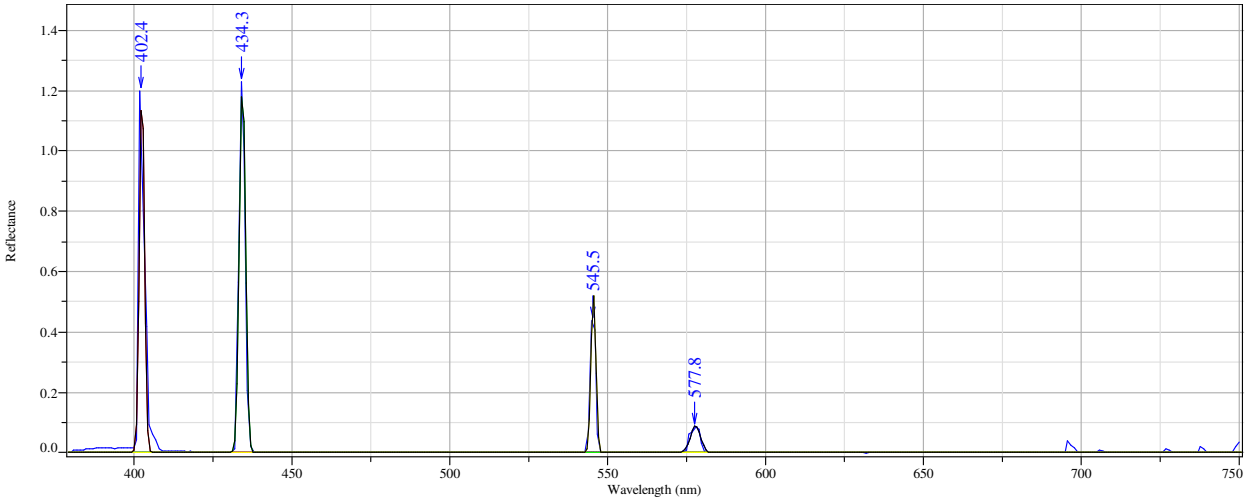

Figure A3.4: Example of a CAL-2000 calibration lamp spectrum that has undergone preprocessing functions for peak-fitting with baseline correction. Wavelength values at peak maximums for several peaks across the spectral range were tabulated and used to determine wavelength accuracy and precision, or wavelength dependence on spectral resolution. The results of which are located in the Instrument Qualification and Summary Report.

PHOTOMETRIC NOISE

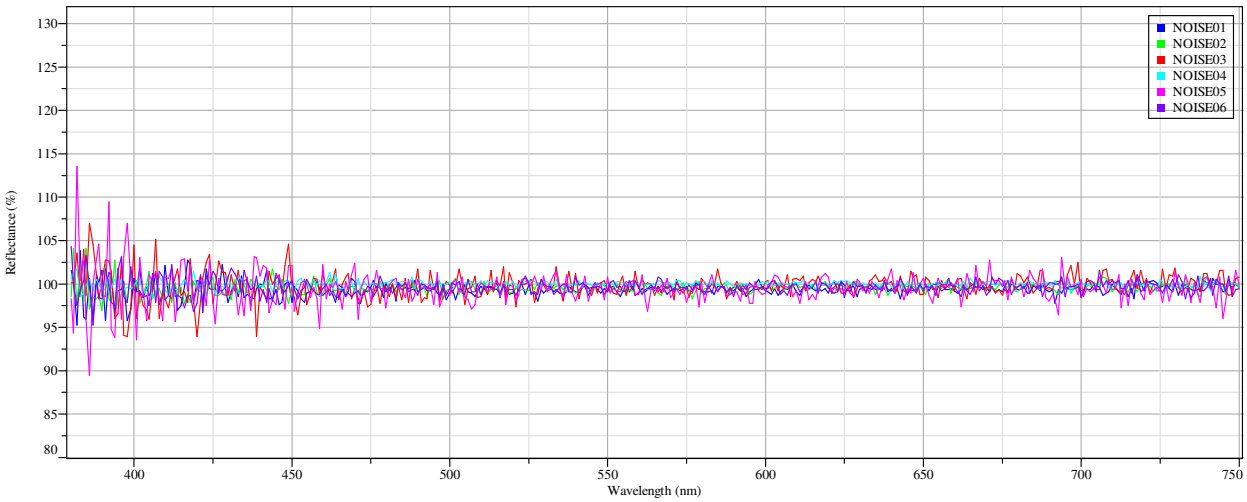

Figure A3.5: Overlay of six 100% Transmittance spectra used to calculate the RMS noise and short-term instrument stability

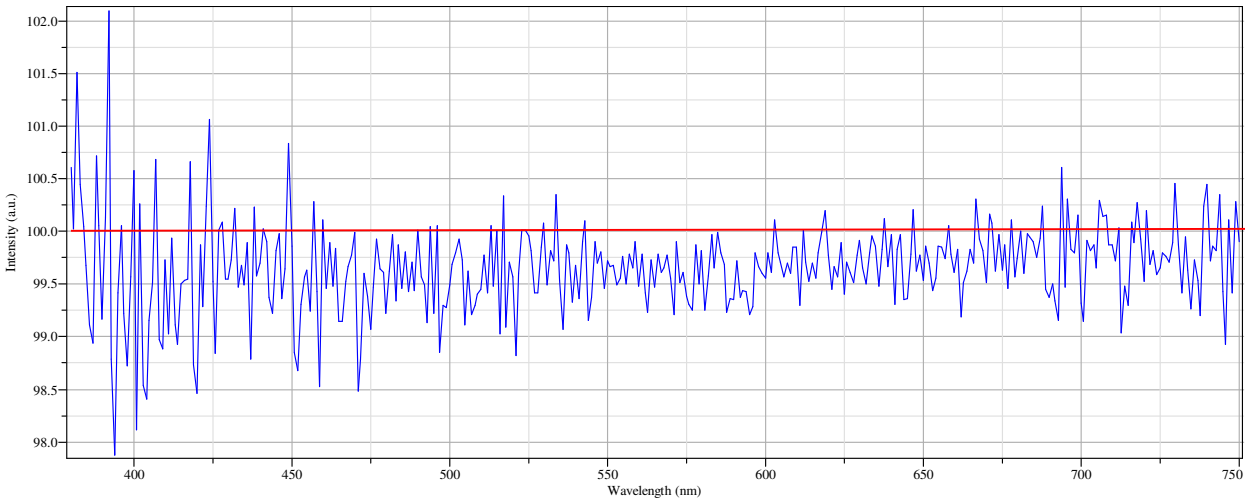

Figure A3.6: RMS Noise, mean spectrum

Reflectance Photometric RMS Noise, 100% R			
λ	slope	y-intercept	RMS noise
400	-2.80E-02	110.7033	0.945354
500	-6.00E-03	102.52	0.318196
600	0.019206	88.0735	0.202129
700	1.44E-02	89.72893	0.380402

Table A3.: Summary tabulation of RMS noise data.

λ	y-intercept	Deviation, 100%R
400	110.7	10.7
500	102.5	2.5
600	88.0	-12.0
700	89.7	-10.3

Table A3.2: Summary table containing short-term baseline stability data where deviations from 100%R is an indication of short term baseline instability and may indicate a malfunction of the microscope spectrophotometer.

SPECTRAL RESOLUTION DEPENDENCE ON WAVELENGTH

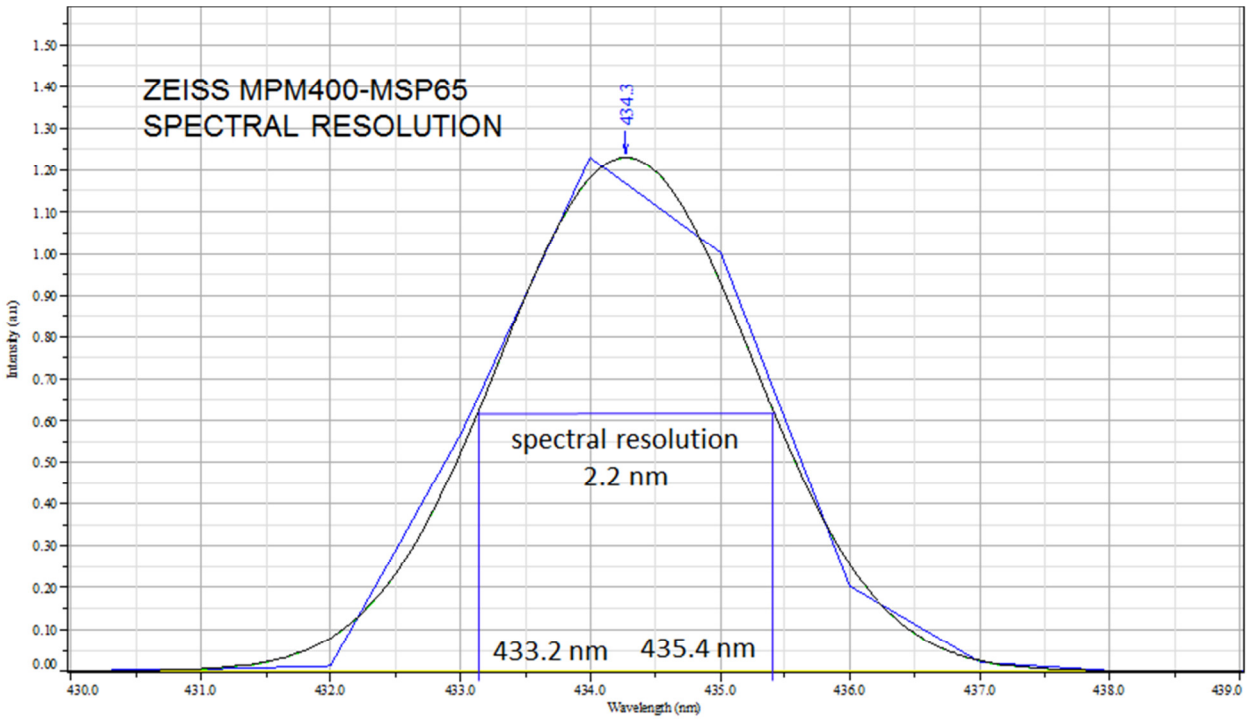

Figure A3.7: Spectral resolution of 2.2 nm at central wavelength 434.3 nm.

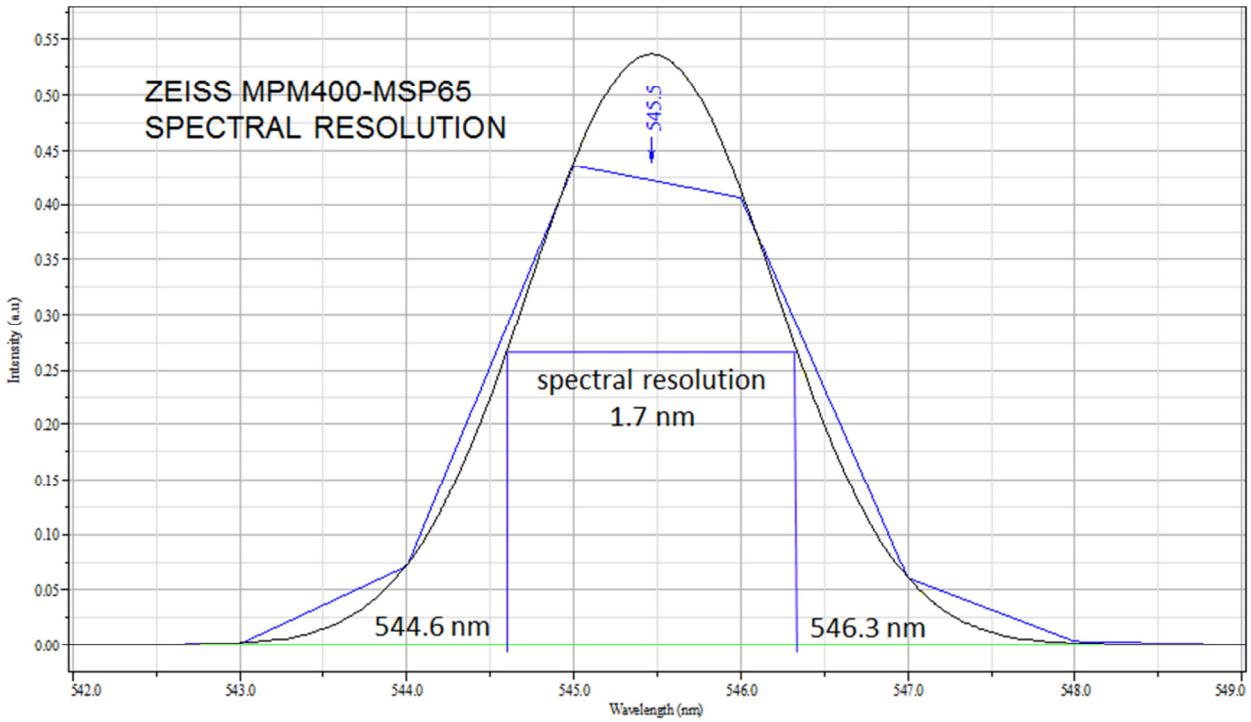

Figure A3.8: Spectral resolution of 1.7 nm at central wavelength 545.5 nm.

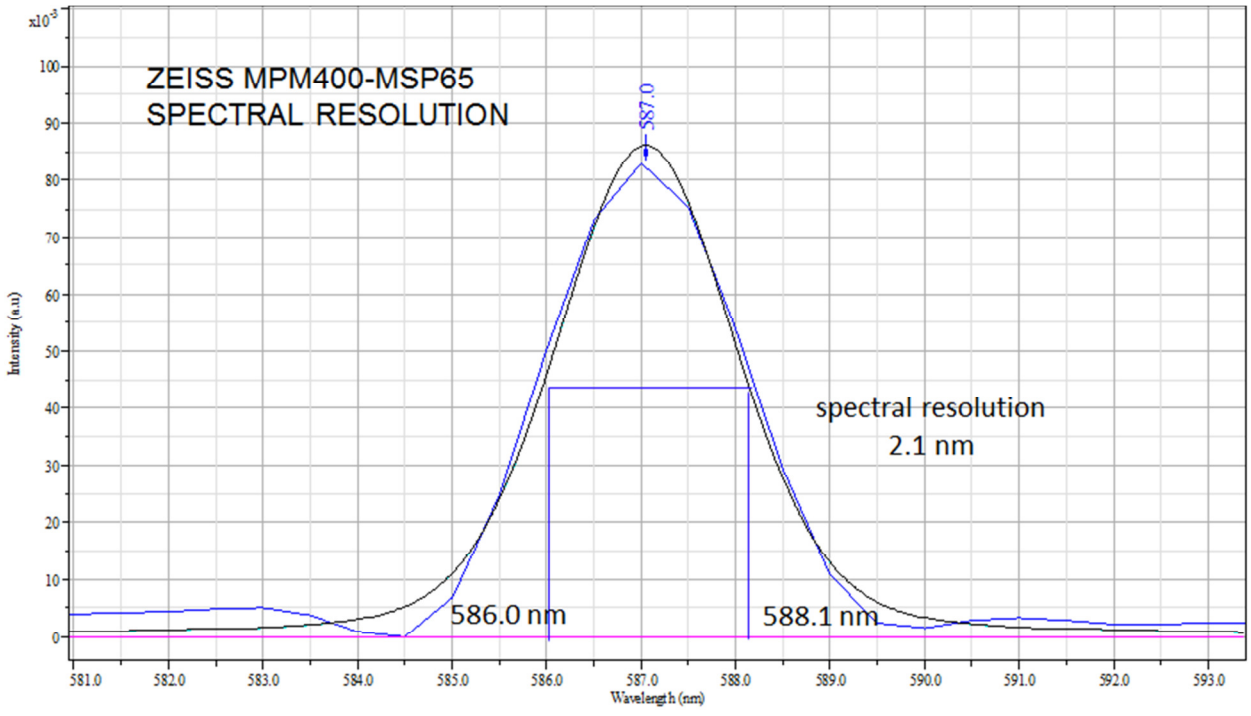

Figure A3.9: Spectral resolution of 2.1 nm at central wavelength 587.0 nm.

APPENDIX IV. SPECTRAL DATA FOR CUSTOM BUILT HORIBA XPLORA RAMAN-VISIBLE POLARIZED LIGHT MICROSPECTROMETER

WAVELENTH ACCURACY AND PRECISION

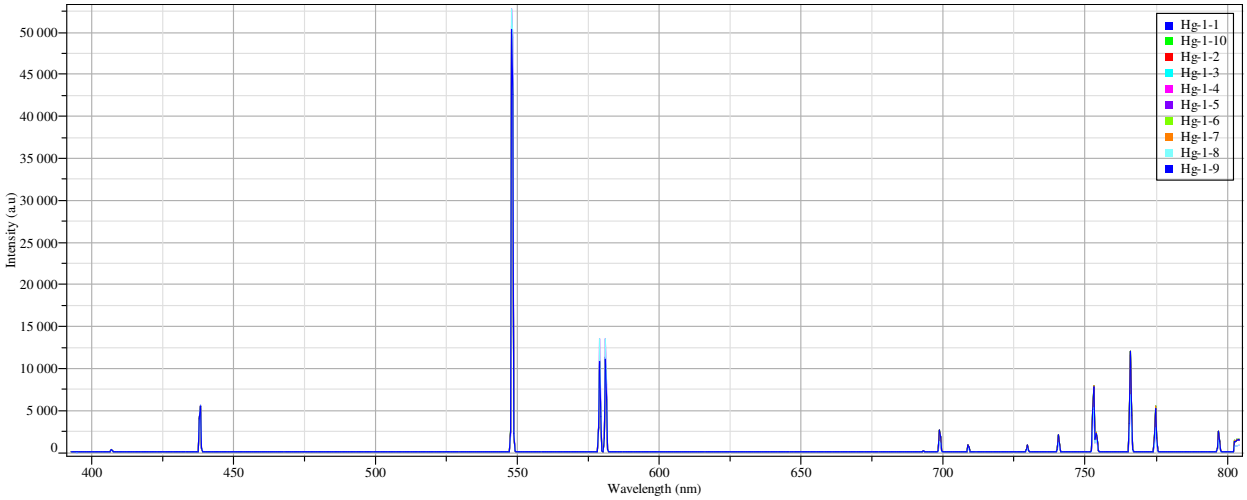

Figure A4.1: Example of an overlay spectrum consisting of ten measurements of a HG-1 calibration lamp.

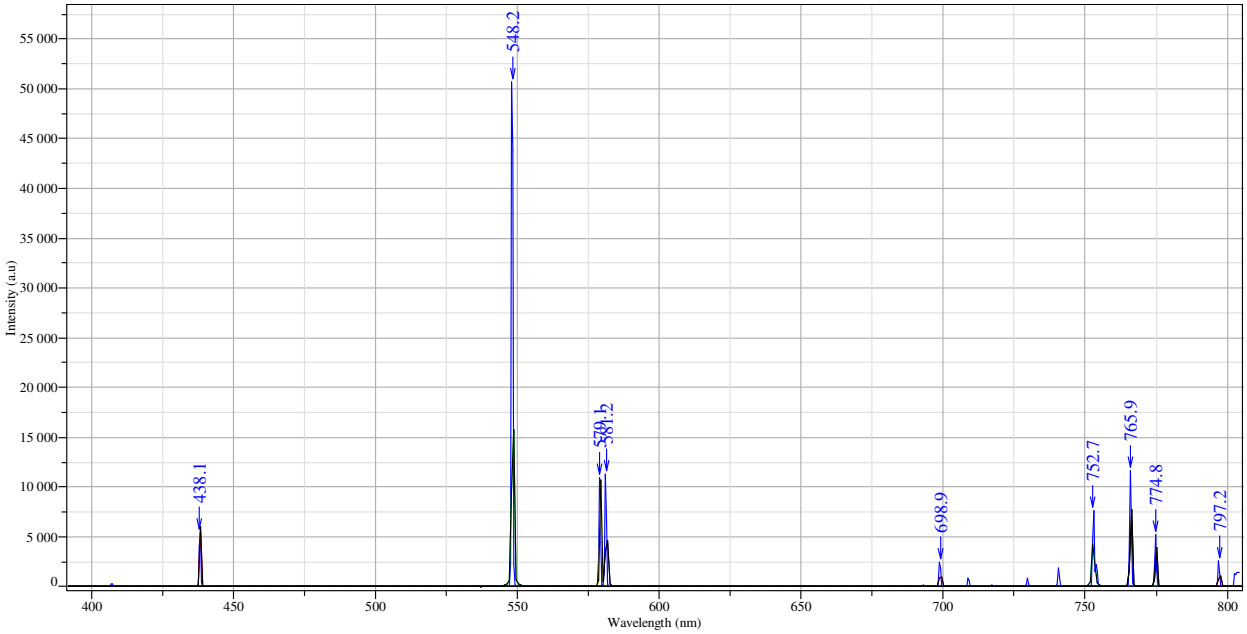

Figure A4.2: Example of a HG-1 calibration lamp spectrum that has undergone preprocessing functions for peak-fitting with baseline correction. Wavelength values at peak maximums for several peaks across the spectral range were tabulated and used to determine wavelength accuracy and precision, or wavelength dependence on spectral resolution. The results of which are located in the Instrument Qualification and Summary Report.

Wavelength Accuracy and Wavelength Precision Data													
*λ (nm)	1	2	3	4	5	6	7	8	9	10	Ave. λ	stdev	*λ – Ave.λ
435.93	438.1	438.0	438.0	438.0	438.1	438.1	438.0	438.0	438.1	438.0	438.05		-2.12
546.07	548.2	548.2	548.2	548.2	548.2	548.2	548.2	548.2	548.2	548.2	548.2		-2.13
578.01	581.2	581.2	581.2	581.2	581.2	581.2	581.2	581.2	581.2	581.2	581.2		-3.19
763.51	765.9	765.9	765.9	765.9	765.9	765.9	765.9	765.9	765.9	765.9	765.9		-2.39
772.42	774.8	774.8	774.8	774.8	774.8	774.8	774.8	774.8	774.8	774.8	774.8		-2.27

Table A4.1: Summary table containing wavelength accuracy, precision, and deviation data calculated from ten independent measurements of Ocean Optics HG-1 mercury-argon calibration low-pressure gas discharge calibration lamp. *Standard spectral data wavelength values were obtained from ASTM E275-08.

PHOTOMETRIC ACCURACY, PRECISON AND LINEARITY

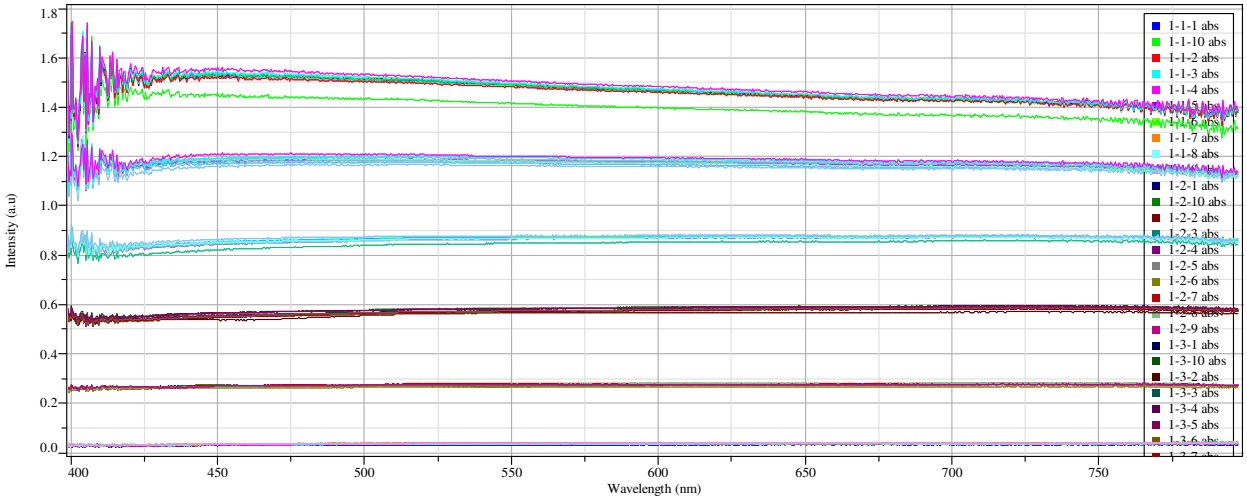

Figure A4.3: Overlay spectra of five measurements at each of eight steps on Edmund Optics® stepped optical density slide #1.

Reference Material: Edmund Optics® Optical Density Stepped Slide #1								
Optical Density (*True) - Step	400 nm		500 nm		600 nm		700 nm	
	Mean	St Dev	Mean	St Dev	Mean	St Dev	Mean	St Dev
(0.04) – step 1	0.03	0.010	0.03	0.006	0.03	0.005	0.03	0.005
(0.34) – step 2	0.26	0.011	0.27	0.003	0.27	0.003	0.27	0.002
(0.63) – step 3	0.57	0.024	0.57	0.020	0.57	0.019	0.58	0.020
(0.93) – step 4	0.89	0.047	0.86	0.026	0.87	0.022	0.87	0.018
(1.22) – step 5	1.26	0.092	1.18	0.034	1.17	0.031	1.16	0.026
(1.52) – step 6	1.68	0.117	1.50	0.080	1.46	0.069	1.42	0.065

Table 4.2: Summary table containing photometric accuracy and photometric precision data for an Edmund Optics® stepped optical density slide. Values represent mean and standard deviation of five measurements. Red-color horizontal data was used to determine photometric accuracy and precision, while the red-colored vertical data was used to determine photometric linearity found in the "Instrument Qualification and Summary Report", which accompanies the discussion of each instrument in the Results chapter. *The true value was obtained from the documented stepped optical density slides.

PHOTOMETRIC NOISE

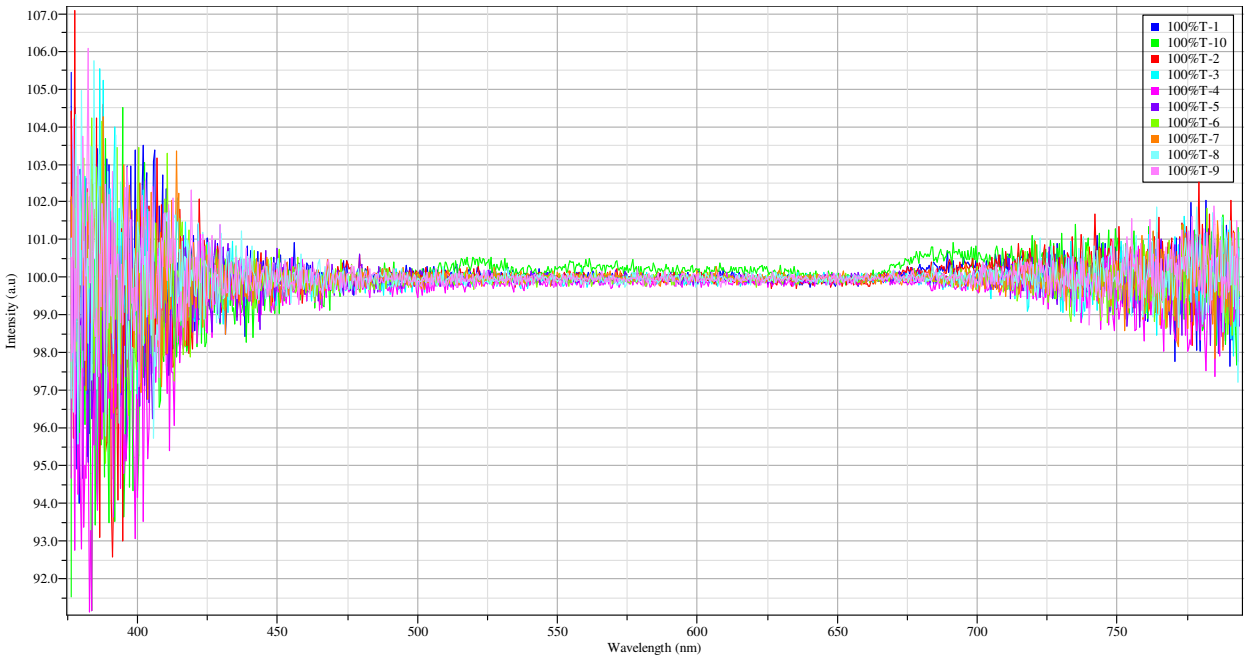

Figure A4.4: Overlay of ten 100% Transmittance spectra used to calculate the RMS noise and short-term instrument stability

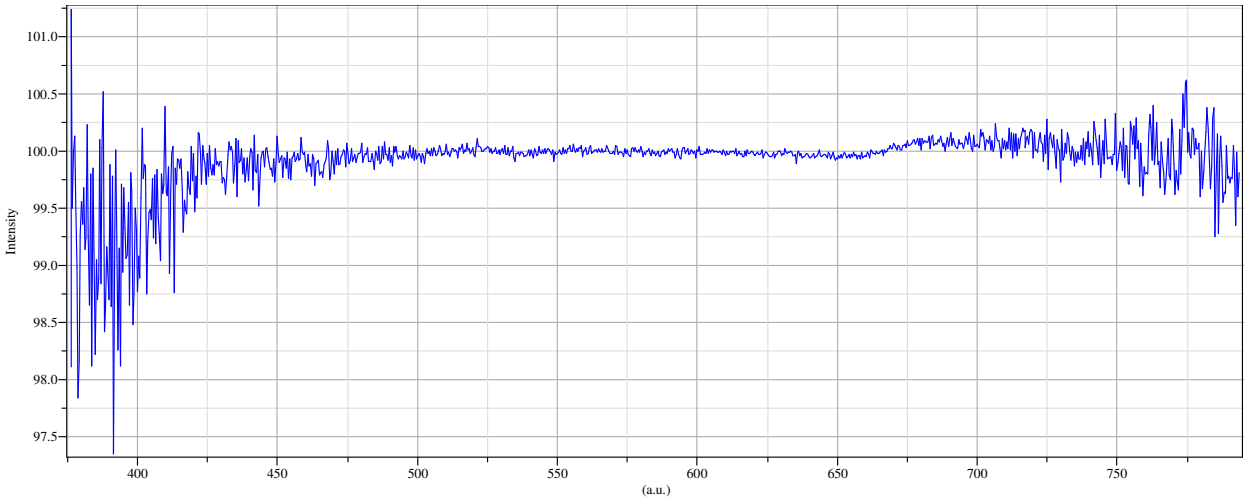

Figure 4.5: RMS Noise, mean spectrum

Photometric RMS noise, 100 %T			
λ	slope	y-intercept	%T RMS noise
500	1.73E-03	99.10125	4.03E-02
600	-5.06E-04	100.2951	2.38E-02
700	-4.01E-04	100.3631	5.34E-02

Table A4.3: Summary Tabulation of RMS noise data.

λ	y-intercept	Deviation, 100% T
500	99.1	-0.9
600	100.2	0.2
700	100.3	0.3

Table A4.4: Summary table containing short-term baseline stability data where deviations from 100% T is an indication of short term baseline instability and may indicate a malfunction of the microscope spectrophotometer.

SPECTRAL RESOLUTION DEPENDENCE ON WAVELENGTH

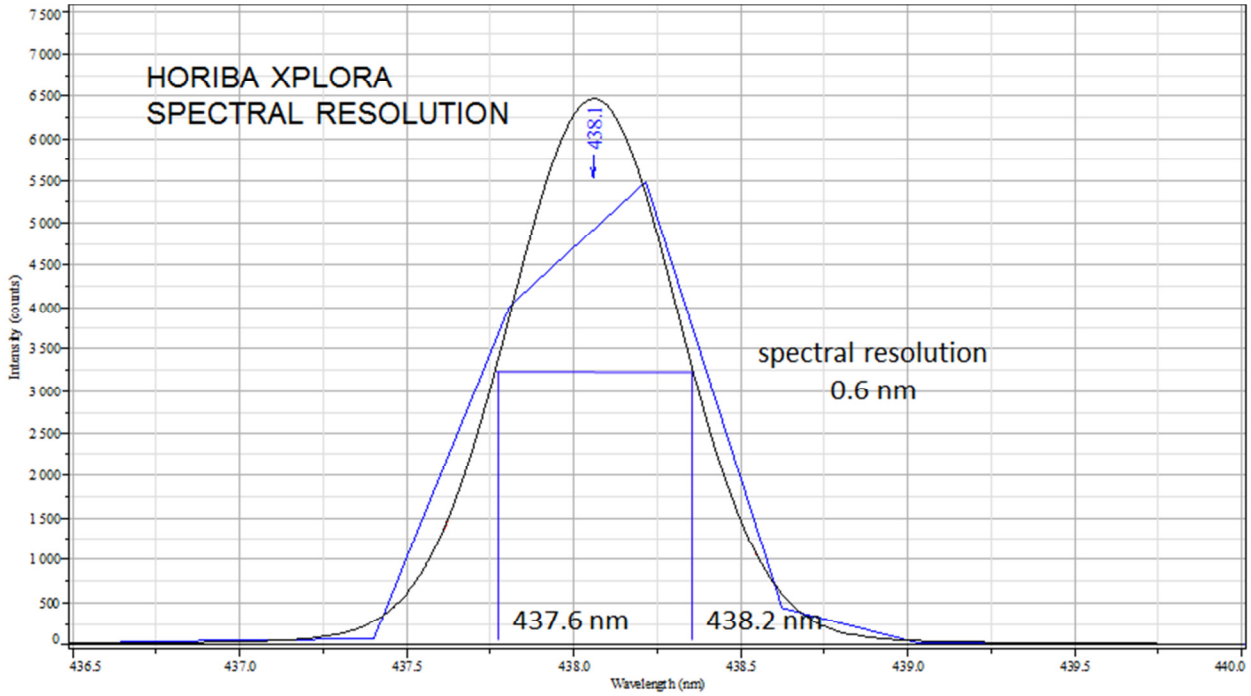

Figure A4.6: Spectral resolution of 0.6 nm at central wavelength 438.1 nm.

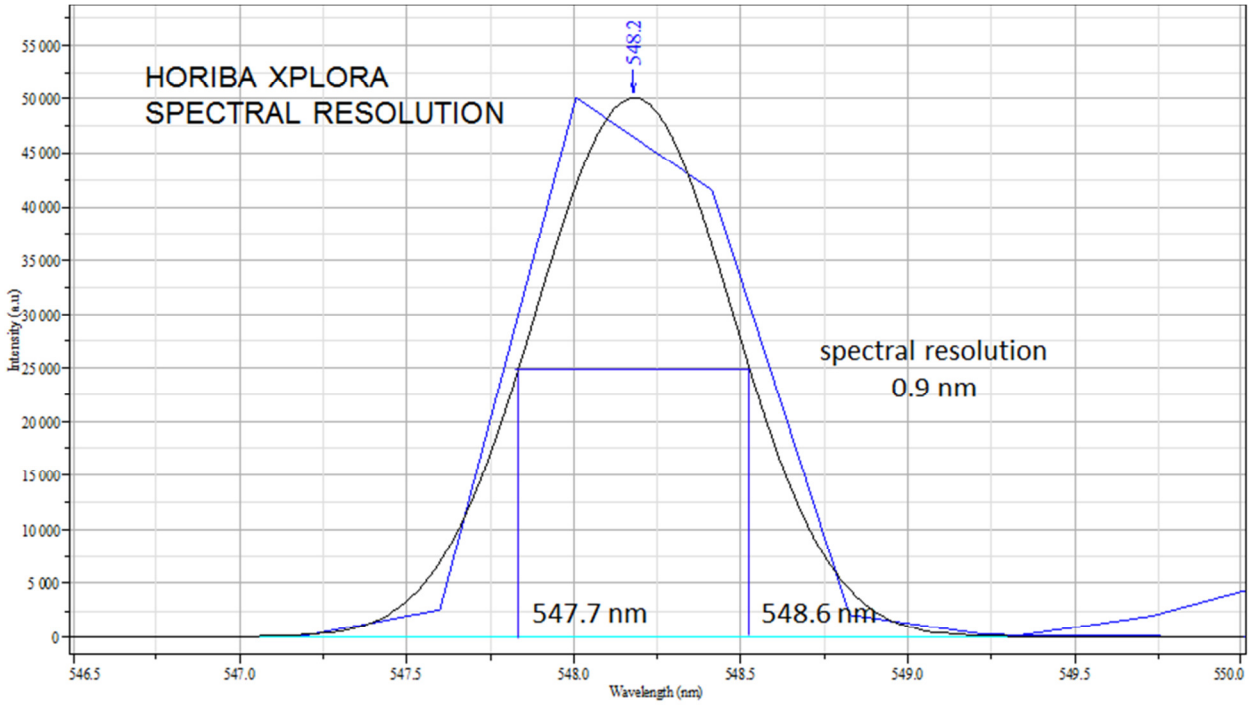

Figure A4.7: Spectral resolution of 0.9 nm at central wavelength 548.2 nm.

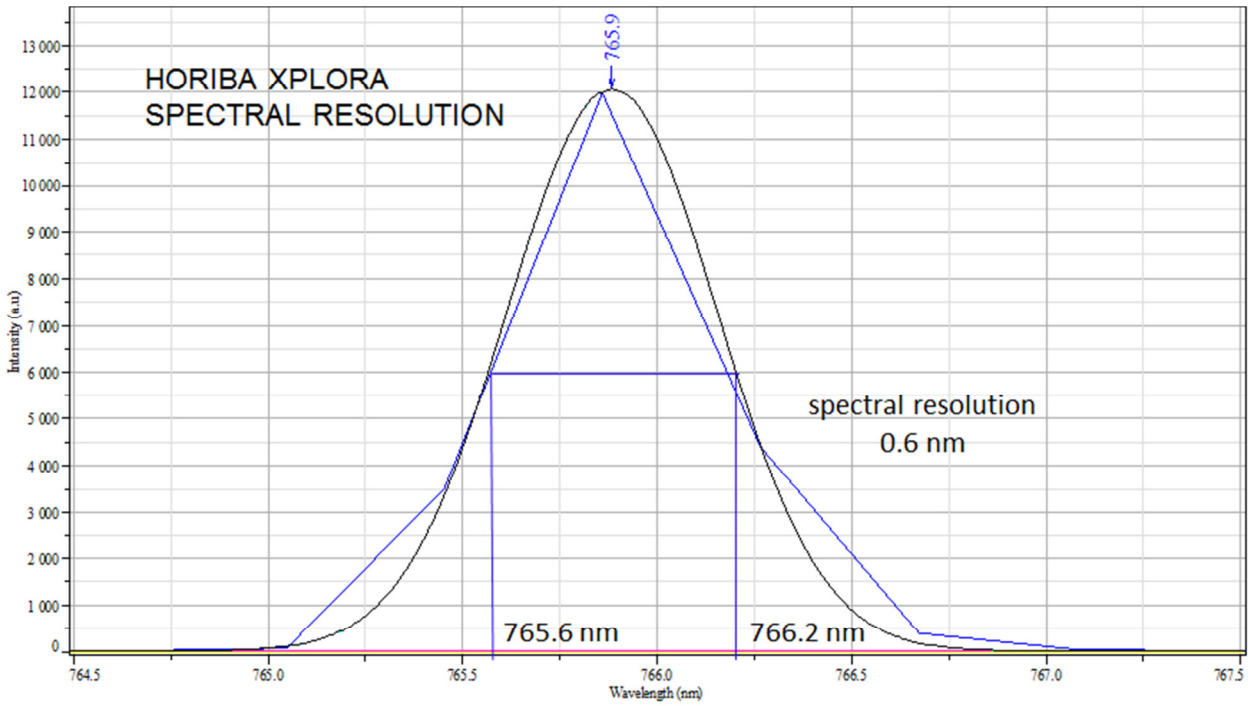

Figure A4.8: Spectral resolution of 0.6 nm at central wavelength 765.9 nm.

ILLUMINATORS

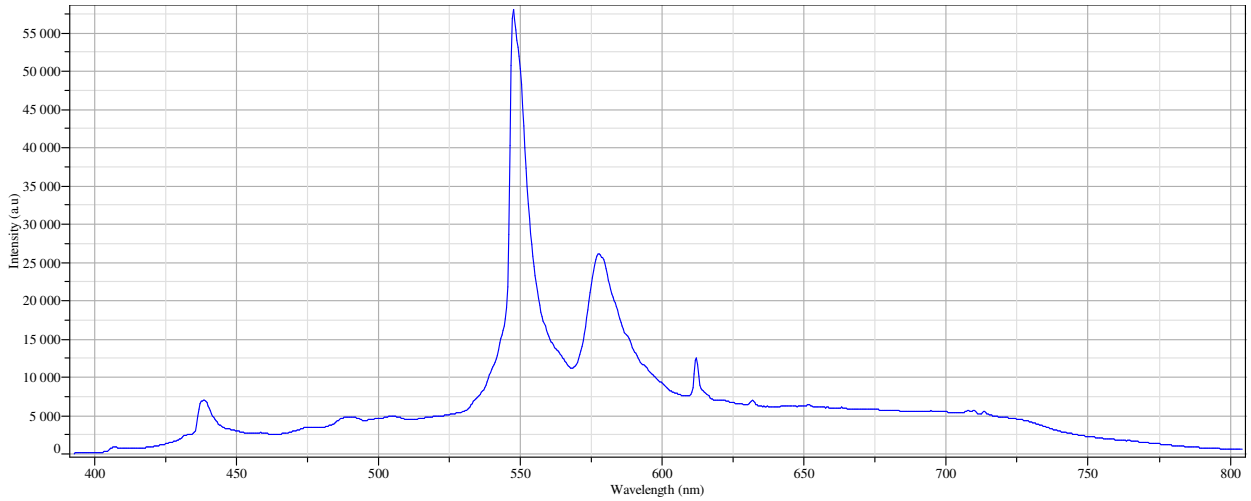

Figure A4.9: Reflectance spectrum of X-cite mercury metal-halide high-pressure discharge lamp reflected off of SRM2017 multiangle white reflection standard.

APPENDIX V. SPECTRAL DATA FOR CUSTOM BUILT OLYMPUS BX51TRF POLARIZED LIGHT MICROSCOPE WITH HORIBA VS140 FIBER OPTIC SPECTROMETER

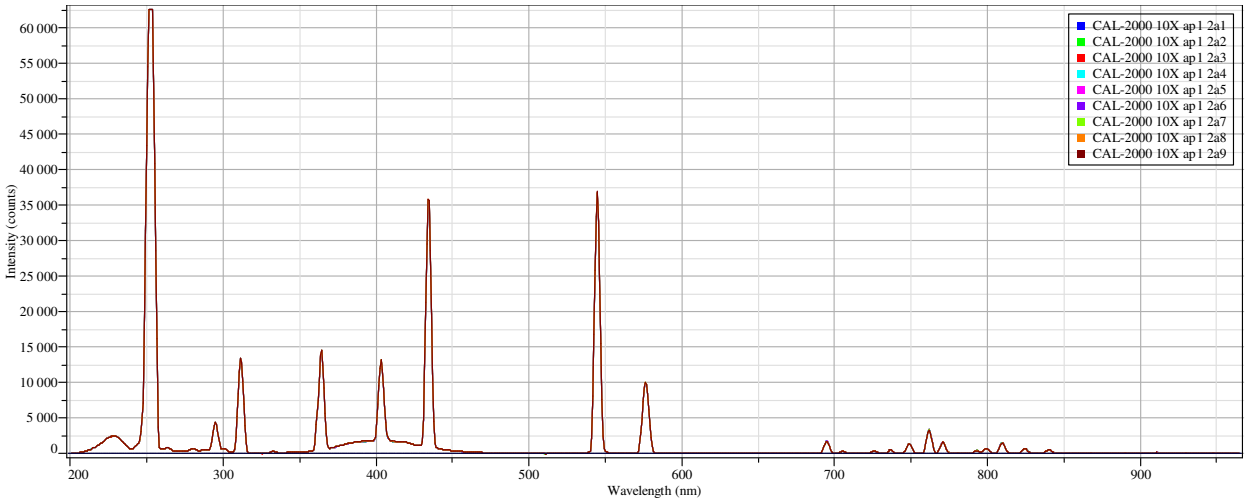

Figure A5.1: Example of an overlay spectrum consisting of nine measurements of a CAL-2000 calibration lamp.

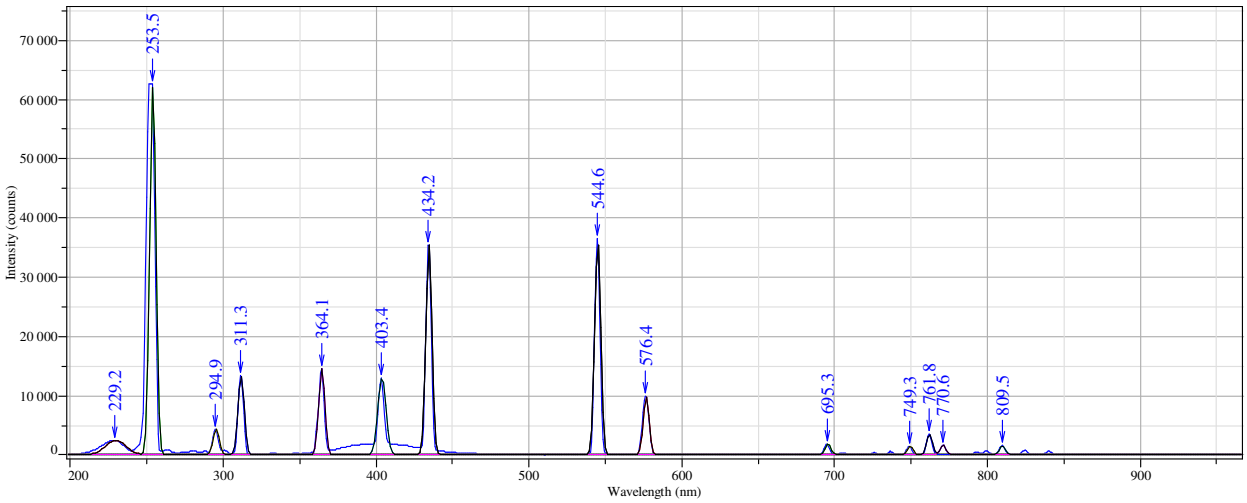

Figure A5.2: Example of a CAL-2000 calibration lamp spectrum that has undergone preprocessing functions for peak-fitting with baseline correction. Wavelength values at peak maximums for several peaks across the spectral range were tabulated and used to determine wavelength accuracy and precision, or wavelength dependence on spectral resolution. The results of which are located in the Instrument Qualification and Summary Report.

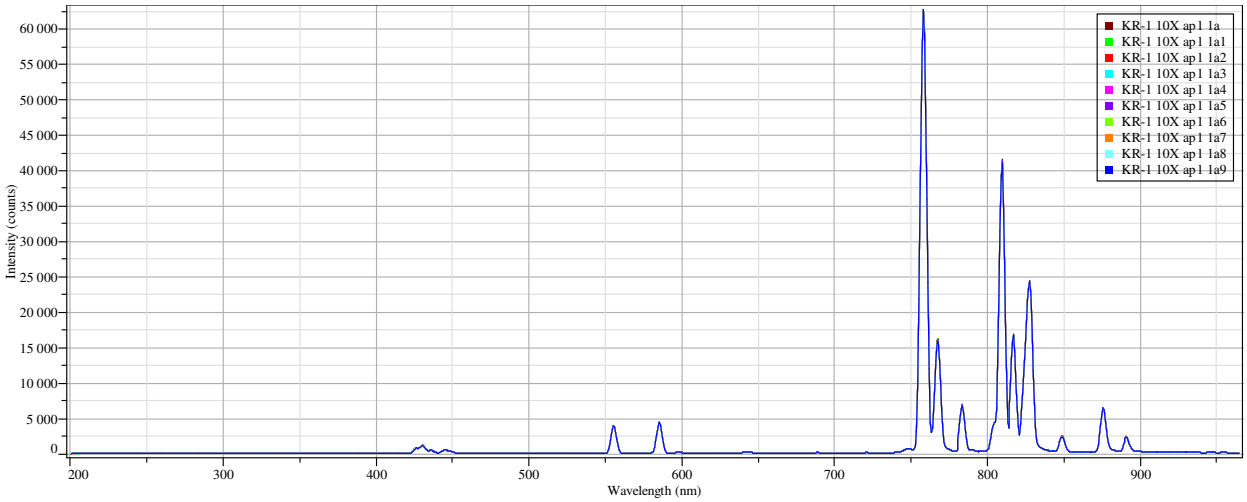

Figure A5.3: Example of an overlay spectrum consisting of nine measurements of a KR-1 calibration lamp.

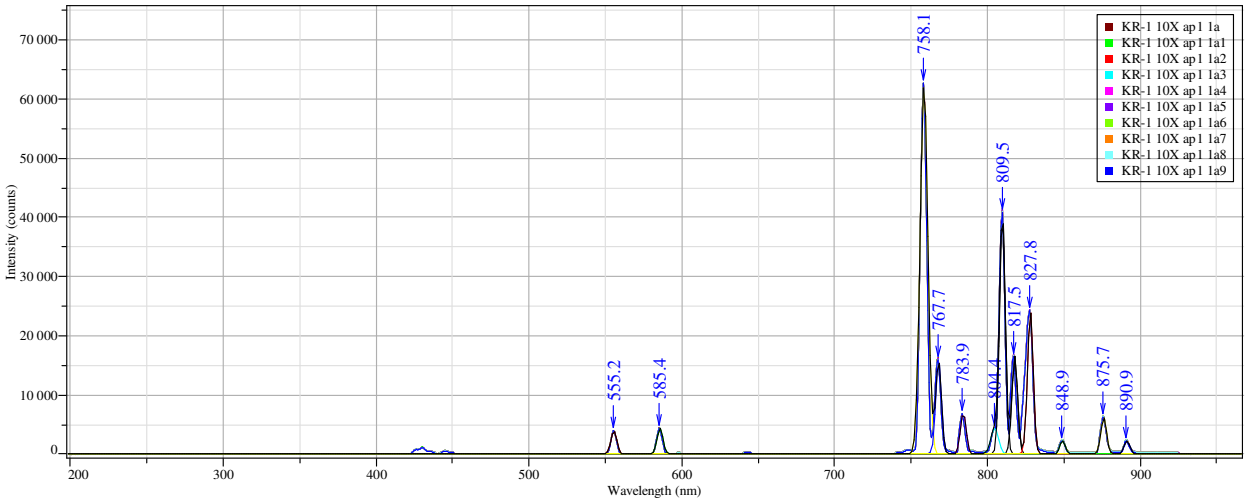

Figure A5.4: Example of a KR-1 calibration lamp spectrum that has undergone preprocessing functions for peak-fitting with baseline correction. Wavelength values at peak maximums for several peaks across the spectral range were tabulated and used to determine wavelength accuracy and precision, or wavelength dependence on spectral resolution. The results of which are located in the Instrument Qualification and Summary Report.

Wavelength Accuracy and Wavelength Precision Data													
*λ (nm)	1	2	3	4	5	6	7	8	9	10	Ave. λ	stdev	*λ – Ave.λ
253.65	252.2	252.2	252.2	252.2	252.2	252.2	252.2	252.2	252.2	252.2	252.2		1.45
296.72	295.1	295.1	295.1	295.1	295.1	295.1	295.1	295.1	295.1	295.1	295.1		1.62
312.57	311.5	311.5	311.5	311.5	311.5	311.5	311.5	311.5	311.5	311.5	311.5		1.07
365.02	363.9	363.9	363.9	363.9	363.9	363.9	363.9	363.9	363.9	363.9	363.9		1.12
404.66	403.4	403.4	403.4	403.4	403.4	403.4	403.4	403.4	403.4	403.4	403.4		1.26
435.93	434.5	434.5	434.5	434.5	434.5	434.5	434.5	434.5	434.5	434.5	434.5		1.43
546.07	544.6	544.6	544.6	544.6	544.6	544.6	544.6	544.6	544.6	544.6	544.6		1.47
578.01	576.6	576.6	576.6	576.6	576.6	576.6	576.6	576.6	576.6	576.6	576.6		1.41
763.51	761.8	761.8	761.8	761.8	761.8	761.8	761.8	761.8	761.8	761.8	761.8		1.71
772.42	770.7	770.7	770.7	770.7	770.7	770.7	770.7	770.7	770.7	770.7	770.7		1.72
811.53	809.4	809.4	809.4	809.4	809.4	809.4	809.4	809.4	809.4	809.5	809.4		2.13

Table A5.1: Summary table containing wavelength accuracy, precision, and deviation data calculated from ten independent measurements of Ocean Optics® CAL-2000™ mercury-argon calibration low-pressure gas discharge calibration lamp. *Standard spectral data wavelength values were obtained from ASTM E275-08.

PHOTOMETRIC ACCURACY, PRECISION AND LINEARITY

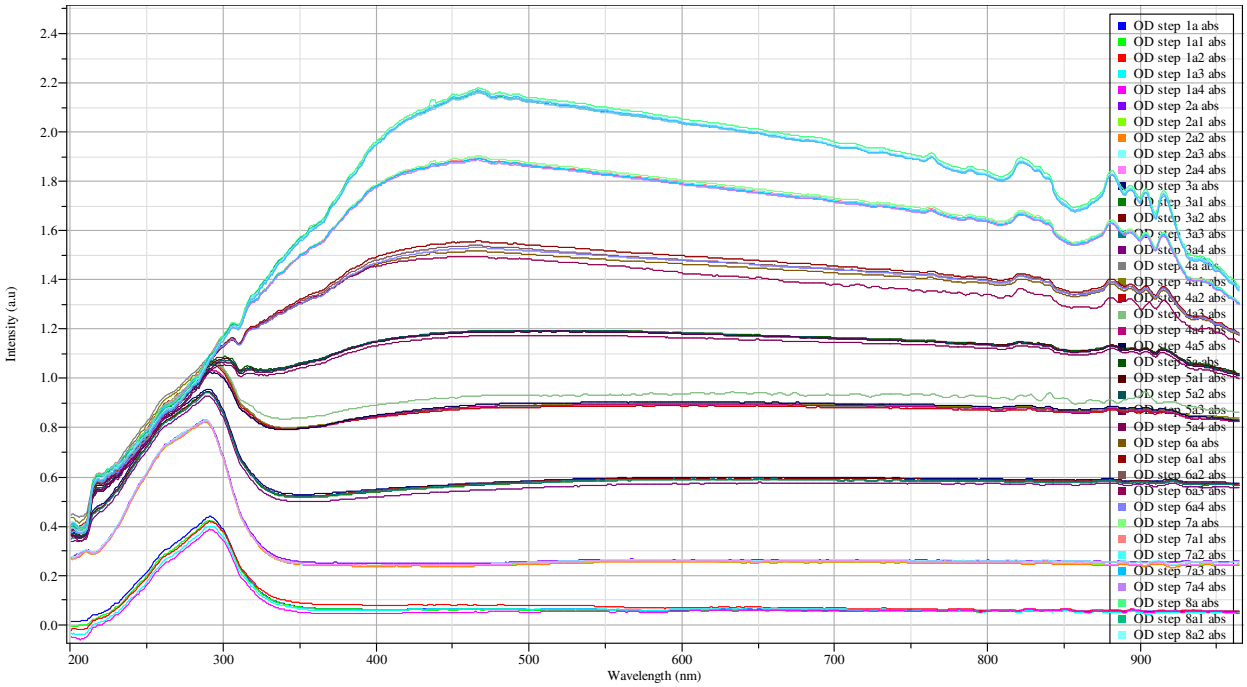

Figure A5.5: Overlay spectra of five measurements at each of eight steps on Edmund Optics® stepped optical density slide #1.

Reference Material: Edmund Optics® Optical Density Stepped Slide #1								
Optical Density (*True) - Step	400 nm		500 nm		600 nm		700 nm	
	Mean	St Dev	Mean	St Dev	Mean	St Dev	Mean	St Dev
(0.04) – step 1	0.06	0.012	0.06	0.009	0.06	0.005	0.06	0.005
(0.34) – step 2	0.24	0.005	0.25	0.004	0.26	0.004	0.26	0.004
(0.63) – step 3	0.54	0.012	0.57	0.011	0.59	0.010	0.59	0.009
(0.93) – step 4	0.85	0.004	0.89	0.006	0.89	0.006	0.89	0.006
(1.22) – step 5	1.15	0.008	1.19	0.008	1.18	0.008	1.16	0.008
(1.52) – step 6	1.47	0.015	1.51	0.022	1.47	0.026	1.43	0.028
(1.82) – step 7	1.78	0.004	1.87	0.006	1.79	0.006	1.72	0.007
(2.11) – step 8	1.95	0.006	2.13	0.008	2.04	0.007	1.95	0.008

Table A5.2: Summary table containing photometric accuracy and photometric precision data for an Edmund Optics® stepped optical density slide. Values represent mean and standard deviation of five measurements. Red-color horizontal data was used to determine photometric accuracy and precision, while the red-colored vertical data was used to determine photometric linearity found in the "Instrument Qualification and Summary Report", which accompanies the discussion of each instrument in the Results chapter. *The true value was obtained from the documented stepped optical density slides.

PHOTOMETRIC NOISE

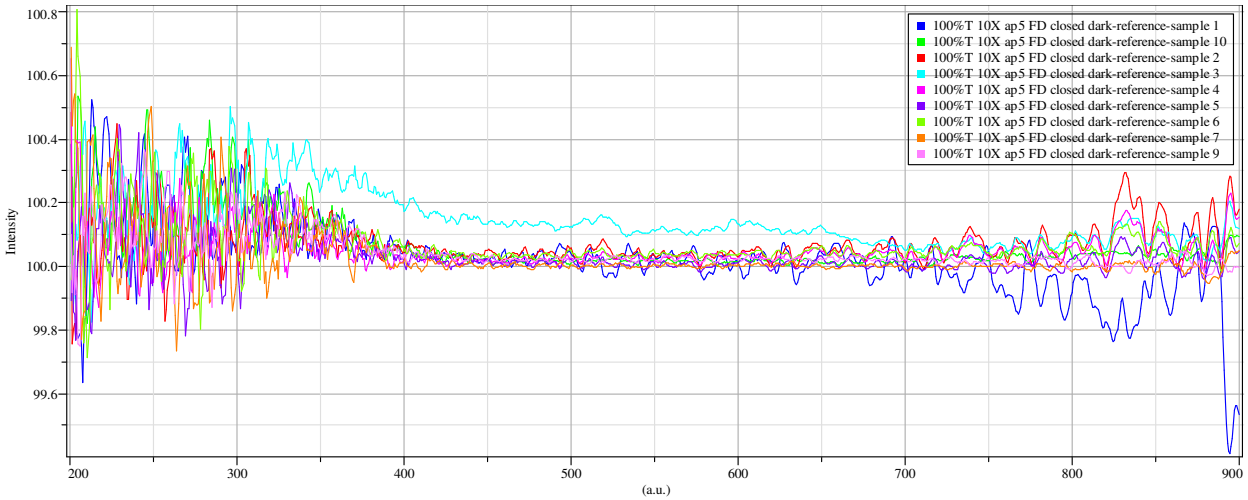

Figure A5.6: Overlay of ten 100% Transmittance spectra used to calculate the RMS noise and short-term instrument stability

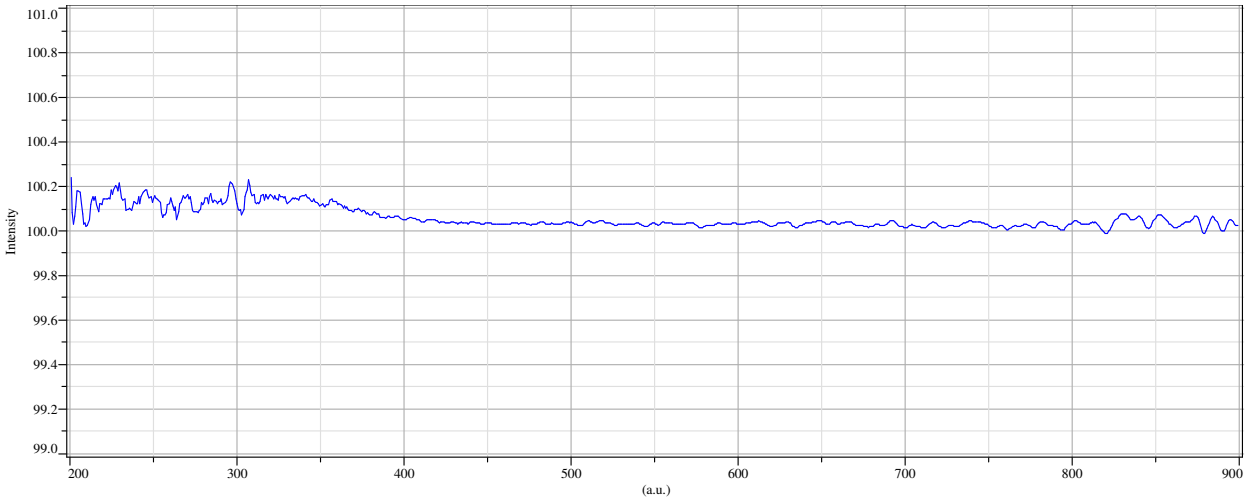

Figure A5.7: RMS Noise, mean spectrum

Photometric RMS noise, 100 %T			
λ	slope	y-intercept	%T RMS noise
300	9.78E-04	99.86134	4.55×10^{-02}
400	-7.72E-04	100.3669	3.97×10^{-03}
500	-2.68E-04	100.167	5.19×10^{-03}
600	3.17E-04	99.84373	1.60×10^{-03}
700	-1.24E-03	100.8959	7.15×10^{-03}

Table A5.3: Summary Tabulation of RMS noise data.

λ	y-intercept	deviation
300	99.8	-0.2
400	100.3	0.3
500	100.1	0.1
600	-0.2	0.1
700	100.8	0.8

Table A5.4: Summary table containing short-term baseline stability data where deviations from 100% T is an indication of short term baseline instability and may indicate a malfunction of the microscope spectrophotometer.

SPECTRAL RESOLUTION DEPENDENCE ON WAVELENGTH

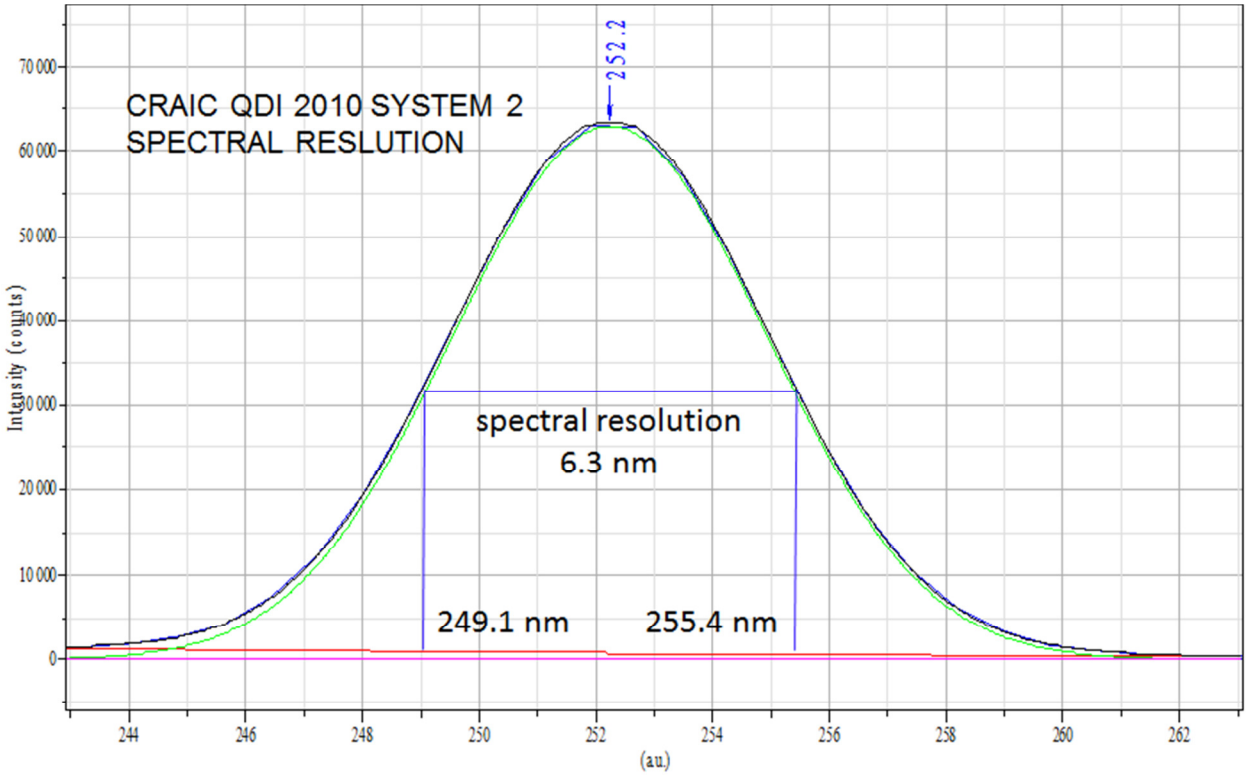

Figure A5.8: Spectral resolution of 6.3 nm at central wavelength 252.2 nm.

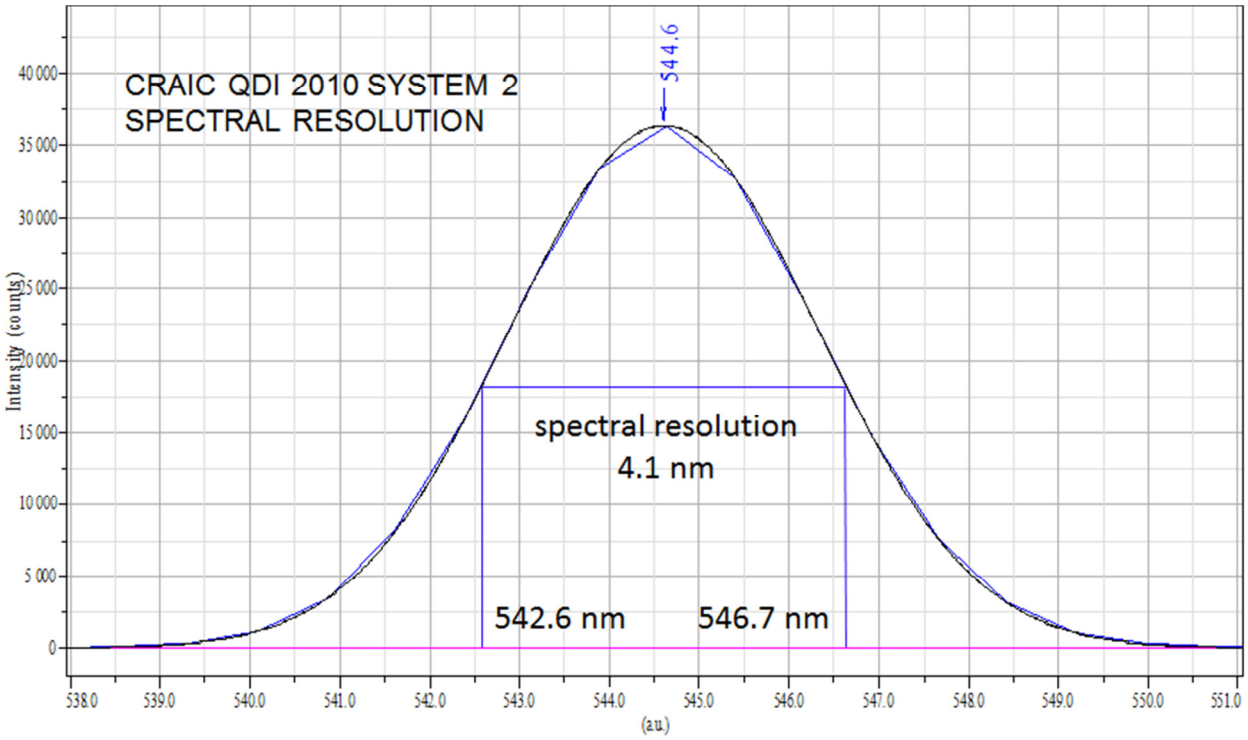

Figure A5.9: Spectral resolution of 4.1 nm at central wavelength 544.6 nm.

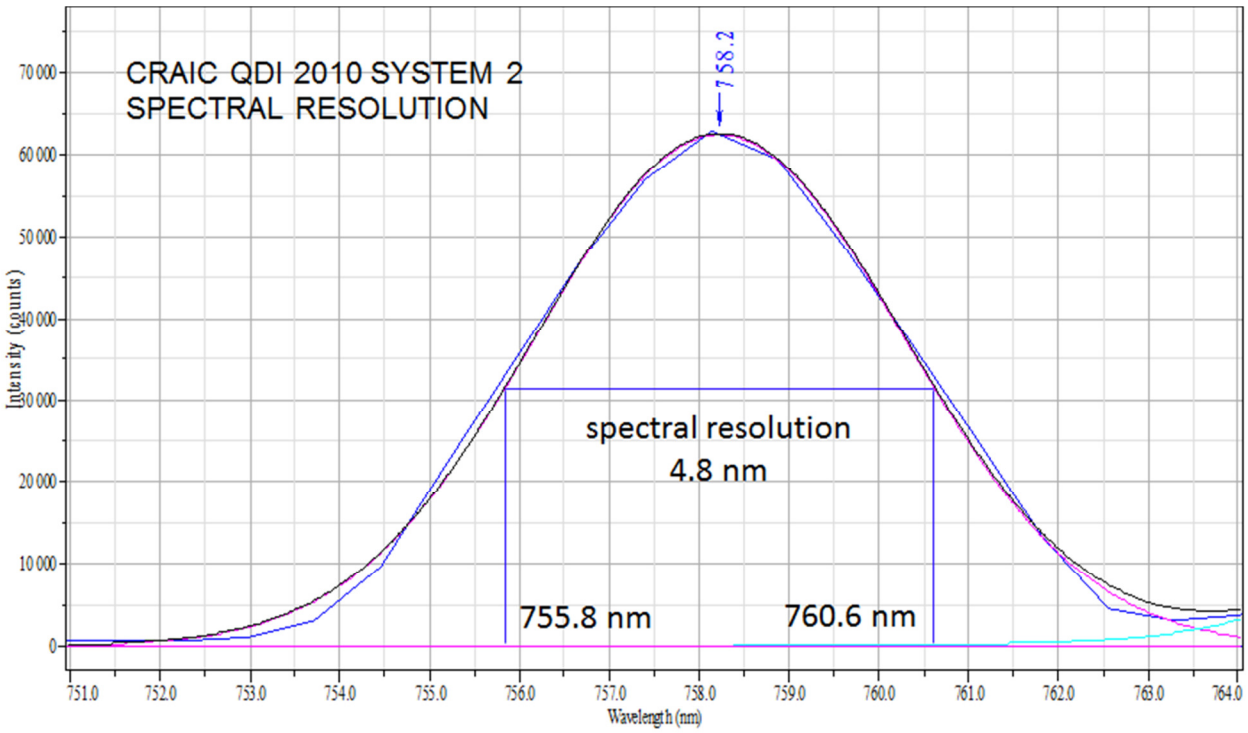

Figure A5.10: Spectral resolution of 4.8 nm at central wavelength 758.2 nm.

APPENDIX VI. SPECTRAL DATA FOR CUSTOM BUILT OLYMPUS BH-BHA-POL POLARIZED LIGHT MICROSCOPE WITH OCEAN OPTICS USB2000+ FIBER OPTIC SPECTROMETER

WAVELENGTH ACCURACY AND PRECISION

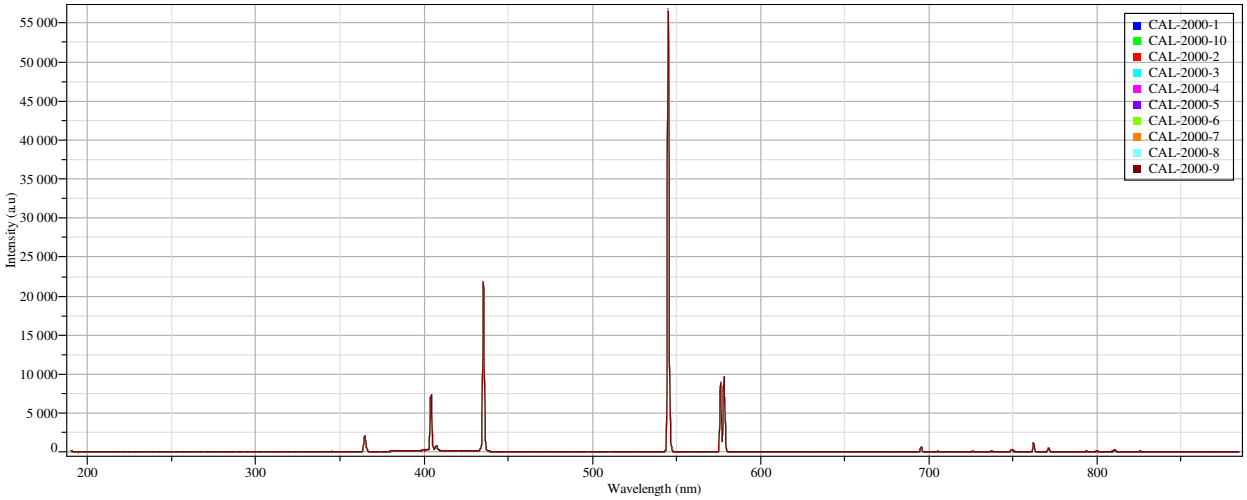

Figure A6.1: Example of an overlay spectrum consisting of ten measurements of a CAL-2000 calibration lamp.

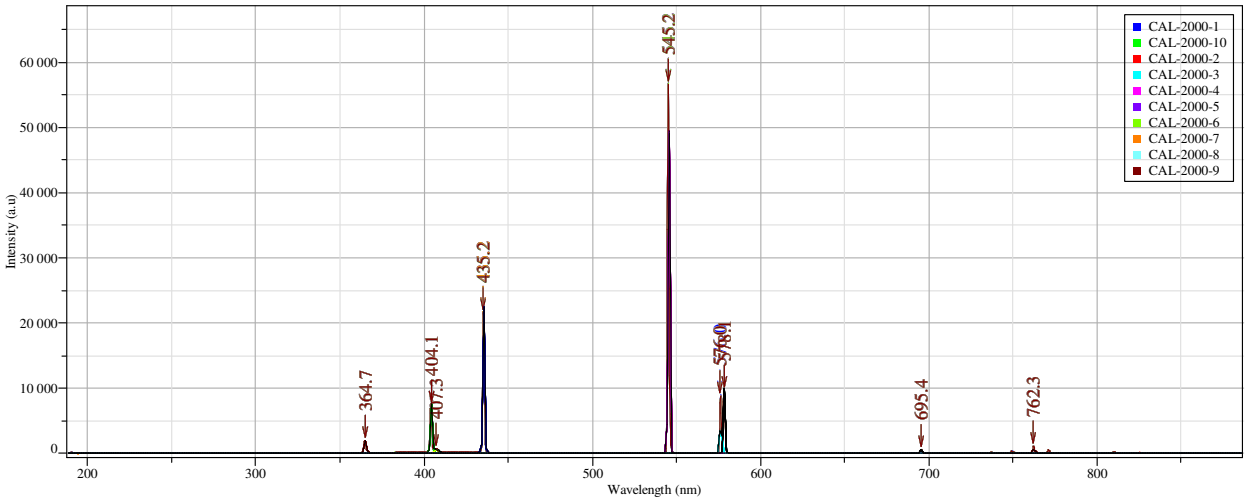

Figure A6.2: Example of a CAL-2000 calibration lamp spectrum that has undergone preprocessing functions for peak-fitting with baseline correction. Wavelength values at peak maximums for several peaks across the spectral range were tabulated and used to determine wavelength accuracy and precision, or wavelength dependence on spectral resolution. The results of which are located in the Instrument Qualification and Summary Report.

Wavelength Accuracy and Wavelength Precision Data													
*λ (nm)	1	2	3	4	5	6	7	8	9	10	Ave. λ	stdev	*λ – Ave.λ
365.02	364.7	364.7	364.7	364.7	364.7	364.7	364.7	364.7	364.7	364.7	364.7	0.000	0.32
404.66	404.1	404.1	404.1	404.1	404.1	404.1	404.1	404.1	404.1	404.1	404.1	0.000	0.56
435.93	435.2	435.2	435.2	435.2	435.2	435.2	435.2	435.2	435.2	435.2	435.2	0.000	0.73
546.07	545.2	545.2	545.2	545.2	545.2	545.2	545.2	545.2	545.2	545.2	545.2	0.000	0.87
578.01	578.1	578.1	578.1	578.1	578.1	578.1	578.1	578.1	578.1	578.1	578.1	0.000	-0.09
763.51	762.3	762.3	762.3	762.3	762.3	762.3	762.3	762.3	762.3	762.3	762.3	0.000	1.21

Table 6.1: Summary table containing wavelength accuracy, precision, and deviation data calculated from ten independent measurements of Ocean Optics® CAL-2000™ mercury-argon calibration low-pressure gas discharge calibration lamp. *Standard spectral data wavelength values were obtained from ASTM E275-08.

PHOTOMETRIC ACCURACY, PRECISION AND LINEARITY

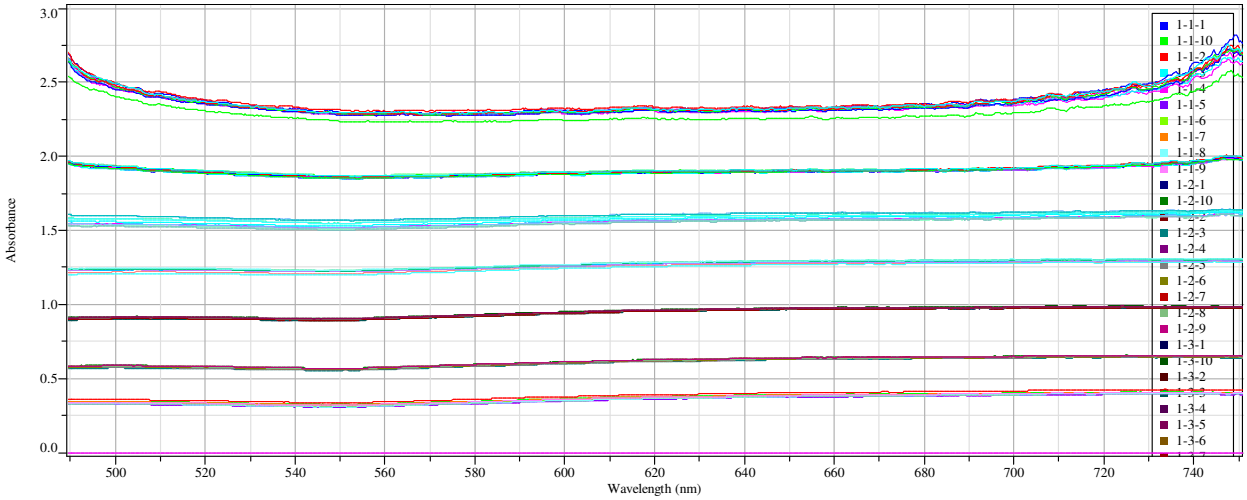

Figure A6.3: Overlay spectra of five measurements at each of eight steps on Edmund Optics® stepped optical density slide #1.

Reference Material: Edmund Optics® Optical Density Stepped Slide #1								
Optical Density (*True) - Step	400 nm		500 nm		600 nm		700 nm	
	Mean	St Dev	Mean	St Dev	Mean	St Dev	Mean	St Dev
(0.04) – step 1								
(0.34) – step 2			0.33	0.030	0.35	0.027	0.39	0.026
(0.63) – step 3			0.57	0.017	0.60	0.012	0.64	0.011
(0.93) – step 4			0.90	0.017	0.94	0.013	0.97	0.040
(1.22) – step 5			1.23	0.033	1.26	0.026	1.29	0.022
(1.52) – step 6			1.56	0.077	1.56	0.063	1.59	0.052
(1.82) – step 7			1.92	0.024	1.88	0.021	1.91	0.015

Table 6.2: Summary table containing photometric accuracy and photometric precision data for an Edmund Optics® stepped optical density slide. Values represent mean and standard deviation of five measurements. Red-color horizontal data was used to determine photometric accuracy and precision, while the red-colored vertical data was used to determine photometric linearity found in the "Instrument Qualification and Summary Report", which accompanies the discussion of each instrument in the Results chapter. *The true value was obtained from the documented stepped optical density slides.

PHOTOMETRIC NOISE

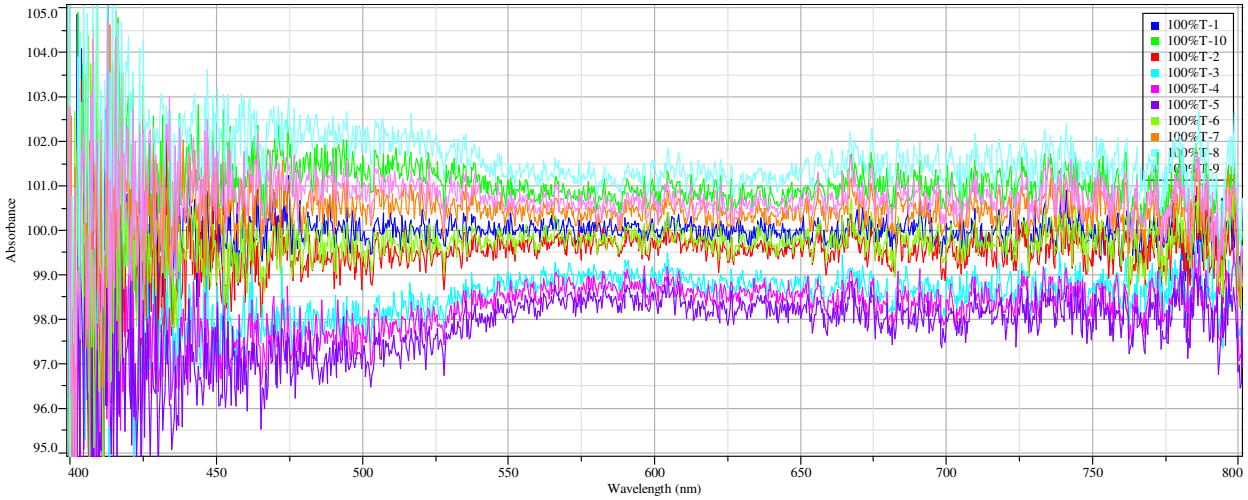

Figure A6.4: Overlay of ten 100% Transmittance spectra used to calculate the RMS noise and short-term instrument stability

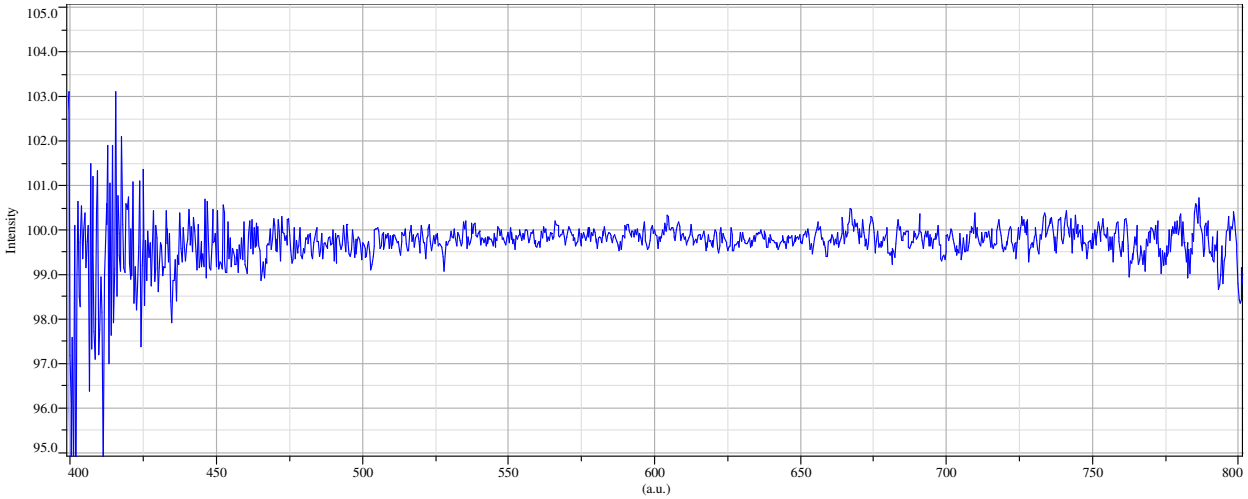

Figure A6.5: 100% transmittance, RMS Noise, mean spectrum

Photometric RMS noise, 100 %T			
λ	slope	y-intercept	%T RMS noise
500	-1.83E-02	108.7	0.2259
600	0.015708	90.4	0.1704
700	-6.70E-03	104.3	0.2426

Table 6.3: Summary tabulation of RMS noise data.

λ	y-intercept	deviation
500	108.7	8.7
600	90.4	-0.6
700	1004.3	4.3

Table A6.4: Summary table containing short-term baseline stability data where deviations from 100% T is an indication of short term baseline instability and may indicate a malfunction of the microscope spectrophotometer.

SPECTRAL RESOLUTION DEPENDENCE ON WAVELENGTH

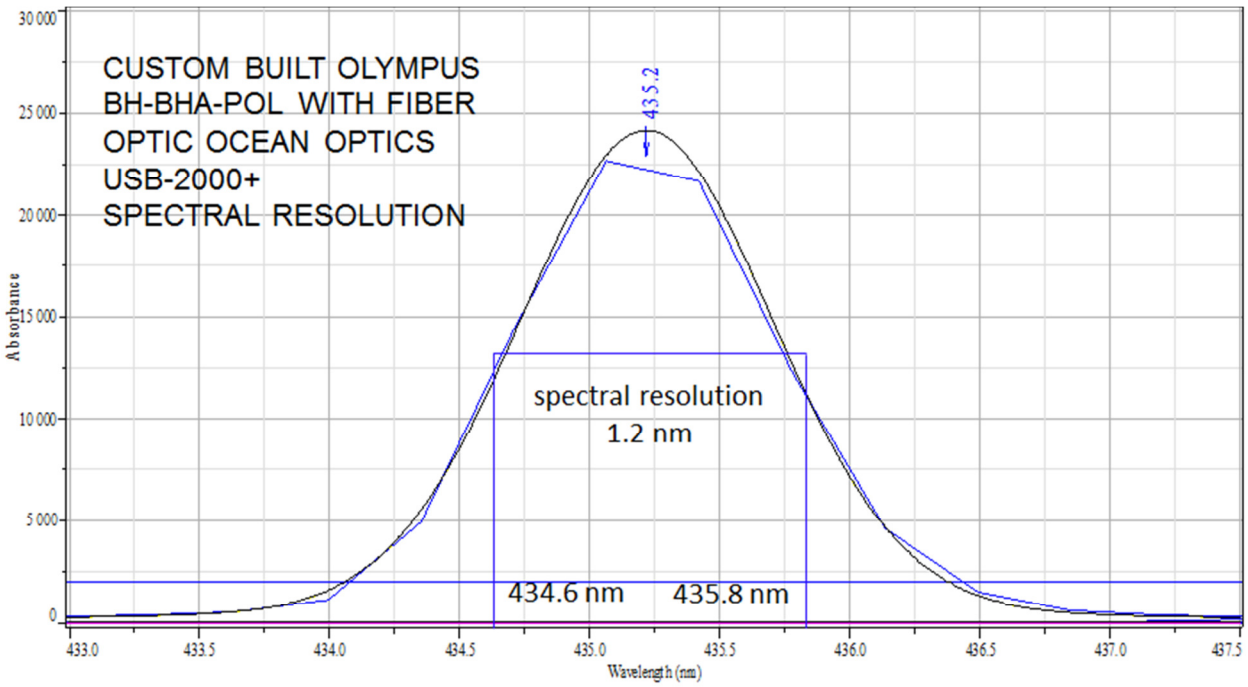

Figure A6.6: Spectral resolution of 1.2 nm at central wavelength 435.2 nm.

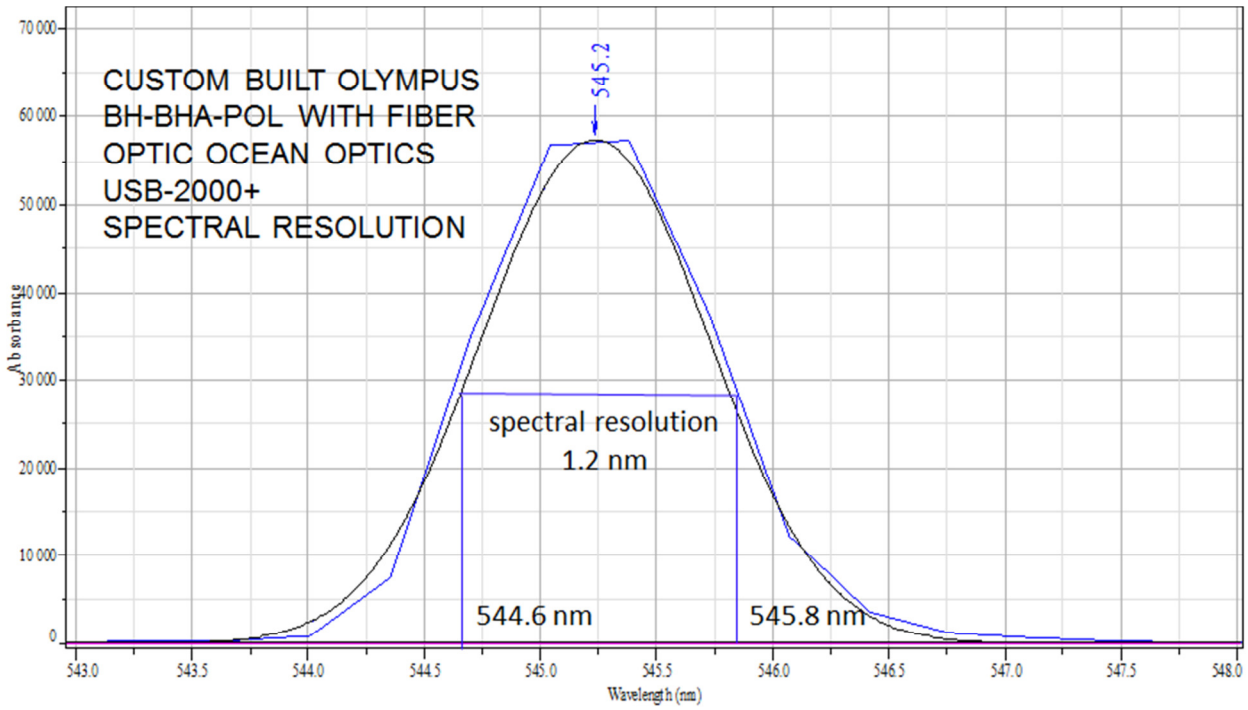

Figure A6.7: Spectral resolution of 1.2 nm at central wavelength 545.2 nm.

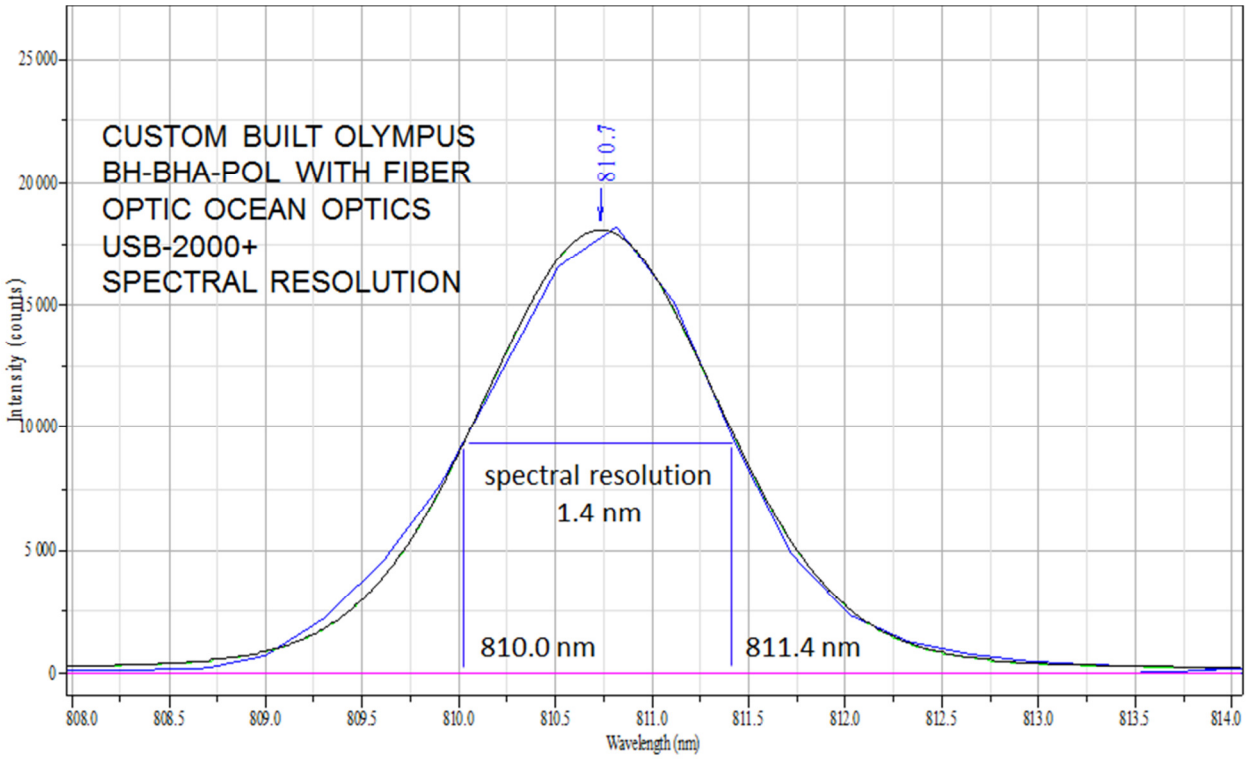

Figure A6.8: Spectral resolution of 1.4 nm at central wavelength 810.7 nm.

APPENDIX VII. CERTIFICATES OF ANALYSIS FOR VALIDATED, CERTIFIED AND STANDARD REFERENCE MATERIALS

Spectral Wavelength Calibration Sources

Model Numbers: CAL-2000; KR-1

The calibration of these wavelength calibration sources is not required as the wavelengths of the atomic emission lines are determined by quantum mechanics and are fixed as a function of time. Therefore, these products do NOT require National Institute of Standards and Technology (NIST) certification.

The wavelength of the atomic emission lines may be verified at the NIST website:

http://physics.nist.gov/cgi-bin/AtData/lines_form

Nick Sebastian
Core Americas Technical Sales Manager

The Americas
830 Douglas Avenue
Dunedin, FL 34698
+1 727-733-2447
+1 727-733-3962 fax
www.oceanoptics.com
info@oceanoptics.com

Europe
Geograaf 24
6921 EW Duiven
The Netherlands
+31 26-319-0500
+31 26-319-0505 fax
www.oceanoptics.eu

Asia
666 Gubei Road, Kirin Tower
Suite 601B - Changning District
Shanghai, PRC 200336
+86 21-6295-6600
+86 21-6295-6708 fax
www.oceanopticschina.cn

National Institute of Standards & Technology

Certificate

Standard Reference Material® 2017

Multi-Angle White Reflectance Standard

Serial No.: 2017-02-8

This Standard Reference Material (SRM) is intended for use in calibrating the reflectance factor scale of multi-angle reflectance instruments for an illumination angle of 45° and aspecular angles of 15°, 25°, 45°, 75°, and 110° at visible wavelengths. SRM 2017 is a polished white Russian opal glass with a diameter of 44 mm, mounted in a Delrin[1] holder with a diameter of 57 mm and a thickness of 13 mm. A mark in the holder indicates the direction of illumination. The serial number is located on the back of the holder.

Certified Values of Reflectance Factor: This SRM was individually calibrated using the NIST High Accuracy Reference Reflectometer [1,2], which determines bi-directional spectral reflectance with an absolute technique. Figure 1 shows typical reflectance factors as a function of wavelength for the reported aspecular geometries. The certified reflectance factor is given in Table 1 for wavelengths from 360 nm to 780 nm at an increment of 10 nm. This reflectance factor is valid for unpolarized light at an illumination angle of 45° from the sample normal and aspecular angles of 15°, 25°, 45°, 75°, and 110°, as shown in Figure 2, over the central 20 mm diameter of the sample. The uncertainty contributions and expanded uncertainty for the certified reflectance factors are given in Table 2.

Expiration of Certification: The certification of this SRM is deemed to be valid, within the uncertainties specified, for a period of **five years** from the date of certification specified in Table 1, provided the sample has been handled in accordance with the handling instructions given in this certificate. This SRM may be recertified if the sample surface has not been altered, contaminated, or damaged; however, acceptance for recertification is contingent upon inspection by NIST. For acceptance inspection and recertification information, contact M.E. Nadal of the NIST Optical Technology Division by phone (301) 975-4632; fax (301) 869-5700; or email maria.nadal@nist.gov.

Handling Instructions: When not in use, the sample should be properly stored in its original container. Improper handling will adversely affect the condition of the front surface. Lint-free gloves (nylon or latex) should be used when handling the sample to prevent fingerprints on the surface. Gently use a clean air bulb to remove dust from the front surface. The polished surface of the sample is very stable. However, care should be exercised while cleaning and handling the sample to avoid scratching the polished surface.

The overall direction and coordination leading to certification was provided by G.T. Fraser of the NIST Optical Technology Division. The initial research, development, and technical measurements leading to certification of this SRM were performed in the NIST Optical Technology Division by M.E. Nadal and E.A. Early.

Statistical consultation was provided by A.I. Aviles of the NIST Statistical Engineering Division.

The support aspects involved in the preparation, certification, and issuance of this SRM were coordinated through the NIST Standard Reference Materials Group by J.W.L. Thomas.

Albert C. Parr, Chief
Optical Technology Division

Gaithersburg, MD 20899
Certificate Issue Date: 3 June 2002

John Rumble, Jr., Chief
Measurement Services Division

---

[1] Certain commercial equipment, instrumentation, or materials are identified in this certificate to specify adequately the experimental procedure. Such identification does not imply recommendation or endorsement by the NIST, nor does it imply that the materials or equipment identified are necessarily the best available for the purpose.

Source of Material: The samples were produced by the Hemmendinger Color Laboratory, Princeton, NJ.

Determination of Reflectance Factor: The bi-directional spectral reflectance measurements were made using the NIST High Accuracy Reference Reflectometer [1,2]. The sample was placed in a mount on the sample goniometer so that its front surface was on the axis of rotation. The collimated illumination beam, with less than 1° divergence, a 14.5 nm spectral bandwidth, and a diameter of 14 mm was centered on the front of the sample. The orientation of the mount was adjusted so that, at a goniometer angle of 0°, the illumination beam was retroreflected. This aligned the normal of the sample parallel to the illumination axis. The geometry is denoted by θ_i/θ_v with respect to the normal of the sample so that, for example, the specular condition $\theta_i = 45°$, $\theta_v = -45°$ is represented by 45°/–45°. The aspecular angle is the viewing angle measured from the specular angle toward the sample normal. Radiant flux was collected and measured using a receiver mounted on an arm of the goniometer. The distance from the center of the illuminated area to the center of the limiting aperture of the collector optics was 670.7 mm. The diameter of the limiting aperture was 31.85 mm. The sources of radiant flux into the monochromator were a xenon arc lamp for wavelengths less than 390 nm and a quartz-tungsten-halogen incandescent lamp for longer wavelengths. The optical detector was a silicon photodiode. During the measurements, the ambient temperature was 20 °C ± 3 °C and the relative humidity was 40 % ± 10 %.

The bi-directional spectral reflectance was measured at wavelengths from 360 nm to 780 nm at a 10 nm increment for polarizations of the illumination beam both parallel and perpendicular to the plane of illumination, an illumination angle of 45°, and aspecular angles of 15°, 25°, 45°, 75°, and 110°. As shown in Figure 2, the sample was positioned so that the projection of the illumination axis onto the surface was aligned with the mark on the Delrin holder. For each wavelength and polarization, the following measurement sequence was followed. With the sample translated out of the illumination beam, a signal proportional to the incident radiant flux was measured by the receiver, termed the incident signal. The reflected radiant flux was measured by centering the sample in the illumination beam and rotating it with the goniometer to obtain a 45° angle of illumination. The receiver was rotated so that the viewing angle was in the desired aspecular direction, and a signal proportional to the reflected radiant flux was measured, termed the reflected signal. The sequence was completed by again measuring the incident signal. Also, after each signal reading, a shutter was closed on the monochromator and a dark signal was measured.

For each wavelength and polarization, the reflectance factor was calculated by subtracting the dark signals from the incident and reflected signals to yield net signals, dividing the net reflected signal by the average of the net incident signals and the projected solid angle of the limiting aperture, and multiplying by the constant π. The reflectance factor for unpolarized incident light was calculated by averaging the reflectance factors of both polarizations.

Discussion of Uncertainties: Uncertainties were calculated according to the procedures outlined in Reference [3]. Type A uncertainty components due to random effects include source stability and detector noise. The uncertainty contribution caused by these effects was evaluated from the standard deviation of repeat measurements (three scans with ten measurements each) of each sample.

Type B uncertainty components due to systematic effects include those that depend on the scattering properties of the sample (wavelength, uniformity, illumination, and viewing angle) and those that are independent of the sample (solid angle and viewing angle). The uncertainty contribution for the solid angle includes the standard uncertainty in the distance from the illuminated area to the center of the limiting aperture of the collector optics and the standard uncertainty in the diameter of the limiting aperture. The standard uncertainties in distance, diameter, wavelength, and angles are given in Reference [2]. The uncertainty contribution for wavelength was evaluated from the derivative of the reflectance factor. The uncertainty contributions for illumination and viewing angles were evaluated from reflectance factors measured at angles differing from the nominal angles by 0.1°. The uncertainty contribution for uniformity was evaluated from reflectance factors measured at 5 mm displacements, both horizontal and vertical, from the center of the sample. All uncertainty components were assumed to have normal probability distributions.

The sources of uncertainty and uncertainty contributions are given in Table 2, categorized by effect and dependence on sample. The expanded uncertainty in reflectance factor is obtained from the root-sum-square of the uncertainty contributions multiplied by a coverage factor $k = 2$.

REFERENCES

[1] Proctor, J.E.; Barnes, P.Y.; *NIST High Accuracy Reference Reflectometer-Spectrophotometer*; J. Res. Natl. Inst. Stand. Technol. **101**, p. 619 (1996).

[2] Barnes, P.Y.; Early, E.A.; Parr, A.C.; *NIST Measurement Services: Spectral Reflectance*; NIST Special Publication 250-48, U.S. Government Printing Office, Washington, DC (1998).

[3] *Guide to the Expression of Uncertainty in Measurement*, ISBN 72-67-10188-9, lst Ed., ISO, Geneva, Switzerland, 1993; see also Taylor, B.N.; Kuyatt, C.E.; *Guidelines for Evaluating and Expressing the Uncertainty of NIST Measurement Results*; NIST Technical Note 1297, U.S. Government Printing Office, Washington, DC; 1994; available at http://physics.nist.gov/Pubs.

Users of this SRM should ensure that the certificate in their possession is current. This can be accomplished by contacting SRM at: telephone (301) 975-6776; fax (301) 926-4751; e-mail srminfo@nist.gov; or via the internet http://www.nist.gov/srm.

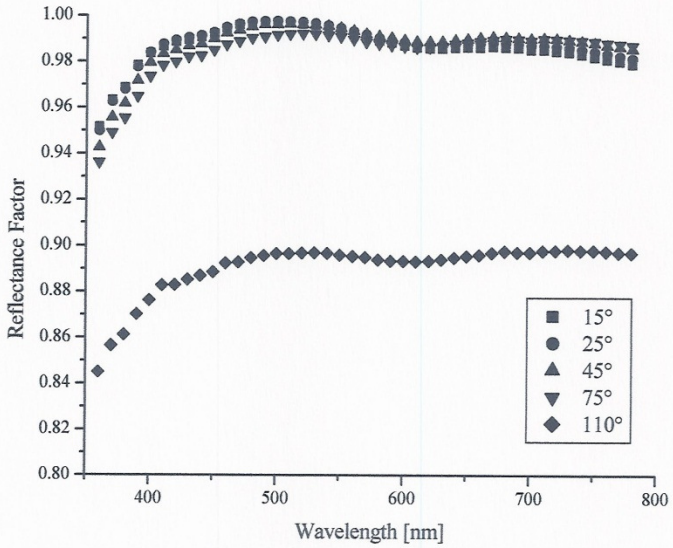

Figure 1. Reflectance factor of SRM 2017 as a function of wavelength for an illumination angle of 45° and aspecular angles of 15°, 25°, 45°, 75°, and 110° at visible wavelengths.

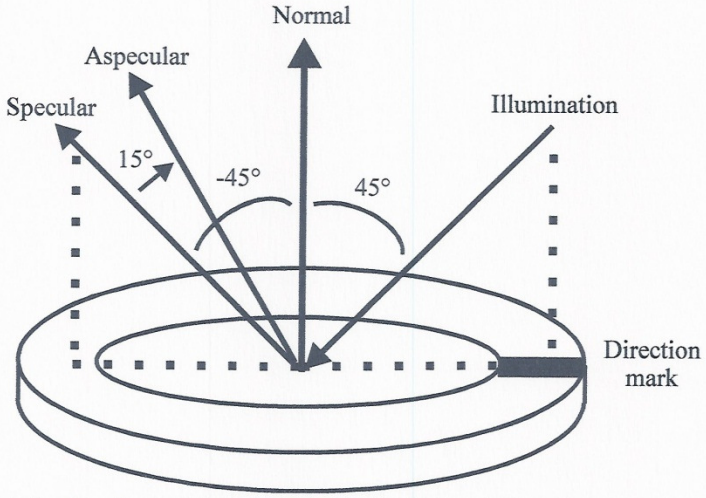

Figure 2. Schematic of sample orientation and angles. The illuminator axis is 45° from the sample normal, and its projection onto the surface is aligned with the mark in the Delrin holder. The aspecular angle is measured from the normal in the illuminator plane.

Table 1. Reflectance factor as a function of wavelength of SRM 2017

Serial No: 2017-02-2 Calibration Date: September 8, 2004

	Aspecular Angle [deg]				
	15	25	45	75	110
Wavelength [nm]	Reflectance Factor				
360	0.944	0.939	0.936	0.927	0.843
370	0.956	0.951	0.947	0.939	0.852
380	0.962	0.957	0.954	0.945	0.857
390	0.972	0.968	0.965	0.955	0.865
400	0.979	0.974	0.969	0.960	0.871
410	0.982	0.979	0.973	0.963	0.873
420	0.984	0.980	0.977	0.966	0.876
430	0.985	0.981	0.977	0.968	0.877
440	0.986	0.982	0.979	0.968	0.877
450	0.988	0.984	0.981	0.970	0.879
460	0.991	0.988	0.983	0.974	0.882
470	0.993	0.989	0.985	0.975	0.885
480	0.994	0.991	0.986	0.977	0.885
490	0.995	0.991	0.987	0.978	0.886
500	0.995	0.992	0.987	0.978	0.887
510	0.995	0.992	0.988	0.979	0.887
520	0.995	0.992	0.988	0.979	0.887
530	0.994	0.992	0.987	0.979	0.888
540	0.994	0.991	0.987	0.978	0.888
550	0.993	0.991	0.986	0.977	0.887
560	0.992	0.990	0.986	0.976	0.885
570	0.991	0.989	0.984	0.975	0.885
580	0.990	0.988	0.983	0.975	0.885
590	0.989	0.987	0.983	0.974	0.884
600	0.988	0.986	0.982	0.974	0.884
610	0.988	0.986	0.982	0.974	0.884
620	0.987	0.986	0.982	0.973	0.884
630	0.988	0.986	0.982	0.974	0.884
640	0.988	0.986	0.983	0.975	0.885
650	0.989	0.987	0.983	0.975	0.886
660	0.989	0.987	0.984	0.976	0.887
670	0.990	0.988	0.984	0.977	0.887
680	0.990	0.988	0.984	0.977	0.887
690	0.989	0.988	0.984	0.977	0.888
700	0.989	0.988	0.984	0.977	0.888
710	0.988	0.987	0.984	0.977	0.888
720	0.988	0.987	0.984	0.977	0.888
730	0.988	0.986	0.984	0.977	0.888
740	0.988	0.986	0.983	0.977	0.888
750	0.987	0.985	0.983	0.976	0.887
760	0.985	0.984	0.982	0.975	0.887
770	0.984	0.983	0.981	0.975	0.887
780	0.984	0.982	0.980	0.974	0.886

Table 2. Uncertainty Contributions and Expanded Uncertainty ($k = 2$) of the Reflectance Factor of SRM 2017 at Each Aspecular Angle

Source of Uncertainty	Aspecular Angle (deg)				
	15	25	45	75	110
	Uncertainty Contribution (%)				
Systematic Effects					
Sample-Independent					
Distance	0.15	0.15	0.15	0.15	0.15
Aperture Area	0.1	0.1	0.1	0.1	0.1
Viewing Angle	0.1	0.06	0	0.1	0.37
Wavelength					
360 nm – 390 nm	0.1	0.1	0.1	0.1	0.1
400 nm – 780 nm	0	0	0	0	0
Sample-Dependent					
Uniformity	0.1	0.1	0.1	0.1	0.1
Illumination Anlge	0.1	0.1	0.1	0.1	0.1
Viewing Angle	0	0	0	0	0
Random Effects					
Repeatability	0.2	0.2	0.2	0.2	0.4
Wavelength Range	**Expanded Uncertainty ($k = 2$) (%)**				
360 nm – 390 nm	0.67	0.65	0.64	0.67	1.20
400 nm – 780 nm	0.64	0.62	0.61	0.64	1.18

Avian Technologies LLC

Certified Reflectance Standards

CERTIFICATE OF CALIBRATION

Total Hemispherical Reflectance
UV-Visible Wavelength Calibration Standard

WCR-UVVis-02c

For:
CUNY/John Jay Institute
P.O. 2471083
Calibration #AT-20120510-WC1

May 10th, 2012

Avian Technologies LLC
P.O. Box 716, Sunapee,NH 03782-0716
Ph: 603-526-2420/ Fax 603-526-2729
info@aviantechnologies.com

Avian
TECHNOLOGIES LLC
Optical Spectroscopy
Materials, Coatings, & Standards

P.O. Box 716
Sunapee, NH
03782-0716

603.526.2420 (P)
603.526.2729 (F)
www.aviantechnologies.com

Avian Technologies LLC

Calibration #AT-201200510-WC1
Calibration Date10 May 2012
Vis-NIR Wavelength Calibration Standard
FW-WC-UVVis-02c
For: CUNY-John Jay Institute of Forensic Science

Customer Name: CUNY-John Jay Institute. Order no: 2471083
Sample: Wavelength Calibration Standard FW-WC UV-Vis-02c (WCR-UVVis-02c)
Measurement Instrument: Perkin-Elmer Lambda-9/19 UV-Vis-NIR Spectrometer Ser. No. 1104
Traceability of measurement to: ASTM Test Method E 1331-96, Test Method E903-96,
NRC Certificate PO1948 (Didymium Oxide Glass)
NRC Certificate PAR-2008-2614 (Holmium Oxide Glass)
NIST SRM-1920a, NIST SRM-2036

Measurement Conditions:
Mean Temperature: 26.8°C Relative Humidity: 28%
Instrument Parameters:
Bandpass: 1 nm. (UV-Vis) NIR Sensitivity: n/a
Reporting Interval: 1 nm. Recording Interval: 1 nm.. Scan Speed: 60 nm/min
Integration time: 1 sec. Number of measurements averaged: 3

Procedure: Procedure: The regular transmittance measurements were performed on a Perkin-Elmer Lambda 9/19 UV-Vis-NIR Spectrophotometer. The instrument was set up in 8° hemispherical geometry with the sample positioned normally to the beam. The measurement beam is well collimated (maximum angle of convergence is ±4°). The transmittance factor measurements were relative to packed PTFE powder (Dupont 7A) at ambient temperature (26.8°C±1°) and humidity (28±5%).

The calibration of the wavelength calibration standard was performed by a scanning over the wavelength range at a slit of 1 nm. and scan speed of 1 nm/sec. Peak picking was done at 0.1 nm. interval over the wavelength range 250-850 nm. Four scans were performed on the standard and the data averaged.

Traceability is to National Research Council Canada, Calibrated artifact AVTDD-02, Didymium oxide glass, Calibration PO-1948. and NIST SRM-1920a and SRM-2036. Traceability to NIST is achieved through NORAMET, the North American Metrological Agreement, and SRM's 1920 and 2065.

Certified by: _____ Date: 05.10.2012
Arthur W. Springsteen Ph.D. May 10th. 2012

Other Pertinent References:
ASTM Standard Practice E 275-93 "Standard Practice for Describing and Measuring Performance of UV, Vis, and NIR Spectrophotometers"
ASTM Standard Practice E 925-94 "Standard Practice for Periodic Calibration of Narrow Band-Pass Spectrophotometers"

Avian Technologies LLC
General Statements of Measurement Uncertainty
Based on Perkin-Elmer Lambda-9/19 Spectrophotometers
and Byk-Gardner ColorView 45:0 Spectrophotometer

Wavelength Accuracy

A precision of measurement of < 0.2 nm. from 250 to 850 nm. is based on repeated measurement of a Corning holmium oxide filter (melt 3131). Accuracy, determined by comparison with a holmium oxide filter calibrated by the National Research Council, Canada is ±0.2 nm. over the same range. Uncertainty in the near-IR range has been calculated to be <±1.5 nm, by repeated measurements of NIST SRM-1920a and the NRC Calibrated holmium oxide filter in total hemispherical reflectance and normal transmittance mode.

Transmittance/Photometric Scale

The precision of measurement of <0.001A between 400-700 nm. at 50% transmittance, <0.001A between 400-700 nm. at 3% transmittance, and ≈0.002 between 400-700 nm has been determined by multiple readings of neutral density filter glasses (Starna Inc. Serial No. 5688). Accuracy in the Visible range (400-700 nm) has been determined to be <±0.005A for a 50% filter, <±0.010A for a 3% filter, and <±0.010A for a 1% filter . Accuracy in the UV is better than ±0.005A for a nominal 10% transmissive filter..(NRC UV-Vis ND Filters, Certificate PAR2007-2532) Expanded uncertainties levels are at confidence level 95% for a coverage factor of k=2

8°/Hemispherical Reflectance Factor

Precision of measurement was determined at 11 wavelengths between 360-760 nm using three CERAM Research tiles. A series of measurements over a three week period showed the overall precision to be no worse than 0.0025 at any wavelength on all three tiles. Accuracy was determined by multiple measurements of a calibrated sintered PTFE plaques (ser. #PO2115, Calibration date 7-20-2002) and calibrated CERAM tiles (PA-2007-2535) from the National Research Council, Canada. Measurements at ten wavelengths showed a variance from the mean NRC values of <0.006. The overall uncertainty of measurement has been calculated to be <0.0045 at 500 and 750 nm. and by interpolation, appx. 0.005 at 300 nm. These are comparable with the uncertainties stated by the National Laboratories of the United States (NIST) and Canada (NRC). Expanded uncertainties levels are at confidence level 95% for a coverage factor of k=2

45:0 Directional Radiance Factor

The uncertainty of 45:0 spectral radiance factor is currently under investigation. Preliminary calculations indicate that uncertainty is <0.003 from 380-720 nm. Based on measurement of standard CERAM tiles measured at National Research Council Canada.

Specular Reflectance (7.5° Absolute Reflectance)

The uncertainty has been determined to be <0.4° for the range 400-2000 nm, as determined by multiple measurements of an first surface aluminum mirror calibrated by National Research Council Canada, Certificate #AVIAN-17947-5-2).

(Revised 02.08.2012)

Avian Technologies LLC
Wavelength Calibration Standard WCR-UVVis-02c
For: John Jay/CUNY
Calibration #AT-20120510-WC1
Peak Positions

Measured at 1 nm bandpass

Wavelength	Refl. At Peak	Wavelength	Refl. At Peak
799.7	0.778	419.6	0.674
664.4	0.725	415.5	0.688
661.3	0.686	407.6	0.748
654.5	0.611	387.0	0.643
648.1	0.594	379.7	0.415
641.4	0.631	376.8	0.386
538.9	0.539	360.0	0.531
536.3	0.568	344.7	0.746
522.4	0.404	290.9	0.708
517.8	0.410	288.1	0.660
483.0	0.686	280.7	0.632
462.2	0.429	278.3	0.717
454.5	0.357	255.6	0.586
448.1	0.353		

Measured at 1 nm bandpass
Hemispherical Reflectance Factor is bandpass dependent

05.10.2012

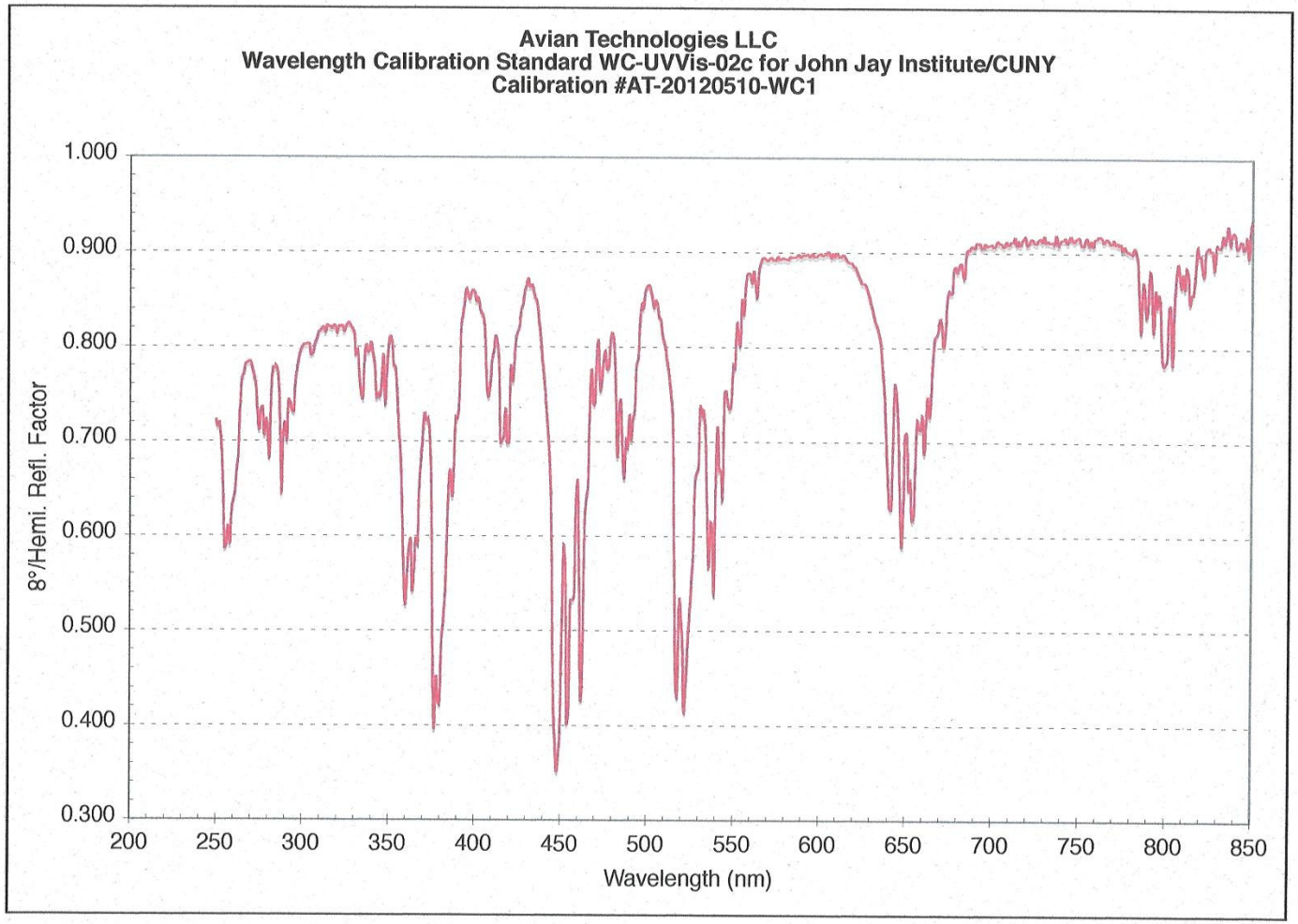

05.10.2012

Avian Technologies LLC
P.O. Box 716,Sunapee,NH 03782-0716 USA
www.aviantechnologies.com

NRC Calibrated Holmium Oxide Filter
Instrument Wavelength Calibration Check

NRC Holmium Oxide Filter
Customer: John Jay/CUNY
Date: 05.10.2012

Peak #	Wavelength Minima	Uncertainty	Found
1	279.26	0.20	279.3
2	287.56	0.20	287.5
3	289.96	0.20	****
4	333.80	0.20	333.8
5	347.78	0.20	347.5
6	360.79	0.20	360.8
7	381.65	0.20	381.6
8	385.86	0.20	385.8
9	418.63	0.20	418.5
10	445.43	0.20	445.4
11	453.41	0.20	453.3
12	459.96	0.20	459.9
13	484.28	0.20	484.3
14	536.44	0.20	536.4
15	637.60	0.50	637.4
16	662.23	0.50	662.2
17	1150.17	1.00	n/a
18	1192.96	1.00	n/a
19	1885.16	1.00	n/a
20	1938.08	1.00	n/a
21	2005.03	1.00	n/a

05.10.2012

Avian Technologies LLC

Avian
TECHNOLOGIES LLC

Certified Reflectance Standards

45:0c bidirectional Radiance Factor

ATBC Color Tile Set

For: **John Jay College**
P.O.: **2471083**

Calibration # **AT201200608-1(450)**

Date: **June 8, 2012**

Avian Technologies LLC
P.O. Box 716, Sunapee, NH 03782-0716
Ph: 603-526-2420/ Fax 603-526-2729
info@aviantechnologies.com

Avian Technologies LLC
P.O. Box 716, Sunapee,NH 03782-0716
Ph: 603-526-2420/ Fax 603-526-2729
info@aviantechnologies.com

Avian TECHNOLOGIES LLC

Calibration Certificate

Customer Supplied Samples:
ATBC Color Tile Set
45:0c Bidirectional Radiance Factor
June 8, 2012
Certificate #AT201200608-1(450)

Customer Name: John Jay College
Purchase order # : 2471083
Sample: ATBC Color Tile Set

Measuring Instrument
Model: BYK-Gardner Colorview
Type: Bidirectional spectrophotometer
Serial number: 90001220
Geometry: 45:0c, large area view

Traceability of measurement
ASTM Test Method E1349-06
NRC Certificates PAR-2007-2528

Measurement Conditions
Mean Temperature: 24°
Relative Humidity: 43%

Instrument and Measurement Details
Bandpass: approximately 10 nm
Wavelength Range: 380-720 nm
Recording Interval: 10 nm
Replicates: 3
Accuracy: 0.5 (mean ΔE^*_{ab} for 14 calibrated ceramic tiles)

Uncertainty:

Wavelength (nm)	μ_{Avian} [1]	μ_{NRC} [2]	μ_{total} [3]
400	0.26%	0.63%	0.68%
500	0.19%	0.49%	0.52%
600	0.18%	0.52%	0.55%
700	0.24%	0.51%	0.56%

[1] Standard deviation of reflectance factor of white tile, measured 30 times with replacement. Stated uncertainty is the average standard deviation at each respective wavelength. Coverage factor k=2.

[2] NRC uncertainty is in percent radiance factor for the white tile B-5 (PAR-2007-2528), averaged over each respective wavelength range. Coverage factor k=2.

[3] Uncertainties combined in quadrature (ie: $\mu_{total} = \sqrt{\mu^2_{Avian} + \mu^2_{NRC}}$)

Procedure
These bidirectional measurements were performed on a recently-standardized BYK-Gardner Colorview Spectrophotometer. This instrument reports bidirectional radiance factor, using circumferential illumination and normal detection (CIE 15.2004 designation 45:0c). For replicate measurements, samples are rotated approximately 90° between measurements. Instrument performance is verified against white and light green NRC transfer standards prior to every measurement suite.

Certified by David R. Wyble Ph.D. Date June 8, 2012

Avian Technologies LLC
Calibration certificate AT201200608-1(450)
June 8, 2012

wavelength	B-1	B-2	B-3	B-4	B-5	B-6	B-7	B-8
380	0.3750	0.0203	0.0633	0.1694	0.7542	0.2380	0.0824	0.0031
390	0.3951	0.0205	0.0646	0.1882	0.7860	0.2410	0.0826	0.0029
400	0.4100	0.0209	0.0660	0.2018	0.8077	0.2411	0.0821	0.0031
410	0.4200	0.0211	0.0679	0.2103	0.8209	0.2395	0.0813	0.0031
420	0.4273	0.0211	0.0713	0.2148	0.8289	0.2377	0.0802	0.0030
430	0.4340	0.0213	0.0770	0.2158	0.8347	0.2369	0.0796	0.0031
440	0.4407	0.0218	0.0863	0.2131	0.8388	0.2373	0.0790	0.0030
450	0.4490	0.0245	0.1057	0.2048	0.8427	0.2388	0.0784	0.0031
460	0.4584	0.0246	0.1271	0.1919	0.8476	0.2410	0.0779	0.0030
470	0.4677	0.0245	0.1585	0.1741	0.8514	0.2427	0.0773	0.0030
480	0.4761	0.0245	0.2057	0.1562	0.8553	0.2438	0.0766	0.0031
490	0.4820	0.0245	0.2723	0.1412	0.8579	0.2437	0.0757	0.0030
500	0.4854	0.0247	0.3581	0.1294	0.8609	0.2429	0.0751	0.0030
510	0.4851	0.0250	0.4520	0.1184	0.8625	0.2411	0.0744	0.0030
520	0.4822	0.0259	0.5396	0.1113	0.8628	0.2394	0.0740	0.0031
530	0.4774	0.0277	0.6069	0.1081	0.8630	0.2385	0.0739	0.0031
540	0.4725	0.0296	0.6512	0.1068	0.8629	0.2390	0.0743	0.0032
550	0.4698	0.0310	0.6828	0.1022	0.8627	0.2399	0.0747	0.0033
560	0.4708	0.0323	0.7086	0.0902	0.8619	0.2399	0.0748	0.0034
570	0.4759	0.0346	0.7307	0.0757	0.8607	0.2386	0.0746	0.0034
580	0.4816	0.0428	0.7445	0.0646	0.8595	0.2368	0.0743	0.0033
590	0.4842	0.0772	0.7582	0.0592	0.8589	0.2359	0.0744	0.0034
600	0.4831	0.1957	0.7782	0.0576	0.8585	0.2363	0.0749	0.0035
610	0.4796	0.4261	0.7932	0.0572	0.8582	0.2364	0.0754	0.0036
620	0.4758	0.6158	0.8002	0.0567	0.8573	0.2358	0.0759	0.0038
630	0.4736	0.7027	0.8054	0.0559	0.8566	0.2349	0.0762	0.0038
640	0.4731	0.7406	0.8074	0.0556	0.8555	0.2342	0.0764	0.0040
650	0.4747	0.7604	0.8038	0.0567	0.8541	0.2346	0.0766	0.0041
660	0.4805	0.7731	0.8089	0.0606	0.8536	0.2368	0.0767	0.0043
670	0.4897	0.7823	0.8172	0.0681	0.8536	0.2409	0.0769	0.0045
680	0.5014	0.7893	0.8207	0.0808	0.8532	0.2468	0.0777	0.0049
690	0.5158	0.7948	0.8222	0.1000	0.8527	0.2541	0.0789	0.0054
700	0.5331	0.8003	0.8268	0.1247	0.8518	0.2617	0.0805	0.0061
710	0.5508	0.8065	0.8300	0.1516	0.8507	0.2693	0.0829	0.0069
720	0.5660	0.8115	0.8321	0.1764	0.8488	0.2771	0.0863	0.0081

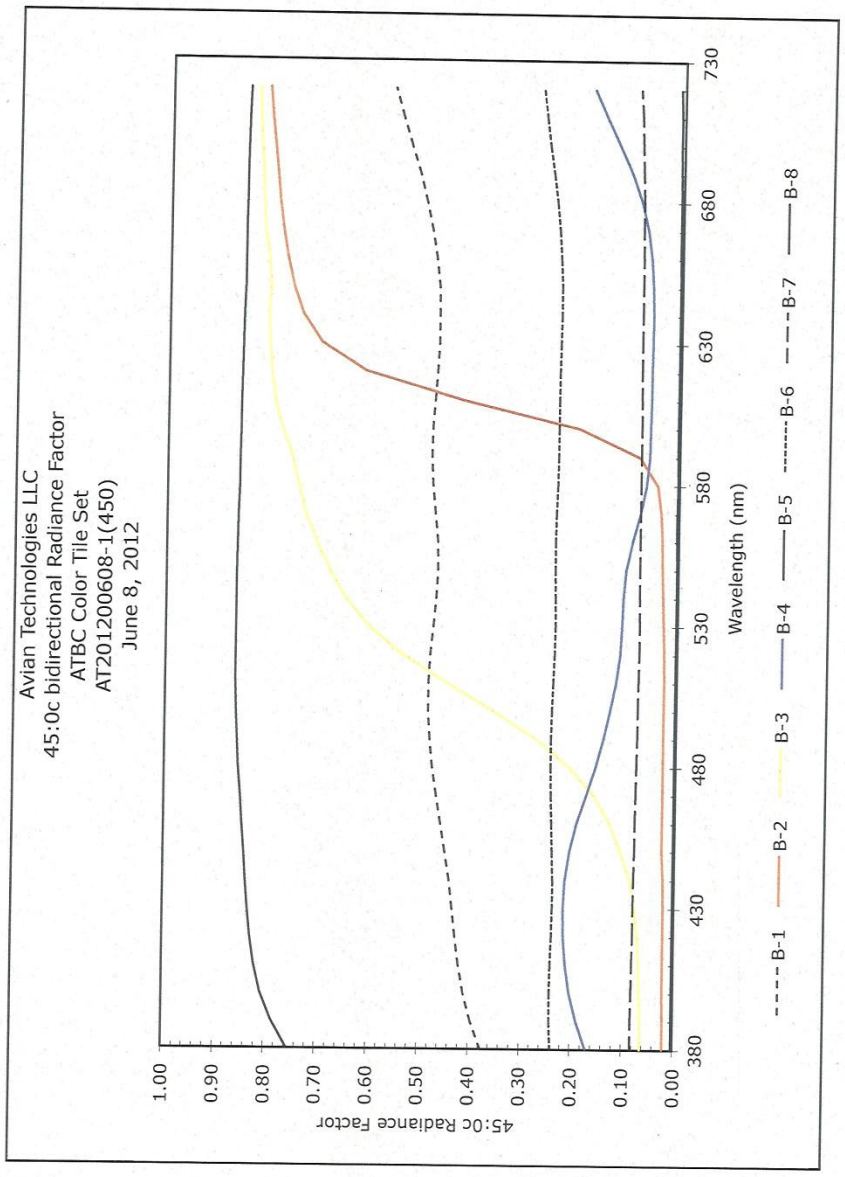
Avian Technologies LLC
45:0c bidirectional Radiance Factor
ATBC Color Tile Set
AT201200608-1(450)
June 8, 2012
45:0c Radiance Factor
1.00
0.90
0.80
0.70
0.60
0.50
0.40
0.30
0.20
0.10
0.00
380
430
480
530
580
630
680
730
Wavelength (nm)
B-1
B-2
B-3
B-4
B-5
B-6
B-7
B-8

Avian Technologies LLC
Calibration certificate AT201200608-1(450)
June 8, 2012

wavelength	B-9	B-10	B-11	B-12	B-13	B-14	B-15	B-16
380	0.0220	0.0864	0.1552	0.0057	0.2182	0.1567	0.0414	0.193
390	0.0233	0.0858	0.1704	0.0058	0.2659	0.1709	0.0431	0.196
400	0.0247	0.0825	0.1817	0.0060	0.3103	0.1763	0.0449	0.193
410	0.0266	0.0794	0.1907	0.0061	0.3470	0.1705	0.0467	0.185
420	0.0297	0.0789	0.1996	0.0062	0.3771	0.1548	0.0495	0.171
430	0.0347	0.0833	0.2061	0.0063	0.4022	0.1329	0.0542	0.155
440	0.0429	0.0909	0.2083	0.0069	0.4230	0.1085	0.0613	0.138
450	0.0603	0.1021	0.2057	0.0099	0.4397	0.0837	0.0749	0.122
460	0.0792	0.1182	0.1992	0.0100	0.4549	0.0624	0.0886	0.107
470	0.1075	0.1369	0.1858	0.0098	0.4629	0.0452	0.1061	0.093
480	0.1510	0.1580	0.1696	0.0096	0.4621	0.0335	0.1277	0.083
490	0.2149	0.1787	0.1552	0.0095	0.4511	0.0264	0.1510	0.074
500	0.3007	0.1949	0.1425	0.0097	0.4294	0.0221	0.1731	0.069
510	0.3970	0.2032	0.1276	0.0099	0.3959	0.0188	0.1911	0.066
520	0.4855	0.1978	0.1133	0.0108	0.3550	0.0171	0.2083	0.065
530	0.5512	0.1816	0.1003	0.0123	0.3111	0.0167	0.2270	0.069
540	0.5949	0.1610	0.0883	0.0141	0.2687	0.0173	0.2437	0.076
550	0.6259	0.1388	0.0776	0.0159	0.2292	0.0177	0.2571	0.087
560	0.6521	0.1165	0.0680	0.0184	0.1949	0.0160	0.2711	0.103
570	0.6764	0.0977	0.0575	0.0240	0.1661	0.0133	0.3005	0.125
580	0.6939	0.0878	0.0488	0.0465	0.1434	0.0113	0.3736	0.154
590	0.7070	0.0815	0.0443	0.1456	0.1267	0.0108	0.5033	0.193
600	0.7271	0.0754	0.0431	0.3679	0.1145	0.0113	0.6282	0.243
610	0.7438	0.0721	0.0429	0.5640	0.1059	0.0121	0.6944	0.300
620	0.7520	0.0743	0.0423	0.6659	0.1001	0.0127	0.7207	0.363
630	0.7584	0.0766	0.0414	0.7200	0.0967	0.0129	0.7326	0.424
640	0.7632	0.0759	0.0418	0.7523	0.0956	0.0132	0.7396	0.478
650	0.7674	0.0741	0.0443	0.7734	0.0969	0.0140	0.7451	0.520
660	0.7718	0.0758	0.0498	0.7902	0.1010	0.0162	0.7511	0.552
670	0.7764	0.0874	0.0586	0.8046	0.1078	0.0210	0.7577	0.577
680	0.7805	0.1169	0.0711	0.8168	0.1179	0.0316	0.7644	0.596
690	0.7843	0.1673	0.0869	0.8270	0.1313	0.0552	0.7710	0.613
700	0.7879	0.2304	0.1050	0.8357	0.1483	0.1013	0.7780	0.629
710	0.7917	0.2902	0.1234	0.8431	0.1672	0.1739	0.7852	0.646
720	0.7950	0.3350	0.1398	0.8483	0.1842	0.2678	0.7914	0.661

Avian Technologies LLC
45:0c bidirectional Radiance Factor
ATBC Color Tile Set
AT201200608-1(450)
June 8, 2012

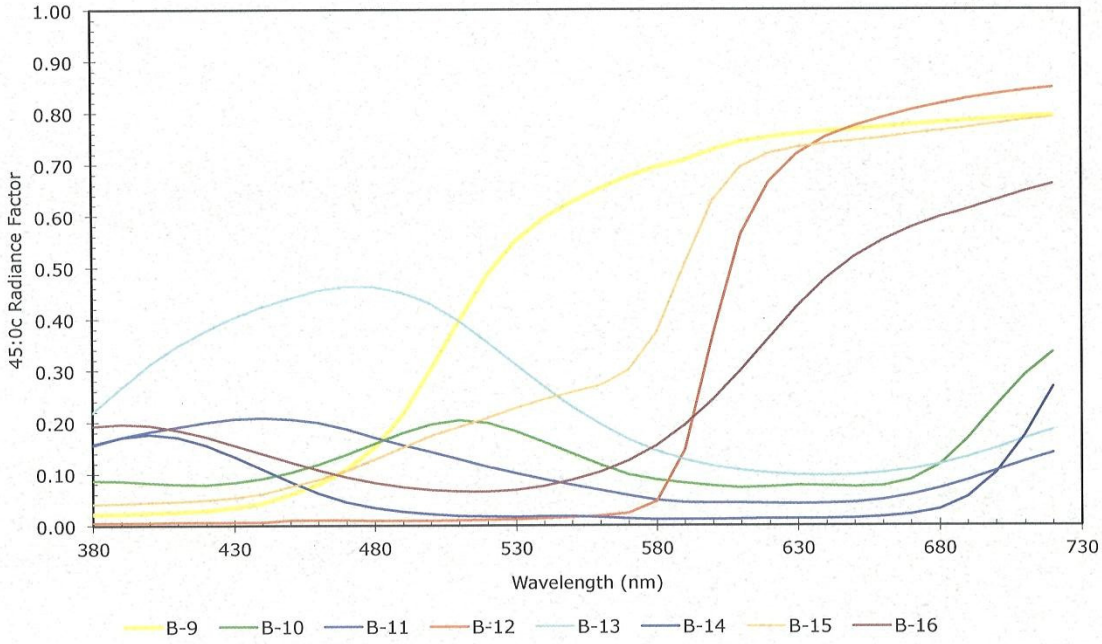

APPENDIX VIII. SPECTRAL DATA FOR MICROSCOPE SUPPLIES, OPTICAL FILTERS, AND DICHROIC MIRRORS

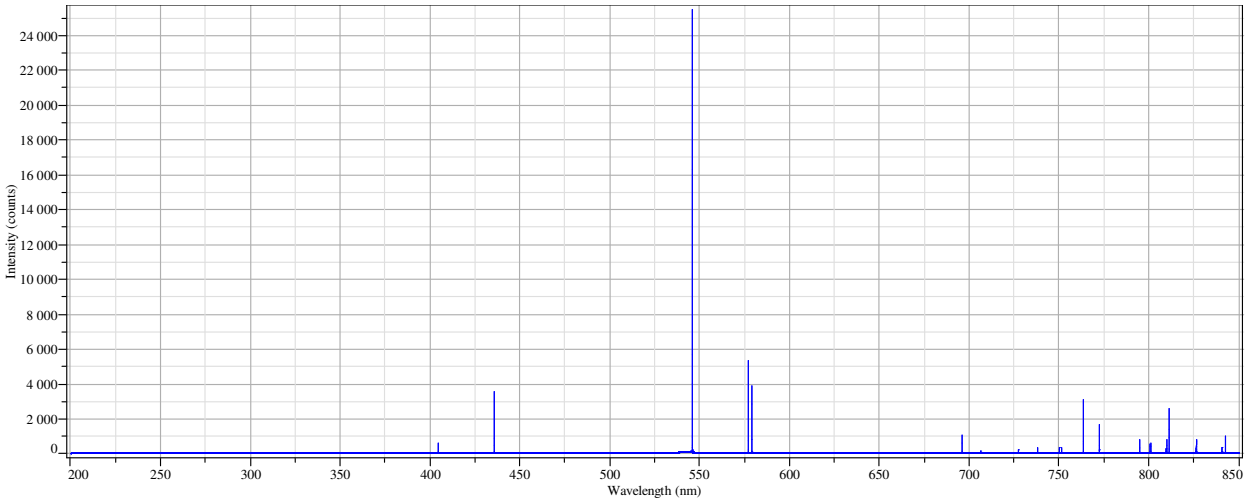

Figure A8.1: Single-beam intensity spectrum of Ocean Optics® CAL-2000™, mercury-argon low-pressure gas discharge lamp collected with a Horiba Scientific LabRAM HR Evolution Raman Spectrometer located at Horiba Scientific, Edison, New Jersey. Instrument spectral collection and measurement parameters: grating, 1800 grooves/mm; wavelength range, 200-850 nm; data acquisition rate, 0.05 seconds, accumulations, 16; hole, 25 micrometer.

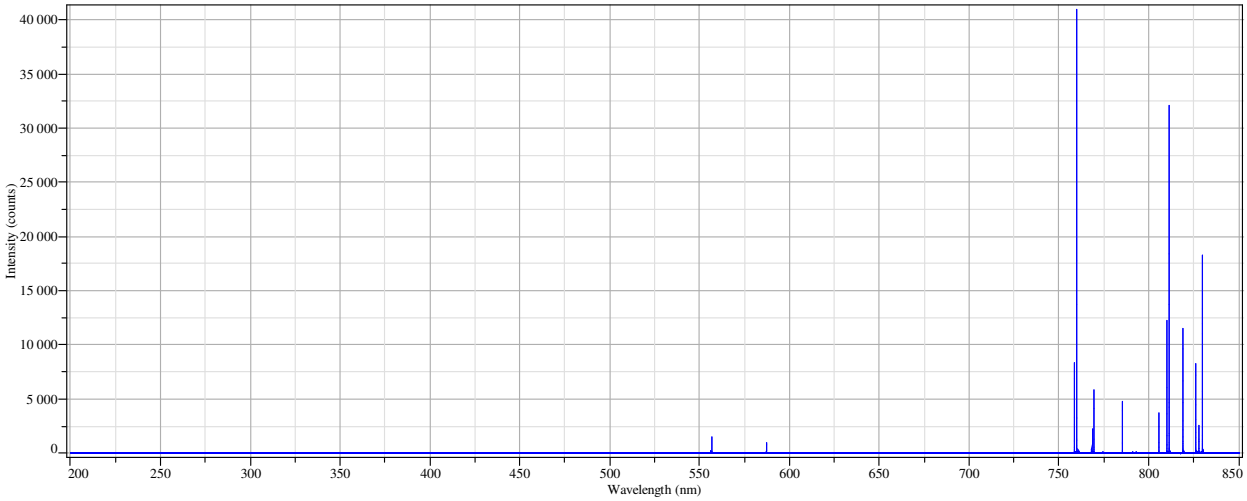

Figure A8.2: Single-beam intensity spectrum from Ocean Optics® KR-1™, krypton low-pressure gas discharge lamp collected with a Horiba Scientific LabRAM HR Evolution Raman Spectrometer located at Horiba Scientific, Edison, New Jersey. Instrument spectral collection and measurement parameters: grating, 1800 grooves/mm; wavelength range, 200-850 nm; data acquisition rate, 0.05 seconds, accumulations, 16; hole, 25 micrometer.

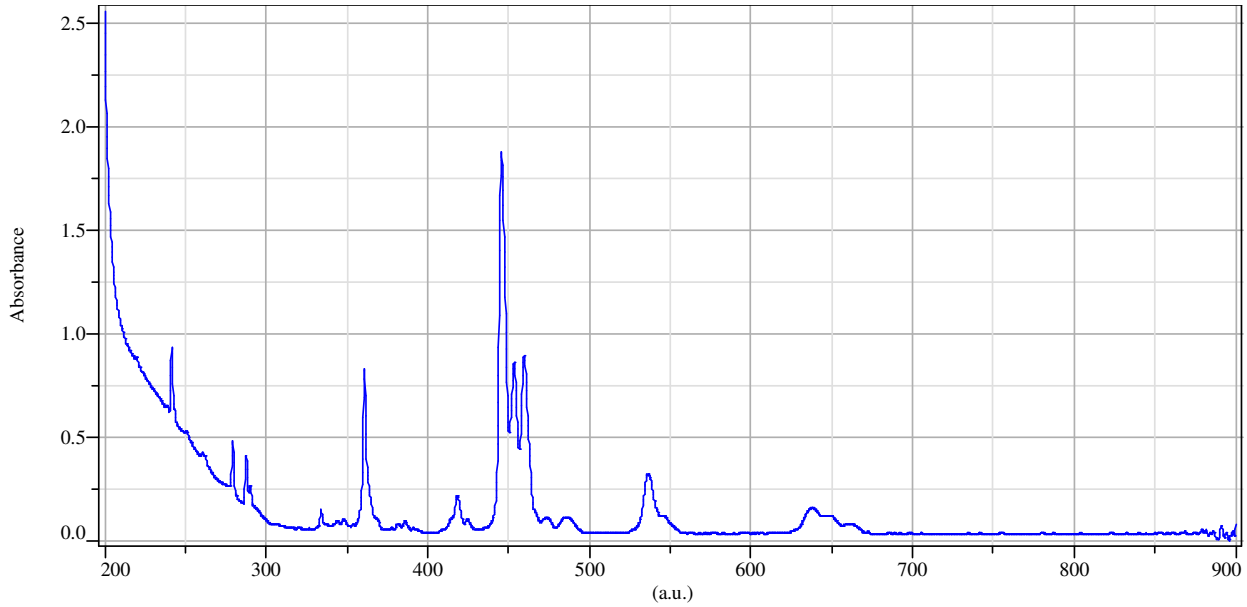

Figure A8.3: An absorbance spectrum of Starna® RM-HG, holmium oxide glass collected with a Shimadzu UV-2450 bench top spectrophotometer located at John Jay College of Criminal Justice. Spectrum measurement parameters: wavelength range, 200-900 nm; scan speed, slow; sampling interval, 0.2 nm; slit width, 0.1 nm bandwidth.

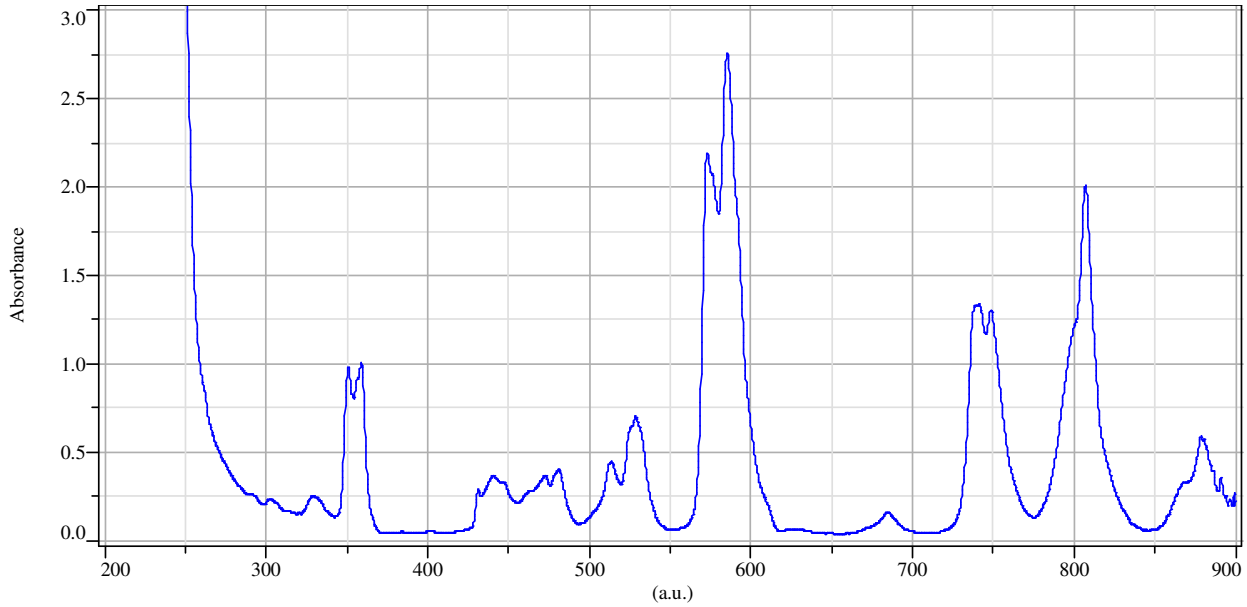

Figure A8.4: An absorption spectrum of the Starna® RM-DG, didymium glass wavelength accuracy standard collected with a Shimadzu UV-2450 bench top spectrophotometer located at John Jay College of Criminal Justice. Spectrum measurement parameters: wavelength range, 200-900 nm; scan speed, slow; sampling interval, 0.2 nm; slit width, 0.1 nm bandwidth.

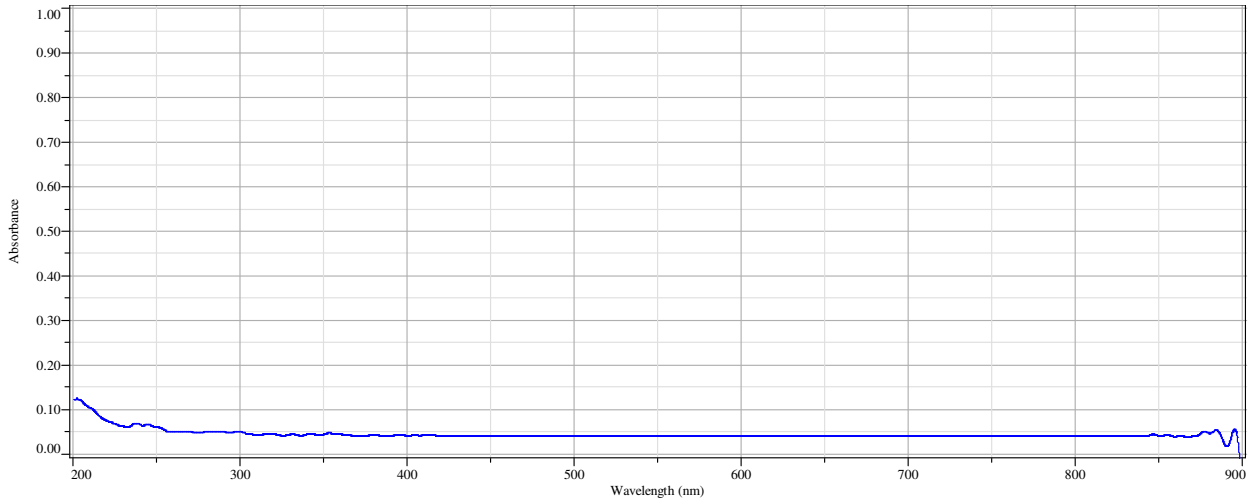

Figure A8.5: An absorbance spectrum of a ChemGlass, CGQ-0640-03, 25 x 25 x 1 mm, quartz slide. Spectrum collected with a Shimadzu UV-2450 bench top spectrophotometer located at John Jay College of Criminal Justice. This slide was referenced against air.

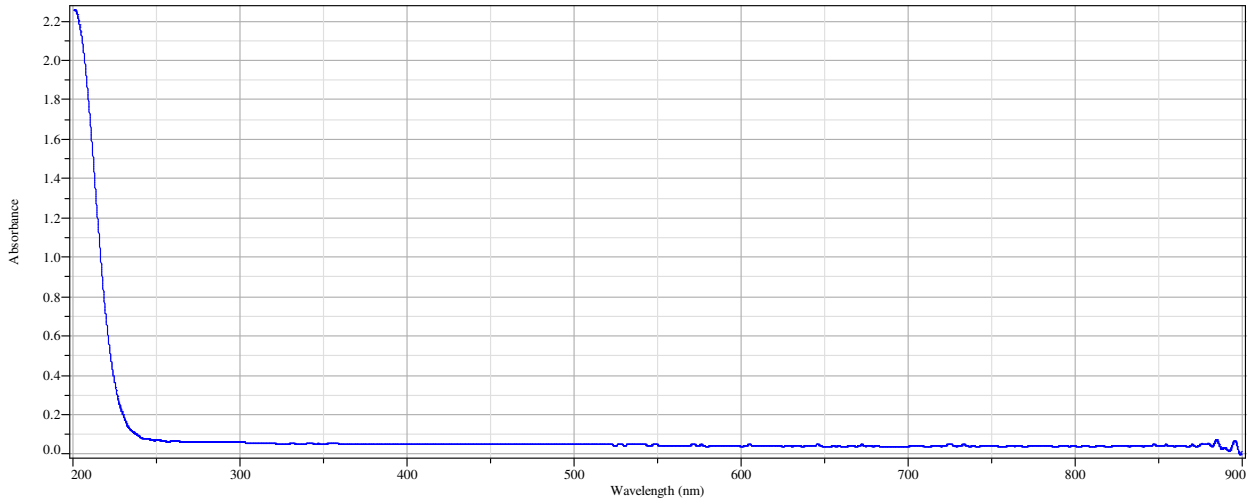

Figure A8.6: An absorbance spectrum of a CRAIC Inc., 25.4 x 25.4 mm, quartz cover slip. Spectrum collected with a Shimadzu UV-2450 bench top spectrophotometer located at John Jay College of Criminal Justice. This cover slip was referenced against air.

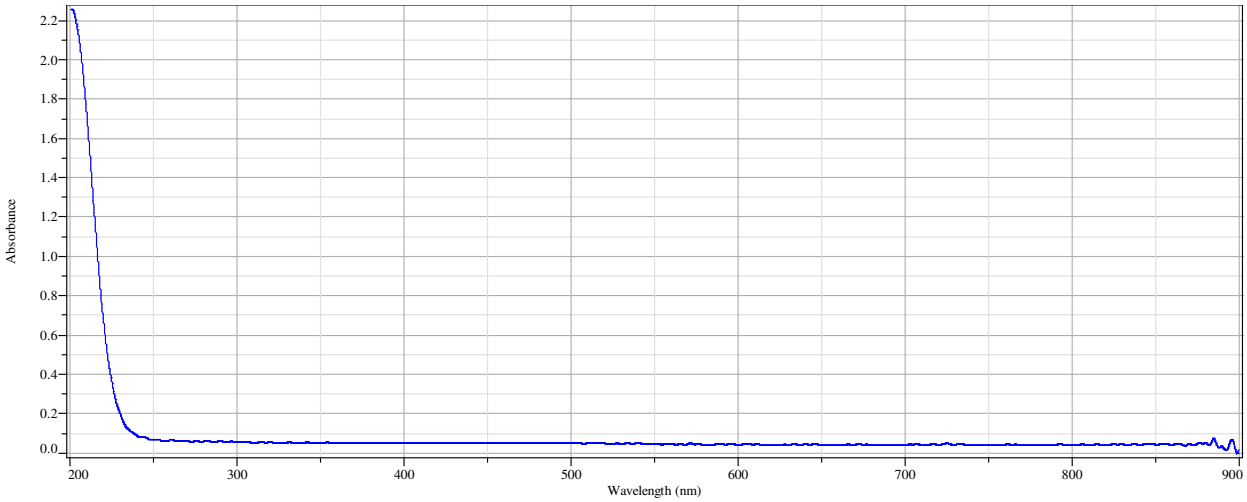

Figure A8.7: An absorbance spectrum of a CRAIC Inc., 25 x 76 x 1 mm, quartz slide. Spectrum collected with a Shimadzu UV-2450 bench top spectrophotometer located at John Jay College of Criminal Justice. This slide was referenced against air.

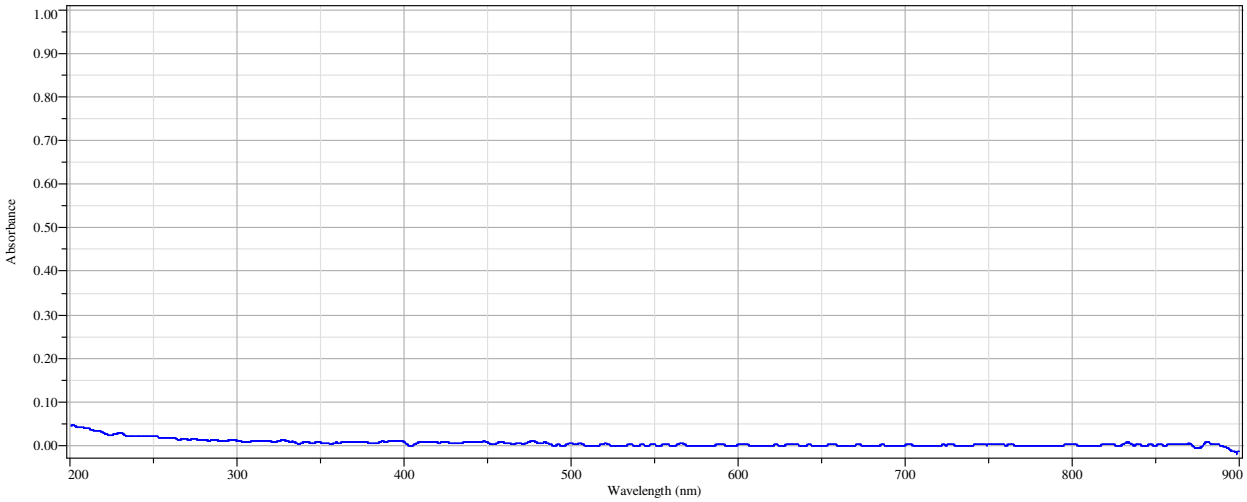

Figure A8.8: An absorbance spectrum of a SPI, Inc. #1001-AB Corning 7980, fused silica, 1 x 25.4 mm diameter disc (LOT# 1170223) collected with a Shimadzu UV-2450 bench top spectrophotometer located at John Jay College of Criminal Justice. The disc was reference against air.

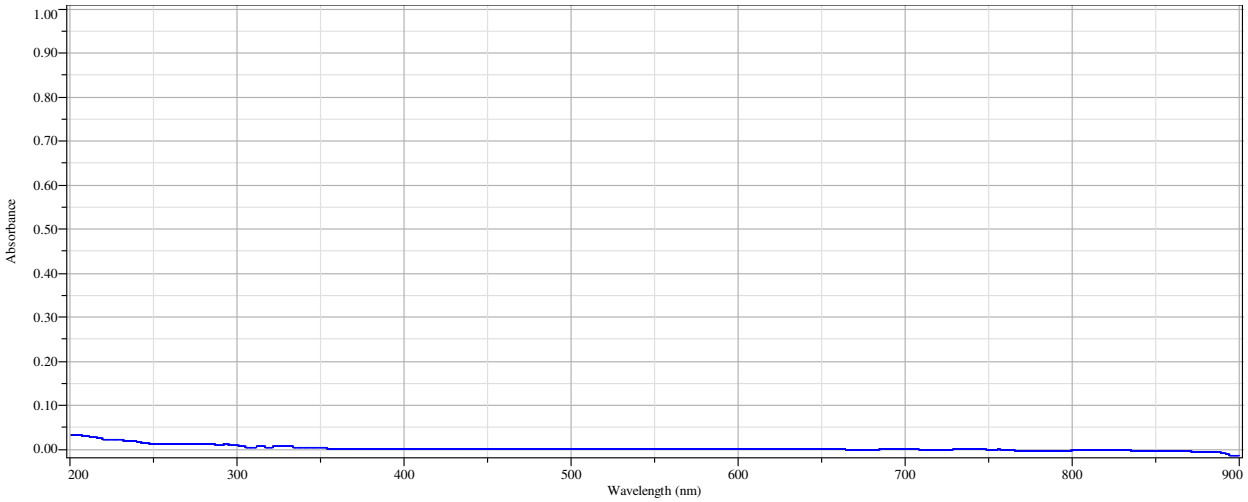

Figure A8.9: An absorbance spectrum of a SPI, Inc. #1003-AB Corning 7980, fused silica, 25.4 x 25.4 x1 mm slide (LOT# 1170223) collected with a Shimadzu UV-2450 bench top spectrophotometer located at John Jay College of Criminal Justice. The slide was referenced against air.

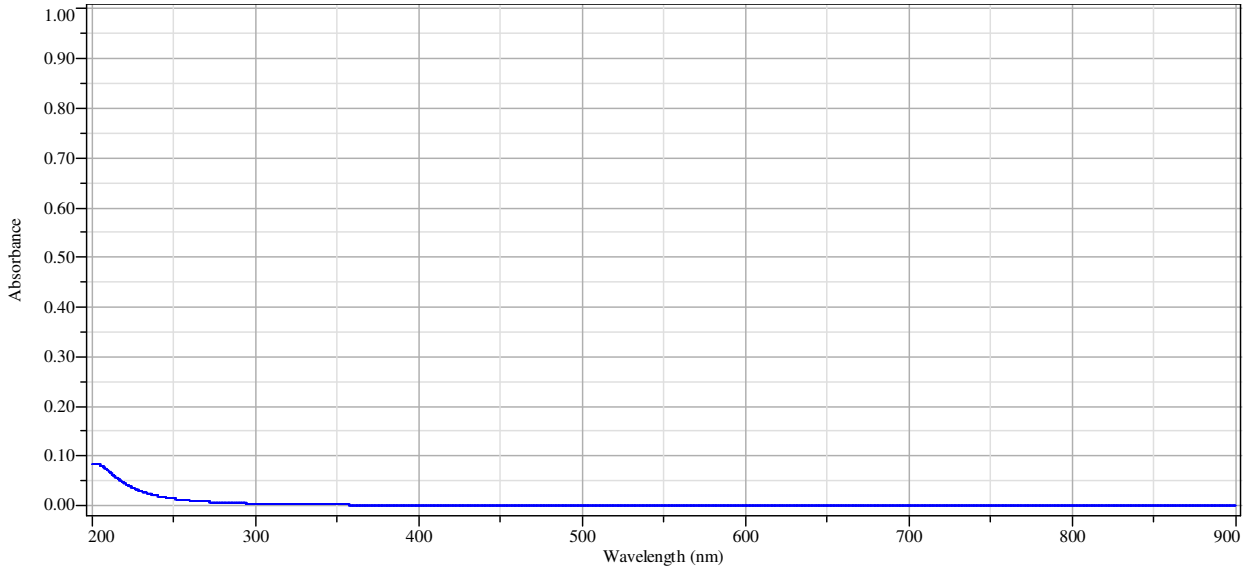

Figure A8.10: An absorbance spectrum of a SPI, Inc. #1015, fused quartz cover slip, 25.4 x 25.4 x 0.2 mm (LOT# 1120917) collected with a Shimadzu UV-2450 bench top spectrophotometer located at John Jay College of Criminal Justice. The slide was referenced against air. This cover slip was obtained with courtesy from Fran Adar, Ph.D.

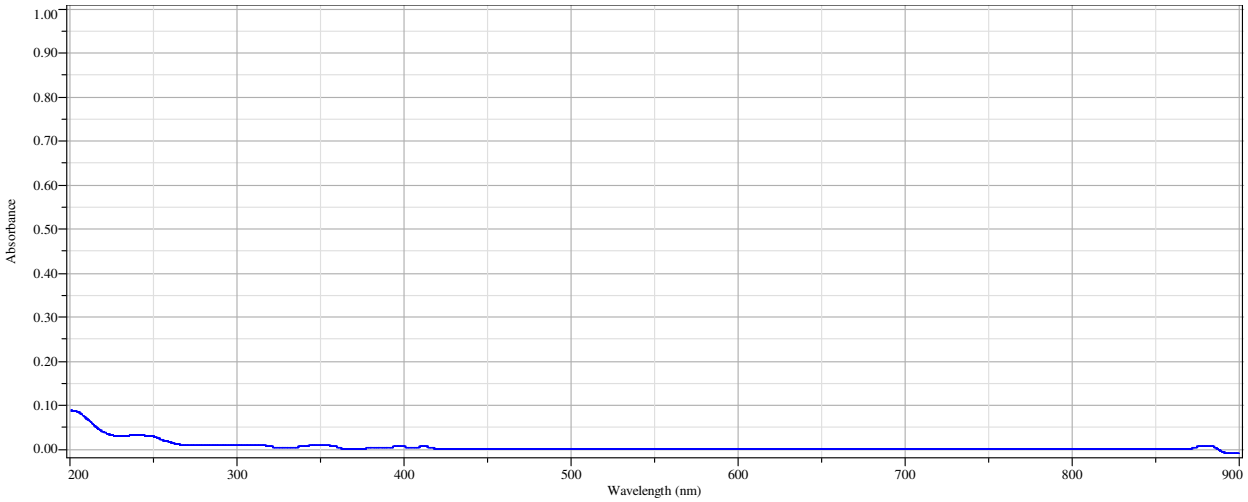

Figure A8.11: An absorbance spectrum of a SPI, Inc. #1016, fused quartz slide, 25.4 x 25.4 x 1 mm (LOT# 1130128) collected with a Shimadzu UV-2450 bench top spectrophotometer located at John Jay College of Criminal Justice. This slide was referenced against air.

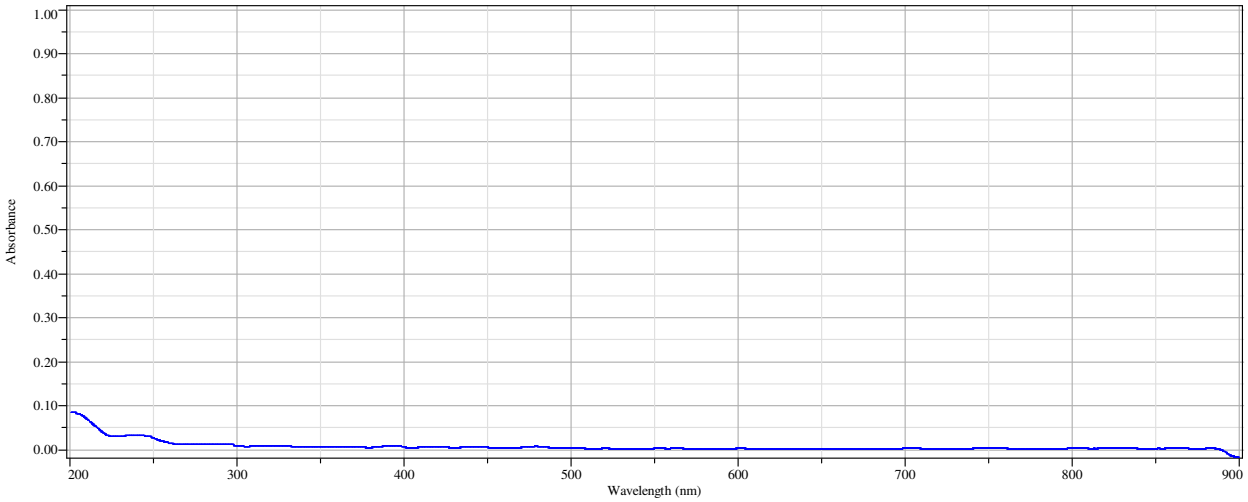

Figure A8.12: An absorbance spectrum of a SPI, Inc. #1018-AB, fused quartz slide, 25 x 76 x 1 mm (LOT# 1140630) collected with a Shimadzu UV-2450 bench top spectrophotometer located at John Jay College of Criminal Justice. This slide was referenced against air.

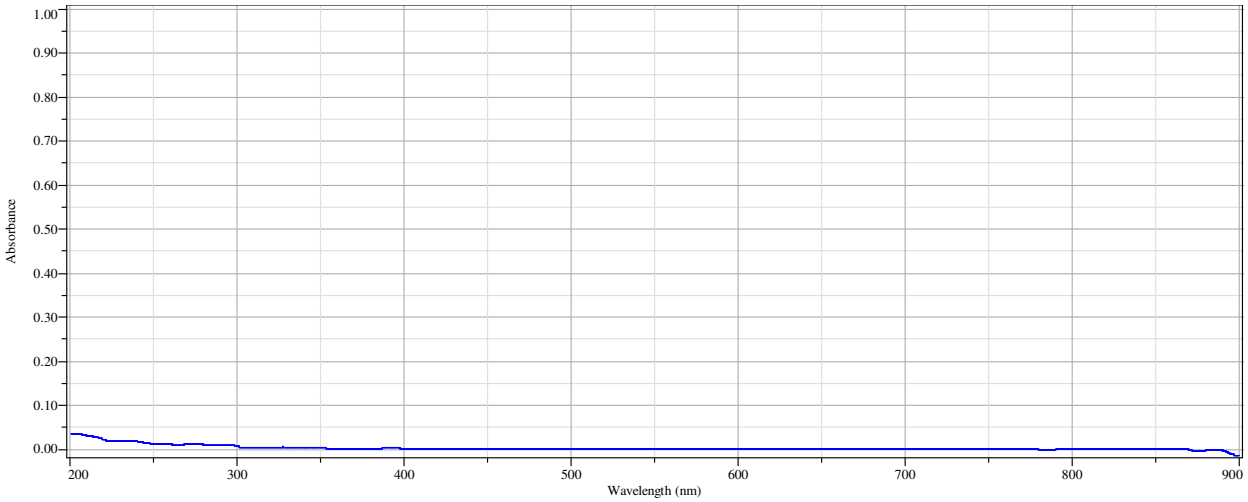

Figure A8.13: An absorbance spectrum of a SPI, Inc. #1019-AB, fused silica quartz cover slip, #2, 25.4mm diameter (LOT# 1140611) collected with a Shimadzu UV-2450 bench top spectrophotometer located at John Jay College of Criminal Justice. This cover slip was referenced against air.

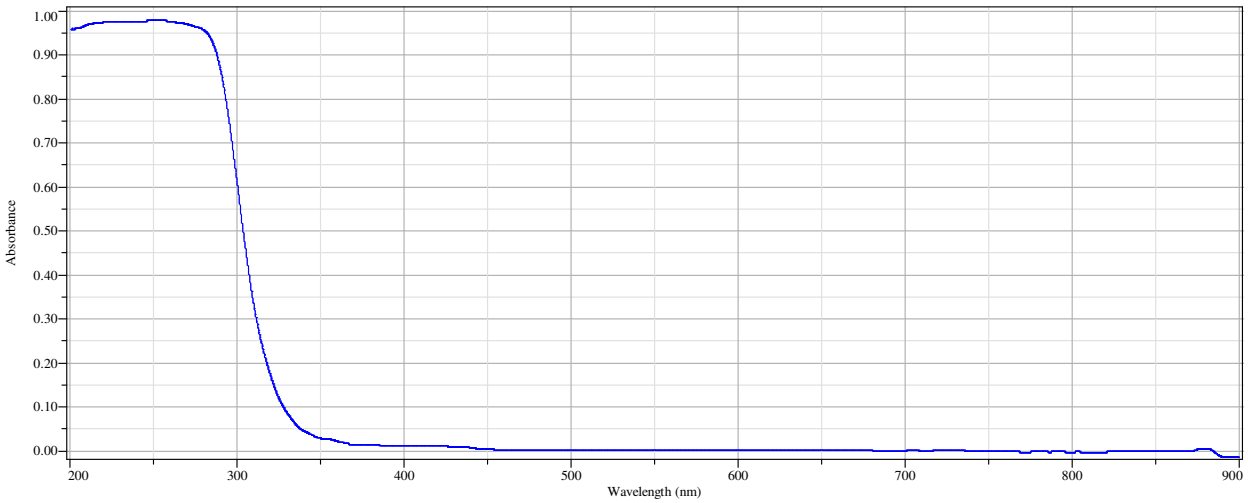

Figure A8.14: An absorbance spectrum of a Perkin Elmer Corporation quartz slide, 16 x 20 x 1 mm, collected with a Shimadzu UV-2450 bench top spectrophotometer located at John Jay College of Criminal Justice. This slide was referenced against air. The slide was obtained with courtesy from John A. Reffner, Ph.D.

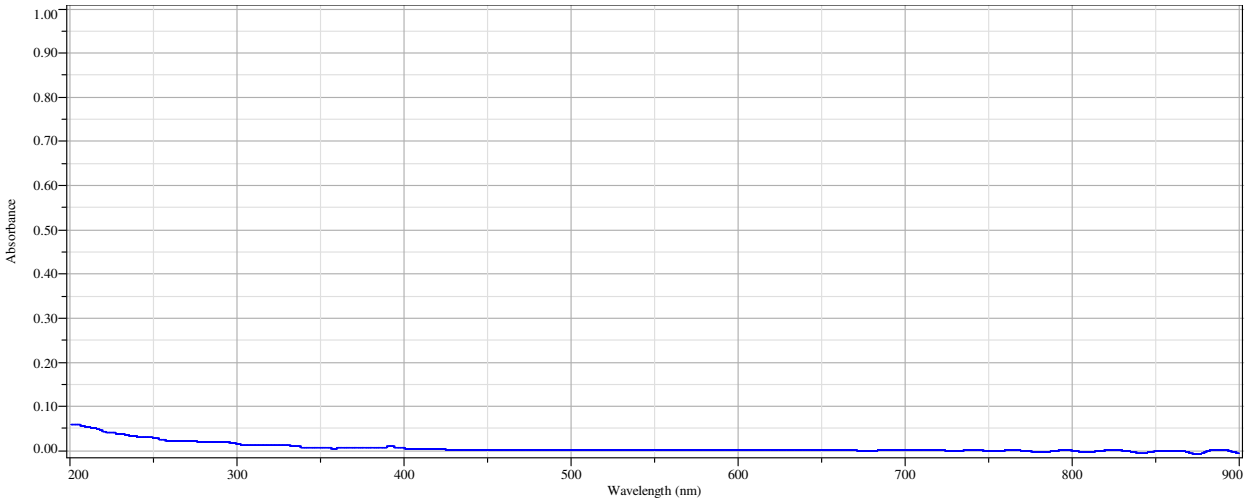

Figure A8.15: An absorbance spectrum of the Starna® 48-Q-0.01, fused-silica quartz flow cell, 0.01 mm path length collected with a Shimadzu UV-2450 bench top spectrophotometer located at John Jay College of Criminal Justice. The flow cell was empty and referenced against air.

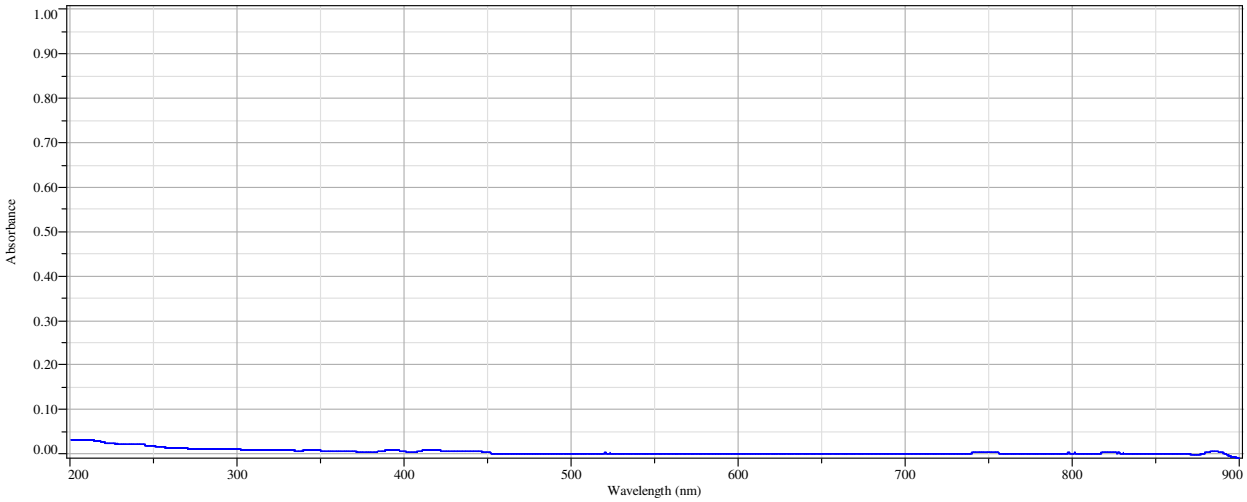

Figure A8.16: An absorbance spectrum of the Starna® 48-Q-0.1, fused quartz flow cell, 0.1 mm path length. Spectrum collected with a Shimadzu UV-2450 bench top spectrophotometer located at John Jay College of Criminal Justice. The flow cell was empty and referenced against air.

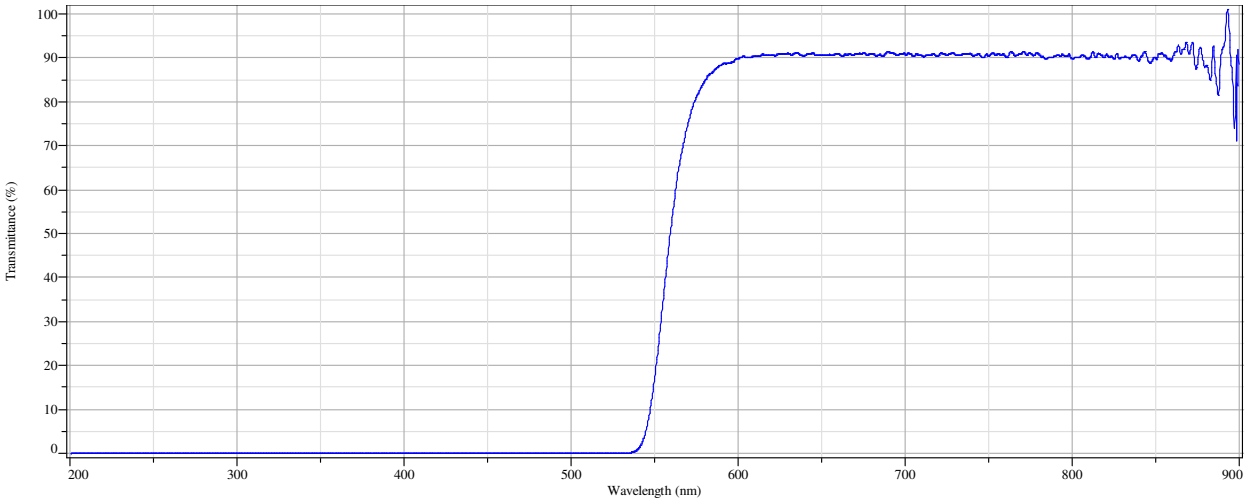

Figure A8.17: A transmittance spectrum of an orange 560 nm long band pass filter collected with a Shimadzu UV-2450 bench top spectrophotometer located at John Jay College of Criminal Justice. The filter was referenced against air.

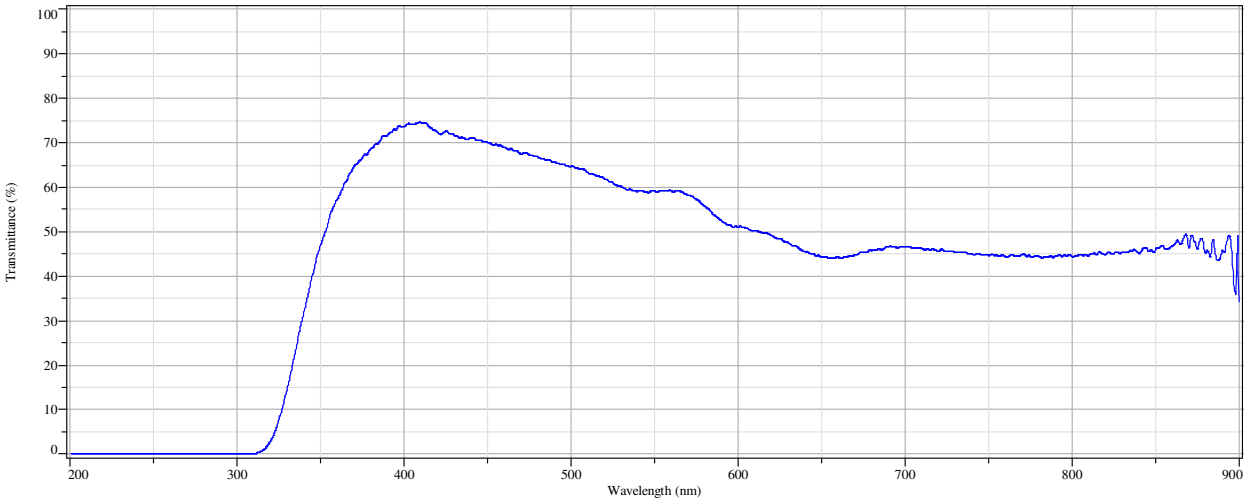

Figure A8.18: A transmittance spectrum of an LB-45 long pass daylight correction filter collected with a Shimadzu UV-2450 bench top spectrophotometer located at John Jay College of Criminal Justice. The filter was referenced against air.

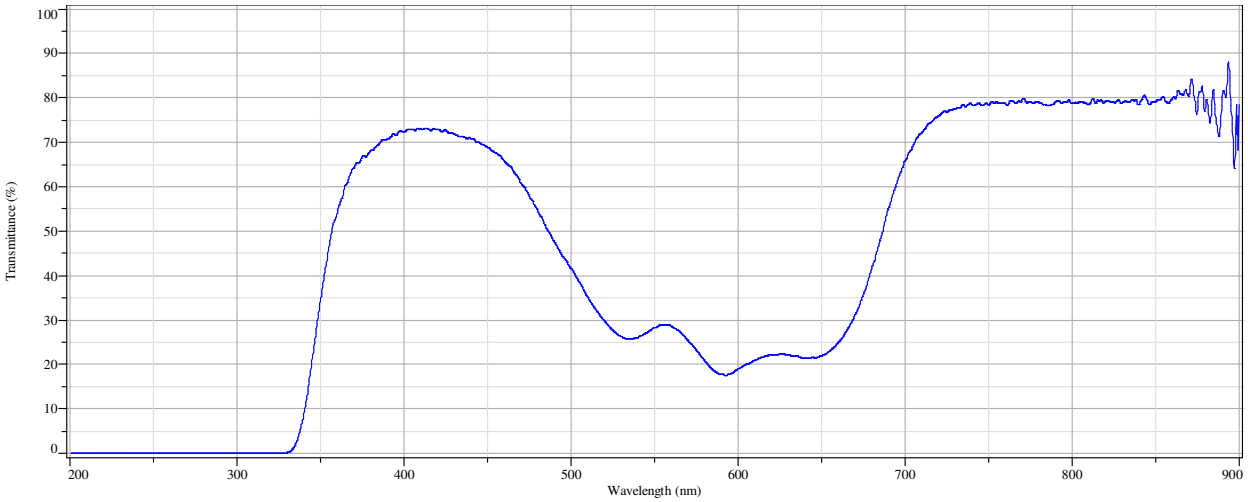

Figure A8.19: A transmittance spectrum of a KB-4 long pass blue filter collected with a Shimadzu UV-2450 bench top spectrophotometer located at John Jay College of Criminal Justice. The filter was referenced against air.

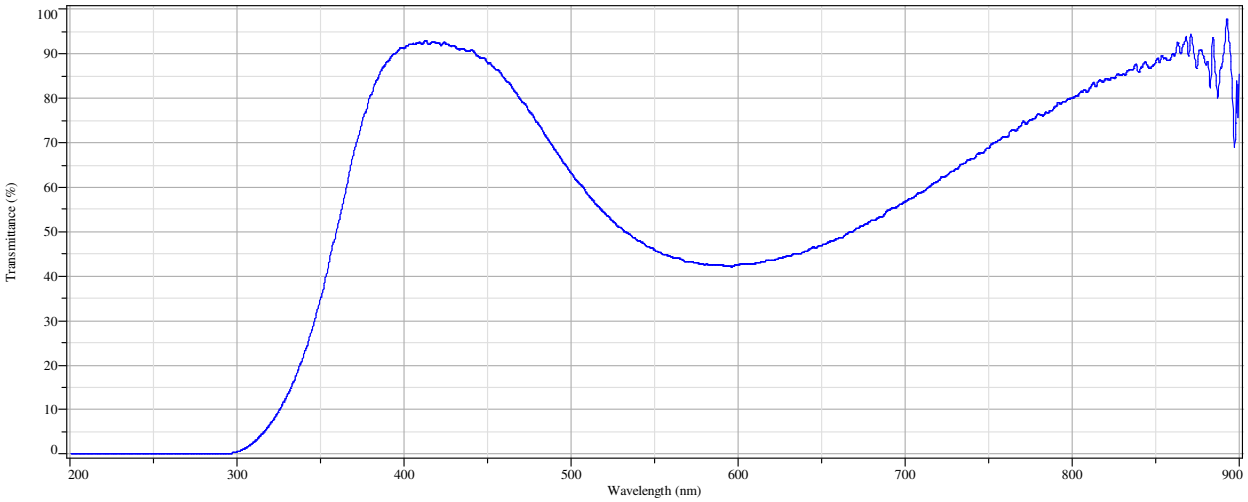

Figure A8.20: A transmittance spectrum of a LBD daylight correction filter collected with a Shimadzu UV-2450 bench top spectrophotometer located at John Jay College of Criminal Justice. The filter was referenced against air.

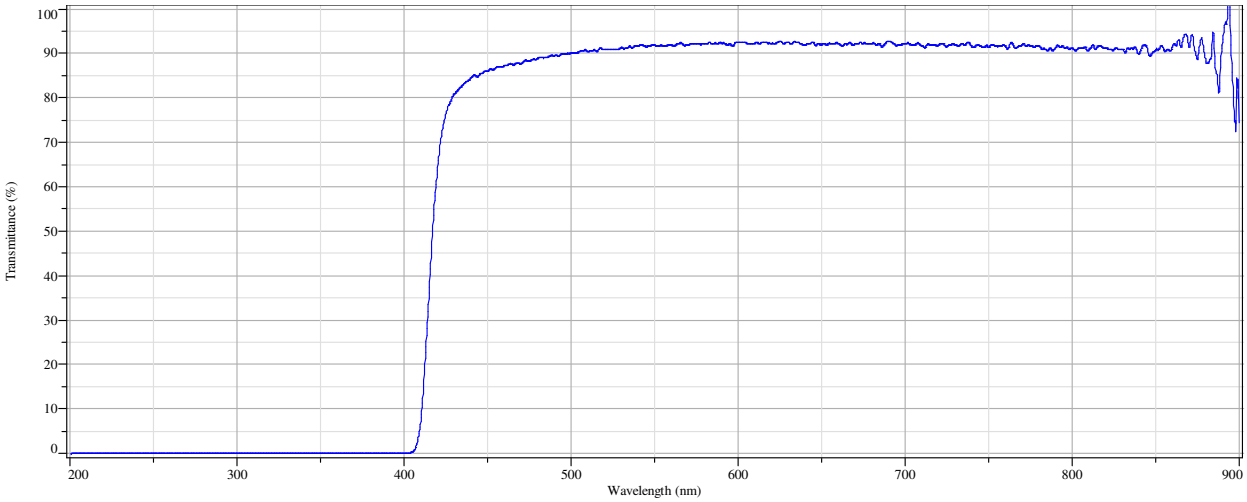

Figure A8.21: A transmittance spectrum of a GG420 long pass filter collected with a Shimadzu UV-2450 bench top spectrophotometer located at John Jay College of Criminal Justice. The filter was referenced against air.

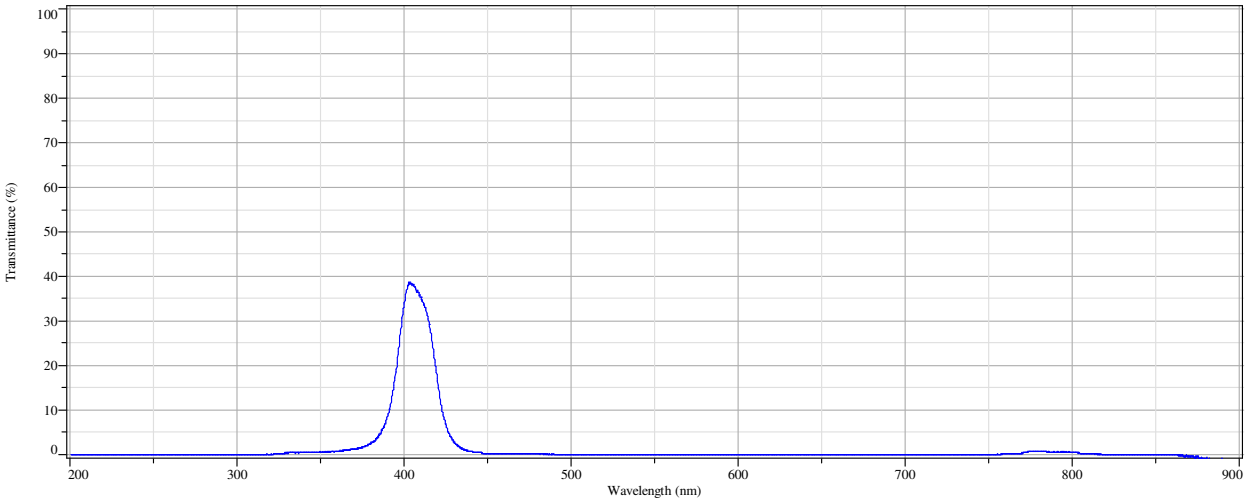

Figure A8.22: A transmittance spectrum of an interference filter, 405 nm, collected with a Shimadzu UV-2450 bench top spectrophotometer located at John Jay College of Criminal Justice. The filter was referenced against air.

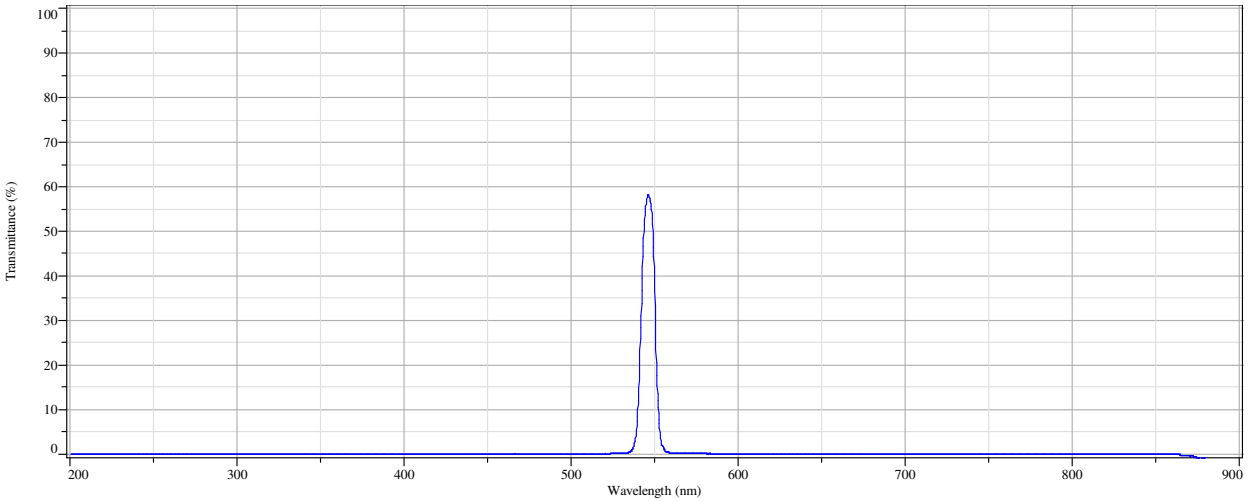

Figure A8.23: A transmittance spectrum of an interference filter, 546 nm, 1-47-09, collected with a Shimadzu UV-2450 bench top spectrophotometer located at John Jay College of Criminal Justice. The filter was referenced against air.

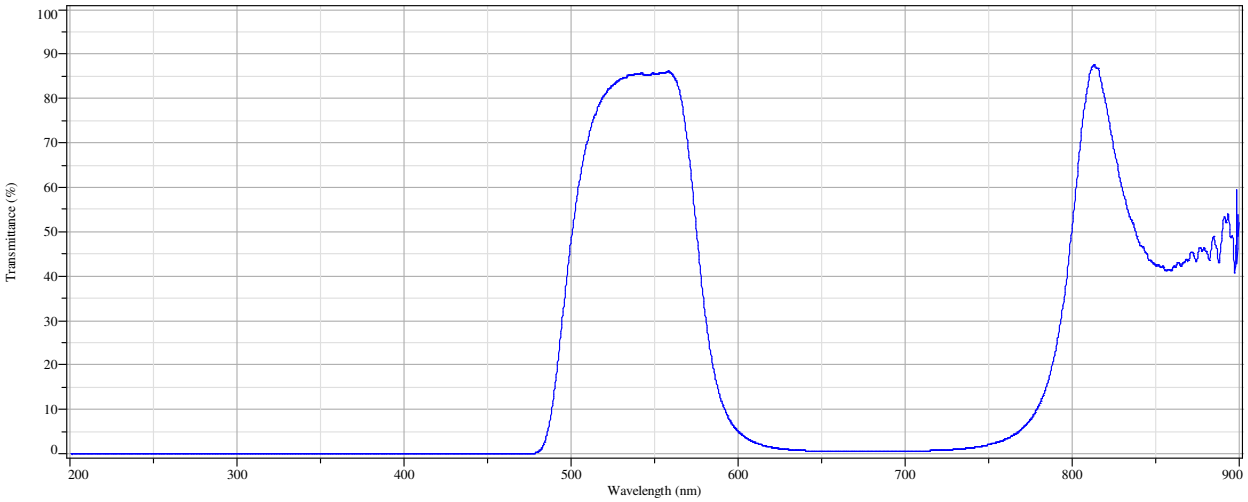

Figure A8.24: A transmittance spectrum of an interference filter, 550 nm, collected with a Shimadzu UV-2450 bench top spectrophotometer located at John Jay College of Criminal Justice. The filter was referenced against air.

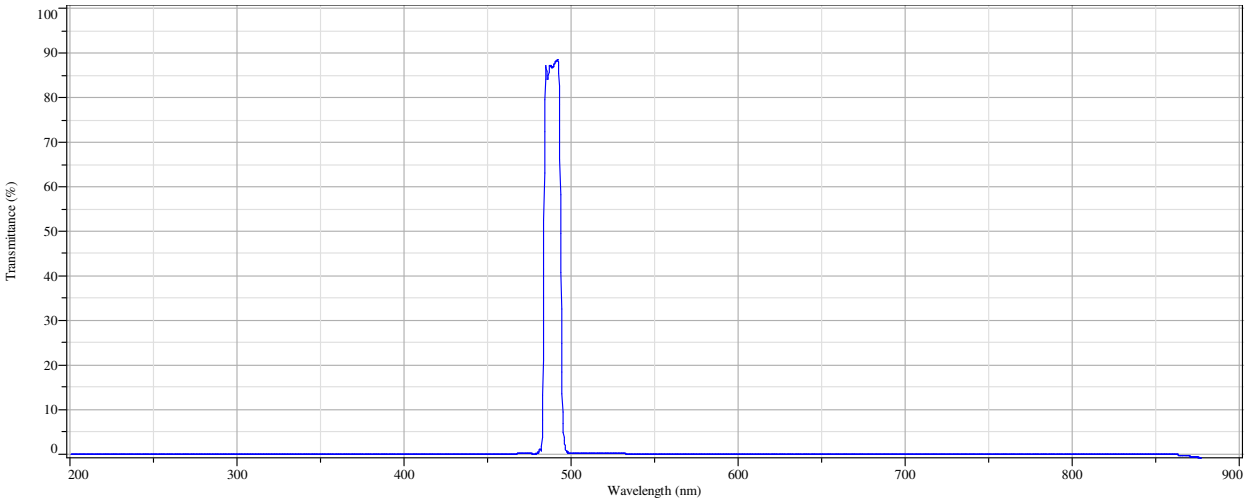

Figure A8.25: A transmittance spectrum of an interference filter, Z488-10, 52430, collected with a Shimadzu UV-2450 bench top spectrophotometer located at John Jay College of Criminal Justice. The filter was referenced against air.

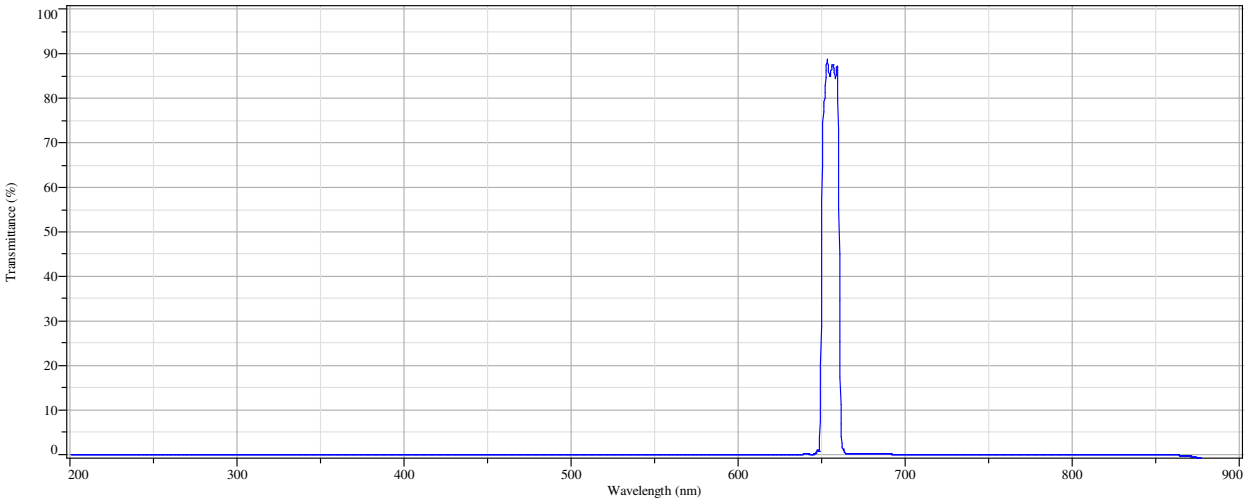

Filter A8.26: A transmittance spectrum of an interference filter, Z656-10, 52489, collected with a Shimadzu UV-2450 bench top spectrophotometer located at John Jay College of Criminal Justice. The filter was referenced against air.

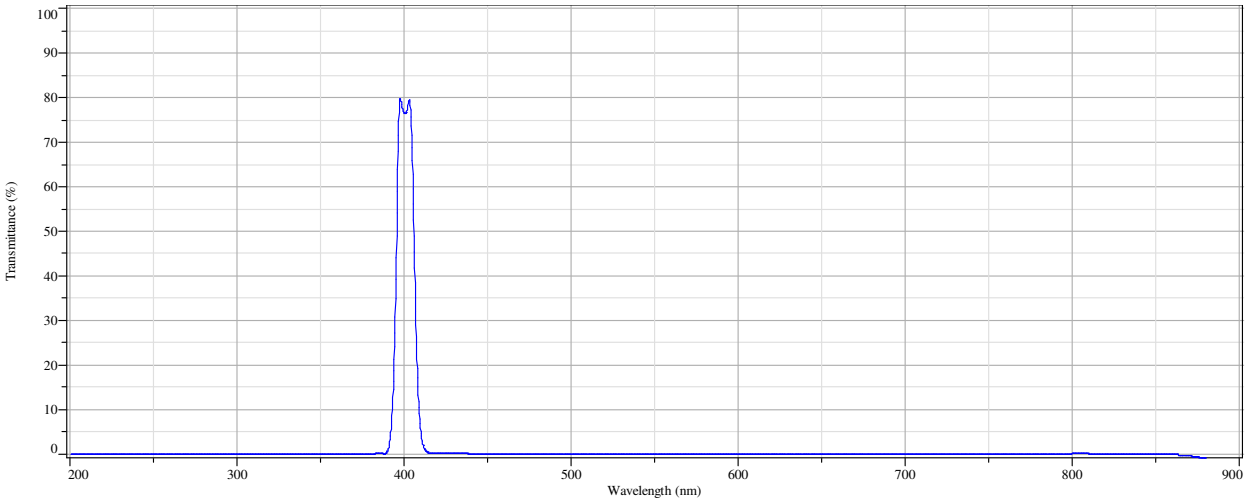

Figure A8.27: A transmittance spectrum of an excitation filter, BP400-410 nm, collected with a Shimadzu UV-2450 bench top spectrophotometer located at John Jay College of Criminal Justice. The filter was referenced against air.

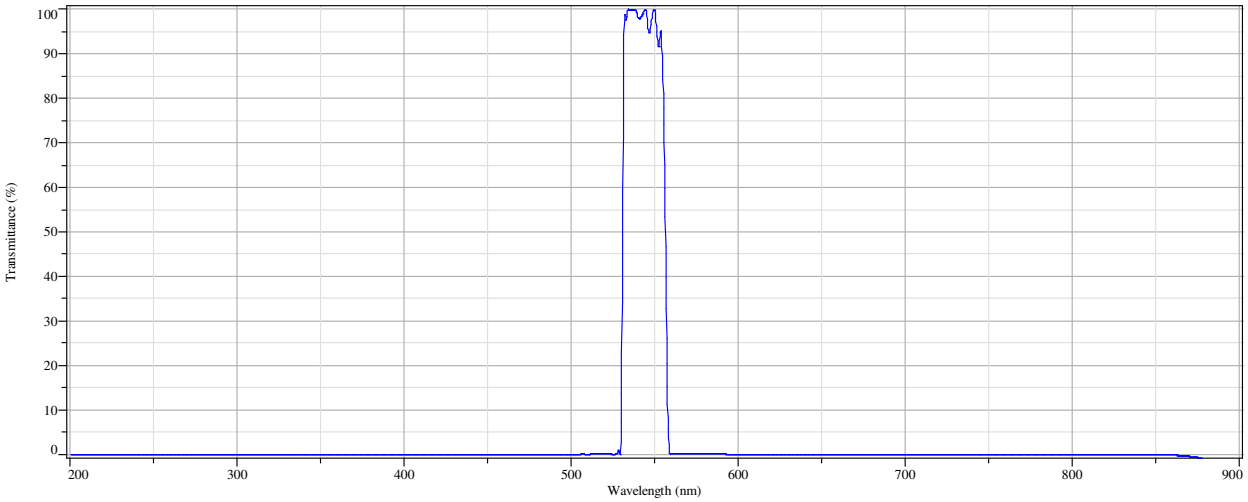

Figure A8.28: A transmittance spectrum of an excitation filter, BP543-22 nm, collected with a Shimadzu UV-2450 bench top spectrophotometer located at John Jay College of Criminal Justice. The filter was referenced against air.

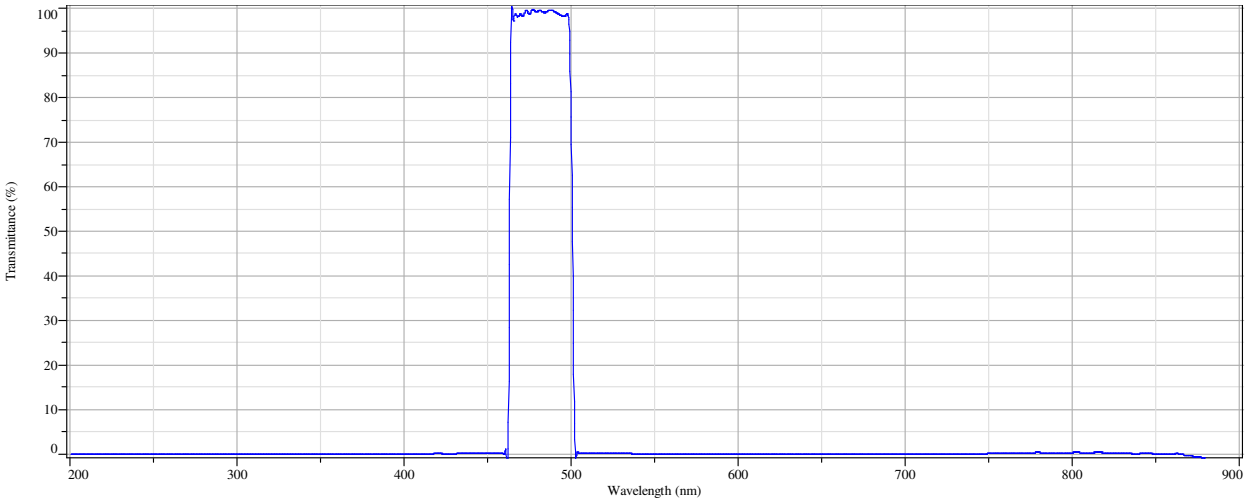

Figure A8.29: A transmittance spectrum of an excitation filter, BP482-35 nm, collected with a Shimadzu UV-2450 bench top spectrophotometer located at John Jay College of Criminal Justice. The filter was referenced against air.

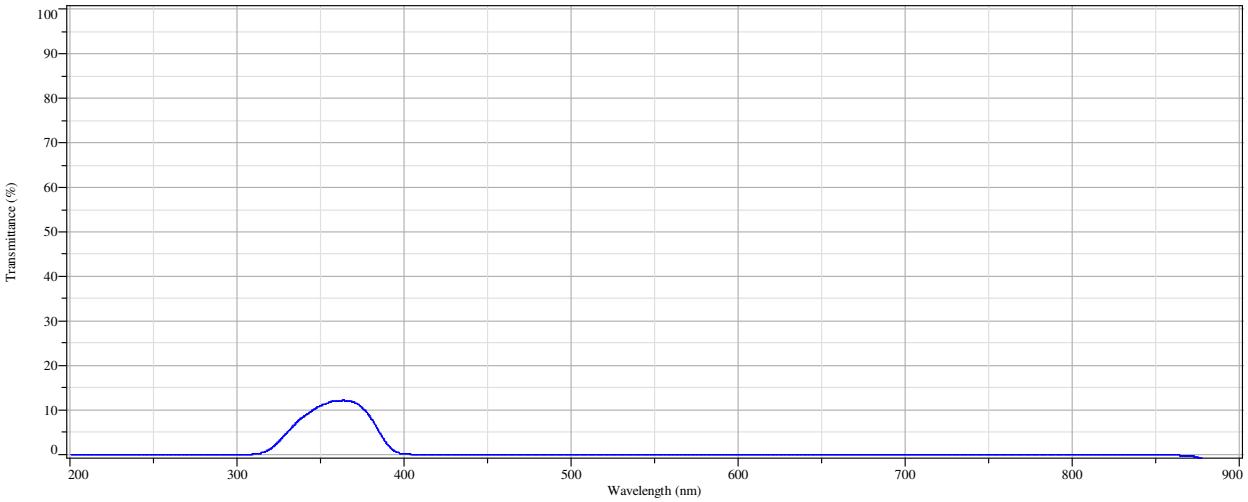

Figure A8.30: A transmittance spectrum of an excitation filter, BP330-380 nm, collected with a Shimadzu UV-2450 bench top spectrophotometer located at John Jay College of Criminal Justice. The filter was referenced against air.

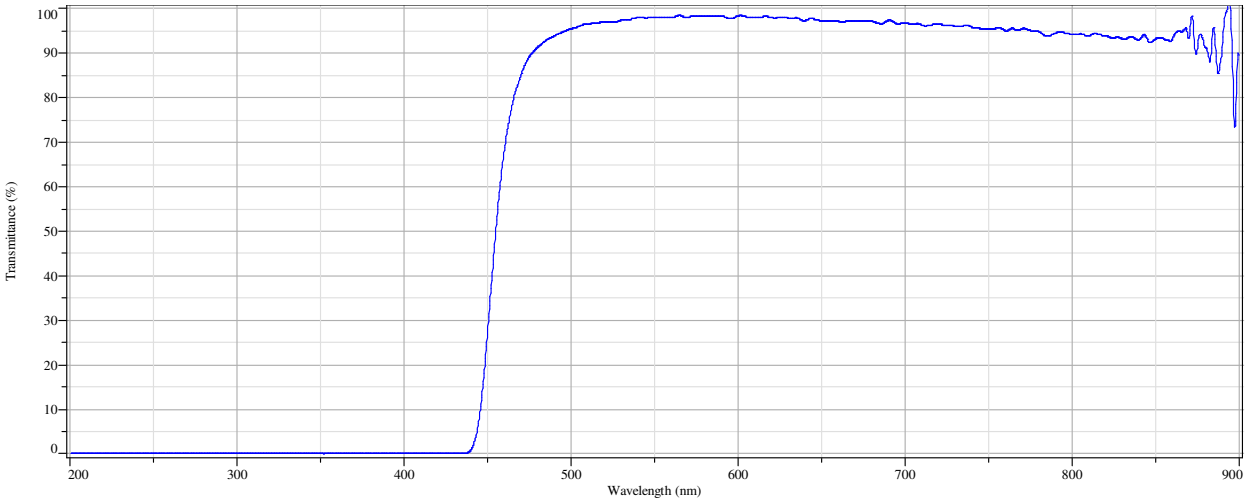

Figure A8.31: A transmittance spectrum of a barrier filter, BA455 nm, collected with a Shimadzu UV-2450 bench top spectrophotometer located at John Jay College of Criminal Justice. The filter was referenced against air.

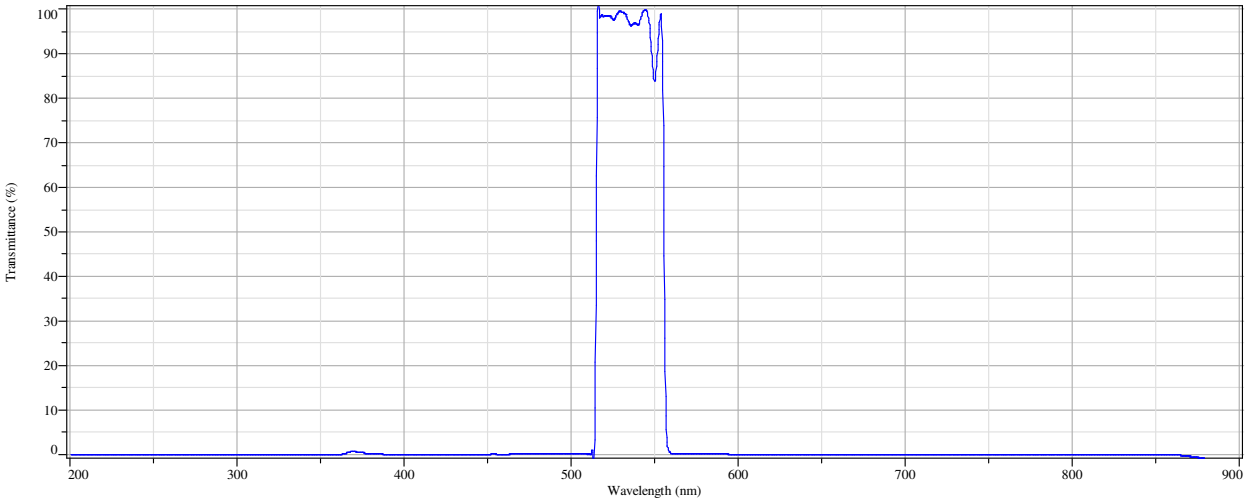

Figure A3.32: A transmittance spectrum of a barrier filter, 536-40 nm, collected with a Shimadzu UV-2450 bench t2p spectrophotometer located at John Jay College of Criminal Justice. The filter was referenced against air.

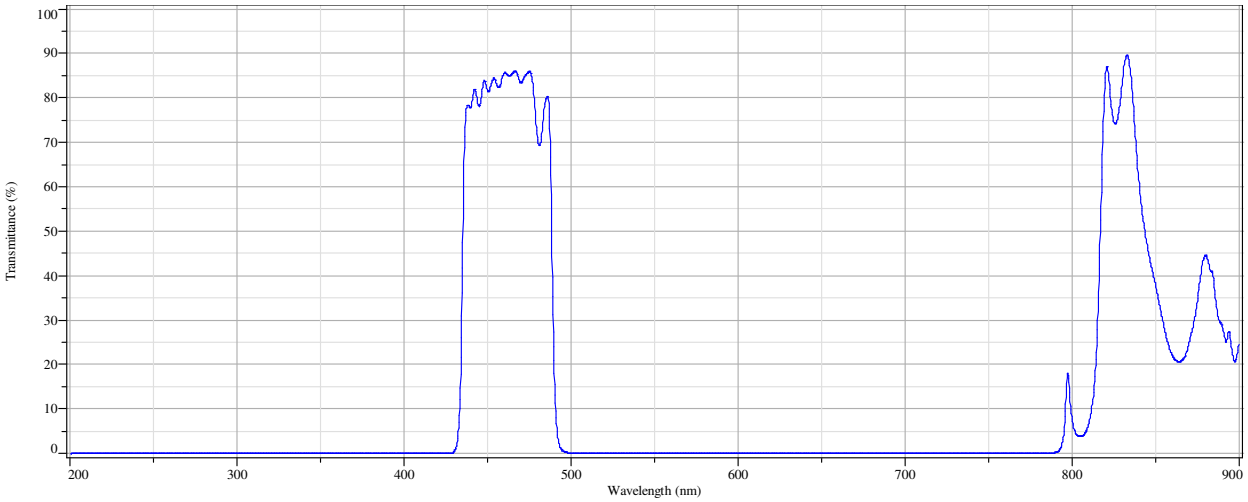

Figure A8.33: A transmittance spectrum of a barrier filter, 435-485 nm, 49185, collected with a Shimadzu UV-2450 bench top spectrophotometer located at John Jay College of Criminal Justice. The filter was referenced against air.

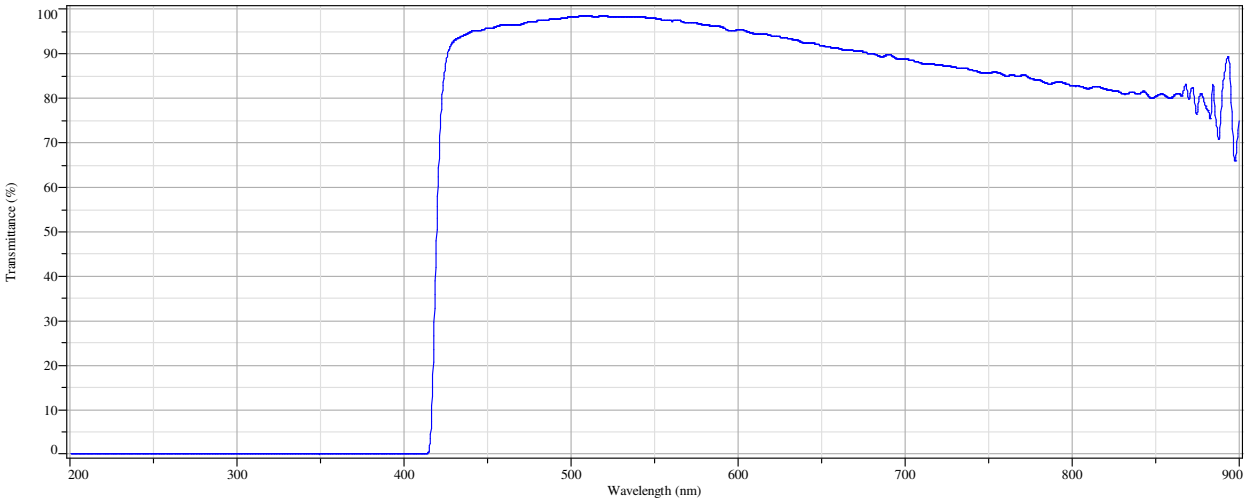

Figure A8.34: A transmittance spectrum of a barrier filter, 420 nm, collected with a Shimadzu UV-2450 bench top spectrophotometer located at John Jay College of Criminal Justice. The filter was referenced against air.

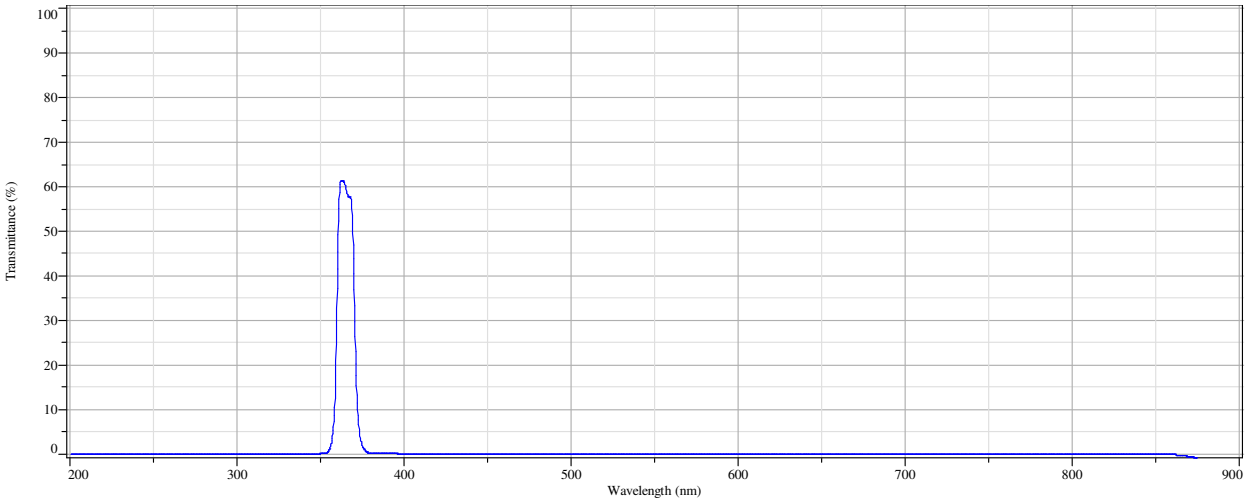

Figure A8.35: A transmittance spectrum of an excitation filter, narrow band pass, 360-370 nm, collected with a Shimadzu UV-2450 bench top spectrophotometer located at John Jay College of Criminal Justice. The filter was referenced against air.

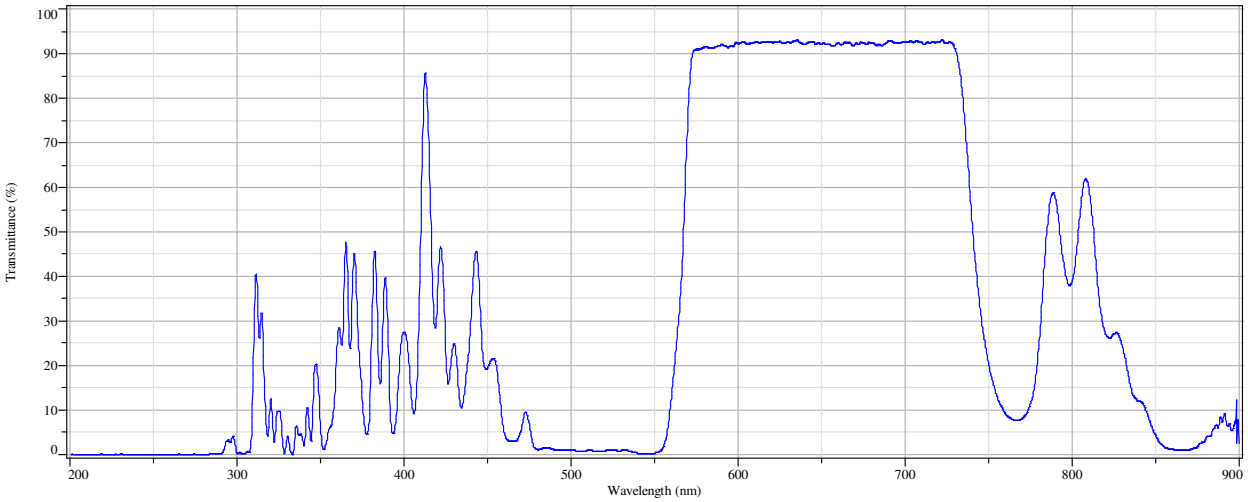

Figure A8.36: A transmittance spectrum of a dichroic mirror, 560 nm, collected with a Shimadzu UV-2450 bench top spectrophotometer located at John Jay College of Criminal Justice. The filter was referenced against air.

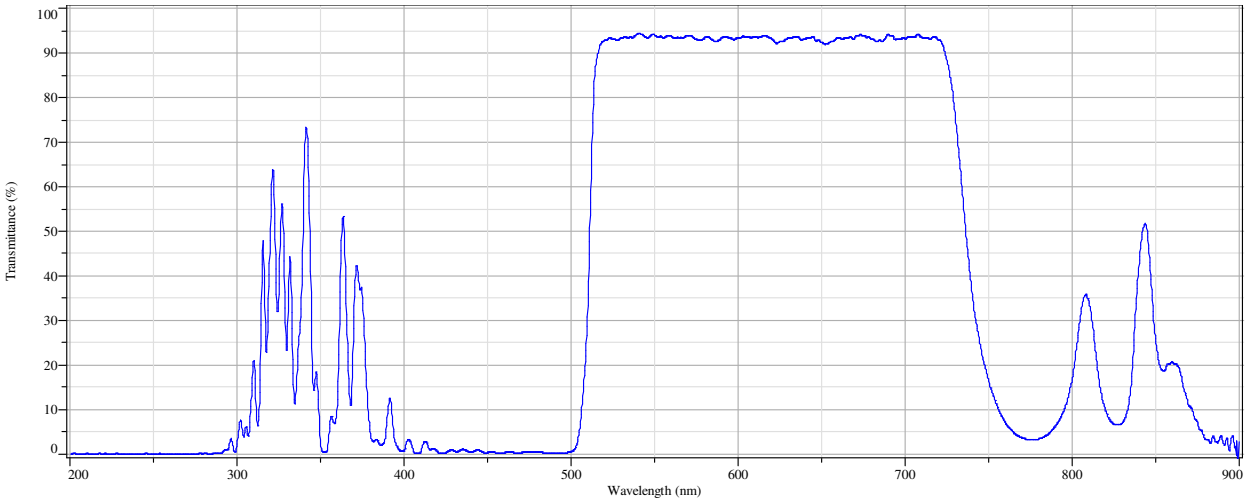

Figure A8.37: A transmittance spectrum of a dichroic mirror, 500 nm, collected with a Shimadzu UV-2450 bench top spectrophotometer located at John Jay College of Criminal Justice. The filter was referenced against air.

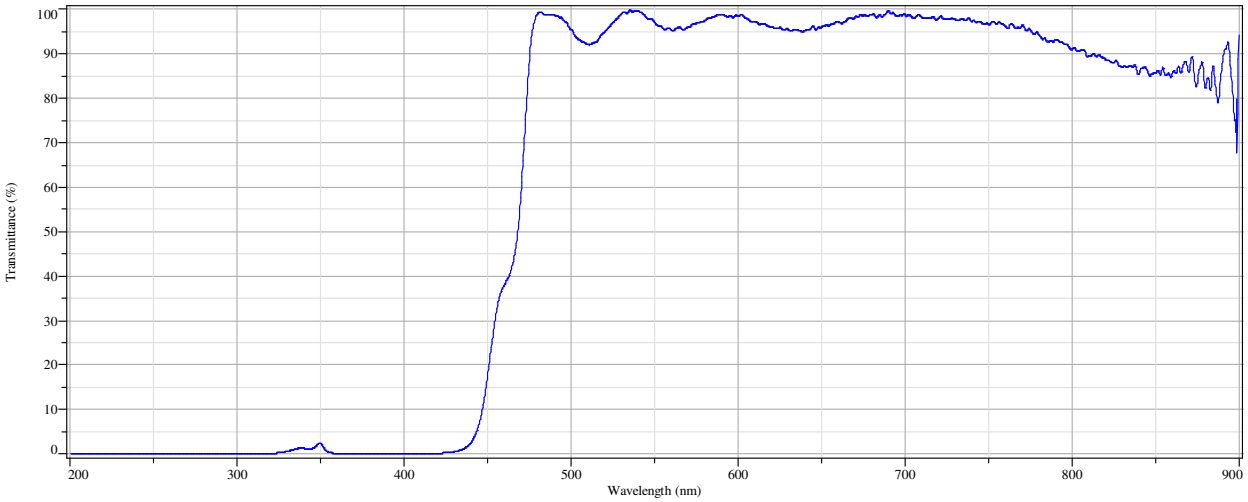

Figure A8.38: A transmittance spectrum of a dichroic mirror, 450 nm, collected with a Shimadzu UV-2450 bench top spectrophotometer located at John Jay College of Criminal Justice. The filter was referenced against air.

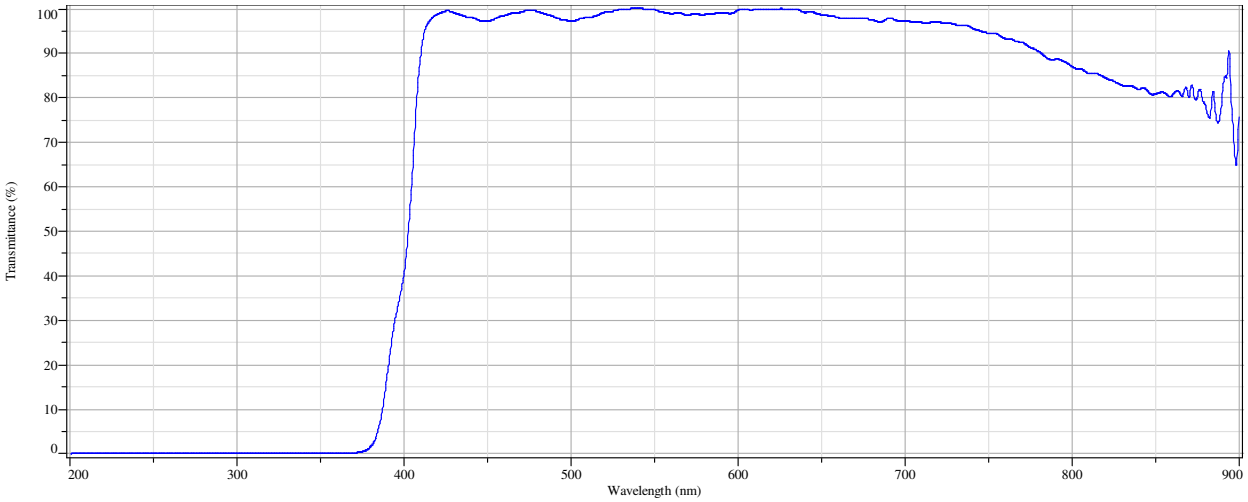

Figure A8.39: A transmittance spectrum of a dichroic mirror, 400 nm, collected with a Shimadzu UV-2450 bench top spectrophotometer located at John Jay College of Criminal Justice. The filter was referenced against air.

CHAPTER 8. BIBLIOGRAPHY

Abramowitz, M., (1985) Microscope Basics and Beyond, Vol. 1, Olympus Corporation: Lake Success, NY.

Abramowitz, M., (1987) Contrast Methods in Microscopy: Transmitted Light, Vol. 2, Olympus Corporation: Lake Success, NY.

Abramowitz, M., (1990) Reflected Light Microscopy: An Overview, Vol. 3, Olympus Corporation: Lake Success, NY.

Abramowitz, M., (1993), Fluorescence Microscopy: The Essentials, Vol. 4, Olympus Corporation: Lake Success, NY.

Abramowitz, M., (1994) Optics: A Primer, Olympus Corporation: Lake Success, NY.

Adar, F. (2013) "Raman Microscopy Analysis of Molecular Orientation in Fibers", *Spectroscopy*, 28(2), 14-22.

Adolf, F.P. & Dunlop, J. (1999) Microspectrophotometry/Colour Measurement, ch. 10, In: Forensic Examination of Fibres, Robertson, J.R and Grieve, M. (Ed.), CRC Press, Taylor & Francis, Inc., New York, NY. 251-289.

Aerneke, M. (2002) An exploration of the potential of hematoporphyrin fluorescence as a test for blood, (Master's Thesis, John Jay College of Criminal Justice, City University of New York, 2002).

Aginsky, V.N., (1993) Some New Ideas for Dating Ballpoint Inks – A Feasibility Study, *Journal of Forensic Sciences*, 38(5), 1134-1150.

Aginsky, V.N., (1995) A Microspectrophotometric Method for Dating Ballpoint Inks – A Feasibility Study, *Journal of Forensic Sciences*, 40(3) 475-478.

Allen, R.D., Brault, J., & Moore, R.D., (1963) A new method of polarization microscopic analysis I: Scanning with a birefringence detection system, *The Journal of Cell Biology*, 18, 223-235.

ASTM Standard E131, 2005, "Standard Terminology Relating to Molecular Spectroscopy", ASTM International, West Conshohocken, PA. ASTM vol. 03.06 (2009).

ASTM Standard E169, 2004, "Standard Practices for General Techniques of Ultraviolet-Visible Quantitative Analysis", ASTM International, West Conshohocken, PA. ASTM vol. 03.06 (2009).

ASTM Standard E275, 2008, "Standard Practice for Describing and Measuring Performance of Ultraviolet and Visible Spectrophotometers", ASTM International, West Conshohocken, PA. ASTM vol. 03.06 (2009).

ASTM Standard E387, 2004, "Standard Test Method for Estimating Stray Radiation Power Ratio of Dispersive Spectrophotometers by the Opaque Filter Method", ASTM International, West Conshohocken, PA. ASTM vol. 03.06 (2009).

ASTM Standard E925, 2002, "Standard Practice for Monitoring the Calibration of Ultraviolet-Visible Spectrophotometers whose Spectral Slit Width does not Exceed 2 nm", ASTM International, West Conshohocken, PA. ASTM vol. 03.06 (2009).

ASTM Standard E958, 1993 (2005), "Standard Practice for Measuring Practical Spectral Bandwidth of Ultraviolet-Visible Spectrophotometers", ASTM International, West Conshohocken, PA. ASTM vol. 03.06 (2009).

ASTM Standard E1866, 1997 (2007) "Standard Guide for Establishing Spectrophotometric Performance Tests", ASTM International, West Conshohocken, PA. ASTM vol. 03.06 (2009).

ASTM Standard E2642, 2009 "Standard Terminology for Scientific Charge-Coupled Device (CCD) Detectors", ASTM International, West Conshohocken, PA. ASTM vol. 03.06 (2009).

ASTM Standard D2244, 1993, "Standard Test Method for Calculation of Color Differences From Instrumentally Measured Color Coordinates", ASTM International, West Conshohocken, PA. ASTM vol. 06.01 (1994).

ASTM Standard E1347, 1990, "Standard Test Method for Color and Color-Difference Measurement by Tristimulus (Filter) Colorimetry", ASTM International, West Conshohocken, PA. ASTM vol. 06.01 (1994).

ASTM Standard E1345, 1990, "Standard Practice for Reducing the Effect of Variability of Color Measurement by Use of Multiple Measurements", ASTM International, West Conshohocken, PA. ASTM vol. 06.01 (1994).

ASTM Standard E1164, 1993, "Standard Practice for Obtaining Spectrophotometric Data for Object-Color Evaluation", ASTM International, West Conshohocken, PA. ASTM vol. 06.01 (1994).

Barrett, J.A., Siegel, J.A., & Goodpaster, J.V., (2010) Forensic Discrimination of Dyed Hair Color: I. UV-Visible Microspectrophotometry, *Journal of Forensic Science*, 55(2), 323-333.

Barrett, J.A., Siegel, J.A., & Goodpaster, J.V., (2011) Forensic Discrimination of Dyed Hair Color: II. Multivariate Statistical Analysis, *Journal of Forensic Science*, 56(1), 95-101.

Bass, M., (Ed.) (1995) Handbook of Optics, Volume I: Fundamentals, Techniques, & Design, 2nd ed., Optical Society of America, McGraw-Hill Inc., New York, NY.

Bass, M., (Ed.) (1995) Handbook of Optics, Volume II: Devices, Measurements, & Properties, 2nd ed., Optical Society of America, McGraw-Hill Inc., New York, NY.

Beebe, K. R., Pell, R.J., & Seasholtz, M.B., (1998) Chemometrics: A Practical Guide. John Wiley & Sons, Inc., New York, NY.

Blackwell, H.R., (1946) Contrast Threshold of the Human Eye, *Journal of the Optical Society of America*, 36, 624-643.

Born, M and Wolf, E. (1975) Principles of Optics: Electromagnetic Theory of Propagation, Interference and Diffraction of Light, 5th ed., Pergamon Press, New York, NY.

Bracegirdle, B. & Bradbury, S., (1995) Modern PhotoMICROgraphy, (RMS Microscopy Handbooks 33), Bios Scientific Publishers, Ltd.: Oxford, UK.

Bradbury, S. & Evennett, P.J., (1996) Contrast Techniques in Light Microscopy, (RMS Microscopy Handbooks 34), Bios Scientific Publishers, Ltd.: Oxford, UK.

Breene, R.J., Jr. (1980) Theories of Spectral Line Shape, John Wiley & Sons, New York, NY.

Burgess, C. & Frost, T. (1999) Standards and Best Practice in Absorption Spectrometry, Blackwell Science: Malden, MA.

Choudhry, M.Y., (1991) Comparison of Minute Smears of Lipstick by Microspectrophotometry and Scanning Electron Microscopy/Energy-Dispersive Spectroscopy, *Journal of Forensic Sciences*, 36(2), 366-375.

Corning Incorporated, (2003) HPFS Fused Silica ArF Grade, Corning 7980, Corning, NY. Available online at http://www.corning.com/specialtymaterials/products_capabilities/HPFS.aspx

Cousins, D.R., Platoni C.R., and Russell, L.W. (1984) The use of microspectrophotometry for the identification of pigments in small paint samples, Forensic Science International, 24(3), 183-196.

Cousins, D. R. (1989) Use of Microspectrophotometry in the Examination of Paints, *Forensic Science Review,* 1(2), 142-161.

Daubert v. Merrell Dow Pharmaceuticals, Inc., 509 U.S. 5791 (1993)

Daubert v. Merrell Dow Pharmaceuticals, Inc., 43 F.3d 1311 (9th Cir. 1995)

De Forest, P.R., (1982) Foundations of Forensic Microscopy, Ch. 9, in Forensic Science Handbook, vol. 1, 1st ed., Richard Saferstein (Ed.), Regents/Prentice-Hall, Englewood Cliffs, NJ, 416-528

De Wael, K., Lepot, L., Gason, F., & Gilbert, B., (2008) In search of blood—Detection of minute particles using spectroscopic methods, *Forensic Science International*, 180, 37-42.

De Wael, K. and Vanden Driessche, T. (2011) "Dichroism measurements in forensic fibre examination Part 1 – Dyed polyester fibres", *Science and Justice*, 51, 57-67.

De Wael, K. and Vanden Driessche, T. (2011) "Dichroism measurements in forensic fibre examination Part 2 – Dyed polyamide, wool and silk fibres", *Science and Justice*, 51, 163-172.

De Wael, K. and Lepot, L. (2011) "Dichroism measurements in forensic fibre examination Part 3 – Dyed cotton and viscose fibres", *Science and Justice*, 51, 173-186.

De Wael, K. (2012) "Dichroism measurements in forensic fibre examination Part 4 – Dyed acrylic and acetate fibres", *Science and Justice*, 52, 81-89.

De Wael, K. (2012) "Dichroism measurements in forensic fibre examination Part 5 – Pigmented fibres", *Science and Justice*, 52, 161-167.

De Wael, K. (2012) "Dichroism measurements in forensic fibre examination Part 6 – Validation and practical aspects of MSP-PPL", *Science and Justice*, 52, 249-258.

Donati, S. (2002) Photodetectors: Devices, Circuits, and Applications, Prentice Hall, Inc., Upper Saddle River, NJ.

Eaton, W.A. and Hofrichter, J. (1981) "Polarized Absorption and Linear Dichroism Spectroscopy of Hemoglobin", *Methods in Enzymology*, 46, 175-261.

Edisbury, J.R., (1967) Practical Hints on Absorption Spectrometry: Ultra-Violet and Visible. Plenum Press, New York, NY.

Eyring, M. B. (2002) "Visible microscopical spectrophotometry in the forensic sciences" Ch. 6. In Forensic Science Handbook, Volume I, 2nd Edit., Richard Saferstein, Ed., Prentice Hall, Upper Saddle River, NJ.

Federal Rules of Evidence, 2009. Available online at http://judiciary.house.gov/hearings/printers/111th/evid2009.pdf

Fouweather, C., May, R.W., & Porter, J., (1976) The Application of a Standard Color Coding System to Paint in Forensic Science, *Journal of Forensic Sciences*, 21(3), 629-635.

Garcia, A.M. (1965) A one-wavelength, two-area method in microspectrophotometry for pure amplitude objects, *The Journal of Histochemistry and Cytochemistry*, 13(3), 161-167.

Garvin, E.J. and Koons, R.D. (2011) Evaluation of Match Criteria Used for the Comparison of Refractive Index of Glass Fragments, *Journal of Forensic Sciences*, 56(2), 491-500.

Gibson, E.P., (1977) Review: Applications of Luminescence in Forensic Science, *Journal of Forensic Sciences*, 22(4), 680-696.

Goldberg, O., (1980) Köhler Illumination, *The Microscope*, 28, 15-21.

Goldstein, D.J., (1969) Detection of dichroism with the microscope, *J Microscope*, 89(1), 19-36.

Grams/AI Help Resource. (2012) [Computer Software Version 9.1]. Thermo Scientific.

Grieve, M. & Deck, S., (1995) A new mounting medium for the forensic microscopy of textile fibres, *Science and Justice*, 35(2), 109-112.

Griffin, R.M.E., Lewis, R., Bennett, J., Hamill, J., & Kee, T.G., (1996) Analysis of cling films and coloured cellophanes and the application to casework, *Science and Justice*, 36(4), 219-227.

Grossman, W.E.L. (1993) The optical characteristics and production of diffraction gratings, *Journal of Chemical Education*, 70(9), 741-748.

Halliday, D., Resnick, R., and Walker, J. (1993) Fundamentals of Physics, 4th ed., John Wiley & Sons, Inc., New York, NY.

Hartshorne, N.H. & Stuart, A. (1950) Crystals and the polarising microscope: A handbook for chemists and others, 2nd ed., Edward Arnold & Co.; London, England.

Hartshorne, A.W. & Laing, D.K. (1984) The measurement of birefringence of single fibers using a microscope mounted spectrometer, *The Microscope*, 32, 11-22.

Hartshorne, A.W. & Laing, D.K., (1991) Microspectrofluorimetry of fluorescent dyes and brighteners on single textile fibres: Part 1 — Fluorescence emission spectra, *Forensic Science International*, 51(2), 203-220.

Hartshorne, A.W. & Laing, D.K., (1991) Microspectrofluorimetry of fluorescent dyes and brighteners on single textile fibres: Part 2 — Colour measurements, *Forensic Science International*, 51(2), 221-237.

Hartshorne, A.W. & Laing, D.K., (1991) Microspectrofluorimetry of fluorescent dyes and brighteners on single textile fibres: Part 3 — Fluorescence decay phenomena, *Forensic Science International*, 51(2), 239-250.

Hartshorne, A.W. & Laing, D.K., (1991) An absorption standard for microspectrophotometry: Results of a collaborative exercise, *Forensic Science International*, 51(2), 263-272.

Heath, J.P., (2005) Dictionary of Microscopy, John Wiley & Sons, Ltd.: West Sussex, England.

Horiba Jobin Yvon, (2006) Scientific diffraction gratings / custom gratings: Product catalog and capabilities.

Houck, M. (1997) "Measuring Dichroism in Fibers by use of the Microspectrophotometer", *Proceedings of the 5th European Fibres Group Meeting*, Berlin, Germany, 75-82.

Howling, D.H. & Fitzgeralds, P.J. (1959) The nature, significance, and evaluation of the Schwarzschild-Villiger (SV) effect in photometric procedures, *Journal of Biophysical and Biochemical Cytology*, 6(3), 131-337.

Ingle, J.D. & Crouch, S.R. (1988) Spectrochemical Analysis, Prentice Hall, Upper Saddle River, NJ.

Inoué, S. & Spring, K.R., (1997) Video Microscopy: The Fundamentals, 2nd ed., Plenum Press: New York, NY.

Isaka, H. (1972) Introduction to Microspectrophotometry: Application to Biomedical Research, Olympus Optical Co., Ltd, Tokyo, Japan.

Johannsen, A. (1914) Manual of Petrographic Methods, McGraw-Hill Book Company, Inc., New York, NY.

Kotowski, T.M. & Grieve, M.C., (1986) The Use of Microspectrophotometry to Characterize Microscopic Amounts of Blood, *Journal of Forensic Sciences*, 31(3), 1079-1085.

Kirk, P.L. (1953) Crime Investigation, Interscience Publishers, New York, NY.

Kubic, T.A., King, J.E., & DuBey, I.S. (1983) Forensic analysis of colorless textile fibers by fluorescence microscopy, *The Microscope*, 31, 213-222.

Kubin, I.D. (2013) Personal communication, Washington, DC, American Academy of Forensic Sciences, Annual Meeting.

Laing, D.K., Dudley, R.J., & Isaacs, M.D.J., (1980) Colorimetric measurements on small paint fragments using microspectrophotometry, *Forensic Science International*, 16(2), 159-171.

Laing, D.K., Dudley, R.J., Home, J.M., & Isaacs, M.D.J., (1982) The discrimination of small fragments of household gloss paint by microspectrophotometry, *Forensic Science International*, 20(2), 191-200.

Laing, D.K., Hartshorne, A.W., & Harwood, R.J, (1986) Colour measurements on single textile fibres", *Forensic Science International*, 30(1), 65-77.

Losev, A. (1994) On a Model Line Shape for Asymmetric Spectral Peaks, *Applied Spectroscopy*, 48(10), 1289-1290.

Macrae, R., Dudley, R.J., & Smalldon, K.W., (1979) The Characterization of Dyestuffs on Wool Fibers with Special Reference to Microspectrophotometry, *Journal of Forensic Sciences*, 24(1), 117-129.

Martin, P. and Puerta, J. (1981) "Generalized Lorentzian approximation for the Voigt line shape", *Applied Optics*, 20(2), 259-263.

McCrone, W.C. (1957) Fusion Methods in Chemical Microscopy: A Textbook and Laboratory Manual, Interscience Publishers, New York, NY.

McCrone, W.C., McCrone, L.B., & Delly, J.G. (1984), Polarized Light Microscopy, McCrone Research Institute: Chicago, IL.

Mendelsohn, M.L. (1958) The two-wavelength method of microspectrophotometry I. A microspectrophotometer and tests on model systems, *The Journal of Biophysics and Biochemical Cytology*, 4(4), 407-414.

Mendelsohn, M.L. (1958) The two-wavelength method of microspectrophotometry II. A set of tables to facilitate the calculations, *The Journal of Biophysics and Biochemical Cytology*, 4(4), 415-424.

Mendelsohn, M.L. (1958) The two-wavelength method of microspectrophotometry III. An extension based on photoghraphic color transparencies, *The Journal of Biophysics and Biochemical Cytology*, 4(4), 425-431.

Mendelsohn, M.L. (1961) The two-wavelength method of microspectrophotometry IV. A new solution, *The Journal of Biophysics and Biochemical Cytology*, 11, 509-513.

Mickols, W.E. (1991) "Differential Polarization Microscopy", Ch. 6, In: New Techniques of Optical Microscopy and Microspectroscopy, Richard J. Cheery (Ed.), CRC Press, Inc., Boca Raton, FL, 153-176.

Michl, J. and Thulstrup, E.W. (1986) Spectroscopy with Polarized Light: Solute Alignment by Photoselection, in Liquid Crystals, Polymers, and Membranes. VCH Publishers, Inc., Deerfield Beach, FL.

Naora, H. (1951) Microspectrophotometry and Cytochemical Analysis of Nucleic Acids, *Science*, 114, 279-280.

National Research Council (2009). Strengthening forensic science in the United State: A path forward. Washington, DC: The National Academies Press.

Nofi, M. R. (2007) The color determination of optically variable paint flakes pigments, ch. 14, In: Forensic Analysis on the Cutting Edge, Robert D. Blackledge (Ed.), John Wiley & Sons, Inc., Hoboken, NJ, 375-397.

Norden, B. (1978) Applications of linear dichroism spectroscopy, *Applied Spectroscopy Reviews*, 14(2), 157-248.

Norden, B., Rodger, A., and Dafforn, T. (2010) Linear Dichroism and Circular Dichroism: A Textbook on Polarized-Light Spectroscopy, The Royal Society of Chemistry, Cambridge, UK.

Nowicki, J. & Patten, R., (1986) Examination of U.S. Automotive Paints: I. Make and Model Determinations of Hit-and-Run Vehicles by Reflectance Microspectrophotometry, *Journal of Forensic Sciences*, 31(2), 464-470.

Olson, L.A., (1986) Color Comparison in Questioned Document Examination Using Microspectrophotometry, *Journal of Forensic Sciences*, 31(4), 1330-1340.

Olivero, J.J. and Longbothum, R.L. (1977) Empirical fits to the Voigt line width: A brief review, *Journal of Quantitative Spectroscopy and Radiative Transfer*, 17l2), 233-236.

Palenik, C.S. & Buscaglia, J., (2007) Applications of cathodoluminescence in forensic science, ch. 6, In: Forensic Analysis on the Cutting Edge, Robert D. Blackledge (Ed.), John Wiley & Sons, Inc., Hoboken, NJ, 141-173.

Palmer, R. & Turnbull, L.D., (1995) A survey of dye batch variation, *Science and Justice*, 35(1), 59-64.

Palmer, C. (2005) Diffraction Grating Handbook, 6th ed., Newport Corporation, Rochester, NY.

Parsons, N.S. & Mountain, C.-A., (2007) Investigating polyurethane foam as a form of trace evidence", *Science and Justice*, 47(1), 24-33.

Patau, K. (1952) Absorption microphotometry of irregular-shaped objects, Chromosoma, 5(1), 341-362.

Pawley, J. (1995) Fundamental Limits in Confocal Microscopy, ch. 2, In: Handbook of Biological Confocal Microscopy, 2nd ed., James B. Pawley (Ed.), Plenum Press, New York, NY, 19-37.

Petraco, N. & Kubic, T.A. (2004) Color Atlas and Manual of Microscopy for Criminalists, Chemists, and Conservators, CRC Press LLC: Boca Raton, FL.

Pfefferli, P.W., (1983) Applications of microspectrophotometry in document examination, *Forensic Science Internationa*l, 23(2-3), 129-136.

Piller, H. (1977) Microscope Photometry, Springer-Verlag Berlin, Germany.

Pollister, A.W. & Moses, M.J. (1949) A simplified apparatus for photometric analysis and photomicrography, *The Journal of General Physiology*, 567-577.

Roux, C., Novotny, M., Evans, I., & Lennard, C, (1999) A study to investigate the evidential value of blue and black ballpoint pen inks in Australia, *Forensic Science International*, 101, 167-176.

Saarinen, P.E., Kauppinen, J.K. and Partanen, J.O. (1995) "New Method for Spectral Line Shape Fitting and Critique on the Voigt Line Shape Model", *Applied Spectroscopy*, 49(10), 1438-1453.

Savitzky, A. and Golay, M.J.E., (1964) Smoothing and Differentiation of Data by Simplified Least Squares Procedures, *Analytical Chemistry*, 36(8), July, 1627-1639.

Sawyer, L.C., Grubb, D.T., & Meyers, G.F. (2008) Polymer Microscopy, 3rd ed., Springer Science LLC: New York, NY.

Schubert, E.F., (2010) Light-Emitting Diodes, 2nd ed., Cambridge University Press, New York, NY.

Scientific Working Group for Materials Analysis (SWGMAT). (2004) A Forensic Fiber Examiner Training Program, Forensic Science Communications, 7(2), Accessed November 2010 from http://www.fbi.gov/about-us/lab/forensic-science-communications/fsc/april2005/standards/SWGMAT_fiber_training_program.pdf

Shier, D., Butler, J. and Lewis, R. (2006) Hole's Essentials of Human Anatomy and Physiology, 9th ed., McGraw Hill, New York, NY.

Sims, G.R. (1994) Principles of Charged-Transfer Devices, ch. 2, In: Charge-Transfer Devices in Spectrocopy, Sweedler, J.V., Ratzlaff, K.l. and Denton, M.B, (Eds.), VHC Publishers, Inc., New York, NY.

Skoog, D.A., Holler, F.J., & Crouch, S.R. (2007) Principles of Instrumental Analysis, 6th ed., Thomson, Brooks/Cole: Belmont, CA.

Slater, E.M. & H.S. Slater, H.S. (1992) Light and Electron Microscopy, Cambridge University Press: New York, NY.

Stoecklein, W. & Fujiwara, H., (1999) The examination of UV-absorbers in 2-coat metallic and non-metallic automotive paints, *Science and Justice*, 39(3), 188-195.

Stoecklein, W. (2001) “The role of colour and microscopic techniques for the characterization of paint fragments”, ch. 8, In: Forensic Examination of Glass and Paint: Analysis and Interpretation, Brian Caddy (Ed.), CRC Press, Taylor & Francis, Inc., New York, NY, 143-163.

Suzuki, S., Suzuki, Y., Ohta, H., Sugita, R., & Marumo, Y., (2001) Microspectrophotometric discrimination of single fibres dyed by indigo and its derivatives using ultraviolet-visible transmittance spectra, *Science and Justice*, 41(2), 107-111.

Swatland, H.J., (1998) Computer Operation for Microscope Photometry, CRC Press LLC, Boca Raton, FL.

Thorwald, J. (1967) Crime and Science: The New Frontier in Criminology, Harcourt, Brace & World, Inc., New York, NY

Totty,R.N., Ordidge, M.R., & Onion, L.J., (1985) A comparison of the use of visible microspectrometry and high performance thin layer chromatography for the discrimination of aqueous inks used in porous tip and roller ball pens, *Forensic Science International*, 28(2) 137-144.

Travis, J.C., Smith, M.V., Rasberry, S.D. and Kramer, B.W. “Standard Reference Materials: Technical Specifications for Certification of Spectrophotometric NTRMs”, NIST Special Publication 260-140, U.S. Department of Commerce, National Institute of Standards and Technology, Gaitherburg, MD (Feb. 2000).

Walbridge-Jones, S. (2009) Microspectrophotometry for textile fiber color measurement, ch. 9, In: Identification of textile fibers, Houck, M.M. (Ed.), CRC press, LLC, Boca Raton, FL, 165-180.

Walsh, J.W.T. (1958) Photometry, Constable & Company Ltd., London, UK.

Webb, R.H. and Dorey, C.K. (1995) The Pixelated Image, ch. 4. In: Handbook of Biological Confocal Microscopy, 2nd ed., James B. Pawley (Ed.), Plenum Press, New York, NY, 55-67.

Wiggins, K.G., (2001) Forensic textile fiber examination across the USA and Europe, *Journal of Forensic Sciences*, 46**(X),** 1303-1308.

Wilkinson, J.M. , Locke, J., & Laing, D.K., (1988) The examination of paints as thin sections using visible microspectrophotometry and Fourier transform infrared microscopy, *Forensic Science International*, 38(1-2), 43-52.

Young, M. (2000) Optics and Lasers: Including Fibers and Optical Waveguides, 5th ed, Springer-Verlag: New York, NY.

Zeichner, A., Levin, N., Klein, A., & Novoselsky, Y., (1988) Transmission and Reflectance Microspectrophotometry of Inks, *Journal of Forensic Sciences*, 33(5), 1171-1184.

Zeiler, H.W. (1969) What Resolving Power Formula Do You Use?, *The Microscope*, 17**,** 249-270.

Zukauskas, A., Shur, M.S., & Gaska, R. (2002) Introduction to solid-state lighting, John Wiley & Sons, Inc., New York, NY.